UNIVERSIDAD COMPLUTENSE DE MADRID

FACULTAD DE CIENCIAS QUÍMICAS

TESIS DOCTORAL

Tratamiento de efluentes acuosos con contaminantes emergentes presentes en las Listas de Observación de la Unión Europea

MEMORIA PARA OPTAR AL GRADO DE DOCTOR

PRESENTADA POR

Pablo Gutiérrez Sánchez

DIRECTORES

Juan García Rodríguez
Silvia Álvarez Torrellas

UNIVERSIDAD COMPLUTENSE DE MADRID

FACULTAD DE CIENCIAS QUÍMICAS

PROGRAMA DE DOCTORADO DE INGENIERÍA QUÍMICA

TESIS DOCTORAL

Tratamiento de efluentes acuosos con contaminantes emergentes presentes en las Listas de Observación de la Unión Europea

MEMORIA PARA OPTAR AL GRADO DE DOCTOR

PRESENTADO POR:

Pablo Gutiérrez Sánchez

DIRECTORES:

Juan García Rodríguez

Silvia Álvarez Torrellas

Madrid, 2023

UNIVERSIDAD COMPLUTENSE
MADRID

D. Juan García Rodríguez, Catedrático de Universidad, y Dña. Silvia Álvarez Torrellas, Profesora Contratada Doctor, del Departamento de Ingeniería Química y de Materiales de la Facultad de Ciencias Químicas de la Universidad Complutense de Madrid.

CERTIFICAN:

Que la presente memoria, titulada: "*Tratamiento de efluentes acuosos con contaminantes emergentes presentes en las Listas de Observación de la Unión Europea*", constituye la Tesis Doctoral en la modalidad por publicaciones presentada por D. Pablo Gutiérrez Sánchez como requisito para optar al grado de Doctor en Ingeniería Química, y que ha sido realizada en las instalaciones del Departamento de Ingeniería Química y de Materiales de la Facultad de Ciencias Químicas de la Universidad Complutense de Madrid.

Y para que así conste, firman el presente certificado en Madrid, a 28 de junio de 2023.

Fdo.: Juan García Rodríguez

Fdo.: Silvia Álvarez Torrellas

La realización del presente trabajo ha sido posible gracias al apoyo económico prestado a través de los proyectos de la Comunidad de Madrid IND2017/AMB-7720 y S2018/EMT-4341 REMTAVARES-CM.

Agradecimientos

La Tesis Doctoral es el reflejo del compromiso, la perseverancia y la pasión por el conocimiento y la investigación. Es un viaje de descubrimiento personal y profesional donde las preguntas, más allá de convertirse en respuestas, generan el germen de nuevas preguntas, haciendo que las ideas naveguen a través de nuestra imaginación hasta materializarse. Es el comienzo de un sueño en el que desafiamos nuestras limitaciones, nos atrevemos a salir de nuestra zona de confort y nos comprometemos a perseguir lo que realmente nos apasiona. Es el punto de partida de un viaje extraordinario. Y es que, en esta andadura, a veces pedregosa, han sido muchas las personas que han aliviado la intensidad de la carga y han compartido el peso de una mochila que, en ocasiones, parecía no poder levantarse. Por eso, este trabajo no es un logro individual, sino que evidencia el esfuerzo de todos aquellos que, de una forma u otra, han contribuido a su consecución.

Como no podía ser de otra forma, el mayor y más profundo de los agradecimientos es para mi familia, que ha estado en todos los pasos de mi trayectoria vital, personal y profesional. Y es que, sin su apoyo, esto no habría sido posible. A mi madre, Pilar, le debo todas y cada una de las metas que he alcanzado en estos años, porque su amor incondicional, su paciencia infinita y su capacidad para desvanecer todo lo complicado han sido la solución a un gran número de dificultades. A mi padre, Pablo, le debo el valor del esfuerzo, de la constancia, del afán por conocer, por crecer, por nunca estancarse y por enseñarme que el saber es la llave que abre todas las puertas. Y es que, a pesar de haber emprendido tu viaje antes de lo que tendría que haber sido, solo puedo dar las gracias por todas tus enseñanzas. A mis hermanas, Scherezade y Amanda, no puedo más que agradecerles el haber estado, el estar y el tener la certeza de que estarán. Porque las enseñanzas que me han regalado a lo largo de estos años no han hecho más que construir la persona que soy hoy. A Álex, por haber irrumpido en mi vida de una forma tan maravillosa, por haber supuesto un oasis de paz en los momentos en los que la oscuridad parecía inundarlo todo, gracias por ser, simplemente.

A mis amigas, Carmen y Vanesa, con las que comencé mi trayectoria universitaria, y que han sido una pieza fundamental a lo largo de estos años, mi más eterna gratitud. Porque con vosotras el tiempo se detiene, las agujas del reloj se congelan, y el hoy sigue teniendo

el mismo dulce sabor que el ayer. Gracias por hacer que cada minuto de estos años haya sido tan estupendo.

A mis compañeros, y amigos, del Grupo de Catálisis y Operaciones de Separación, a las personas que han estado codo con codo a mi lado en esta etapa, a todos y cada uno de ellos, gracias. Y es que he tenido la suerte de conocer a un gran número de personas maravillosas que se han colado en mi vida como una brisa de aire fresco. Rubén, Elisa, Eva Portillo, Diego Huber, Loren, Naby, Nacho, Marcos Tierno, gracias a todos por los momentos que han hecho de esta una experiencia inolvidable. Pero, como en el cielo, siempre hay estrellas que brillan con una luz más intensa y especial, que te acompañan y hacen que cualquier momento sea importante. Andrés, un referente de nobleza y bondad, un compañero de vida (y de piso), y sin duda, un hogar al que acudir. Gracias amigo, por tu apoyo, por escucharme, por tus risas, por nuestras confidencias en el sofá, y por estar cuando se te necesita. Eva, contigo las palabras y los sentimientos se agolpan al intentar expresarlos para definirte, porque eres eso, un todoterreno, una mujer increíble con una fuerza sobrehumana que ha demostrado con creces su valía. Gracias por ser la mejor compañera de laboratorio que podría haber tenido, por nuestros momentos de desahogo y nuestras innumerables risas. A Diego, porque sin duda eres una de las personas con más potencial que he conocido, porque trabajar a tu lado ha sido toda una experiencia, y porque tu capacidad para relativizar los problemas es algo que se debería patentar. Gracias por haber constituido un pilar fundamental. A Cañas, eres todo un ejemplo de madurez y sensatez. Gracias, amigo, por aconsejarme en todos aquellos momentos en los que parecía no haber una decisión fácil, y por nuestras conversaciones nocturnas de reflexión en el piso. A mi última estrella, Laura, que apareció de forma inesperada, pero que se ha convertido en una pieza fundamental, gracias amiga mía. Tu capacidad de trabajo, tu dedicación, tu entrega a los amigos, tu integridad, tus valores, tu fortaleza, y también tu sensibilidad, hacen que seas todo un referente para cualquiera. Gracias a los cinco por vuestra amistad incondicional.

Por último, agradecer a Juan García, Silvia Álvarez y Marcos Larriba la oportunidad que me ofrecieron para realizar esta Tesis Doctoral, porque ellos han sido el detonante de una reacción en cadena que, más allá de conducirme a incontables vivencias y experiencias personales y profesionales, me ha permitido conocer a personas que, sin duda, formarán parte de mi vida.

Índice general

Índice de figuras

Índice de tablas

Resumen

El agua constituye un recurso esencial para la vida, por lo que su escasez, contaminación y mala gestión suponen un gran impacto sobre la salud humana, el desarrollo económico y el medio ambiente. Para afrontar esta problemática, es preciso la elaboración de un marco regulatorio a nivel global, nacional y local, que promueva, no solo una gestión equitativa y sostenible, sino el desarrollo de tecnologías innovadoras que garanticen la disponibilidad de agua de calidad para las generaciones presentes y futuras.

En este contexto, aquellas sustancias químicas, cuya información es escasa y que no tienen un control medioambiental habitual, pero que presentan un potencial impacto sobre la salud humana o el medio ambiente, conocidas como contaminantes emergentes, están generando una gran repercusión social y política. De esta forma, la Unión Europea ha intensificado sus esfuerzos en las últimas décadas para desarrollar un marco normativo dirigido a la protección de los recursos hídricos frente a este tipo de compuestos, surgiendo las denominadas Listas de Observación.

La presente Tesis Doctoral, titulada "*Tratamiento de efluentes acuosos con contaminantes emergentes presentes en las Listas de Observación de la Unión Europea*", se centra en el estudio de diversas alternativas para el tratamiento de fármacos y pesticidas, evaluándose procesos como la extracción líquido-líquido, la adsorción, la oxidación húmeda catalítica (CWAO), y no catalítica (WAO), y la oxidación promovida por peróxido

de hidrógeno (CWPO). Es decir, el contexto político actual parece estar demandando a la comunidad científica una solución a estos desafíos, por lo que este trabajo aborda el planteamiento de procesos eficaces de eliminación de contaminantes de los que se sospecha pueden presentar un impacto en el ecosistema, pero que se encuentran en fase de evaluación para determinar si es necesario establecer normas de calidad ambiental que los regulen.

En los procesos de extracción líquido-líquido, el empleo de disolventes alternativos, como los terpenoides y mezclas eutécticas, mostró resultados prometedores, alcanzándose rendimientos de extracción considerablemente superiores y pérdidas en la fase acuosa inferiores a los obtenidos para disolventes convencionales. Para los pesticidas neonicotinoides, el carvacrol presentó rendimientos de extracción próximos al 95, 98 y 99 % para el tiametoxam, imidacloprid y acetamiprid, respectivamente, empleando una relación S/F de 0,1, una temperatura de 30 ºC y matriz de agua ultrapura. Además, el efecto de la matriz, el pH del alimento y la temperatura no fueron significativos para la extracción de pesticidas con este terpenoide. Para los antibióticos analizados, ningún pH permitió alcanzar un óptimo para la extracción simultánea de los tres compuestos, lo que se vio influido según sus equilibrios de disociación. Aunque los disolventes eutécticos mostraron una menor sensibilidad a los cambios de pH en el alimento, el carvacrol se posicionó como disolvente de extracción más favorable, mostrando rendimientos del 98,9, 99,5 y 97,0 % para la trimetoprima, ciprofloxacina y sulfametoxazol, respectivamente, empleando matrices reales a pH 5,0 y relación S/F 1,00. También se evaluó con éxito la reutilización del carvacrol durante cinco etapas consecutivas de extracción de fármacos y su recuperación mediante un evaporador rotatorio a 164 °C y 20 mbar.

Los materiales sintetizados a partir de lodos de depuradora de diferente procedencia mediante procesos pirolíticos, empleando diversos agentes activantes químicos ($NiCl_2$ y $FeCl_3$), mostraron propiedades adsorbentes y catalíticas prometedoras. En este sentido, los sólidos exhibieron una combinación de isotermas de adsorción-desorción de nitrógeno tipo I-IV, con ciclos de histéresis tipo H3-H4. Es decir, el tamaño medio de poro indicó una naturaleza mesoporosa, con una contribución moderada de la microporosidad, mientras que las áreas superficiales BET se encontraron en el intervalo 397-713 m^2/g. Las capacidades de adsorción de ciprofloxacina variaron entre 32,1 y 73,9 mg/g en función del tipo de material y las condiciones en las que se realizaron los blancos de adsorción. Además, el

proceso de síntesis propuesto pareció alcanzar una elevada fijación de los metales de transición incorporados durante la activación química, como haluros metálicos, a la matriz sólida. Este hecho fue considerablemente notable para el agente activante $FeCl_3$, que además proporcionó materiales con una gran actividad catalítica en procesos CWPO y CWAO. La viabilidad técnica de los procesos catalíticos verificó a través de su eficacia con matrices reales y/o en ciclos consecutivos de reutilización del catalizador.

Abstract

Water is essential for life, and its scarcity, pollution and mismanagement have a major impact on human health, economic development and natural environment. Therefore, it is imperative to develop a global, national and local regulatory framework that promotes not only an equitable and sustainable access to water, but also the implementation of innovative technologies. That is to say, guaranteeing the availability of quality water for present and future generations.

Against this background, those chemicals that are not commonly monitored or regulated in the environment, but which may have a potential impact on human health or the environment, known as emerging pollutants, are raising a great social and political concern. As a result, the European Union has intensified its efforts in the last decades to build a regulatory framework aimed at protecting water resources against this type of pollutants, creating the so-called Watch Lists.

This PhD dissertation, entitled "Treatment of aqueous effluents to remove emerging pollutants included in the EU Watch Lists", is focused on the study of several approaches for the removal of pharmaceuticals and pesticides, assessing processes such as liquid-liquid extraction, adsorption, catalytic wet air oxidation (CWAO) and non-catalytic wet air oxidation (WAO), and catalytic wet peroxide oxidation (CWPO). The current political context seems to be demanding a solution to these challenges from the scientific

community, so this work addresses the development of effective techniques for the removal of pollutants that are suspected of having an impact on the environment, but which are currently being evaluated to decide whether it is required to set out environmental quality standards to regulate them.

In liquid-liquid extraction processes, the use of bio-based solvents, such as terpenoids and eutectic mixtures, revealed promising results, achieving considerably higher extraction yields and lower losses in the aqueous phase than those obtained for conventional solvents. Concerning neonicotinoid pesticides, carvacrol showed extraction yields close to 95, 98 and 99 % for thiamethoxam, imidacloprid and acetamiprid, respectively, using an S/F ratio of 0.1, a temperature of 30 °C and ultrapure water as matrix. Furthermore, the effect of matrix, feed pH value and temperature were not significant for the pesticide extraction with this terpenoid. Regarding the antibiotics tested, no single pH was optimal for the simultaneous extraction of the three compounds, which was influenced by their dissociation equilibria. Although the eutectic solvents showed a lower sensitivity to pH changes in the feed, carvacrol was placed as the most favourable extraction solvent, showing yields of 98.9, 99.5 and 97.0 % for trimethoprim, ciprofloxacin and sulfamethoxazole, respectively, using real matrices at pH 5.0 and S/F 1.00. The reuse of carvacrol during five consecutive extraction steps and its recovery using a rotary evaporator at 164 °C and 20 mbar was also successfully evaluated.

Carbonaceous materials synthesised from different sewage sludge sources by pyrolytic processes, using chemical activating agents ($NiCl_2$ and $FeCl_3$), showed promising adsorption and catalytic properties. In this regard, the solids exhibited a combination of type I-IV nitrogen adsorption-desorption isotherms with H3-H4 hysteresis loops. The average pore widths indicated a mesoporous nature, with a moderate contribution from microporosity, while BET areas were in the range 397-713 m^2/g. The adsorption capacities of ciprofloxacin were found to be between 32.1 and 73.9 mg/g, depending on the carbonaceous material and the operating conditions during the adsorption blanks. Moreover, the proposed synthesis process seemed to achieve a high attachment of the transition metals incorporated during the chemical activation to the solid matrix. This was considerably marked for the activating agent $FeCl_3$, which also provided materials with high catalytic activity in CWPO and CWAO processes. The technical feasibility of the

catalytic processes was verified through their efficiency with real matrices and/or in consecutive cycles of catalyst reuse.

Capítulo I

Introducción

La escasez, la contaminación y la mala gestión del agua plantean amenazas significativas para la salud humana, el desarrollo económico y el medio ambiente. La solución a este desafío requiere la elaboración de políticas a nivel global, nacional y local, que promuevan una gestión sostenible y equitativa y la aplicación de soluciones innovadoras para el tratamiento de este recurso vital, garantizando su disponibilidad para las generaciones presentes y futuras.

En este contexto, los contaminantes emergentes han atraído la atención de la comunidad científica, generando un contundente impacto económico, social y político a nivel mundial. De esta forma, la Unión Europea ha intensificado sus esfuerzos en las últimas dos décadas para desarrollar un marco normativo cuyo objeto es la protección de los recursos hídricos, surgiendo las denominadas listas de observación europeas.

La eliminación eficaz de contaminantes emergentes en las aguas todavía constituye un reto. Procesos de tratamiento como la extracción líquido-líquido, la adsorción o la oxidación avanzada podrían posicionarse como técnicas efectivas en el tratamiento de contaminantes como los fármacos y los pesticidas.

1.1 Problemática actual del agua

El agua no solo constituye un recurso esencial para la vida, sino que es indispensable para la mayor parte de las actividades económicas que se realizan de manera diaria. Sin embargo, el incremento de la población mundial ha conducido a un aumento de la demanda de agua, lo que ha intensificado los desafíos relacionados con la escasez, la contaminación y la mala gestión de este recurso vital (Programa Mundial de Evaluación de los Recursos Hídricos (WWAP), 2016, 2019).

A pesar de ser un derecho humano fundamental, millones de personas en todo el mundo carecen de acceso a agua de calidad o a servicios de saneamiento gestionados de manera segura. Concretamente, el Fondo de las Naciones Unidas para la Infancia cifra en 2.200 millones el número de personas sin servicios de agua potable, lo que pone en peligro su salud y bienestar (UNICEF, 2019). Se prevé que 3.500 millones de personas sufran escasez de agua en el año 2025 y que más del 40% de la población mundial viva en condiciones de estrés hídrico severo (Otto & Schleifer, 2020; Programa Mundial de Evaluación de los Recursos Hídricos (WWAP), 2020).

La escasez de agua plantea uno de los principales desafíos a los que se enfrenta la sociedad actual. En este sentido, a medida que la población y las demandas industriales y agrícolas crecen, la presión sobre los recursos hídricos también lo hace. Parece evidente, por tanto, que la escasez de agua limita el desarrollo económico y la producción agrícola, siendo esta última uno de los mayores consumidores a nivel mundial. La falta de acceso a agua para riego reduce la producción de alimentos y afecta a la seguridad alimentaria. También tiene implicaciones en la generación de energía, la industria y otros sectores económicos (Engelbert & Scheuring, 2022; Seckler et al., 1999; Unfried et al., 2022).

Además, el cambio climático está causando una alteración en los patrones de precipitación, así como un aumento en la frecuencia e intensidad de sequías y eventos climáticos extremos, lo que agrava la escasez de agua en muchas regiones (Programa Mundial de Evaluación de los Recursos Hídricos (WWAP), 2016, 2020). Factores como el desarrollo económico, el crecimiento de la población, y los cambios en los patrones de consumo serían los principales causantes de un incremento del 600 % en el uso de agua

dulce a nivel mundial en los últimos cien años. El ritmo de crecimiento se ha estabilizado en cerca de un 1 % anual desde la década de los 80 (Programa Mundial de Evaluación de los Recursos Hídricos (WWAP), 2021).

La mala gestión del agua ha agravado aún más la problemática actual, contribuyendo a este hecho factores como la falta de infraestructura adecuada para el suministro y saneamiento, la sobreexplotación de acuíferos, la falta de normativa y la escasa concienciación y educación sobre el uso sostenible del agua. Todo ello resulta en una distribución desigual de este recurso, afectando especialmente a las comunidades más vulnerables. En términos de salud, la falta de acceso a agua de calidad y saneamiento adecuado contribuye a la propagación de enfermedades, como el cólera y la diarrea, causando millones de muertes cada año, especialmente en los países en desarrollo (Chua et al., 2023; Programa Mundial de Evaluación de los Recursos Hídricos (WWAP), 2020).

Por otro lado, la contaminación se ha visto agravada por otros factores, como la industrialización, el uso irracional del agua y el incremento de la población (Programa Mundial de Evaluación de los Recursos Hídricos (WWAP), 2021). Las actividades agrícolas, industriales y domésticas liberan una amplia variedad de contaminantes a los recursos hídricos, incluyendo productos químicos, nutrientes y plaguicidas, residuos industriales y productos farmacéuticos. Es decir, más del 80 % de las aguas residuales generadas a nivel mundial regresan al medio ambiente sin un tratamiento adecuado (Programa Mundial de Evaluación de los Recursos Hídricos (WWAP), 2017). La introducción de estos contaminantes en los ecosistemas acuáticos presenta un gran impacto y representa un riesgo para la salud humana y el medio ambiente. Además, la exposición a contaminación fecal a través del agua potable está muy extendida en países en vías de desarrollo, lo que supone un riesgo elevado en la transmisión de enfermedades. Concretamente, se estima que alrededor de 2.000 millones de personas emplean fuentes de agua contaminada con heces para consumo humano. (World Health Organization, 2021, 2022).

Para afrontar la problemática actual del agua es preciso la adopción de medidas integrales a nivel local, nacional e internacional, por lo que una gestión sostenible y equitativa de los recursos hídricos es fundamental (Englezos et al., 2023). Esto implica la

implementación de políticas y normativas efectivas, la inversión en infraestructuras hídricas adecuadas, la adopción de prácticas agrícolas sostenibles, la promoción de la conservación del agua y el fomento de la eficiencia en su uso (Seijger & Hellegers, 2023). También es crucial la educación y la concienciación sobre la importancia del agua, pudiéndose realizar a través de campañas de sensibilización, programas educativos en colegios y la participación de la sociedad civil en la toma de decisiones relacionadas con el agua (Stoker et al., 2022; Williams et al., 2023). A nivel internacional, resulta imprescindible la cooperación y la solidaridad entre los países, mediante acuerdos y tratados para la gestión compartida de los recursos hídricos transfronterizos, la transferencia de tecnologías y conocimientos, y el apoyo financiero para proyectos y programas relacionados con el agua en los países en desarrollo (Hayat et al., 2022; Shams & Muhammad, 2022; Ziganshina & de Schutter, 2022).

En cuanto a las perspectivas futuras, la innovación tecnológica desempeñará un papel decisivo en el futuro de la gestión del agua. En este contexto, el desarrollo de tecnologías de tratamiento de agua más eficientes, la implementación de técnicas de agricultura que optimicen el uso del agua, y la aplicación de soluciones medioambientalmente sostenibles, pueden contribuir a la mejora de la situación actual (Linh et al., 2023; Xiuling et al., 2023).

1.2 Contaminantes emergentes

1.2.1 Definición y clasificación

En los últimos años, la preocupación por los denominados “contaminantes emergentes” ha generado un contundente impacto económico, social y político a nivel mundial. Según la UNESCO, este grupo de contaminantes se define como cualquier sustancia química, natural o sintética, o cualquier microorganismo, que no tenga una regulación o control medioambiental habitual y que presente un potencial impacto sobre la salud humana o el medio ambiente (Cavero et al., 2023). Además, la mayoría de ellos se emplean y se liberan de manera continuada en los medios acuáticos, en concentraciones

normalmente bajas, pudiendo generar toxicidad crónica, alteraciones endocrinas y el desarrollo de bacterias resistentes, entre otros (Ngo et al., 2015; Petrović et al., 2003).

La presencia en los recursos hídricos, la acumulación en el medio ambiente y los riesgos para la salud humana y los ecosistemas todavía se presentan como los principales interrogantes para la gran mayoría de contaminantes emergentes. Por esta razón, normalmente no se encuentran regulados en las normativas medioambientales, de calidad del agua y de vertidos de aguas residuales, lo que refuerza la necesidad de realizar investigaciones encaminadas a la adopción de enfoques tecnológicos y políticos para controlar el vertido de estos contaminantes (Kosma et al., 2010; Tran & Gin, 2017).

La monitorización de los contaminantes emergentes en las aguas es un desafío debido a la gran cantidad de compuestos diferentes y la diversidad de sus fuentes. La detección y cuantificación de estos compuestos requieren métodos analíticos avanzados y sensibles que puedan identificar incluso bajas concentraciones en muestras de agua. Además, es necesario desarrollar y mejorar continuamente las tecnologías de tratamiento de agua para eliminar o reducir la presencia de estos compuestos en los suministros de agua potable (Petrović et al., 2003). Los contaminantes emergentes abarcan una amplia gama de sustancias, como pesticidas, fármacos, cosméticos, productos para el cuidado personal y del hogar, tensioactivos, subproductos de desinfección, retardantes de llama, nanomateriales, compuestos perfluorados, colorantes, entre otros, que se utilizan en todo el mundo y son esenciales en la sociedad moderna (Cavero et al., 2023; Kumar et al., 2022).

Dentro del amplio espectro de compuestos, los grupos predominantes en el medio ambiente han sido los pesticidas y los productos farmacéuticos y de cuidado personal, incluyendo antibióticos, antiinflamatorios, cosméticos y protectores solares, entre otros (Bell et al., 2012; González-González et al., 2022; Ortúzar et al., 2022; Rajmohan et al., 2020; Riyaz et al., 2021). También se han detectado otros compuestos asociados a la actividad industrial u originados en la degradación de plásticos, como tensioactivos, retardantes de llama, plastificantes o colorantes (Barceló & Petrovic, 2008; Calvo-Flores et al., 2017; Eggen et al., 2010). Además, la presencia simultánea de varios compuestos podría tener efectos tóxicos sinérgicos, lo que supondría una amenaza mayor (Kümmerer, 2009b).

1.2.1.1 Fármacos

Los medicamentos constituyen uno de los factores más eficaces para la mejora de la salud y el control de algunas enfermedades, lo que ha propiciado un incremento en las inversiones de este campo y un desarrollo exponencial de la industria farmacéutica. Este sector presenta una supervisión estricta y minuciosa por parte de los gobiernos, por lo que la trayectoria normativa pertinente ha influido en su crecimiento y desarrollo (Safari et al., 2018).

El aumento progresivo de la esperanza de vida en los países desarrollados como consecuencia de los grandes avances en el área médica conducirá a una población más envejecida y, por ende, a un aumento en la demanda de medicamentos. Todo esto no hace más que dibujar una tendencia positiva en la ampliación de los mercados farmacéuticos a medio-largo plazo (Safari et al., 2018).

Los mercados emergentes también parecen representar un factor clave en la industria farmacéutica. Países como Rusia, India, Brasil, China, México, Indonesia, Sudáfrica, Corea del Sur y Turquía han duplicado sus ventas en cinco años, consiguiendo una cuota de mercado cercana al 20 %. Por tanto, la expansión de las empresas farmacéuticas en estos mercados dependerá del grado de adecuación al ritmo de desarrollo del país. Además, aunque tradicionalmente han dominado los medicamentos contra enfermedades infecciosas y transmisibles, como las de transmisión sexual, el aumento de la riqueza y la esperanza de vida están generando un cambio en el estilo de vida y en los patrones de enfermedades. Concretamente, se ha incrementado de forma notable la incidencia de enfermedades no transmisibles, como la diabetes, las cardiovasculares, y las oncológicas, en los mercados emergentes, acercándose a lo observado en los países occidentales (Tannoury & Attieh, 2017).

Existen distintos subgrupos de fármacos en función de su uso, incluyéndose entre ellos los siguientes: antibióticos; antiepilépticos; analgésicos y antiinflamatorios; hormonas; betabloqueantes; reguladores de lípidos en sangre; citostáticos; y agentes de contraste. Algunos de los medicamentos más representativos empleados en la actualidad se encuentran recogidos en la Tabla 1 (Liu & Wong, 2013).

Tabla 1. Clasificación de los principales fármacos empleados en la actualidad.

Subgrupo	Ejemplos
Antibióticos	Claritromicina
	Eritromicina
	Sulfametoxazol
	Sulfadimetoxina
	Amoxicilina
	Ciprofloxacina
	Norfloxacino
	Trimetoprima
Hormonas	Estrona
	Estradiol
	Etinilestradiol
Analgésicos y antiinflamatorios	Diclofenaco
	Ibuprofeno
	Paracetamol
	Ácido acetilsalicílico
	Celecoxib
Antiepilépticos	Carbamazepina
	Primidona
	Fenobarbital
Reguladores de lípidos en sangre	Clofibrato
	Gemfibrozil
	Fenofibrato
Betabloqueantes	Metoprolol
	Propranolol
	Atenolol
Agentes de contraste	Diatrizoato
	Iopromida
Citostáticos	Ifosfamida
	Ciclofosfamida

Los antibióticos son considerados como uno de los principales medicamentos empleados a nivel mundial, debido a su amplia aplicación para el tratamiento de infecciones fúngicas y bacterianas, tanto en humanos como en animales (Tambosi et al., 2010). Entre los principales grupos de antibióticos, se encontrarían las sulfonamidas

(sulfametoxazol, sulfadimetoxina), los macrólidos (eritromicina, roxitromicina) y las fluoroquinolonas (norfloxacino, ciprofloxacina) (Liu & Wong, 2013).

Según los datos publicados por el Centro Europeo para la Prevención y el Control de las Enfermedades, España fue el séptimo país europeo con mayor consumo de antibióticos en 2021, después de Rumanía, Chipre, Bulgaria, Grecia, Francia y Polonia. En este sentido, España presentó alrededor de 20 dosis diaria definidas por 1000 habitantes y día, frente a la media 18 dosis diaria definidas por 1000 habitantes y día para el conjunto de países europeos (European Centre for Disease Prevention and Control, n.d.).

Otro de los subgrupos más estudiado que más atención ha atraído es el de las hormonas, entre las que se incluyen los estrógenos naturales, excretados por humanos y animales (estrona, estradiol o estriol), y sintéticos, empleados como anticonceptivos orales (principalmente etinilestradiol). Aunque los estrógenos esteroides naturales no se engloban en realidad dentro de los productos farmacéuticos, generalmente se estudian junto con las hormonas sintéticas por sus efectos de alteración endocrina en agua contaminada (Liu & Wong, 2013).

1.2.1.2 Pesticidas

Los pesticidas los constituyen todas aquellas sustancias, puras o mezclas, destinadas a prevenir, repeler, destruir o mitigar una plaga, incluyendo aquellas empleadas como defoliantes, desecantes o reguladores de crecimiento vegetal. Estas características han convertido a los productos fitosanitarios en compuestos indispensables para erradicar enfermedades transmitidas por insectos y para producir alimentos y fibras de manera sostenible, confiriéndoles un papel económico muy significativo en el mercado mundial. Entre los plaguicidas más consumidos destacarían los herbicidas, insecticidas y fungicidas, mientras que las principales potencias productoras las constituirían, en orden decreciente, Asia, Latinoamérica, Europa y los integrados dentro del Tratado de Libre Comercio de América del Norte (Matthews, 2016; Plakas & Karabelas, 2012; Primo Yúfera, 2007; Salem & Olajos, 1988; Sierra & Gómez Gallego, 2007).

Los pesticidas han evolucionado, no solo en términos económicos y geográficos, sino también en su estructura y propiedades químicas. Es decir, mientras que inicialmente se

caracterizaban por su carácter inorgánico (sulfato de cobre, polisulfuro de calcio o arsenato de plomo) o su origen botánico (piretrinas, nicotina y rotenona), en la actualidad son frecuentes los compuestos orgánicos sintéticos. La Segunda Guerra Mundial supuso un hito en el progreso de los pesticidas sintéticos, propiciándose la aparición acelerada de un gran número de plaguicidas durante las décadas posteriores, como se muestra en la Tabla 2. Todo ello, ha permitido disminuir de un 42 a un 9 % las pérdidas de las cosechas debidas a las plagas (Matthews, 2016; Salem & Olajos, 1988; Sierra & Gómez Gallego, 2007).

Tabla 2. Evolución de los pesticidas y año de síntesis.

Año	Tipo	Pesticida	Año	Tipo	Pesticida
900	I	Arsénicos	1948	I	Aldrin, Dieldrin
1690	I	Nicotina	1949	F	Captan
1800	I	Piretrinas	1956	I	Carbaril
1867	I	París Green	1965	N	Aldicarb
1930	H	DNOC	1990	I	Imidacloprid, Spinosad
1939	I	DDT	1998	I	Tiametoxam
1942	H	2,4-D	2002	I	Pyridalyl
1943	F	Zineb	2005	I	Flonicamid, Spinetoram, Spirodiclofen
1944	I	HCH (Lindano)	2007	H	Pyraxosulfone
1946	I	Paratión	2012	I	Sulfoxaflor, Flupyradifurone

Nota: Insecticida (I); Herbicida (H); Nematicida (N); Fungicida (F)

A pesar de los beneficios que ha implicado el uso masivo de pesticidas, también ha tenido graves repercusiones sobre el medio ambiente, la biodiversidad, la calidad de los alimentos y la salud del ser humano. Las propiedades fisicoquímicas, junto con su modo de acción y de aplicación, ha posicionado a alguno de estos compuestos, como los pesticidas organoclorados, dentro de los denominados contaminantes orgánicos persistentes. Por esta razón, en las últimas décadas se ha promovido la síntesis de productos fitosanitarios con menores dosis de aplicación, persistencia y toxicidad hacia otras especies no objetivo. En este contexto, ha cobrado cada vez más interés los pesticidas neonicotinoides, que representan el 25 % del total de insecticidas empleados a nivel mundial y requieren dosis de aplicación entre 0,01 y 0,1 Kg/ha, frente a los 3 Kg/ha de los compuestos organoclorados (Goulson, 2013; Mehran Anjum, 2017; Rathore & Nollet, 2012; Sierra & Gómez Gallego, 2007).

El término neonicotinoide agrupa a todas aquellas sustancias sintéticas y sistémicas cuyo modo de acción se asemeja al de la nicotina, es decir, actúan selectivamente sobre el sistema nervioso central de los insectos como agonistas de los receptores nicotínicos de acetilcolina (Insecticide Resistance Action Committee (IRAC), n.d.; Jeschke & Nauen, 2008). La estructura general de estos insecticidas aparece esquematizada en la Figura 1 y consta de tres segmentos (Jeschke & Nauen, 2008; Wakita et al., 2003):

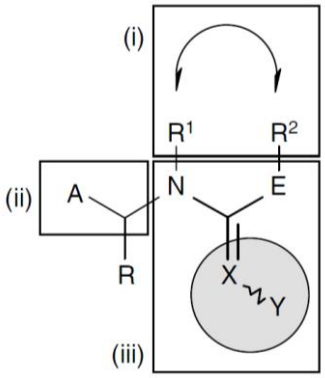

Figura 1. Estructura química general de los insecticidas neonicotinoides (Jeschke & Nauen, 2008).

(i) Para los compuestos de cadena abierta, entre los sustituyentes R^1 y R^2 no se establece ningún enlace simple. Sin embargo, en los compuestos cíclicos se establece un puente de la forma [-R^1-R^2-] o [-R^1-Z-R^2-], donde Z puede ser [-O-] o [-N-Me-].

(ii) Este segmento está constituido por un grupo heteroalicíclico o heterocíclico (A-) unido a una cadena puente [-CHR-], siendo el metileno el grupo empleado como cadena puente para los neonicotinoides sintetizados hasta el momento. Según la composición de este segmento estructural, se distinguen los cloronicotinilos (CPM), los tianicotinilos (CTM) y los furanicotinilos (TFM), cuyas estructuras se detallan en la Tabla 3.

(iii) El segmento [-N-C(E)=X-Y] representa los diferentes farmacóforos, pudiéndose agrupar los compuestos desarrollados en: nitroenaminas o nitrometilenos [–N–C(E)=CH–NO_2], donde E puede ser S ó NH; N-nitroguanidinas o N-nitroiminas [–N–C(E)=N–NO_2], donde E puede ser NH ó NMe; y N-cianoamidinas o N-cianoiminas [–N–C(E)=N–CN], donde E puede ser S ó Me.

Tabla 3. Segmento estructural [A-CHR-] para los insecticidas neonicotinoides comercializados (Jeschke & Nauen, 2008; Wakita et al., 2003).

Estructura del segmento [A-CHR-]	Nomenclatura	Abreviatura
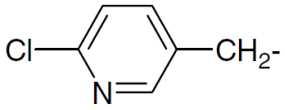	6-**c**loro-**p**irid-3-il**m**etilo	CPM
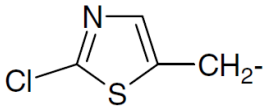	2-**c**loro-1,3-**t**iazol-5-il**m**etilo	CTM
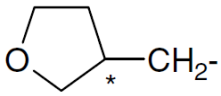	(±)-**t**etrahidro-**f**ur-3-il**m**etilo	TFM

**Mezcla de los enantiómeros (R) y (S).*

En la Tabla 4 se recogen los insecticidas neonicotinoides desarrollados hasta el momento, agrupados según los segmentos estructurales mencionados previamente (Jeschke & Nauen, 2008).

1.2.2 Fuentes de la contaminación

La contribución y la importancia de las distintas fuentes de liberación y transporte de contaminantes emergentes al medio ambiente se encuentra entre los principales objetivos de numerosos proyectos de investigación actuales, valorándose además aspectos tan relevantes como la concentración y el destino de los mismos. Además, este tipo de compuestos se encuentra en concentraciones relativamente bajas (ng/L a µg/L), por lo que su detección y seguimiento ha supuesto un reto técnico y económico (Barbosa et al., 2016).

La presencia de los contaminantes emergentes se ha detectado en un gran número de medios acuáticos, aunque su concentración varía considerablemente según su origen. De esta forma, las concentraciones, tanto en aguas superficiales como subterráneas, suelen ser inferiores a las observadas a la salida de las plantas de tratamiento de aguas residuales, debido a la dilución, a los procesos naturales de atenuación, o a una combinación de ambos (Gurr & Reinhard, 2006; Pal et al., 2010).

Tabla 4. Tipos de compuestos neonicotinoides y ejemplos.

Farmacóforo [–N–C(E)=X–Y]	Compuestos cíclicos (R^1-R^2 ó R^1-Z-R^2)	Compuestos de cadena abierta (R^1, R^2)
Nitroenaminas/ Nitrometilenos [–N–C(E)=CH–NO_2] E = S, NH	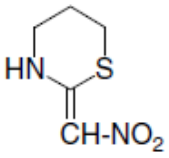 Nitiazina ($CH_2CH_2CH_2$)	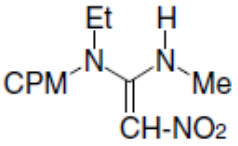 Nitenpiram (Et, Me)
N-nitroguanidinas/ N-nitroiminas [–N–C(E)=N–NO_2] E = NH, NMe	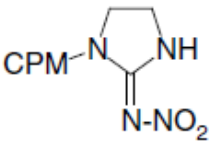 Imidacloprid (CH_2CH_2) 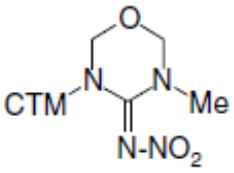 Tiametoxam (CH_2-O-CH_2) 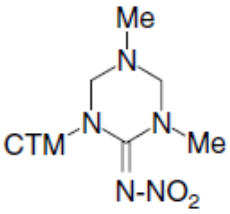 AKD 1022 (CH_2-NMe-CH_2)	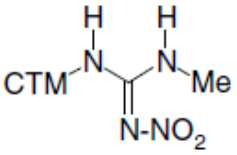 Clotianidina (H, Me) 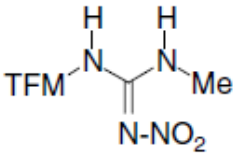 Dinotefuran (H, Me)
N-cianoamidinas/ N-cianoiminas [–N–C(E)=N–CN] E = S, Me	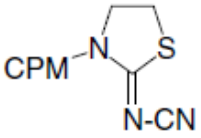 Tiacloprid (CH_2CH_2)	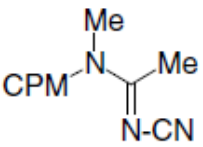 Acetamiprid (Me, Me)

Nota: Etilo (Et); Metilo (Me), CPM, CTM y TFM definidos en la Tabla 3.

La localización geográfica también presenta un gran impacto en su caracterización, pues la frecuencia y dosificación local y regional en el uso de estos productos, así como la eficacia de las instalaciones de tratamiento de aguas residuales, influyen en los niveles de concentración en las masas de agua superficial. Además, la presencia de contaminantes emergentes en las aguas superficiales suele ser superior a la de las aguas subterráneas, debido no solo a que reciben directamente los efluentes de las EDAR, sino a que el tiempo de residencia es considerablemente más corto (Barnes et al., 2008).

El transporte y transformación de los contaminantes emergentes en los ecosistemas acuáticos depende de un gran número de factores, entre los que se encuentran las propiedades fisicoquímicas del contaminante (como la solubilidad en agua, la polaridad, la volatilidad, etc.), y parámetros ambientales (como la temperatura, el pH, el contenido de materia orgánica, las precipitaciones y la altitud). Estos factores están directamente relacionados con el tiempo de vida de un determinado compuesto en el medio ambiente. Por ejemplo, la solubilidad de ciertos contaminantes en el agua puede facilitar su incorporación en el medio acuático mediante procesos de escorrentía. De igual forma, la polaridad indica la afinidad por una fase acuosa u orgánica, por lo que compuestos con un elevado coeficiente octanol-agua tienden a bioacumularse.

Las fuentes de los contaminantes emergentes se pueden clasificar atendiendo a si la contaminación se produce a través de una fuente específica e identificable (puntual) o si se produce a través de varios puntos dispersos o procedentes de una amplia zona (difusa) (Lapworth et al., 2012). En la Figura 2 se esquematizan las principales fuentes de entrada de los contaminantes emergentes en el medio acuático.

1.2.2.1 Fuentes puntuales

Las principales fuentes puntuales de contaminación las constituyen los efluentes procedentes de las plantas de tratamiento de aguas residuales en zonas industriales, urbanas y agrícolas (Glassmeyer et al., 2005; Pal et al., 2010; Lapwoth et al., 2012). Debido a sus propiedades fisicoquímicas, es decir, baja volatilidad y elevado carácter refractario y solubilidad, se ha observado que las EDAR convencionales resultan ineficaces para el tratamiento de contaminantes emergentes, lo que, aunque en bajas concentraciones,

implicaría la presencia de estos compuestos en el efluente de las instalaciones (Asano et al., 2007; Stefanakis et al., 2014). Otras fuentes puntuales las constituirían las instalaciones industriales, las plantas de procesamiento de alimentos, las actividades mineras, y los vertederos.

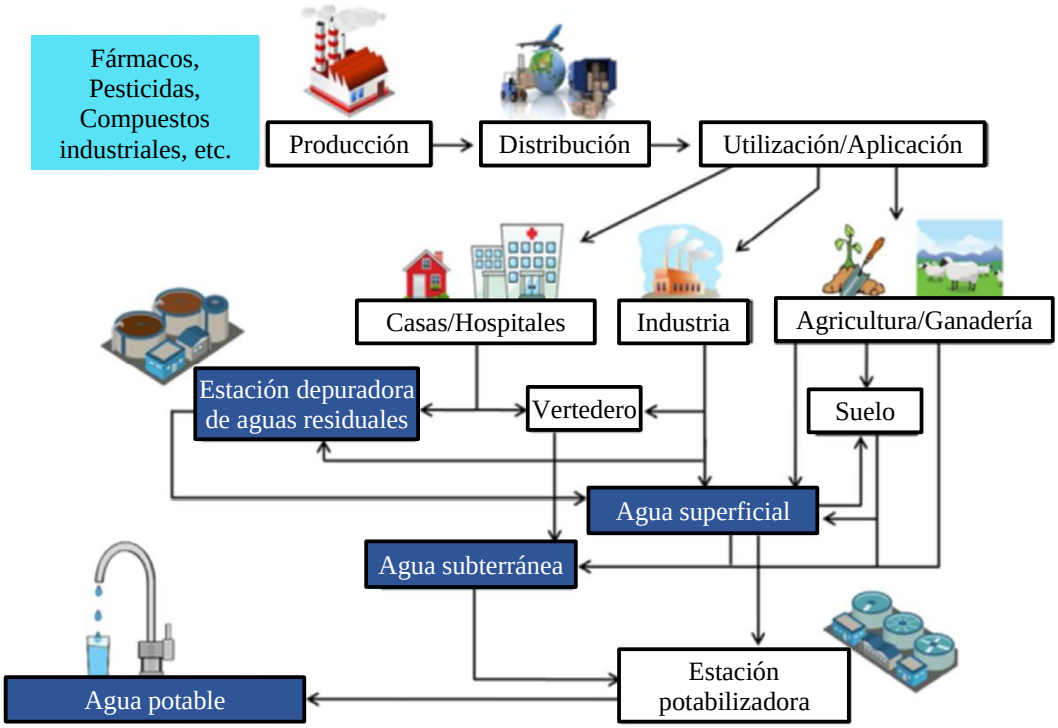

Figura 2. Fuentes y rutas más representativas de los contaminantes emergentes en el medio ambiente (Barbosa et al., 2016).

Los hogares son otra de las fuentes puntuales más significativas, especialmente de productos farmacéuticos y de cuidado personal. En este sentido, diversos estudios realizados en Europa y Estados Unidos han reportado que la mayor parte de los medicamentos que no se usan, o que se encuentran caducados, suelen eliminarse junto con los residuos sólidos domésticos o se tiran por el inodoro (Bound & Voulvoulis, 2005; Glassmeyer et al., 2009; Khan, 2012; Vollmer, 2010). En Alemania y Austria, por ejemplo, se estima que más de un 30 y 25 % de los fármacos comercializados, respectivamente, se desechan de esta forma (Kümmerer, 2008, 2009a). Además, los fármacos se excretan a través de las heces o la orina sin sufrir ningún cambio o como metabolitos activos, introduciéndose en el sistema de alcantarillado. Concretamente, se ha observado que hasta el 95% de la dosis puede excretarse en las aguas residuales domésticas (Gezahegn et al.,

2019; Karungamye, 2020). La eliminación de compuestos farmacéuticos con los residuos sólidos domésticos suele propiciar la presencia de estos contaminantes en los lixiviados de vertederos y, con ello, en las aguas subterráneas si no se realiza ningún tratamiento.

Las aguas residuales hospitalarias se posicionan como otra de las principales fuentes puntuales de contaminantes emergentes, incluyendo un amplio espectro de compuestos, como las sustancias farmacéuticas, disolventes y desinfectantes (Ternes & Hirsch, 2000; Verlicchi et al., 2010). Además, aunque el caudal es inferior al de las aguas residuales municipales, las aguas hospitalarias contienen una mayor concentración de estos compuestos. Algunas de las sustancias procedentes de esta fuente se caracterizan por su alta persistencia en el medio ambiente, llegándose a detectar incluso en aguas subterráneas (Sacher et al., 2001; Schulz et al., 2008; Ternes & Hirsch, 2000).

La recarga de acuíferos es una de las técnicas más utilizadas para mantener y aumentar el nivel de las aguas subterráneas, garantizando su aprovechamiento sostenible, la seguridad de los abastecimientos y la pervivencia de este recurso. Sin embargo, el empleo de aguas de escorrentía pluvial o urbana, o de aguas residuales tratadas, podría introducir en el medio ambiente diversos contaminantes (Díaz-Cruz & Barceló, 2008). Es decir, esta estrategia también podría tener un impacto sobre la calidad de las aguas subterráneas, y sobre la salud humana, si se emplean como fuentes de agua potable (Cordy et al., 2004). Asimismo, también existiría este riesgo cuando se utilizan aguas superficiales para la recarga ya que, como se mencionó anteriormente, la presencia de contaminantes emergentes en las aguas superficiales es normalmente superior a la encontrada en las subterráneas (Díaz-Cruz & Barceló, 2008; Heberer et al., 2001; Heberer & Adam, 2004).

Los vertederos poseen una contribución considerable sobre la emisión de contaminantes emergentes, especialmente de aquellos cuyo destino son las aguas subterráneas. Esta contaminación local de acuíferos cercanos depende, en gran medida, de aspectos como la elección de la ubicación o el diseño, aunque en la mayor parte de los países desarrollados esta problemática se ha reducido de manera exponencial. A pesar de ello, se siguen detectando aguas subterráneas contaminadas en zonas de vertederos en países como Dinamarca, Croacia o Estados Unidos (Ahel et al., 1998; Buszka et al., 2009; Holm et al., 1995).

Las explotaciones ganaderas presentan fuentes puntuales considerables de vertido de compuestos estrogénicos. Es decir, los efluentes de las EDAR procedentes de estas instalaciones contienen niveles de estrógenos (androstenediona, estrona, testosterona, etc.) significativamente superiores a los encontrados en las EDAR municipales. También es muy frecuente la presencia de medicamentos de uso veterinario (Bartelt-Hunt et al., 2011; Furuichi et al., 2006; Kolodziej et al., 2004).

Por último, cabría resaltar la contaminación procedente de los sistemas de tratamiento in situ como las fosas sépticas, especialmente en aquellas zonas donde el nivel del agua subterránea sea elevado. El uso de esta técnica está muy extendido, por lo que su seguimiento plantea ciertas dificultades. En la bibliografía, se ha relacionado la presencia de fármacos y cosméticos en aguas subterráneas con fugas de fosas sépticas (Carrara et al., 2008; Pal et al., 2010; Swartz et al., 2006).

1.2.2.2 Fuentes difusas

A diferencia de las puntuales, la identificación de las fuentes difusas es más compleja, pudiéndose extender por amplias zonas geográficas, dificultando la definición real de las fuentes exactas y vertiendo generalmente cargas más ligeras de contaminantes al medio ambiente. Dentro de esta categoría, se incluirían las aguas de escorrentía pluvial procedentes de carreteras, autopistas, zonas urbanas y terrenos agrícolas (Lapworth et al., 2012).

La principal fuente de contaminación difusa estaría constituida por el uso de pesticidas en la agricultura, llegándose a detectar este tipo de compuestos en aguas superficiales y subterráneas (Heberer et al., 2004). Además, la reutilización de lodos de EDAR como fertilizante en terrenos agrícolas puede suponer que los contaminantes emergentes adsorbidos durante la etapa de tratamiento biológico se reintroduzcan en el medio ambiente y alcancen las aguas subterráneas (Clarke & Smith, 2011; Topp et al., 2008).

1.2.3 Impacto ambiental

En las últimas décadas, el desarrollo de las técnicas analíticas para la medición y evaluación de los contaminantes emergentes ha permitido demostrar la presencia de una gran variedad de estos compuestos tanto en aguas superficiales como subterráneas. Además, la eliminación de estos compuestos en las EDAR convencionales no resulta lo suficientemente efectiva, por lo que siguen llegando al medio acuático de forma continuada (Houtman, 2010; Kümmerer, 2009b).

Los contaminantes emergentes pueden presentar efectos crónicos sobre los seres vivos, como los que muestran a corto plazo ciertos fármacos sobre los artrópodos, aunque las concentraciones evaluadas normalmente son considerablemente mayores a las encontradas en el medio ambiente (Boxall, 2012a; Taheran et al., 2018). Sin embargo, cada vez se utilizan concentraciones más próximas a los niveles ambientales, siendo también un factor crítico las especies consideradas y su correspondiente sensibilidad a los diferentes tipos de contaminantes (Boxall, 2012b; L. Li et al., 2022; Pablos et al., 2015). Además, aunque en la última década se ha incrementado el número de investigaciones relacionadas, la falta de datos sobre los contaminantes emergentes ha conducido a la realización de evaluaciones de riesgos y estudios sobre efectos ecotoxicológicos poco precisos (Noguera-Oviedo & Aga, 2016). En el caso particular de los medicamentos, por ejemplo, la Unión Europea ha publicado directrices para la evaluación del riesgo medioambiental de los medicamentos, siendo obligatoria para los fabricantes e incluyendo estudios relacionados con el destino del medicamento y los efectos potenciales en el medio acuático (Wess, 2021).

En la bibliografía se han reportado algunas bases de datos ecotoxicológicos de ciertos contaminantes emergentes, considerándose aspectos como la información fisicoquímica de los mismos o el alcance y destino del transporte ambiental (Cooper et al., 2008; Molander et al., 2009). A pesar de ello, tan solo un número reducido de los compuestos más recientes se han sometido a una evaluación de riesgos mediante pruebas toxicológicas, entre los que cabría resaltar los fármacos, cuyos datos ecotoxicológicos publicados en la literatura y en las bases de datos de acceso abierto están disponibles para menos del 1% (Tambosi et al., 2010). En este sentido, se ha demostrado que los medicamentos que actúan sobre el sistema nervioso central, cardiovasculares y antiinfecciosos suponen un mayor riesgo para el medio

ambiente, siendo estos últimos los más tóxicos (Cooper et al., 2008; Molander et al., 2009). Además, la información sobre el impacto a largo plazo de este tipo de compuestos, especialmente en el caso de exposiciones prolongadas a bajas concentraciones, es escasa (Y. Li et al., 2014).

Algunos contaminantes emergentes pueden tener efectos biológicos sobre los ecosistemas acuáticos. En este sentido, se ha descubierto que los antineoplásicos, fármacos cardiovasculares, antibióticos y hormonas sexuales afectan a las algas y a las daphnias, mientras que los dos últimos presentan una mayor peligrosidad para la salud humana y la vida acuática (Sanderson et al., 2004).

Además, los organismos acuáticos parecen ser más sensibles que los humanos a este tipo de compuestos, interfiriendo en el funcionamiento de su sistema endocrino y conduciendo a una disfunción reproductiva y a una disminución de la población (Falconer et al., 2006). Los peces constituyen uno de los grupos más estudiados en lo relativo a efectos de sustancias con actividad estrogénica en el desarrollo de anomalías en el aparato reproductor, iniciándose ya en la década de 1980. Algunos autores también han informado de que, dependiendo de la dosis y el tiempo de exposición, la presencia de disruptores endocrinos puede estar relacionados con enfermedades como el cáncer de mama, testicular y de próstata, los ovarios poliquísticos y la reducción de la fertilidad masculina (Tambosi et al., 2010). Entre los principales disruptores endocrinos se encontrarían algunos productos farmacéuticos y de cuidado personal, productos de limpieza domésticos e industriales, retardantes de llama y pesticidas (Mnif et al., 2011; Monneret, 2017).

Entre la gran variedad de contaminantes emergentes, la detección de antibióticos en el medio acuático ha atraído una gran atención en los últimos años. Según los expertos, estos compuestos favorecen el desarrollo de poblaciones bacterianas resistentes. (Moles et al., 2020; Tambosi et al., 2010). Es frecuente la presencia de bacterias resistentes a antibióticos en aguas residuales, incluso en concentraciones superiores a las de las aguas superficiales, lo que indicaría que las EDAR contribuyen a su diseminación (Bouki et al., 2013). Además, las bacterias resistentes a los antimicrobianos de origen animal también pueden transmitirse a los humanos. Es decir, los organismos bacterianos de distinto origen, humano y animal, pueden mezclarse y desarrollar resistencia mediante el intercambio de genes (Baquero et

al., 2008). Este hecho, supone una potencial amenaza para la salud humana y animal, pudiendo crear problemas en el control de infecciones. Se han asociado infecciones, enfermedades e incluso muertes a bacterias resistentes (Bouki et al., 2013). En 2011, por ejemplo, se produjo un brote en Alemania del síndrome urémico hemolítico causado por la Escherichia coli enterohemorrágica multirresistente (Rubino et al., 2011).

La presencia de contaminantes emergentes en el agua potable parece ser una cuestión crucial para el medio ambiente y la salud humana. Además, aunque se encuentran en concentraciones relativamente bajas, los efectos asociados a una exposición continuada para la mayoría de estos compuestos aún se desconocen. Por esta razón, los controles periódicos, especialmente en regiones donde las condiciones locales pueden implicar posibles concentraciones más elevadas en las aguas locales, parece un buen punto de partida desde el que realizar un seguimiento más exhaustivo. La presencia combinada de diversos contaminantes emergentes podría presentar efectos diferentes a los mostrados para los compuestos aislados, por lo que el estudio de las posibles interacciones y efectos de mezclas multicomponentes también supondría un gran avance en este campo (Hernando et al., 2011).

1.2.4 Marco regulatorio: Listas de observación

La preocupación por la contaminación del agua está conduciendo a la elaboración de nuevos marcos regulatorios que permitan abordar este desafío y proteger la calidad de los recursos hídricos.

En España, la primera normativa en materia de aguas fue la Ley de Aguas de 1879, que establecía que todas las corrientes naturales, cauces y riberas de ríos eran de dominio público. Sin embargo, presentaba grandes carencias, como la especificación del dominio de las aguas subterráneas por parte de los dueños del terreno. Este aspecto no se modificó hasta su derogación por la aprobación de la Ley de Aguas 29/1985, que no solo exponía la íntima relación entre las aguas superficiales y subterráneas, sino que planteaba aspectos como la regulación del dominio público hidráulico, del uso del agua y del ejercicio de las competencias atribuidas al Estado.

En 1986, España se incorporó a la Unión Europea, desencadenando el desarrollo de un gran número de normativas ambientales encaminadas a la protección de los recursos hídricos existentes. En este contexto, surge la Directiva 91/271/CE, sobre el tratamiento de aguas residuales urbanas, que se incorporó al ordenamiento jurídico español a través del Real Decreto-ley 11/1995, y se completó con el Real Decreto 509/1996. Posteriormente, se modificó parte del cuerpo de esta normativa europea mediante la Directiva 98/15/CE, y se transpuso con la aprobación del Real Decreto 2116/1998, que especificaba algunas variaciones del Real Decreto 509/1996. Estos avances en la política de aguas permitieron definir conceptos tan relevantes como el de las aguas residuales urbanas e industriales, así como los sistemas de recogida, tratamiento y vertido de las aguas residuales urbanas.

La calidad de las aguas de consumo humano es otro de los enfoques clave que se ha ido abordando. En este sentido, a principios de 2023 ha entrado en vigor la Directiva 2020/2184, que derogaba a la anterior Directiva 98/83/CE con efectos de 13 de enero de 2023. La transposión de esta normativa implicó la aprobación de los Reales Decretos 3/2023 y 2/2023, que derogaban el Real Decreto 140/2003 y modificaban los Reales Decretos 1798/2010 y 1799/2010, estos tres últimos provenientes de la Directiva anterior. De esta forma se configura un marco jurídico para proteger la salud humana de los efectos adversos de cualquier contaminación del agua de consumo, garantizando su salubridad y limpieza mediante la evaluación de parámetros microbiológicos, químicos e indicadores de calidad, entre otros.

Desde una perspectiva legal, la Directiva 2000/60/CE, comúnmente conocida como Directiva Marco del Agua, constituye la piedra angular para la protección de las aguas superficiales continentales, las aguas costeras, las aguas de transición, y las aguas subterráneas. En este sentido, estableció un marco global y estratégico cuyos objetivos eran prevenir el deterioro y mejorar el estado de los ecosistemas acuáticos, fomentar un uso sostenible del agua, prevenir y reducir la contaminación y paliar los efectos de las sequías y las inundaciones. Poco tiempo después, y previo a la incorporación de la Directiva Marco del Agua a la legislación española, se dictó el Real Decreto Legislativo 1/2001, que refundía la legislación vigente en materia de aguas y derogaba a la anterior Ley 29/1985. Una vez aprobado el texto refundido, se transpuso la Directiva 2000/60/CE, dando lugar a la Ley 62/2003, que, en su artículo 129, modificaba el Real Decreto Legislativo 1/2001

para armonizarlo dentro del marco comunitario de actuación en el ámbito de la política de aguas.

La Directiva Marco del Agua propició el desarrollo de otras normativas estrechamente relacionadas y que la complementaban, entre las que destacan:

- Decisión 2455/2001/CE, por la que se aprueba la lista de 33 sustancias prioritarias en el ámbito de la política de aguas, incluidas las sustancias identificadas como sustancias peligrosas prioritarias, que se contempla en los apartados 2 y 3 del artículo 16 de la Directiva 2000/60/CE.
- La Directiva 2006/118/CE, relativa a la protección de las aguas subterráneas contra la contaminación y el deterioro, y cuyo objetivo es prevenir y luchar contra la contaminación de las aguas subterráneas de la Unión Europea, incluyendo tanto medidas de evaluación del estado químico de las aguas como medidas para reducir la presencia de contaminantes. De esta forma, atiende a la exigencia de la Directiva 2000/60/CE, que anunciaba la adopción de medidas para prevenir y controlar la contaminación de las aguas subterráneas. Esta normativa se transpuso a través del Real Decreto 1514/2009.
- La Directiva 2008/105/CE, relativa a las normas de calidad ambiental en el ámbito de la política de aguas, que planteaba entre sus objetivos el establecimiento de normas de calidad ambiental para las 33 sustancias prioritarias identificadas en la Decisión 2455/2001/CE y otros 8 contaminantes que ya estaban regulados en la Unión, según lo dispuesto en el artículo 16 de la Directiva 2000/60/CE, y que se incorporó a la legislación española mediante el actualmente derogado Real Decreto 60/2011.
- La Directiva 2013/39/UE, que modifica las Directivas 2000/60/CE y 2008/105/CE en cuanto a las sustancias prioritarias en el ámbito de la política de aguas, ampliando la lista de contaminantes prioritarios de 33 a 45 compuestos. Además, se introduce, por primera vez, en su artículo 8, el concepto de "lista de observación", que ha de recoger temporalmente un número limitado de contaminantes emergentes, es decir, sustancias cuya información disponible indique que pueden suponer un riesgo significativo para el medio acuático pero

cuyos datos de seguimiento son insuficientes para la evaluación del riesgo. De esta forma, las listas de observación se actualizan cada 2 años, aunque se dispone de un periodo de seguimiento de hasta 4 años para proporcionar datos representativos que permitan realizar el proceso de asignación de prioridad de la Unión y, si fuera el caso, incluirlas en las listas de sustancias prioritarias. Esta normativa se introduce en el sistema jurídico español a través del Real Decreto 817/2015, derogando el Real Decreto 60/2011. Esta regulación incluye en su anexo V una lista propia de 16 compuestos, denominados sustancias preferentes, que presentan un riesgo significativo para las aguas superficiales españolas debido a su especial presencia, toxicidad, persistencia y bioacumulación.

- La Decisión de Ejecución (UE) 2015/495, que incluye la primera lista de observación, con 17 contaminantes emergentes recogidos en 10 grupos de sustancias.
- La Decisión de Ejecución (UE) 2018/840, que deroga la primera lista de observación y configura la segunda, con 15 contaminantes emergentes recogidos en 8 grupos de sustancias.
- La Decisión de Ejecución (UE) 2020/1161, que deroga la segunda lista de observación y constituye la tercera, con 19 contaminantes emergentes recogidos en 9 grupos de sustancias.
- La Decisión de Ejecución (UE) 2022/1307, que deroga la tercera lista de observación y configura la cuarta, con 26 contaminantes emergentes recogidos en 12 grupos de sustancias.

El marco legislativo descrito hasta el momento, cuyo resumen se ilustra en la Figura 3, no hace más ahondar en la necesidad de avances tecnológicos que permitan el tratamiento de aquellas sustancias con un impacto medioambiental considerable. Este proyecto pretende investigar algunos de los contaminantes emergentes recogidos en las listas de observación europeas, que son candidatos potenciales para ser incluidos en las listas prioritarias. De esta forma, se dispondría de un conocimiento tecnológico previo al posible establecimiento de normas de calidad ambiental que limiten su vertido en un futuro próximo.

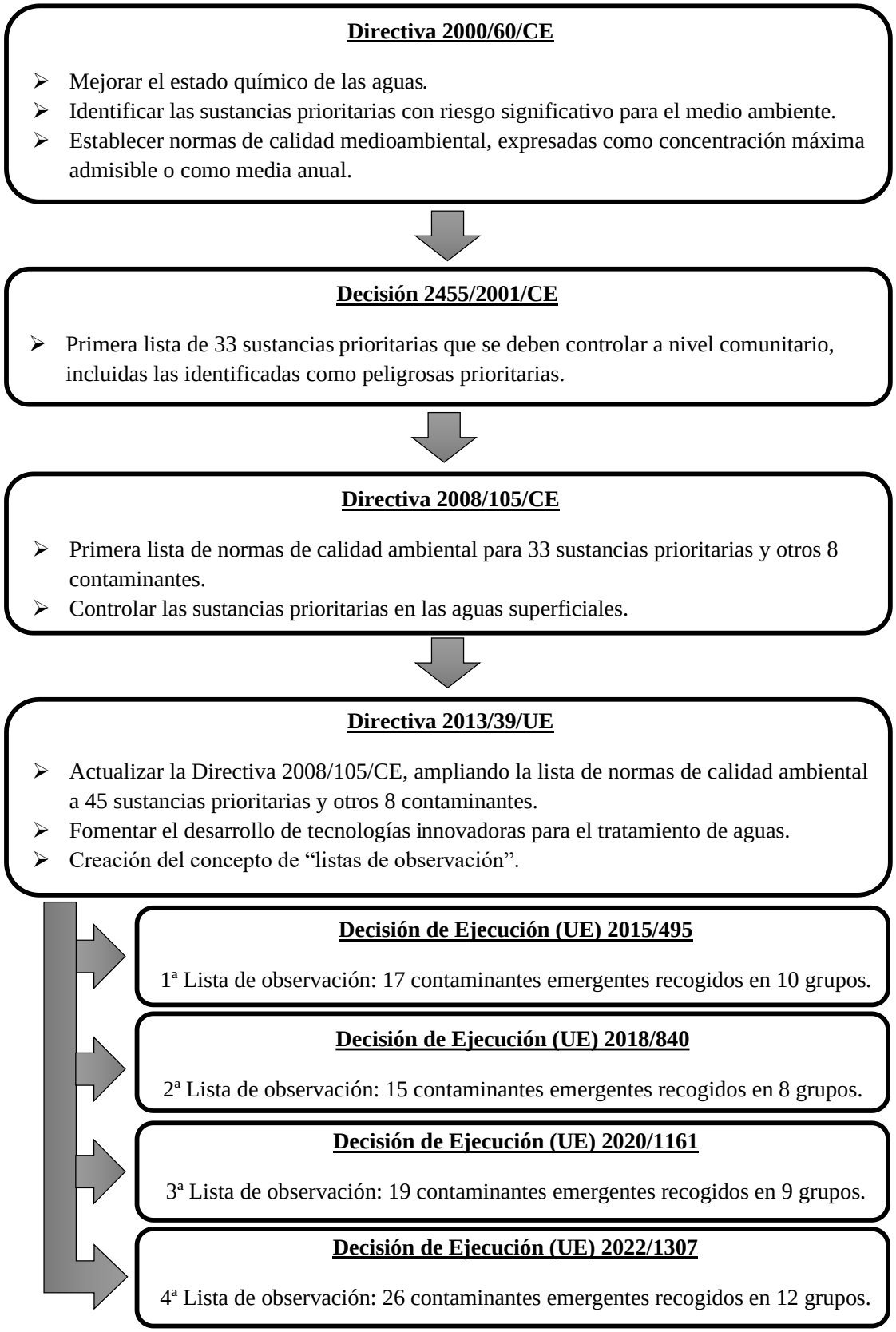

Figura 3. Evolución de la legislación europea más relevantes en materia de protección de calidad de aguas contra las sustancias prioritarias y emergentes.

1.3 Eliminación de contaminantes emergentes en disolución acuosa

Los métodos convencionales para el tratamiento de aguas, entre los que se encuentran procesos como la sedimentación, la coagulación-floculación, la filtración con arena o los tratamientos biológicos, generalmente no son adecuados para la eliminación de gran parte de los contaminantes emergentes. Por esta razón, el rendimiento de eliminación de estos compuestos recalcitrantes no alcanza valores significativos en las estaciones depuradoras de aguas residuales (Ahmed et al., 2017; Petrović et al., 2003; Plakas & Karabelas, 2012; Saleh et al., 2020; Vagı & Petsas, 2017).

La problemática asociada al agua hará que el desarrollo de alternativas que permitan un tratamiento eficaz para la eliminación de los contaminantes emergentes sea un aspecto clave en los próximos años. En este sentido, tecnologías como la extracción líquido-líquido, la adsorción y los procesos de oxidación química se posicionan como candidatos potenciales en este campo (A. Quiroz et al., 2011; Karungamye, 2020; Kaur et al., 2019; Kumar et al., 2022; Narenderan et al., 2019; Narenderan & Meyyanathan, 2019; Rodriguez-Narvaez et al., 2017; Saleh et al., 2020; Samsidar et al., 2018; Timofeeva et al., 2017; Vagı & Petsas, 2017).

1.3.1 Extracción líquido-líquido

La extracción líquido-líquido permite la separación de uno o varios solutos presentes en una mezcla, denominada alimento, por contacto con una segunda fase líquida, el disolvente, que ha de presentar una inmiscibilidad total o parcial con la primera. De esta forma, se produce una transferencia de materia desde el disolvente portador al disolvente de extracción, generándose una fase rica en el disolvente de extracción (extracto) y otra en la que predominará el disolvente portador (refinado). Resulta evidente, por tanto, que esta operación precisa de una primera etapa de mezclado del alimento con el disolvente, durante un cierto periodo de tiempo para alcanzar el equilibrio, seguido de una segunda etapa de separación de fases. Ambos pasos se encuentran íntimamente relacionados ya que, por ejemplo, una agitación vigorosa favorece la transferencia del soluto de una fase a otra,

disminuyendo el tiempo para alcanzar el equilibrio termodinámico, pero puede dificultar la separación de fases debido a la formación de emulsiones, lo que requeriría el empleo de centrifugación (Berk, 2018; Dahuron et al., 2008).

Los procesos de extracción comerciales generalmente incluyen otras operaciones unitarias auxiliares, a fin de aislar el producto deseado, recuperar el disolvente del extracto para su reutilización o purgar los compuestos no deseados del proceso. Otros aspectos relevantes implicados en la implantación del proceso de extracción a escala industrial son la elección del tipo de equipo empleado para el contacto líquido-líquido y la separación de fases, la temperatura de operación o la eliminación de los residuos del disolvente de extracción en el refinado (Dahuron et al., 2008).

La viabilidad del proceso de extracción depende principalmente de la correcta elección del disolvente, que depende de multitud de factores: elevados coeficientes de reparto, capacidad de carga, estabilidad química y selectividad hacia el soluto deseado; viscosidad y solubilidad mutua entre el disolvente de extracción y portador pequeñas; seguridad y requerimientos medioambientales favorables; bajo punto de congelación para evitar la necesidad de calentamiento; disponibilidad y coste adecuados; capacidad para regenerar el disolvente de forma sencilla y económica; etc (Dahuron et al., 2008). En muchas ocasiones, se ha de llegar a una situación de compromiso entre todos ellos, dándose más peso a unos u otros en función del contexto social, económico y político del momento.

El endurecimiento de la política medioambiental en los últimos años ha propiciado la búsqueda de disolventes alternativos a los tradicionales que supongan un menor impacto en el ecosistema, cobrando cada vez más interés los terpenos, terpenoides y sus mezclas eutécticas.

Incluidos dentro de los metabolitos secundarios, los terpenos y terpenoides constituyen el grupo de compuestos de origen vegetal más numeroso y variado, conociéndose más de 80.000 sustancias hasta la fecha (Zhou & Pichersky, 2020). Inicialmente, el término terpeno hacía referencia a hidrocarburos simples derivados de la unidad básica de isopreno (2-metil-1,3-butadieno), mientras que los terpenoides englobaban aquellas moléculas orgánicas que presentaban un esqueleto de isopreno recurrente, pero contenían diferentes

grupos funcionales. Sin embargo, en la actualidad ambos términos se emplean, con carácter general, indistintamente (Boncan et al., 2020; Croteau et al., 2000; Eggersdorfer, 2000; LaLonde, 2005; Perveen, 2018; Rodríguez-Llorente et al., 2020; Yadav et al., 2014). Esta es la razón por la que a lo largo de este documento ambos términos se considerarán sinónimos.

Los terpenos se clasifican en función del número de unidades de isopreno (C_5H_8) que, como se muestra en la Tabla 5, configura su esqueleto hidrocarbonado. Dentro de cada grupo, se distinguen estructuras monocíclicas, policíclicas y acíclicas, siendo los sesquiterpenoides los que mayor variedad estructural presentan (LaLonde, 2005).

Tabla 5. Clasificación de los terpenos.

Tipo	Nº de átomos de carbono	Nº de unidades del isopreno
Hemiterpenoides	5	1
Monoterpenoides	10	2
Sesquiterpenoides	15	3
Diterpenoides	20	4
Sesterterpenoides	25	5
Triterpenoides	30	6
Tetraterpenoides	40	8
Politerpenoides	> 40	> 8

Según la denominada regla del isopreno, los terpenos se construyen mediante uniones cabeza-cola de unidades de isopreno, también llamadas acoplamientos regulares, aunque se han encontrado otros tipos de uniones en la naturaleza, como los acoplamientos irregulares cabeza-cabeza, cabeza-cola o cabeza-mitad. En la Figura 4, se representan los diez patrones de acoplamiento de unidades de isopreno más comunes en estos productos naturales (Carsanba et al., 2021; Christianson, 2017; Croteau et al., 2000; Kobayashi & Kuzuyama, 2019; Zhang et al., 2017).

Los terpenos presentan una gran variedad de aplicaciones, entre las que destacan aquellas relacionadas con la industria farmacéutica, cosmética y alimentaria (Ben Salha et al., 2019; Perveen, 2018; Zwenger & Basu, 2008). Actualmente se están investigando como posibles sustitutos de los disolventes derivados del petróleo, pues se trata de compuestos

renovables que presentan una menor peligrosidad e impacto ambiental. Además, debido a su naturaleza hidrofóbica, los terpenos se han empleado recientemente en la extracción de compuestos orgánicos de soluciones acuosas (Boutekedjiret et al., 2014; Rodríguez-Llorente et al., 2020).

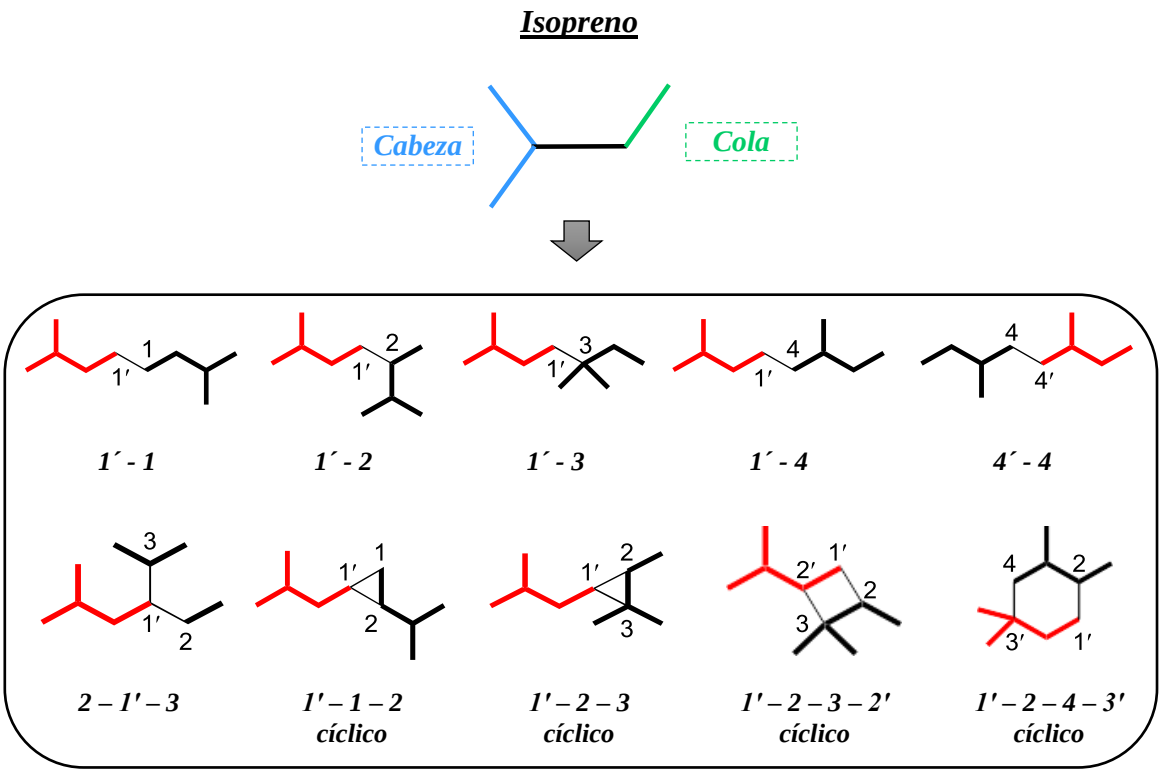

Figura 4. Patrones de acoplamiento de unidades de isopreno en la formación de terpenos (Kobayashi & Kuzuyama, 2019).

También han cobrado cada vez más relevancia los denominados "disolventes eutécticos", sistemas formados por dos o más compuestos que presentan un valor mínimo en su temperatura de fusión en comparación con cualquiera de los constituyentes puros de partida (Zainal-Abidin et al., 2017). En este sentido, la formulación de disolventes eutécticos a partir de terpenos amplía el número de disolventes naturales disponibles para su aplicación a temperatura ambiente, manteniendo las ventajas que caracterizan a los compuestos puros, como son su biodegradabilidad y baja toxicidad (Rodríguez-Llorente et al., 2020). El gran potencial que presentan los terpenos y sus mezclas eutécticas como agentes de extracción los ha posicionado en el punto de mira de numerosas investigaciones.

1.3.2 Adsorción

La adsorción es un fenómeno de superficie que describe la transferencia de materia de uno o más compuestos desde el seno de un fluido, líquido o gas, hasta la superficie de una fase líquida o sólida. De esta forma, el adsorbato es el compuesto que se transfiere de una fase a otra y el adsorbente el que proporciona la superficie sobre la que se quedará adsorbido. Al tratarse de un proceso superficial, el adsorbato no se difunde en la estructura del adsorbente, lo que lo diferencia de los procesos de absorción. El proceso de transferencia de materia inverso se denomina desorción (Artioli, 2008).

Entre los diversos tipos de adsorción, uno de los más comunes y relevantes es aquel en el que interviene una fase sólida como adsorbente. En estos casos, y al tratarse de un fenómeno superficial, la porosidad del material posee una influencia considerable en el proceso. Las interacciones entre la superficie sólida y las sustancias adsorbidas pueden ser de naturaleza física (fisisorción), química (quimisorción) o una combinación de ambas. Es decir, mientras que la primera describe todas las interacciones electrostáticas débiles, incluidas las interacciones de Van Der Waals, dipolo-dipolo y fuerzas de London, la quimisorción se produce cuando el adsorbato forma un enlace químico (normalmente covalente) con el sólido, compartiendo o transfiriendo electrones. Las interacciones de naturaleza química suelen ser dos órdenes de magnitud más fuertes que las de las especies fisisorbidas (Alaqarbeh, 2021; Artioli, 2008; Sims et al., 2019).

La transferencia de materia en los procesos de adsorción tiene lugar en tres etapas. En primer lugar, se transporta el adsorbato desde el seno de la fase fluida hasta la superficie externa del sólido a través de la capa límite (difusión externa). A continuación, ocurre la transferencia del adsorbato desde la superficie hasta los centros activos de adsorción que se encuentran en el interior de los poros (difusión interna o intrapartícula), donde finalmente el soluto se adhiere al centro activo mediante interacciones físicas o químicas (adsorción). Desde el punto de vista cinético, las etapas controlantes suelen ser la difusión externa o interna, ya que la adsorción es prácticamente instantánea. No obstante, se puede mejorar la cinética del proceso aumentando la agitación (que favorece la difusión externa disminuyendo el espesor de la capa límite) y reduciendo el tamaño de partícula (favorece la difusión interna). Algunos de los modelos cinéticos más empleados son el de pseudo-

primer orden, pseudo-segundo orden, Elovich, Weber-Morris o Bangham (Bonilla-Petriciolet et al., 2017; Largitte & Pasquier, 2016; J. Wang & Guo, 2020).

En los procesos de adsorción fluido-sólido, la representación del equilibrio a una determinada temperatura se realiza mediante la relación entre la cantidad adsorbida y la presión parcial, en sistemas gas-sólido, o la concentración en la fase líquida en sistemas líquido-sólido. Estas curvas se conocen como isotermas de adsorción y, en sistemas gas-sólido, son ampliamente utilizadas para la caracterización de la estructura porosa de los adsorbentes, clasificándose según la IUPAC en los 6 grupos mostrados en la Figura 5 (Thommes et al., 2015).

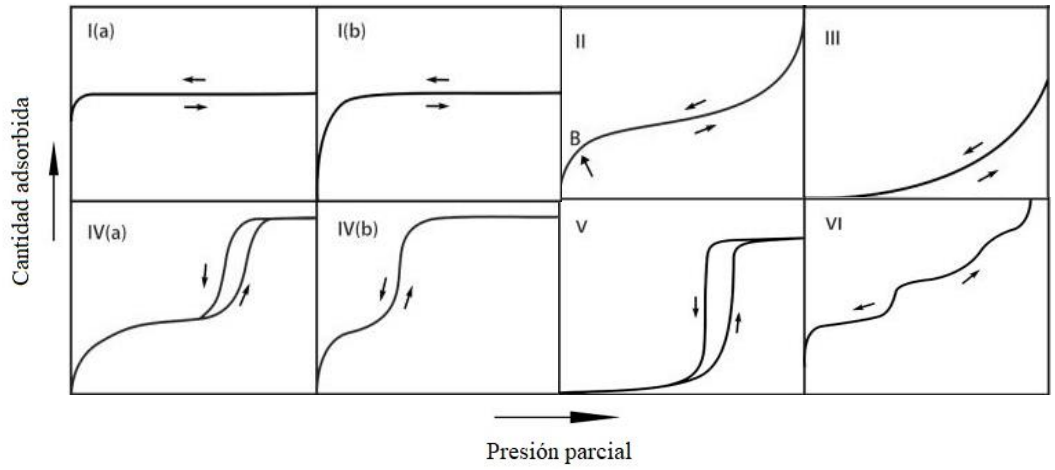

Figura 5. Clasificación de las isotermas de adsorción en fase gas recomendada por la IUPAC (Thommes et al., 2015).

Por otro lado, las isotermas de adsorción en sistemas líquido-sólido suelen clasificarse atendiendo a su forma y curvatura según lo mostrado en la Figura 6, aportando información sobre la naturaleza física del adsorbato y la superficie del adsorbente, así como sobre la superficie específica de este último. Estas curvas de equilibrio se dividen en 4 clases según su pendiente inicial, dividiéndose a su vez en otros cuatro subgrupos en función de la parte superior de la curva y los cambios en la pendiente. Cabe resaltar que este criterio se propuso atendiendo a una descripción cualitativa, carente de fundamento matemático. Sin embargo, se han desarrollado multitud de modelos matemáticos que permiten describir las isotermas de adsorción, entre los que destacan los modelos de Langmuir, Freundlich, Dubinin-Radushkevich y Brunauer-Emmet-Teller (Bonilla-Petriciolet et al., 2017).

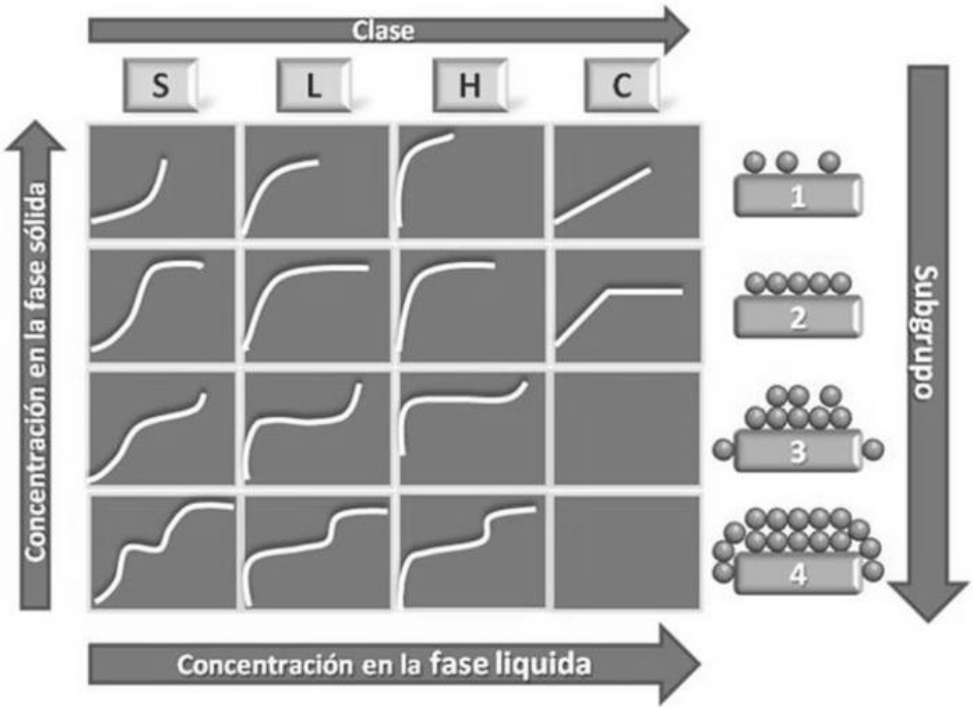

Figura 6. Clasificación de Giles para las isotermas de adsorción en fase líquida.

La capacidad y la cinética de adsorción están relacionadas, no solo con la fase sólida empleada como adsorbente, sino con la naturaleza fisicoquímica del adsorbato y las condiciones del medio líquido. Entre las principales variables asociadas a las propiedades del adsorbente destacarían: la superficie específica, el tamaño de partícula y la distribución de tamaño de poro. Dentro de la naturaleza físicoquímica del adsorbato se incluirían: el peso y tamaño molecular; la solubilidad, polaridad y grado de ionización; y sus grupos funcionales. Por último, las condiciones del medio líquido consideran aspectos como: el pH y la fuerza iónica; la temperatura; y la presencia de otros compuestos que puedan interferir en el proceso de adsorción (Ahnert et al., 2003; Cheremisinoff, 2019; Saravia & Frimmel, 2008; Suzuki & Suzuki, 1990).

El adsorbente es una pieza fundamental para la viabilidad del proceso de adsorción, siendo preciso que disponga no solo de una estructura porosa que genere una elevada área superficial, sino que el tiempo de equilibrio sea lo más corto posible. Además, los materiales deben de ser económicos, fácilmente regenerables e inocuos. Entre los principales adsorbentes convencionales destacan las resinas poliméricas, las zeolitas, las arcillas, el gel de sílice o la alúmina. Sin embargo, el material adsorbente más utilizado a

nivel mundial, y el más antiguo, es el carbón activado. Este sólido se ha aplicado con éxito en la eliminación de una gran variedad de contaminantes, orgánicos e inorgánicos, caracterizándose por sus elevadas superficies específicas. Además, la síntesis del carbón activo precisa de un precursor con un contenido en carbono elevado, por lo que abre la posibilidad al empleo de precursores biomásicos, como los lodos de depuradora, que puedan propiciar la valorización de residuos y favorecer la economía circular (Bonilla-Petriciolet et al., 2017; Gupta et al., 2009; Singh et al., 2018).

1.3.3 Procesos de oxidación

Los procesos de oxidación agrupan una serie de técnicas, entre las que destacan la oxidación húmeda (catalítica y no catalítica), la oxidación húmeda supercrítica y los procesos avanzados de oxidación. La inclusión, o no, de los procesos de oxidación húmeda dentro de los procesos de oxidación avanzada atiende a criterios arbitrarios en función de la fuente bibliográfica consultada. Es decir, si estos últimos se definen como procesos basados en la generación de radicales libres para la eliminación de contaminantes, la oxidación húmeda podría incluirse dentro de los procesos de oxidación avanzada, mientras que si se considera como requisito adicional para su inclusión la necesidad de operar en condiciones cercanas a la presión atmosférica y temperatura ambiente han de clasificarse como un grupo aparte (Benitez et al., 2011; Rodríguez et al., 2006; Serra-Pérez et al., 2019).

1.3.3.1 Procesos de oxidación húmeda catalítica y no catalítica

Los procesos de oxidación húmeda no catalítica (WAO, *Wet Air Oxidation*) y oxidación húmeda catalítica (CWAO, *Catalytic Wet Air Oxidation*) se fundamentan en el empleo de oxígeno molecular disuelto en la fase acuosa, procedente de una corriente de aire u otra enriquecida en oxígeno, como agente oxidante (Garcia et al., 2005).

Aunque la naturaleza de los compuestos orgánicos influye, las condiciones de operación de los procesos WAO generalmente oscilan en el intervalo 150-350 ºC y 20-200 bar, siendo imprescindible que la presión se encuentre por encima de la de vapor a la temperatura de operación fijada para garantizar el estado líquido de la mezcla. Sin embargo, el empleo de catalizadores, como ocurre en los procesos CWAO, permite

disminuir el tiempo de residencia del reactor y operar en condiciones más suaves de temperatura (120-250 ºC) y presión (15-50 bar), reduciendo los costes de inversión y operación. Esta moderación en las condiciones de operación dependerá de la actividad del catalizador empleado (Garcia et al., 2005; Mantzavinos et al., 1999; Rodríguez et al., 2006).

Otra de las características clave es la formación de sustancias orgánicas refractarias, normalmente compuestos oxigenados de bajo peso molecular, entre los que destacan los ácidos fórmico, acético y oxálico. En el caso de los procesos WAO, la proporción de estos productos a la salida del reactor se encuentra entre el 5 y el 10 % del carbono orgánico total del influente de partida. Sin embargo, los procesos catalizados permiten obtener grados de oxidación más elevados, pudiéndose alcanzar incluso la mineralización completa de los contaminantes. Por tanto, mientras que los procesos WAO presentan una eliminación de DQO entre el 75 y 90%, los procesos CWAO alcanzan valores de hasta un 99 % (Imamura, 1999; Kolaczkowski et al., 1999; Luck, 1996, 1999; Pariente et al., 2022).

En lo referente al mecanismo de reacción y a la cinética de los procesos de oxidación húmeda, cabe resaltar el carácter bifásico, o multifásico, de los mismos. Es decir, intervienen una fase gaseosa (que contiene el oxígeno que actúa como agente oxidante), una líquida (donde se produce la oxidación a partir de la fase activa formada a partir del oxígeno disuelto) y, en procesos CWPO con catalizadores heterogéneos, una sólida (Levenspiel, 1998). Este hecho hace que las cinéticas de difusión posean una influencia considerable, actuando como resistencias, representadas en la Figura 7, y disminuyendo la velocidad del proceso.

De forma general, las etapas en este tipo de sistemas, que presentan 1 (WAO y CWAO con catalizadores homogéneos) o 2 (CWAO con catalizadores heterogéneos) interfases, incluyen:

(i) Transferencia de materia del oxígeno en la fase gas a la interfase gas/líquido.

(ii) Transferencia de materia del oxígeno molecular en la interfase gas/líquido al seno del fluido.

(iii) Transferencia de materia de las especies disueltas a la superficie del catalizador.

(iv) Difusión intrapartícula de las especies reactivas a los centros activos.

(v) Adsorción de especies en los sitios activos y reacción en la superficie del catalizador.

(vi) Desorción y difusión a la fase líquida.

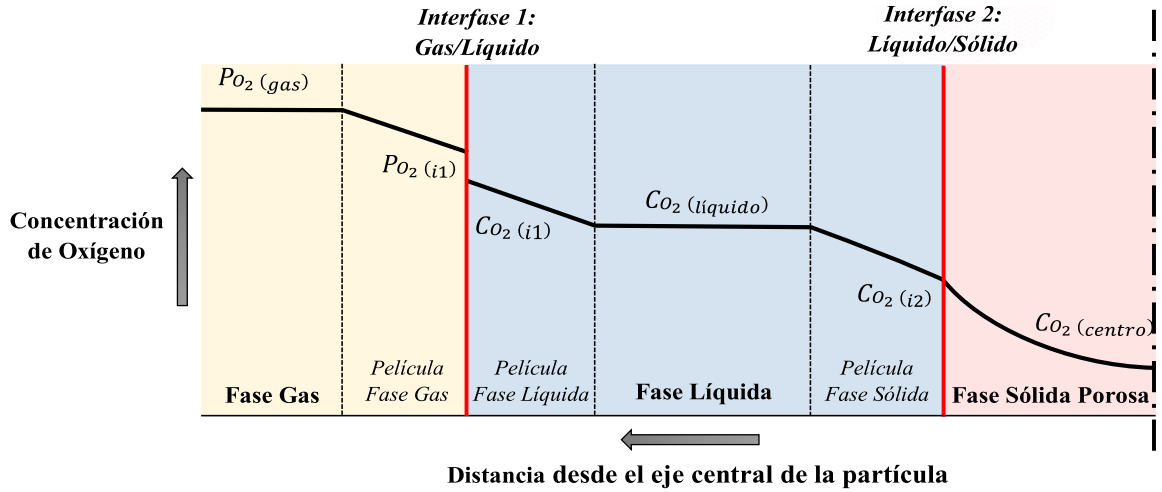

Figura 7. Resistencias desde un reactivo en fase gas hasta el catalizador sólido.

En el caso de los gases poco solubles, como el oxígeno, la resistencia a la transferencia de materia en la película de la fase gas es despreciable en comparación con la de la película de la capa líquida, por lo que la etapa controlante en la interfase gas/líquido sería esta última (Bhargava et al., 2006).

Los procesos de oxidación húmeda no catalíticos normalmente ocurren por vía radicalaria, cuyas reacciones se agrupan en las siguientes etapas (Bhargava et al., 2006):

1º. <u>Iniciación:</u>

$$RH \rightarrow R\bullet + H\bullet \quad [1]$$

$$O_2 \rightarrow O\bullet + O\bullet \quad [2]$$

$$H_2O \rightarrow OH\bullet \rightarrow H\bullet \quad [3]$$

$$RH + O_2 \rightarrow R\bullet + HO_2\bullet \quad [4]$$

$$H_2O + O_2 \rightarrow H_2O_2 + O_2\bullet \quad [5]$$

$$H_2O + O_2 \rightarrow HO_2\bullet + HO\bullet \quad [6]$$

$$RH + O_2 + RH \rightarrow 2R\bullet + H_2O_2 \quad [7]$$

2º. Propagación:

$$R\bullet + O_2 \rightarrow ROO\bullet \quad [8]$$

$$ROO\bullet + RH \rightarrow ROOH + R\bullet \quad [9]$$

$$O\bullet + H_2O \rightarrow HO\bullet + HO\bullet \quad [10]$$

$$RH + HO_2\bullet \rightarrow R\bullet + H_2O_2 \quad [11]$$

$$H\bullet + H_2O \rightarrow HO\bullet + H_2 \quad [12]$$

$$ROOH \rightarrow RO\bullet + HO\bullet \quad [13]$$

$$RH + HO\bullet \rightarrow R\bullet + H_2O \quad [14]$$

3º. Terminación:

$$2ROO\bullet \rightarrow ROOR + O_2 \quad [15]$$

$$2HO_2\bullet \rightarrow H_2O_2 + O_2 \quad [16]$$

$$HO_2\bullet + OH\bullet \rightarrow H_2O + O_2 \quad [17]$$

Sin embargo, los mecanismos de reacción para los procesos CWAO dependen del catalizador empleado, siendo los más comunes:

- Mecanismo radicalario: la etapa de iniciación ocurre sobre la superficie del catalizador, la propagación en la fase líquida y la terminación lo hace en la fase líquida o en la fase sólida en función de la dosis de catalizador empleada. En este último caso, se produce por un mecanismo de radicales libres heterogéneo-homogéneo (Bhargava et al., 2006; Kolaczkowski et al., 1999; Levec & Pintar, 2007; Makatsa et al., 2021; Pintar & Levec, 1992; Sadana & Katzer, 1974).

- Mecanismo de coordinación: implica la oxidación de un sustrato coordinado por un ion metálico. La forma oxidada del metal se regenera posteriormente por reacción de la forma reducida con el oxígeno (Bhargava et al., 2006; Vaschetto et al., 2019).

- Mecanismo redox o de Mars-Van Krevelen: el sustrato es oxidado a través del oxígeno de la red de la capa superficial del catalizador, y la forma reducida resultante es posteriormente reoxidada por el oxígeno, regenerando el catalizador (Bhargava et al., 2006; Chorkendorff & Niemantsverdriet, 2017; Q. Jing & Li,

2019; Ou, Daly, Chansai, et al., 2022; Ou, Daly, Fan, et al., 2022; L. Wang et al., 2023).

- Modelos de adsorción: suponen que la reacción tiene lugar entre varias especies adsorbidas sobre la superficie del catalizador (modelo de Langmuir-Hinshelwood Hougen-Watson) o sobre una especie adsorbida que reacciona con otra especie adsorbida (modelo de Eley-Rideal). El mecanismo Eley-Rideal es menos común en sistemas multifásicos (Bhargava et al., 2006; Chorkendorff & Niemantsverdriet, 2017; Makatsa et al., 2021; Ou, Daly, Fan, et al., 2022).

Entre los aspectos fundamentales para los catalizadores heterogéneos, destacan su preparación y caracterización, la estabilidad y desactivación, y la reutilización y regeneración, mientras que para los catalizadores homogéneos influyen factores como el estado de oxidación del ion metálico, el tipo de contraanión, su solubilidad y posterior separación y recuperación. La etapa de separación final en los sistemas homogéneos suele encarecer los costes de inversión y operación, especialmente si el compuesto a recuperar es tóxico. Los primeros estudios de CWAO se realizaron empleando catalizadores heterogéneos, normalmente procedentes de sales solubles de metales de transición, entre los que destacan el cobre, hierro, níquel, cobalto y manganeso (Bhargava et al., 2006; G. Jing et al., 2016; Kolaczkowski et al., 1999).

Los catalizadores heterogéneos pueden dividirse en dos categorías: los basados en metales nobles y los que emplean otros tipos de metales como fase activa, aunque en los últimos años también se ha descrito el empleo de carbones activos sin ninguna fase activa. Con respecto al primero de los grupos, destaca principalmente el empleo de metales como el cobre, manganeso, cobalto, níquel y bismuto, entre otros. Su principal ventaja frente a los metales nobles es su bajo coste, aunque la actividad catalítica es menor y la lixiviación del metal supone que la estabilidad del catalizador se vea comprometida. Por tanto, el principal reto de estos catalizadores está relacionado principalmente con la síntesis de materiales que mejoren la integración de la fase activa en la matriz sólida, disminuyendo la lixiviación y favoreciendo su estabilidad. Por otro lado, entre los metales nobles empleados en los catalizadores para procesos CWAO se incluyen el rutenio, rodio, platino, iridio, oro y plata, entre otros. Algunos de los soportes más empleados en los procesos

heterogéneos son la alúmina (Al_2O_3), ceria (CeO_2), titania (TiO_2) y zirconia (ZrO_2), así como carbón activo o grafitos de alta superficie específica (G. Jing et al., 2016; Rodríguez et al., 2008). El desarrollo de catalizadores soportados en carbón activo procedente de lodos de depuradora permite la valorización de estos residuos y promueve la economía circular (Bonilla-Petriciolet et al., 2017; Gupta et al., 2009; Singh et al., 2018).

1.3.3.2 Procesos de oxidación avanzada

Los Procesos de Oxidación Avanzada (AOPs, *Advanced Oxidation Processes*) suelen aplicarse en condiciones de operación de presión y temperatura cercanas a las ambientales. Estos procesos se basan en la oxidación de los contaminantes mediante la generación de radicales hidroxilo, que no solo presentan elevados potenciales de oxidación (2,8 V), sino que además su baja selectividad les confiere una gran versatilidad en cuando a la diversidad de contaminantes que degradan. La inestabilidad de los radicales hidroxilo, debido a su elevada reactividad, precisa de una generación in situ de manera continuada para este tipo de procesos. En este sentido, atendiendo al empleo, o no, de radiación ultravioleta para la producción de radicales, los AOPs pueden clasificarse según se muestra en la Tabla 6 (Mahamuni & Adewuyi, 2010; Oller et al., 2011; Oturan & Aaron, 2014; Rodriguez-Narvaez et al., 2017).

Tabla 6. Clasificación de los Procesos de Oxidación Avanzada.

Fotoquímicos	No fotoquímicos
Fotólisis con radiación UV (UV)	Ozonización en medio alcalino (O_3/OH^-)
Peróxido de hidrógeno y radiación ultravioleta (H_2O_2/UV)	Ozonización con peróxido de hidrógeno (O_3/H_2O_2)
Ozono y radiación ultravioleta (O_3/UV)	Ozonización catalítica (O_3/Catalizador)
Ozono, peróxido de hidrógeno y radiaciónultravioleta (O_3/H_2O_2/UV)	Procesos Fenton y relacionados (Fe^{2+}-Fe^{3+} /H_2O_2 ó H_2O_2/catalizador sólido)
Foto-Fenton y relacionados (Fe^{2+}/H_2O_2/UV ó catalizador/H_2O_2/UV)	Oxidación electroquímica/electrocatalítica Electro-Fenton
Fotocatálisis heterogénea (catalizador/O_2/UV)	Tratamientos con ultrasonidos (O_3/US ó H_2O_2/US) Sono-Fenton (Fe^{2+}-Fe^{3+}/H_2O_2/US)

El coste de los reactivos empleados, como de O_3, H_2O_2 y radiación UV, hace que estos procesos se empleen principalmente en efluentes con niveles de DQO relativamente bajos, menores de 1 g/L (Mahamuni & Adewuyi, 2010; Oller et al., 2011; Oturan & Aaron, 2014; Rodriguez-Narvaez et al., 2017).

Entre todas las técnicas agrupadas en los AOPs, los procesos Fenton homogéneos y heterogéneos constituyen uno de los más antiguos y efectivos. Esta técnica se basa en la adición de sales de hierro (Fenton homogéneo), o de catalizadores sólidos que contienen este metal como fase activa (Fenton heterogéneo, también denominada oxidación húmeda promovida por peróxido de hidrógeno, *Catalytic Wet Peroxide Oxidation* o CWPO), para iniciar la descomposición catalítica del peróxido de hidrógeno en radicales hidroxilo, a través de un esquema de reacciones radicalarias que puede resumirse según las siguientes ecuaciones (Bracamontes-Ruelas et al., 2022; Pera-Titus et al., 2004; Rueda Márquez et al., 2018):

1º. Iniciación:

$$H_2O_2 + Fe^{2+} \rightarrow Fe^{3+} + OH^- + \bullet OH \quad [18]$$

$$H_2O_2 + Fe^{3+} \rightarrow Fe^{2+} + H^+ + \bullet OOH \quad [19]$$

2º. Propagación:

$$\bullet OH + H_2O_2 \rightarrow \bullet OOH + H_2O \quad [20]$$

$$\bullet OOH + H_2O_2 \rightarrow \bullet OH + H_2O + O_2 \quad [21]$$

3º. Terminación:

$$Fe^{2+} + \bullet OH \rightarrow Fe^{3+} + OH^- \quad [22]$$

$$\bullet OOH + Fe^{3+} \rightarrow Fe^{2+} + H^+ + O_2 \quad [23]$$

$$\bullet OOH + Fe^{2+} \rightarrow Fe^{3+} + HOO^- \quad [24]$$

$$\bullet OH + \bullet OOH \rightarrow H_2O + O_2 \quad [25]$$

Los radicales hidroxilo generados oxidan la materia orgánica mediante: eliminación de un átomo de hidrógeno, produciendo radicales libres orgánicos y agua (ecuación [26]); adición de los radicales a un compuesto insaturado, alifático o aromático, generando

especies radicalarias (ecuación [27]); sustitución del heteroátomo por el grupo hidroxilo en compuestos aromáticos sustituidos, como los clorofenoles (ecuación [28]) (Carey, 2003; Chen & Pignatello, 1997; Huang et al., 1993; Rueda Márquez et al., 2018).

$$C_xH_yOH + \bullet OH \rightarrow C_xH_{y-1}HO \bullet + H_2O \quad [26]$$

$$C_xH_y + \bullet OH \rightarrow C_xH_y(OH) \bullet \quad [27]$$

$$C_xH_yClOH + \bullet OH \rightarrow C_xH_y(HO)_2 \bullet + HCl \quad [28]$$

Estos procesos han destacado en el tratamiento de aguas debido, no solo a la abundancia de hierro y su carácter relativamente inocuo, sino a su capacidad para activar el peróxido de hidrógeno sin un aporte de energía externo, permitiendo operar a presión atmosférica y temperatura ambiente. El medio de reacción de estos procesos se encuentra en condiciones ácidas, presentando actividades catalíticas óptimas a valores de pH cercanos a 3. De esta forma, se garantiza que la concentración de especies activas de hierro sea máxima y la velocidad de descomposición del agua oxigenada menor. Valores de pH inferiores a 2 no generan la descomposición del peróxido de hidrógeno, mientras que la pérdida de eficacia en medio básico se relaciona con la transición del hierro de la forma ferrosa hidratada a especies férricas coloidales, que descomponen el peróxido de hidrógeno en oxígeno y agua sin promover la formación de radicales libres (Kwon et al., 1999; Rodríguez et al., 2006). La temperatura del proceso presenta efectos contrapuestos, favoreciendo su cinética, pero disminuyendo la estabilidad del agua oxigenada, que se descompone directamente en agua y oxígeno sin formar radicales. En este sentido, temperaturas cercanas a 50 ºC permiten alcanzar una mejora en la cinética, sin comprometer la estabilidad del peróxido de hidrógeno para reducir su dosis (Jones, 1999; Pignatello et al., 2006; Sievers, 2011; Zazo et al., 2005, 2006).

A diferencia de las desventajas de los procesos Fenton homogéneos, las reacciones CWPO evitan la necesidad de eliminar los lodos de hierro en el efluente, ya que el metal se encuentra localizado en la superficie del catalizador sólido. Esto facilita su recuperación y reutilización. Al igual que lo mencionado en los procesos heterogéneos CWAO, la viabilidad de los catalizadores sólidos está condicionada a su actividad y estabilidad física, química y mecánica en las condiciones de operación. La elevada solubilidad de las especies de hierro, especialmente a valores de pH bajos, generalmente implica lixiviados de la fase

activa en el medio acuoso considerables, lo que compromete la estabilidad y eficacia del catalizador. Aunque sigue siendo la fase activa más empleada, también se están estudiando otras especies que permitan sustituir al hierro en los procesos CWPO, entre las que destacan Cu^{2+}, Mn^{2+}, y Co^{2+}. Los soportes más frecuentes incluyen el carbón activo, las arcillas pilareadas, la sílice, las zeolitas, los tamices moleculares mesoporosos y la alúmina (Matatov-Meytal & Sheintuch, 1998; Rueda Márquez et al., 2018). Por tanto, la síntesis de carbones activos a partir de lodos de depuradora que actúen como soporte en los catalizadores permite la valorización de estos residuos y promueve la economía circular (Bonilla-Petriciolet et al., 2017; Gupta et al., 2009; Singh et al., 2018).

CAPÍTULO II

Objetivos y alcance

2.1 Objetivos generales

La presente Tesis Doctoral se centra en el estudio de diversas alternativas para el tratamiento de contaminantes emergentes presentes en disolución acuosa y recogidos en las Listas de Observación de la Unión Europea.

Entre los principales grupos de contaminantes que más preocupación e interés están suscitando se encontrarían los fármacos y los pesticidas. Por esta razón, se han seleccionado como las sustancias más representativas para la propuesta y evaluación de procesos de extracción líquido-líquido, adsorción, oxidación húmeda (catalítica y no catalítica) y oxidación promovida por peróxido de hidrógeno.

2.2 Objetivos específicos

La consecución de los objetivos generales mencionados previamente se ha concretado en los siguientes objetivos específicos:

- Propuesta y evaluación de disolventes de extracción alternativos, basados en terpenoides y disolventes eutécticos, que presenten una elevada afinidad por los contaminantes emergentes y que supongan una toxicidad menor a los convencionales.
- Síntesis de materiales con propiedades fisicoquímicas prometedoras para su aplicación en procesos catalíticos y/o de adsorción.
- Valorización de residuos mediante procesos pirolíticos para la síntesis de materiales carbonosos.
- Realización de pruebas de concepto en las que se empleen matrices acuosas reales y/o se evalúe la reutilización de disolventes de extracción, catalizadores o adsorbentes.
- Influencia de diversas variables de operación según la técnica de tratamiento analizada: relación disolvente/alimento; pH; temperatura; presión; dosis de catalizador; etc.
- Desarrollo de modelos cinéticos representativos de los procesos de reacción.

CAPÍTULO III

Materiales y métodos

En este capítulo se resume el procedimiento experimental seguido para la consecución de los resultados obtenidos en las publicaciones recogidas en los Anexos, así como de las instalaciones utilizadas y las técnicas de análisis requeridas.

Para ello, se han agrupado los procesos de extracción, por un lado, y los procesos de oxidación y adsorción, por otro. Dentro de los primeros se han detallado aspectos como la selección del disolvente mediante simulación molecular, la preparación de las mezclas eutécticas, los procesos de extracción en discontinuo y en continuo, la regeneración y reutilización del disolvente y las técnicas analíticas para la caracterización del refinado. Con respecto al segundo grupo, se ha abordado la síntesis y caracterización de los materiales carbonosos empleados como catalizadores y/o adsorbentes, las reacciones WAO y CWAO, el proceso CWPO, los blancos de adsorción y la caracterización del efluente acuoso tras las reacciones de oxidación.

3.1 Extracción líquido-líquido

3.1.1 Selección del disolvente de extracción mediante simulación molecular con COSMO-RS

La selección inicial de los disolventes de extracción se realizó mediante simulación molecular con el método COSMO-RS (Conductor-like Screening Model for Real Solvents), utilizando el software COSMOtherm (versión 19.0.4). Sin embargo, puesto que los contaminantes emergentes (ciprofloxacina, trimetoprima, sulfametoxazol, acetamiprid, imidacloprid y tiametoxam) y los terpenos considerados no se encuentran en su base de datos, se empleó el software Turbomole 7.4 para obtener y optimizar las geometrías moleculares, seleccionando el método de solvatación continua COSMO con un nivel computacional BP86/TZVP y obteniendo la geometría de mínima energía mediante un cálculo de punto único. De esta forma, la información completa de la molécula optimizada se almacena en un archivo que se puede introducir en el software COSMOtherm para el cálculo de una gran variedad de parámetros termodinámicos. La afinidad de los disolventes de extracción por cada uno de los antibióticos y pesticidas neonicotinoides se evaluó a partir de los coeficientes de actividad a dilución infinita, considerando una temperatura de 50 °C y una fracción molar del contaminante en el disolvente de $5 \cdot 10^{-5}$, a fin de garantizar la región de dilución infinita. Los disolventes eutécticos se han simulado como una mezcla de dos compuestos diferentes con la composición del punto eutéctico.

3.1.2 Preparación de disolventes eutécticos

Las tres mezclas eutécticas seleccionadas como disolventes de extracción se prepararon a partir de sus compuestos puros, empleando como proporción la composición en el punto eutéctico característica para cada una de ellas. Las fracciones molares de timol empleadas fueron 0,56, 0,44 y 0,33 en las mezclas (timol + ácido dodecanoico), (timol + ácido decanoico) y (timol + ácido octanoico), respectivamente. Para agilizar el proceso de síntesis, puesto que las temperaturas de fusión para los disolventes eutécticos anteriores son aproximadamente -2, 14 y 33 °C, se empleó un baño termostático a 50 °C con agitación magnética hasta obtener una mezcla líquida homogénea.

3.1.3 Proceso en discontinuo

La extracción líquido-líquido en discontinuo se llevó a cabo introduciendo el alimento acuoso junto con el disolvente de extracción en viales de vidrio de 8 mL. Las relaciones volumétricas disolvente/alimento empleadas fueron: 0,10; 0,25; 0,50; 1,00 y 2,00. El contacto entre fases se realizó bajo agitación magnética y a temperatura constante, empleando una placa de agitación con calefacción IKA C-MAG HS 7, durante un total de 12 horas. A continuación, se dejó reposar las fases durante 4 horas, a fin de facilitar la separación del extracto y del refinado mediante el uso de pipetas Pasteur de vidrio. En la Figura 8 se representa un esquema de la instalación empleada en el proceso de extracción en discontinuo.

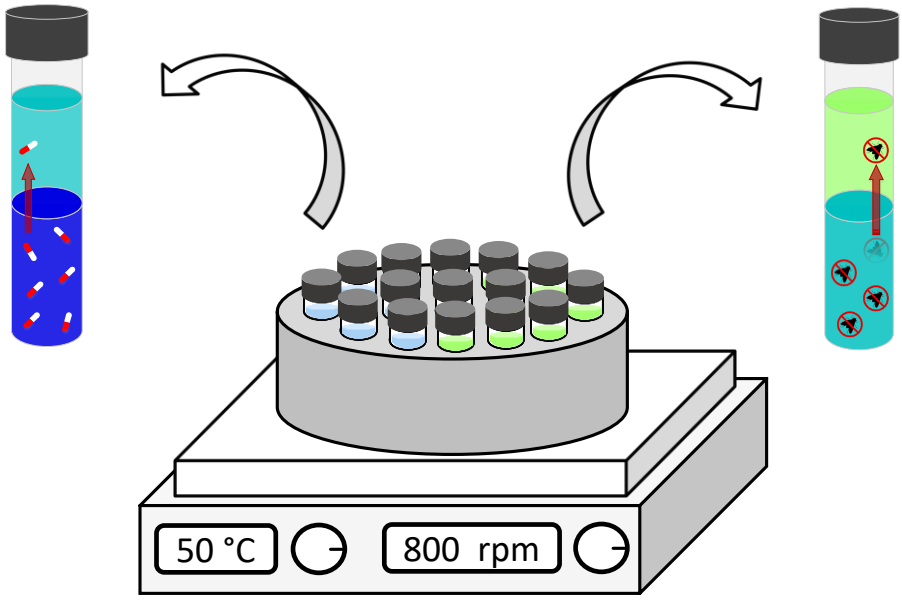

Figura 8. Instalación experimental para la extracción líquido-líquido en discontinuo.

Los disolventes de extracción empleados para los procesos de extracción en discontinuo fueron 2 terpenoides (timol y carvacrol), 3 disolventes eutécticos (timol + ácido dodecanoico, timol + ácido decanoico y timol + ácido octanoico) y 2 disolventes convencionales (MIBK y acetato de etilo).

Para el caso de los pesticidas acetamiprid, imidacloprid y tiametoxam, se evaluó la influencia de la temperatura (30 y 50 °C), la matriz acuosa (agua ultrapura y agua de río), el pH del alimento (valores de 1,0; 3,0; 5,0; 7,0 y 9,0) y la presencia de otros pesticidas (disoluciones monocomponentes a 50 mg/L y disoluciones multicomponentes con 50 mg/L de cada pesticida, es decir, con una concentración total de pesticidas de 150 mg/L).

Por otra parte, el estudio de la extracción de los antibióticos ciprofloxacina, trimetoprima y sulfametoxazol se centró únicamente en disoluciones acuosas multicomponentes con 50 mg/L de cada fármaco, es decir, con una concentración total de fármacos de 150 mg/L. Además, se evaluó el efecto de la matriz acuosa (agua ultrapura y agua hospitalaria), y el pH del alimento (valores de 5,0; 6,5 y 8,0).

3.1.4 Proceso en continuo

Para evaluar el efecto de la transferencia de materia se realizó un proceso de extracción en continuo, operando en paralelo y empleando una columna de relleno de 8 mm de diámetro interno y 80 mm de longitud con un lecho de esferas de vidrio de 2 mm de diámetro. De esta forma, con una bomba de jeringa KDS 100 Legacy y otra Orion Sage M361, se introdujeron la alimentación (disolución acuosa multicomponente de antibióticos en una matriz de agua residual hospitalaria a pH 5,0) y el disolvente (carvacrol) a temperatura ambiente, de acuerdo con las siguientes relaciones volumétricas disolvente/alimento: 2,00; 1,00 y 0,50. El caudal volumétrico total se mantuvo constante durante los experimentos en 10 mL/h y el tiempo de residencia en la columna fue de 21 min. En la Figura 9 se representa un esquema de la instalación para el proceso de extracción en continuo y flujo en paralelo.

3.1.5 Reutilización y regeneración del disolvente

Uno de los aspectos clave para la implantación de un proceso de extracción a escala industrial es la reutilización del disolvente. Para ello, se realizó un proceso de extracción de múltiples etapas consecutivas en discontinuo, empleando como alimento una disolución acuosa multicomponente de ciprofloxacina, trimetoprima y sulfametoxazol en agua residual hospitalaria a un pH ajustado de 5,0. En cuanto al disolvente, se seleccionó

únicamente el carvacrol a una relación S/F volumétrica de 1,00. Las extracciones se realizaron en frascos de vidrio de 500 mL a temperatura ambiente y con agitación magnética durante 12 h. La separación de las fases se realizó de manera análoga a la descrita en el proceso de extracción en vial descrito anteriormente.

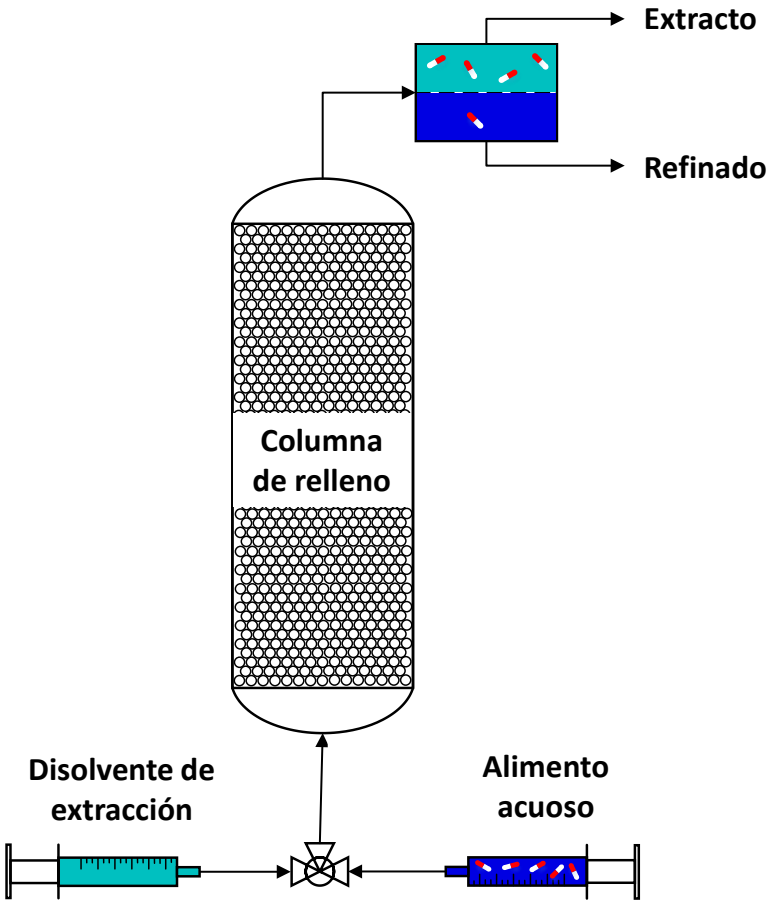

Figura 9. Instalación experimental para la extracción líquido-líquido en continuo.

Por último, la regeneración del disolvente procedente del extracto de la última etapa de extracción se realizó mediante un evaporador rotativo Büchi R-200 a 164 °C y 20 mbar. Para comprobar las propiedades extractivas del disolvente regenerado, se aplicó a una extracción en vial de vidrio de 8 mL con agitación magnética y temperatura ambiente durante 12 h. En la Figura 10 se esquematiza el procedimiento seguido para la reutilización y regeneración del disolvente.

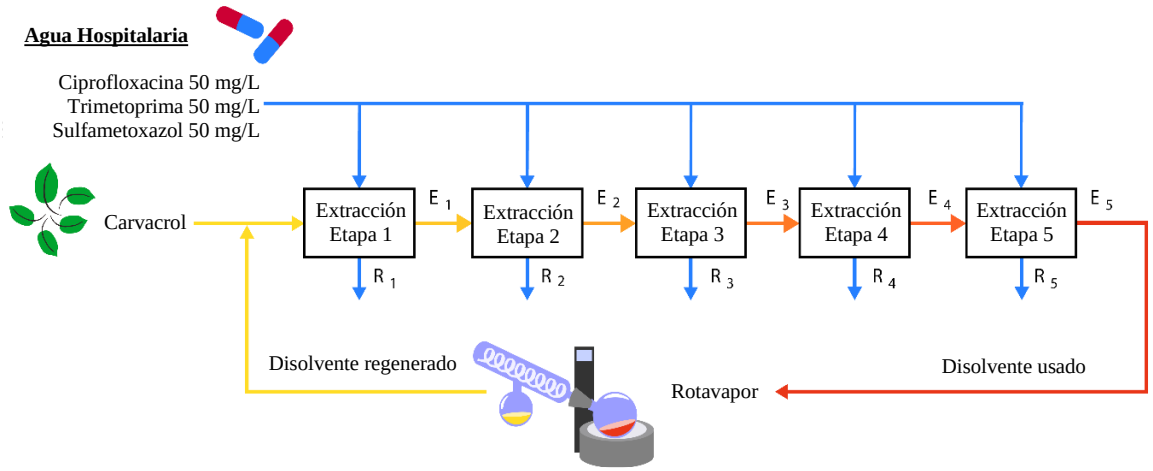

Figura 10. Procedimiento experimental para la reutilización y regeneración del disolvente de extracción.

3.1.6 Caracterización tras el proceso de extracción

La concentración de los compuestos orgánicos en el refinado, tanto para evaluar el rendimiento de extracción de los contaminantes emergentes como las pérdidas del disolvente de extracción en el refinado, se determinó por cromatografía líquida.

Para los antibióticos se empleó un HPLC Agilent 1260 Infinity II acoplado a un detector de matriz de diodos y una columna cromatográfica Poroshell 120 EC-C18 (4,6 × 150 mm; 4 µm). El método cromatográfico desarrollado consistió en una fase móvil compuesta por una mezcla de acetonitrilo y ácido acético 75 mM, operando en gradiente a un caudal volumétrico constante de 0,90 mL/min, un volumen de inyección de 50 µL, una temperatura de columna de 40 ºC y longitudes de onda de 233 y 275 nm.

Por otro lado, en el caso de los pesticidas, el equipo empleado fue un HPLC Varian ProStar acoplado a un detector de matriz de diodos y una columna cromatográfica Teknokroma (4,6 x 250 mm; 5 µm). El método cromatográfico consistió en una fase móvil compuesta por una mezcla 70 % acetonitrilo y 30 % ácido acético 75 mM, un caudal volumétrico de 0,85 mL/min, una temperatura de columna de 30 ºC, un volumen de inyección de 20 µL y longitudes de onda de 223 nm y 275 nm.

El pH de las disoluciones empleadas se determinó mediante un pH-metro Crison 2002.

3.2 Procesos de oxidación y adsorción

3.2.1 Síntesis y caracterización de los catalizadores/adsorbentes

Los materiales carbonosos empleados como catalizadores y/o adsorbentes se prepararon a través de procesos de activación química en los que los lodos de depuradora fueron los precursores biomásicos. Se evaluaron lodos de diferentes procedencias, como los generados en estaciones depuradoras de aguas residuales urbanas y plantas de tratamiento industriales.

La síntesis se llevó a cabo a través de una primera etapa de secado de los lodos en un horno a 105 ºC. Tras una molienda, el lodo en polvo se sometió a una activación química mediante una técnica de impregnación a humedad incipiente, empleando diferentes agentes activantes (dicloruro de hierro y tricloruro de níquel) para estudiar su influencia en la caracterización, actividad catalítica y capacidad de adsorción de los materiales finales. En cualquier caso, la proporción fue de 1 gramo de agente activante, o de mezcla de haluros metálicos, por gramo de lodo seco. Para favorecer el acceso del agente activante a los poros del lodo y homogeneizar la mezcla, tras la impregnación se introdujo en un baño de ultrasonidos a 40 ºC durante 90 min, se dejó durante 12 h a temperatura ambiente y, finalmente, se secó en un horno a 105 ºC durante 24 h. El sólido obtenido se pirolizó en un reactor vertical de cuarzo durante 2 horas a 800 ºC, manteniendo un caudal constante de nitrógeno de 100 mL/min y una rampa de temperatura hasta alcanzar la temperatura de pirólisis de 10 ºC/min. Para eliminar el exceso de metal, y aquel que se encuentra débilmente unido a la matriz sólida, cada gramo de material procedente de la pirólisis se molió, se lavó con 100 mL de ácido clorhídrico 1 M durante 1 h con agitación magnética, se filtró y se enjuagó con agua ultrapura hasta pH neutro. Finalmente, se realizó un secado a 105 °C durante 24 h y se tamizó hasta obtener un tamaño de partícula inferior a 250 µm.

En lo relativo a la caracterización, los parámetros macroscópicos de los lodos se determinaron mediante métodos estándar, incluyendo la demanda química de oxígeno y la concentración de sólidos totales, fijos y volátiles (American Public Health Association, 2017). La composición química, tanto del precursor biomásico como de los materiales sintetizados, se cuantificó mediante espectroscopia de fluorescencia de rayos X y análisis

elemental, empleando un espectrómetro PANalytical Axios y un microanalizador LECO CHNS-932, respectivamente. La química superficial se estudió mediante espectroscopía infrarroja con transformada de Fourier, con un equipo Thermo Nicolet Nexus 670, en un rango de longitudes de onda de 400-4000 cm^{-1}.

Las isotermas de adsorción-desorción de nitrógeno a -196 ºC, obtenidas con un analizador Micromeritics ASAP 2020, proporcionaron información sobre la porosidad. La morfología y propiedades estructurales se observaron mediante difracción de rayos X, microscopía electrónica de barrido, y microscopía electrónica de transmisión, llevadas a cabo en un difractómetro Bruker D8 Advance A25, un microscopio JEOL JSM 6335F y un microscopio JEOL JEM-2100 equipado con una fuente de electrones LaB6 de 200 kV y con una cámara CCD ORIUS SC1000 de alta resolución, respectivamente. La estabilidad térmica de los materiales se comprobó mediante análisis termogravimétrico en una termobalanza STAR 6000 PerkinElmer, fijando una rampa de temperatura de 10 °C/min, un caudal de nitrógeno de 30 mL/min y un intervalo de temperatura de 30-1000 °C.

3.2.2 Oxidación húmeda catalítica y no catalítica

La instalación experimental, esquematizada en la Figura 11, consta de un reactor autoclave Hastelloy C, con un diámetro interno de 3,5 cm y altura de 14,3 cm, equipado con un agitador mecánico de palas situado a 12,1 cm del borde superior y una camisa de calentamiento. La lectura de la temperatura en la camisa y en el interior del reactor se obtiene mediante termopares tipo K, acoplados a un sistema de control TOHO TTM-005. De esta forma, si la temperatura en el reactor difiere de la de consigna, se regula la potencia suministrada a la camisa. La lectura de la presión en el reactor se obtiene mediante un manómetro McDaniel, y se libera a través de una válvula de aguja. El reactor también cuenta con un disco de ruptura y un sistema de toma de muestras a través de una conducción ubicada a una profundidad de 9,8 cm del borde superior del reactor.

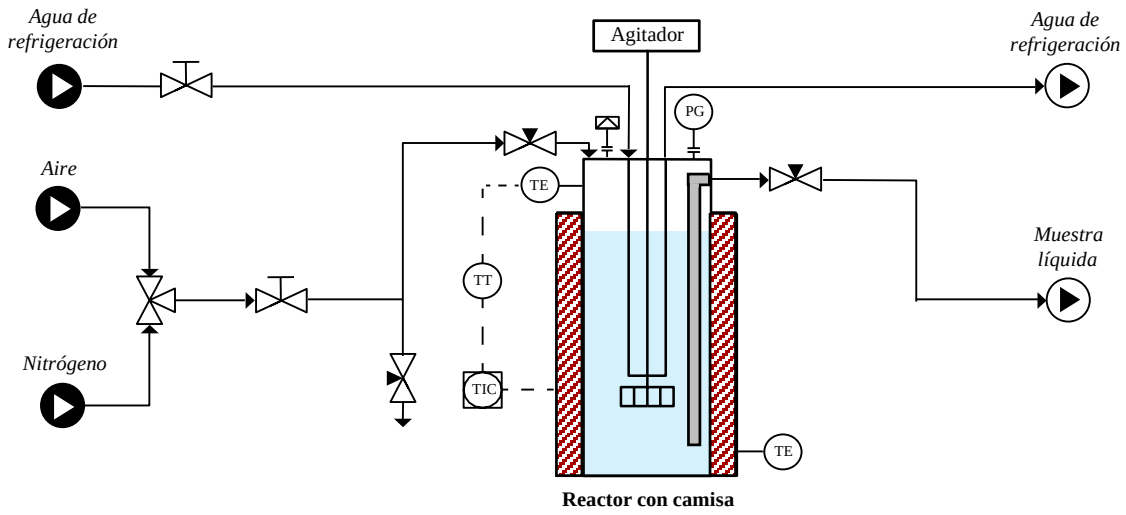

Figura 11. Instalación experimental de oxidación húmeda catalítica y no catalítica.

La reacción WAO se realizó empleando 100 mL de una disolución de ciprofloxacina 50 mg/L, a pH natural, en el interior del reactor, mientras que para los experimentos CWAO se añadió también la dosis deseada del catalizador sólido sintetizado. Una vez posicionado el reactor, se realiza una purga con N_2 a fin de eliminar del sistema cualquier traza, asegurando que la temperatura de operación se alcanza en atmósfera inerte. A continuación, se inicia el calentamiento y la agitación, fijando la velocidad en 700 rpm para evitar limitaciones a la transferencia de materia en la fase líquida. Una vez se alcanza la temperatura de operación deseada en el interior del reactor, se presuriza con aire, considerando ese momento como el tiempo cero del proceso. Durante las tres primeras horas, se tomaron muestras de manera periódica. Para el caso particular del proceso CWAO, las muestras líquidas recogidas se filtraron inmediatamente para eliminar el catalizador arrastrado, empleando filtros de jeringa de PTFE de 0,45 μm.

El proceso WAO se llevó a cabo a 140 ºC y 20 bar, mientras que en el proceso catalítico se investigó la influencia de diferentes condiciones de operación, como la dosis de catalizador (0,1-0,7 g/L), la temperatura (120-160 °C), la presión total (10-30 bar), la matriz acuosa (agua ultrapura y agua superficial) y la reutilización del catalizador.

3.2.3 Oxidación promovida por peróxido de hidrógeno

Las reacciones CWPO se realizaron introduciendo 250 mL de una disolución de ciprofloxacina 50 mg/L, a un pH corregido de 3,2, en el interior de frascos de vidrio de 500 mL, junto con la dosis deseada del catalizador sintetizado (0,3 g/L) y el peróxido de hidrógeno (1,1 mL/L). Para mantener la temperatura de operación a 70 ºC se empleó un baño termostático, acoplado a una placa de agitación que permitía fijar este parámetro a 300 rpm. En la Figura 12 se representa un esquema de la instalación experimental descrita.

Durante las tres primeras horas de reacción, se tomaron muestras periódicamente, filtrándose de manera inmediata mediante filtros de jeringa de PTFE de 0,45 μm. Además, se evaluó la influencia de la matriz acuosa, empleando disoluciones preparadas en agua ultrapura, agua superficial y en un efluente procedente de una estación depuradora de aguas residuales urbana.

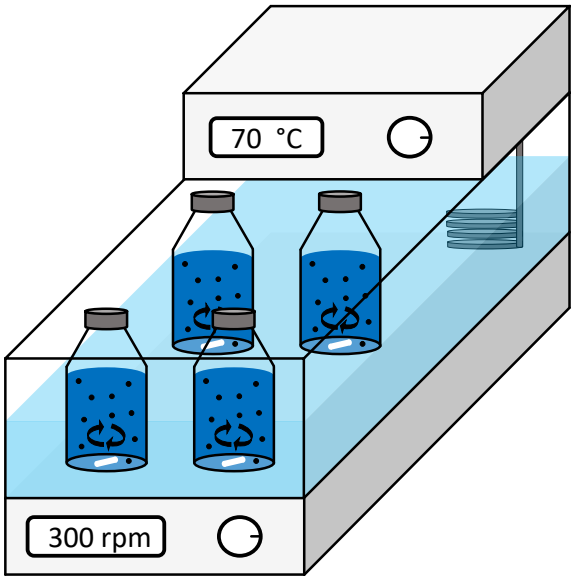

Figura 12. Instalación experimental de oxidación promovida por peróxido de hidrógeno.

3.2.4 Blancos de adsorción

La contribución de la adsorción en los procesos de oxidación húmeda catalítica y con peróxido de hidrógeno se analizó empleando las mismas instalaciones descritas para cada uno de ellos, es decir, las representadas en la Figura 11 y Figura 12, respectivamente. Sin embargo, dichos experimentos se realizaron en ausencia del agente oxidante empleado para la generación de los radicales hidroxilo. Concretamente, el blanco de adsorción en el proceso CWAO tuvo lugar presurizando el reactor hasta la presión deseada con una corriente gaseosa de nitrógeno, en lugar de aire. Para el proceso CWPO, el efecto de la adsorción se estudió mediante el mismo procedimiento seguido para la reacción, pero sin adicionar el peróxido de hidrógeno.

3.2.5 Caracterización tras el proceso de oxidación

La evolución del proceso de degradación de ciprofloxacina en los procesos de oxidación se analizó mediante cromatografía líquida, empleando un HPLC Agilent 1260 Infinity II acoplado a un detector de matriz de diodos y una columna cromatográfica Poroshell 120 EC-C18 (4,6 × 150 mm; 4 μm). El método cromatográfico consistió en una fase móvil compuesta por 17,5 % acetonitrilo y 82,5 % ácido acético 75 mM, fijando un caudal de 0,85 mL/min, un volumen de inyección de 50 μL, una temperatura de columna de 30 ºC y una longitud de onda de 275 nm.

Los compuestos intermedios originados en el transcurso de la reacción se identificaron en un espectrómetro de masas QTOF Bruker modelo Impact II acoplado a un UHPLC. El contenido de carbono orgánico total se midió mediante un analizador Shimadzu TOC-V CPH. La lixiviación de la fase activa del catalizador en los procesos CWAO y CWPO se determinó mediante espectroscopia de emisión óptica con plasma de acoplamiento inductivo en un equipo Spectro Arcos.

CAPÍTULO IV

Resultados

En este capítulo se destacan los resultados y las aportaciones científicas más relevantes obtenidas en la Tesis Doctoral. Si se desea profundizar en alguno de los aspectos mencionados a lo largo de esta sección, se recomienda acudir a las publicaciones de referencia, recogidas en los Anexos.

Además, la estructuración del contenido se ha realizado siguiendo cada uno de los artículos que fundamentan el cuerpo de este documento:

- Publicación 1: Extracción líquido-líquido de pesticidas neonicotinoides.
- Publicación 2: Extracción líquido-líquido de antibióticos.
- Publicación 3: Procesos CWPO y de adsorción para la eliminación de ciprofloxacina.
- Publicación 4: Procesos WAO, CWAO y de adsorción para la eliminación de ciprofloxacina.

4.1 Publicación 1: Extracción líquido-líquido de pesticidas neonicotinoides

Separation and Purification Technology

"Extraction of neonicotinoid pesticides from aquatic environmental matrices with sustainable terpenoids and eutectic solvents"

Factor de impacto (2021): 9,136

Posición: Primer Cuartil (Q1)

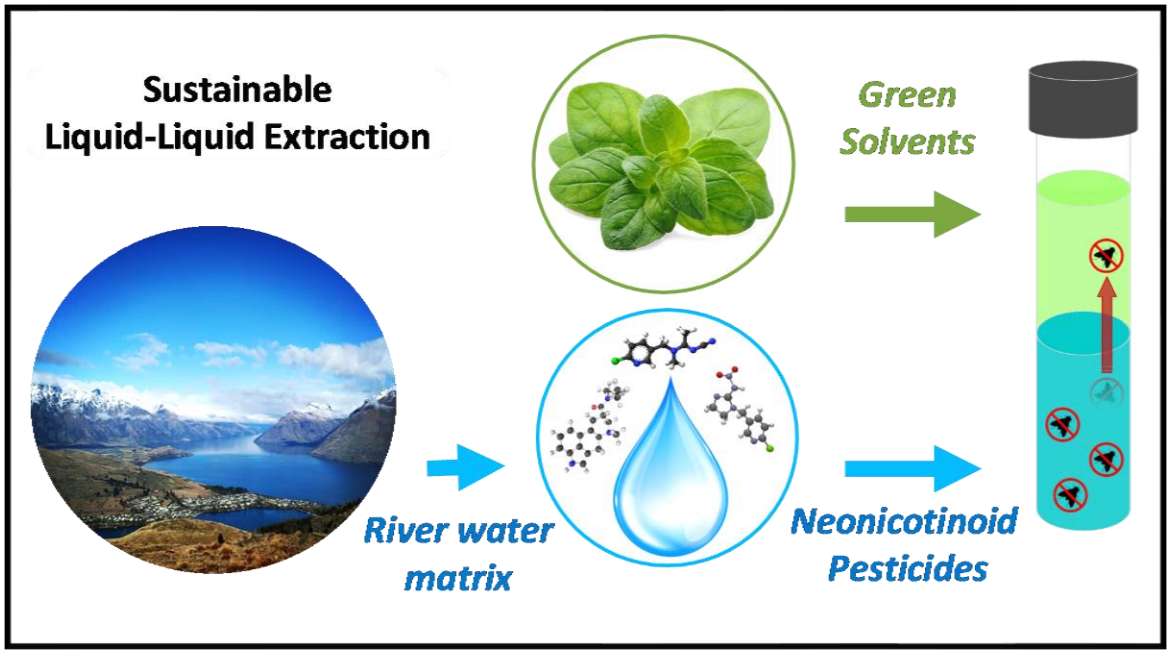

DOI: 10.1016/j.seppur.2022.122148

4.1.1 Selección del disolvente con el método COSMO-RS

Uno de los métodos más empleados para la selección de disolventes en procesos de extracción líquido-líquido se basa en los coeficientes de actividad. En este sentido, un menor coeficiente de actividad a dilución infinita del soluto indicaría una mayor afinidad por el disolvente de extracción.

Según las estimaciones de los coeficientes de actividad mediante el método COSMO-RS, el timol y el carvacrol presentaron los valores más bajos dentro del grupo de terpenos puros. Además, en general, los 11 compuestos que no contienen heteroátomos en su esqueleto hidrocarbonado (mirceno, ocimeno, sabineno, limoneno, felandreno, terpineno-alfa, 3-careno, pineno-beta, canfeno, pineno-alfa y pinano) se caracterizaron por tener una menor afinidad por los tres pesticidas neonicotinoides. Este comportamiento podría asociarse a una menor contribución de los enlaces de hidrógeno y las interacciones dipolo-dipolo. Por otro lado, los disolventes eutécticos presentaron valores de los coeficientes de actividad en el intervalo de los mostrados por los compuestos puros, aunque en la bibliografía se ha señalado que los rendimientos experimentales para estas mezclas pueden ser ligeramente superiores a los estimados por simulación molecular. Dentro de este grupo, destacaron los disolventes formados por timol y ácidos carboxílicos: timol + ácido octanoico, timol + ácido decanoico y timol + ácido dodecanoico. Finalmente, los disolventes convencionales que presentaron una mayor afinidad por los pesticidas fueron el acetato de etilo y la metil isobutil cetona.

A partir de esta metodología, se han seleccionaron 7 candidatos potenciales para extracción de neonicotinoides en disolución acuosa: 2 terpenos (carvacrol y timol), 3 mezclas eutécticas (timol + ácido octanoico, timol + ácido decanoico y timol + ácido dodecanoico) y 2 disolventes convencionales (acetato de etilo y metil isobutil cetona).

4.1.2 Extracción en discontinuo

4.1.2.1 Proceso monocomponente

Los resultados experimentales para extracciones monocomponentes en agua ultrapura a 50 ºC revelaron capacidades de extracción de los tres pesticidas muy similares para los dos terpenoides. Los altos rendimientos con timol y carvacrol podrían deberse a la presencia del grupo hidroxilo en sus estructuras moleculares, lo que potenciaría las interacciones moleculares de tipo enlace de hidrógeno. La deslocalización de electrones como consecuencia de la resonancia en el anillo aromático aumentaría la acidez del hidrógeno presente en este grupo, favoreciendo, aún más, su capacidad como donadores de enlaces de hidrógeno. Este hecho, junto con su capacidad para comportarse también como aceptores de este tipo de enlaces, podría explicar la elevada afinidad de estos dos terpenoides por los tres pesticidas. Además, en sintonía con las predicciones obtenidas con COSMO-RS, los terpenos puros mostraron rendimientos superiores a los de sus mezclas eutécticas, observándose en estos últimos un ligero aumento de acuerdo con la longitud de la cadena alquílica: (timol + ácido octanoico) < (timol + ácido decanoico) < (timol + ácido dodecanoico). El tiametoxam fue el plaguicida con la variación más pronunciada.

Según lo reportado en la bibliografía, únicamente se ha aplicado un número limitado de terpenos, en forma de mezclas eutécticas, para la extracción de pesticidas. Es decir, hasta el desarrollo de esta investigación no se había evaluado el uso de estos compuestos puros, resaltando de nuevo la relevancia de investigaciones relacionadas en este campo. Algunos autores han propuesto el uso de disolventes eutécticos formados por ácidos orgánicos naturales (ácidos octanoico, decanoico y dodecanoico) y el terpenoide DL-mentol, alcanzando rendimientos de extracción de hasta el 75, 70 y 40 % para el acetamiprid, imidacloprid y tiametoxam, respectivamente, utilizando una relación S/F de 1,00. Sin embargo, en las mismas condiciones de operación, las mezclas eutécticas sugeridas en este trabajo (timol + ácidos carboxílicos) permiten alcanzar rendimientos del 98,6-99,6, 96,4-98,4 y 77,5-89,7 % para el acetamiprid, imidacloprid y tiametoxam, respectivamente. Por tanto, el timol parece formular disolventes eutécticos capaces de extraer una mayor cantidad de pesticida. Aunque los disolventes eutécticos descritos en este estudio consiguen rendimientos superiores a los descritos hasta ahora en la bibliografía, el uso de

terpenoides puros mostró resultados aún más favorables, y evitó el uso de un disolvente binario. Es decir, tanto el timol como el carvacrol exhibieron rendimientos de extracción superiores al 99,6, 99,4 y 97,6 % para el acetamiprid, el imidacloprid y el tiametoxam, respectivamente.

De los tres grupos de disolventes empleados, los convencionales presentaron los rendimientos más bajos, incluso para relaciones S/F elevadas. Los tres pesticidas actúan como aceptores de enlaces de hidrógeno, y el imidacloprid lo hace también como donante. Por ello, puesto que el MIBK y el acetato de etilo actúan únicamente como aceptores de enlaces de hidrógeno, es decir, no poseen hidrógenos ácidos unidos a un elemento de alta electronegatividad, las interacciones intermoleculares entre estos disolventes y los neonicotinoides implicarían un menor impacto en comparación con los terpenos. Consecuentemente, la capacidad de extracción de los disolventes convencionales no se debería tanto a la formación de enlaces de hidrógeno, sino a otros tipos de interacciones intermoleculares, como las interacciones de Van der Waals y electrostáticas.

Los terpenos puros presentaron mayores capacidades de extracción que las mezclas eutécticas, y estas, a su vez, superiores a las de los disolventes convencionales. Por tanto, aunque los precios de los terpenoides (carvacrol 10-25 $/kg y timol 9-11 $/kg) pueden ser más elevados que los de los disolventes convencionales (MIBK 1,0-1,5 $/kg y acetato de etilo 1,3 $/kg), los bajos requerimientos de disolvente para alcanzar rendimientos superiores al 90%, junto con su baja toxicidad y escasas pérdidas en la fase acuosa, los posicionan en una situación más favorable. Concretamente, las pérdidas del disolvente de extracción en la fase acuosa superaron el 1,52 y el 10,18 % en peso para el MIBK y el acetato de etilo, respectivamente, mientras que los terpenos puros mostraron solubilidades del 0,17 y 0,25 % en peso para el carvacrol y el timol, respectivamente. Los disolventes eutécticos compuestos por timol + ácido carboxílico presentaron menores pérdidas de timol en agua, obteniéndose valores inferiores al 0,10 % en peso.

Sus elevados rendimientos de extracción, baja solubilidad en agua y temperatura de fusión muy por debajo de la temperatura ambiente convierten al carvacrol en un candidato potencial para la eliminación de pesticidas en disolución acuosa.

4.1.2.2 Proceso multicomponente: Efecto de la matriz, la relación S/F, el pH y la temperatura

Los resultados de las extracciones individuales condujeron al estudio de nuevas cuestiones, estrechamente relacionadas con la aplicación del proceso a escala industrial. Entre ellas, destacarían la influencia de la matriz acuosa, el pH y la temperatura.

La extracción multicomponente se vio favorecida al disminuir la temperatura, obteniéndose un ligero aumento de los rendimientos de extracción individuales y globales tanto para el carvacrol como para el MIBK. Por tanto, el proceso a temperatura ambiente no solo evitaría los requerimientos energéticos asociados al acondicionamiento térmico del proceso, sino que favorecería el rendimiento de extracción.

Los estudios de pH del alimento acuoso en el proceso de extracción con carvacrol evidenciaron una influencia poco significativa sobre los rendimientos, lo que hace que este terpeno sea aún más versátil para su aplicación a escala industrial. Aunque la variación es muy pequeña, a valores de pH del alimento cercanos a 1, el carvacrol parece mostrar una ligera disminución del rendimiento, posiblemente asociado al aumento de la concentración de las especies catiónicas de los tres pesticidas, según evidencian sus equilibrios de disociación.

En lo relativo al efecto de la matriz acuosa, se observaron tendencias diferentes en función del tipo de pesticida. Para el imidacloprid y el tiametoxam, los rendimientos en la matriz de agua de río fueron inferiores a los obtenidos para el agua ultrapura. Es decir, los solutos presentes en el agua real favorecieron la solvatación de los dos neonicotinoides en la fase acuosa, disminuyendo la transferencia de materia al disolvente orgánico. Sin embargo, con el acetamiprid ocurrió lo contrario. Aunque estas tendencias se mantienen para el carvacrol y el MIBK, el efecto de la matriz fue considerablemente menor para el terpeno.

La relación S/F más adecuada para el carvacrol es 0,10, ya que permite alcanzar rendimientos globales de extracción cercanos al 98 %. El uso de un volumen mayor de disolvente no justificaría el ligero aumento del rendimiento de extracción, que incrementaría los costes de operación e inversión.

4.2 Publicación 2: Extracción líquido-líquido de antibióticos

Separation and Purification Technology

“ Extraction of antibiotics identified in the EU Watch List 2020 from hospital wastewater using hydrophobic eutectic solvents and terpenoids”

Factor de impacto (2021): 9,136

Posición: Primer Cuartil (Q1)

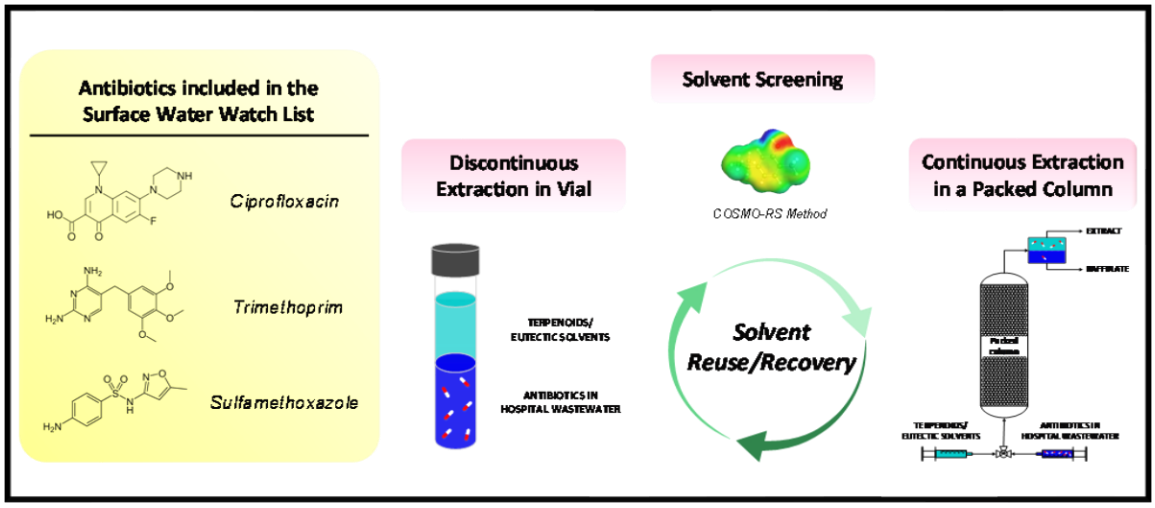

DOI: 10.1016/j.seppur.2021.120117

4.2.1 Selección del disolvente con el método COSMO-RS

La selección de disolventes puede realizarse comparando la magnitud de los coeficientes de actividad del soluto en cada uno de los disolventes considerados. En este sentido, cuanto menor es este valor, mayor su afinidad. En disoluciones multicomponentes es esencial seleccionar un disolvente que alcance la situación de compromiso óptimo para todos los solutos.

Entre los terpenoides, los disolventes con los coeficientes de actividad más bajos para los tres antibióticos fueron el timol y el carvacrol. Además, los terpenos sin heteroátomos en su esqueleto hidrocarbonado presentaron los valores más elevados, lo que indicaría una menor afinidad por los antibióticos al no presentar contribuciones mediante enlaces de hidrógeno o interacciones dipolo-dipolo. En el caso de los disolventes convencionales, los compuestos que mostraron una mayor situación de compromiso para los tres antibióticos fueron el acetato de etilo y el MIBK.

En cuanto a los disolventes eutécticos, las mezclas con timol se caracterizadon por su mayor afinidad, especialmente aquellas formadas por ácidos carboxílicos: timol + ácido dodecanoico, timol + ácido decanoico y timol + ácido octanoico. Los resultados obtenidos para la ciprofloxacina y la trimetoprima fueron considerablemente menores a los del sulfametoxazol. Dentro de este grupo, cabría señalar que, como se menciona en la bibliografía, los rendimientos experimentales pueden ser ligeramente superiores a los predichos por simulación molecular.

El sulfametoxazol fue el antibiótico que presentó una menor afinidad por los terpenoides y disolventes eutécticos, mientras que el comportamiento fue el opuesto para disolventes convencionales. Por tanto, el sulfametoxazol limitaría el rendimiento global de extracción para el primer grupo de disolventes, y la trimetoprima y ciprofloxacina para el segundo.

Según lo mencionado previamente, los compuestos seleccionados para la extracción de disoluciones acuosas multicomponentes de antibióticos fueron: 2 terpenoides (timol y carvacrol), 3 disolventes eutécticos (timol + ácido dodecanoico, timol + ácido decanoico y timol + ácido octanoico) y 2 disolventes convencionales (acetato de etilo y MIBK).

4.2.2 Extración en discontinuo: Efecto de la matriz, la relación S/F, el pH

Las principales variables evaluadas en el proceso de extracción líquido-líquido de disoluciones acuosas multicomponentes de antibióticos a 50 ºC fueron la relación S/F, el pH del alimento y el efecto de la matriz acuosa. En este sentido, los equilibrios de disociación de la ciprofloxacina, trimetoprima y sulfametoxazol jugaron un papel determinate en los rendimientos de extracción. Además, la transferencia de materia de parte del disolvente de extracción a la fase acuosa, debido a su solubilidad, puede modificar el pH del refinado y, con ello, la carga del antibiótico (especies catiónicas, aniónicas y neutras). En el caso de los disolventes convencionales y los terpenoides, el pH del refinado se mantuvo igual al del alimento, mientras que para los 3 disolventes eutécticos considerados, formados con ácido dodecanoico, ácido decanoico y ácido octanoico, el pH varió entre 4,9 y 6,5 con alimentos en aguas residuales hospitalarias a pH 8,0, y entre 3,7 y 4,5 para alimentos en aguas residuales hospitalarias a pH 5,0.

En el caso de la trimetoprima, la disminución del pH del alimento en matrices de aguas residuales hospitalarias redujo los rendimientos de extracción con todos los disolventes, lo que estaría relacionado con su equilibrio de disociación. Generalmente, el agua presenta una mayor afinidad por las especies cargadas, mientras que la fase orgánica lo hace por los compuestos no iónicos. Por tanto, puesto que un aumento del pH incrementa la concentración de trimetoprima en su forma neutra, los rendimientos de extracción se ven mejorados. La aplicación de disolventes convencionales resultó considerablemente más desfavorable en comparación con los terpenoides y mezclas eutécticas a cualquier valor de pH y matriz. Además, en el caso de los disolventes eutécticos, los rendimientos bajaron al hacerlo la longitud de la cadena alquílica del ácido carboxílico, lo que estaría causado por su menor hidrofobicidad y, por ende, por el aumento de la solubilidad parcial del ácido carboxílico en agua. Es decir, la concentración del ácido en la fase acuosa acidifica el medio y favorece la presencia de la forma protonada de este antibiótico. A valores de pH lo suficientemente elevados predomina la trimetoprima en estado neutro para los terpenoides y los disolventes eutécticos, por lo que sus capacidades de extracción son similares. Sin embargo, cuando predomina el soluto en su estado iónico (pH < 6,76), los disolventes eutécticos parecen estabilizar más eficazmente el ion cargado positivamente, y los

rendimientos de extracción son considerablemente superiores a los de los terpenoides, posiblemente debido a la mayor influencia de las interacciones de enlace de hidrógeno.

Por otro lado, la variación del valor de pH del alimento evidenció dos tendencias para la ciprofloxacina en función del disolvente de extracción empleado. Tanto para los terpenoides como para los disolventes convencionales, los rendimientos de extracción aumentaron en el siguiente orden: pH 6,5 > pH 8,0 > pH 5,0. Es decir, a pesar de ser aproximadamente equidistantes al punto isoeléctrico ($pH_{IEP} \approx 7,4$), en el que la concentración de la forma zwitterionica (carga neutra) es máxima, la solvatación de la ciprofloxacina en su estado catiónico fue mayor a la de la especie aniónica para estos dos grupos de disolventes. La tendencia en los rendimientos de extracción para los disolventes eutécticos fue diferente: pH 8,0 > pH 6,5 > pH 5,0. Este hecho se debería a la disminución del pH en la fase acuosa al transferirse parte del ácido carboxílico, haciendo que se aproxime al punto isoeléctrico en el caso de alimentos a pH 8,0 y se aleje cada vez más con alimentos a pH 6,5 y 5,0. Los rendimientos de los disolventes convencionales resultaron considerablemente inferiores a los de los terpenoides y los disolventes eutécticos a cualquier pH y matriz. Además, para todos los alimentos, el valor de pH del refinado al emplear las mezclas eutécticas fue inferior a 6,5 ($pH < pH_{IEP}$), por lo que el rendimiento disminuyó con la longitud de la cadena alquílica de los ácidos, atribuyéndose al descenso del pH del refinado al favorecerse su solubilidad en agua y, con ello, al aumento de la concentración de las especies cargadas. En general, los terpenoides mostraron rendimientos inferiores a los de los disolventes eutécticos, acentuándose esta diferencia al incrementarse la concentración de la especie iónica de la ciprofloxacina (alimento en agua residual a pH 5,0) y destacando la capacidad de los disolventes eutécticos para alcanzar una mayor solvatación de las especies cargadas.

Para el sulfametoxazol, la acidificación del alimento en la matriz real se tradujo en unos mayores rendimientos de extracción. Puesto que el intervalo de pH considerado en el alimento se encontró entre 5,0 y 8,0, una disminución del pH implicó un aumento de la concentración de sulfametoxazol en su estado neutro, favoreciendo su transferencia a la fase orgánica. En el caso de los disolventes convencionales, el MIBK presentó resultados similares a los de los terpenoides a cualquier pH, mientras que con el acetato de etilo el proceso se vio considerablemente favorecido al emplear alimentos con valores de pH entre

6,5 y 8,0, es decir, cuando el soluto predomina en su estado aniónico. Sin embargo, en su estado neutro (alimento a pH 5,0), los terpenoides superaron ligeramente al etilacetato. Entre las mezclas eutécticas, los rendimientos aumentaron al reducirse la longitud de la cadena alquílica del ácido carboxílico, debido a una mayor presencia de la especie en estado neutro al incrementarse la solubilidad del ácido en agua y, con ello, bajar el pH. Los rendimientos en las dos matrices acuosas empleadas evidenciaron una disminución notable de los rendimientos al emplear aguas reales.

Según lo discutido hasta el momento, no existe un valor de pH que presente los mejores resultados para la extracción de los tres antibióticos. Por lo tanto, al tratarse de una extracción multicomponente, es necesario analizar el rendimiento global de extracción. En este sentido, los disolventes convencionales fueron los que presentaron una menor afinidad, en términos generales, a cualquier pH y matriz. Los disolventes eutécticos parecen tener una menor sensibilidad a los cambios de pH en el alimento, debido a su mayor facilidad para solvatar especies iónicas y a la disminución del pH en el refinado al solubilizarse parte del ácido carboxílico. Sin embargo, las condiciones de operación con una mayor capacidad para extraer antibióticos, en términos globales, fue con el alimento a pH 5,0 y terpenoides puros. Por ejemplo, para un alimento en matriz real a pH 5,0 y S/F 0,25, el carvacrol alcanzó rendimientos del 93,2, 90,3 y 89,4 % para la trimetoprima, la ciprofloxacina y el sulfametoxazol, respectivamente, mientras que el disolvente eutéctico timol + ácido octanoico presentó valores del 97,4, 98,6 y 68,0 %.

En lo relativo al efecto de la matriz, la trimetoprima y la ciprofloxacina alcanzaron rendimientos de extracción superiores al emplear agua residual hospitalaria, indicando que los solutos presentes en la matriz real favorecían la transferencia de los antibióticos a la fase orgánica (*salting-out*). El sulfametoxazol mostró el comportamiento contrario, es decir, los solutos presentes en la matriz real favorecieron su solvatación en la fase acuosa (*salting-in*).

La relación S/F seleccionada como valor más adecuado para el proceso de extracción es 1,00, ya que permite obtener rendimientos globales de extracción superiores al 98 % para los terpenoides (superiores al 99 % para la trimetoprima y la ciprofloxacina, y al 97

% para el sulfametoxazol). Mayores cantidades de disolvente no justificarían el aumento de los costes de inversión y operación.

En cuanto a las pérdidas de disolventes orgánicos en la fase acuosa, se observó una mayor solubilidad de los disolventes convencionales en comparación con los terpenoides. Es decir, mientras se obtuvieron valores del 0,12-0,15 y 0,12-0,14 % en masa para el timol y el carvacrol, respectivamente, los asociados al etilacetato y el MIBK fueron 6,84-7,96 y 1,38-1,48 %, respectivamente. Por esta razón, aunque los precios de venta del timol (9-11 $/kg) y el carvacrol (10-25 $/kg) son más elevados que los del acetato de etilo (1,3 $/kg) y el MIBK (1,0-1,5 $/kg), su menor toxicidad, solubilidad en agua y relación S/F necesaria para alcanzar rendimientos elevados los posicionan como sustitutos potenciales de los disolventes derivados del petróleo.

En general, para simplificar el proceso de extracción y facilitar su recuperación, es preferible el uso de disolventes puros a escala industrial. Por tanto, dado que los rendimientos de extracción globales para los terpenoides y los disolventes eutécticos son comparables, se selecciona el carvacrol como disolvente óptimo, pues, a diferencia del timol puro, tiene un punto de fusión lo suficientemente bajo para operar a temperatura ambiente.

4.2.3 Extracción en continuo

Los procesos en continuo en columnas de relleno pueden presentar limitaciones a la transferencia de materia, especialmente con aquellos disolventes que, como el carvacrol, presentan una viscosidad relativamente alta (36,66 mPa·s a 20 °C) en comparación con el alimento acuoso (1,002 mPa·s a 20 °C).

Los resultados de extracción en columna (tiempo de residencia de 21 min) empleando disoluciones multicomponente en matrices de agua residual hospitalaria a pH 5,0 fueron comparables a los obtenidos en los ensayos en discontinuo (12 h de agitación). Esto implica que no hay limitación a la transferencia de materia en el intervalo de S/F considerado, es decir, entre 0,50 y 2,00.

4.2.4 Reutilización y regeneración del disolvente

Uno de los aspectos clave para la viabilidad del escalado de un proceso de extracción es la reutilización y regeneración del disolvente. En este sentido, la realización de etapas de extracción consecutivas con alimentos en agua residual hospitalaria a pH 5,0, carvacrol como disolvente de extracción y una relación S/F de 1,00, mostró una disminución de los rendimientos en cada etapa. Esta tendencia fue más pronunciada para el sulfametoxazol, seguido de la ciprofloxacina y la trimetoprima. Sin embargo, durante las primeras 5 etapas, la reutilización del disolvente condujo a rendimientos de extracción superiores al 83, 96 y 98 % para el sulfametoxazol, ciprofloxacina y trimetoprima, respectivamente.

Por otro lado, los rendimientos de extracción con el disolvente regenerado se encontraron muy próximos a los obtenidos con el disolvente fresco (etapa 1). El carvacrol, por tanto, no sólo permitió la eliminación de más del 98 % del contenido global de antibióticos en una sola etapa de extracción, sino que su regeneración mediante destilación a vacío y su aplicación en procesos en continuo también resultaron viables técnicamente.

4.3 Publicación 3: Procesos CWPO y de adsorción para la eliminación de ciprofloxacina

Journal of Molecular Liquids

"Influence of transition metal-based activating agent on the properties and catalytic activity of sewage sludge-derived catalysts. Insights on mechanism, DFT calculation and degradation pathways"

Factor de impacto (2021): 6,633

Posición: Primer Cuartil (Q1)

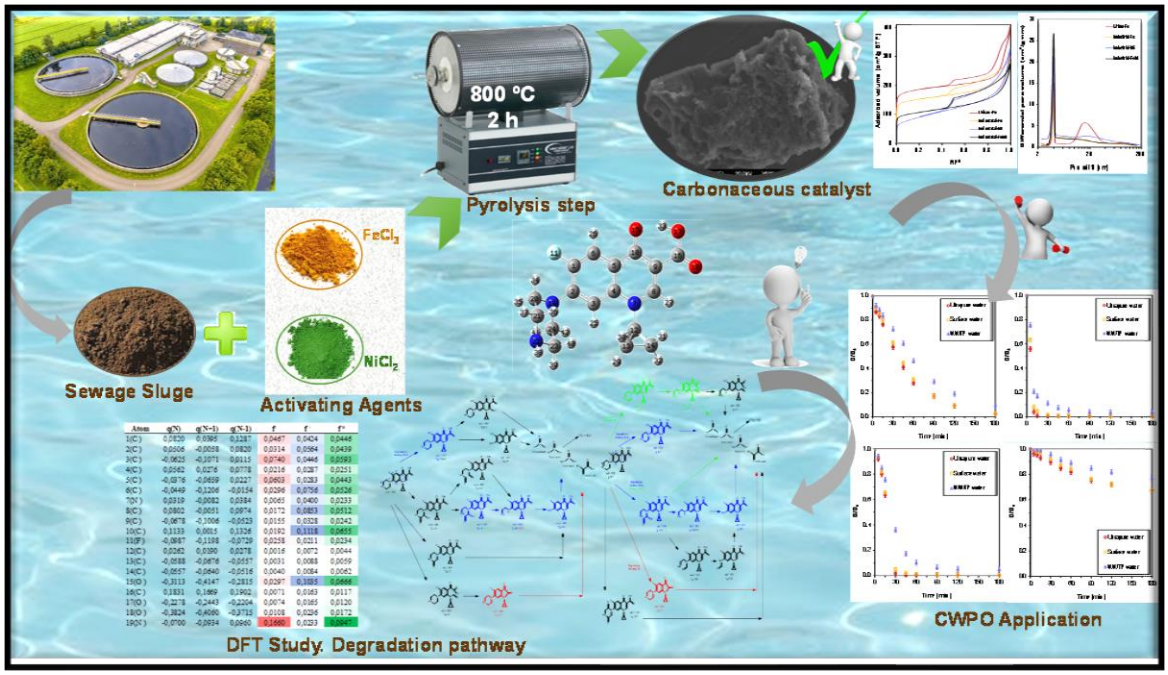

DOI: 10.1016/j.molliq.2023.121840

4.3.1 Caracterización de los materiales carbonosos

Aunque el contenido inicial de carbono fue muy similar en los lodos industriales (42,4 %) y urbanos (37,9 %), el origen del precursor biomásico tuvo una influencia significativa en la composición final. Es decir, los lodos industriales proporcionaron materiales con un contenido en carbono superior al 70 %, y los procedentes de los lodos urbanos tan sólo alcanzaron el 23 %. Por tanto, mientras que el proceso pirolítico pareció enriquecer en carbono los primeros, con materiales procedentes de lodos urbanos ocurrió lo contrario, evidenciando una diferencia en los mecanismos de reacción durante la pirólisis en función de la composición del lodo utilizado como precursor, tal y como se ha señalado en otros estudios. También fue destacable la contribución del oxígeno en el material Urban-Fe (28,3 %), en comparación con la muestra Industrial-Fe (8,5 %), pudiéndose atribuir al contenido de hierro tan significativo presente en los lodos urbanos (11,6 %), que favorecería su combinación con el oxígeno para generar óxidos metálicos. La presencia de hierro en el biorresiduo urbano, en esa proporción, podría haber promovido su fijación en la matriz sólida, alcanzándose un contenido cercano a 9,3 % para el material Urban-Fe. En este sentido, el carbón procedente del lodo industrial tan solo presentó un contenido de hierro próximo al 5,1 %. El silicio también fue uno de los elementos principales del catalizador Urban-Fe (14,9 %).

En cuanto a la influencia del agente activante, se comparó la composición de tres catalizadores obtenidos a partir del mismo precursor biomásico, es decir, lodos industriales. Los agentes empleados fueron sales de hierro y níquel, y una mezcla de ambos. Se observó un contenido de carbono notablemente más elevado para el catalizador sintetizado con $FeCl_3$ (Industrial-Fe) en comparación con el obtenido utilizando $NiCl_2$ (Industrial-Ni). El catalizador bimetálico (Industrial-FeNi) mostró un valor intermedio a los obtenidos para los anteriores, aunque mucho más próximo al catalizador Industrial-Ni. La contribución de oxígeno fue considerablemente mayor para los dos catalizadores basados en Ni, ya sea puro (13,6 %) o como mezcla con la sal de hierro (14,4 %). Es decir, mientras que para el catalizador Industrial-Fe se redujo el contenido de oxígeno a aproximadamente la mitad del presente en el lodo, los catalizadores de níquel y bimetálicos mostraron una variación poco significativa. A diferencia de lo obtenido para los materiales sintetizados con la sal

de hierro, la de níquel provocó una ligera reducción del contenido en cloro, nitrógeno y silicio, mientras que el contenido en potasio mostró la tendencia opuesta. También se observó una marcada diferencia en la concentración de metal fijada en la matriz carbonosa, es decir, mientras que en el catalizador Industrial-Ni se encontró un 26,8 % de níquel, el material Industrial-Fe sólo alcanzó un 5,1 % de hierro. Además, cabría esperar que, al utilizar una menor cantidad relativa de cloruro de hierro y níquel en la síntesis del catalizador Industrial-FeNi (1 g de lodo seco: 0,5 g de sal de hierro: 0,5 g de sal de níquel), el contenido de estos metales en la muestra final se situara entre los valores de los catalizadores obtenidos a partir de una única sal metálica. Sin embargo, el catalizador bimetálico mostró una mayor concentración de hierro que el Industrial-Fe, mientras que el contenido de níquel fue inferior al encontrado en el Industrial-Ni. El uso de una disolución bimetálica, por tanto, favoreció la fijación del hierro y redujo la de níquel. La etapa de lavado durante la síntesis de los materiales permitió eliminar la mayor parte del calcio presente en los lodos industriales, reduciéndose desde un 11,7 % hasta valores inferiores al 0,6 %.

El comportamiento de los catalizadores sintetizados cuando se sometieron a un proceso de fisisorción de nitrógeno sugirió una combinación de isotermas Tipo I-IV con ciclos de histéresis tipo H3-H4, característico de sólidos mesoporosos con una contribución moderada de microporosidad. Las curvas de desorción mostraron un descenso en forma de escalón a valores de P/P^0 cercanos a 0,5, lo que podría indicar una cavitación inducida por la evaporación del líquido condensado en mesoporos más grandes (efecto de condensación capilar). Las áreas superficiales BET evidenciaron la influencia que presentan tanto el origen del precursor biomásico como el agente activante sobre las propiedades texturales: Urbano-Fe (713 m^2/g) > Industrial-Fe (582 m^2/g) > Industrial-FeNi (397 m^2/g) > Industrial-Ni (319 m^2/g). Estos valores se encuentran dentro del intervalo reportado en la bibliografía para otros materiales carbonosos obtenidos a partir de lodos mediante activación química con $FeCl_3$ (S_{BET} = 468 m^2/g) y $ZnCl_2$ (S_{BET} = 266-558 m^2/g). El volumen total de poros disminuyó en el siguiente orden: Urban-Fe > Industrial-Ni > Industrial-Fe > Industrial-FeNi, mientras que el volumen relativo de microporos mostró una tendencia diferente: Industrial-Fe > Urban-Fe > Industrial-FeNi > Industrial-Ni. Por lo tanto, aunque el cloruro de hierro (III) generó una ligera disminución del volumen total de

poros, el desarrollo de la microporosidad se vio considerablemente favorecido. Además, el uso de una mezcla de haluros metálicos proporcionó un material con un volumen total de poros inferior al de los catalizadores sintetizados con un único agente activante, pero la microporosidad relativa se situó entre ambos. La heterogeneidad en la composición de los lodos según su origen también pareció tener un efecto notable. En este sentido, el desarrollo de una mayor porosidad total con los lodos urbanos podría asociarse, en parte, a su alto contenido en hierro (11,6 %). Por el contrario, la contribución relativa de la microporosidad fue ligeramente inferior a la obtenida para el Industrial-Fe, ya que el precursor industrial presentó un elevado contenido en calcio (11,7 %), que se eliminó durante la etapa de lavado y desbloqueó los poros ocupados en la matriz carbonosa. La distribución del tamaño de poro puso de manifiesto la naturaleza micro-mesoporosa de los materiales, con valores medios que oscilaron entre 6,8 y 10,4 nm.

En lo referente a la química superficial, todos los carbones mostraron una banda entre 3700 y 2800 cm^{-1}, que podría estar relacionada tanto con la presencia de enlaces O-H en la superficie como con la humedad adsorbida. También podría atribuirse a las vibraciones de estiramiento N-H relacionadas con amidas y aminas de las proteínas encontradas en los lodos de depuradora. No obstante, el bajo contenido de nitrógeno en comparación con el oxígeno en los materiales finales parecía sugerir una mayor contribución de los enlaces O-H. Las vibraciones de estiramiento de los enlaces alifáticos C-H se mostraron en la banda a 2650 cm^{-1}, mientras que los enlaces C=O y C=C, de grupos carbonilo y anillos aromáticos, aparecieron a 1600 cm^{-1}. Este último pico resultó extremadamente dependiente del origen del precursor, destacando el Urban-Fe frente al Industrial-Fe. La banda situada entre 1000 y 1200 cm^{-1} podría explicarse por el enlace C-O en alcoholes, fenoles, ácidos, éteres o ésteres. Los picos de absorción entre 900 y 1200 cm^{-1} podrían estar relacionados con enlaces Si-O-Si y enlaces Si-O-C, explicando la elevada intensidad para el Urban-Fe debido a su alto contenido en silicio. Las bandas presentes en el intervalo 400-800 cm^{-1} podrían revelar la presencia de enlaces O-H y C-H.

Las micrografías SEM confirmaron la presencia de muestras con una porosidad altamente desarrollada y heterogénea, visualizándose pequeñas partículas de metal depositadas sobre su superficie.

Por último, con respecto a la estabilidad térmica de los biocarbones, se observó una pérdida de masa en torno a los 100 °C, relacionada con el agua adsorbida. Tanto el origen del precursor como el agente activante influyeron en el contenido de humedad de las muestras: Urban-Fe (12,2 %) > Industrial-FeNi (7,9 %) > Industrial-Fe (7 %) > Industrial-Ni (5,1 %). Es decir, el uso de lodo urbano o de sales de hierro generó catalizadores con una mayor humedad. El catalizador bimetálico mostró una humedad superior a la obtenida para los materiales sintetizados con un solo haluro metálico. Por encima de 100 ºC se evidenció una tendencia ligeramente decreciente en la masa de los sólidos, que podría estar asociada a la descomposición de compuestos que no tuvieron tiempo de degradarse durante el proceso de síntesis. Además, a temperaturas cercanas a la de pirólisis, es decir, entre 700 y 900 °C, se observó una variación más pronunciada, eliminándose todos aquellos compuestos que requieren temperatura y/o tiempos superiores. El catalizador Industrial-Fe fue el material con la menor variación de masa, es decir, el de mayor estabilidad térmica.

4.3.2 Blancos de adsorción

Los materiales carbonosos derivados de procesos pirolíticos presentan generalmente propiedades adsorbentes como resultado de la porosidad generada durante su síntesis. Por lo tanto, para determinar la eficacia de los catalizadores en los sistemas de reacción heterogéneos, se requiere la realización de blancos de adsorción que permitan evaluar la contribución de la adsorción al proceso de eliminación de contaminantes.

En cuanto a la influencia del origen del precursor biomásico, el material sintetizado a partir de lodos industriales mostró una cinética de adsorción considerablemente más lenta en comparación con la del obtenido a partir del biorresiduo urbano. Es decir, mientras que el catalizador Urban-Fe requirió tiempos superiores a 45 min para alcanzar el equilibrio, para el Industrial-Fe fue necesario más de 120 min. Por otro lado, el $ZnCl_2$ permitió obtener biocarbones con cinéticas más rápidas que las mostradas con el $FeCl_3$. Concretamente, el Industrial-Ni requirió tiempos superiores a 60 min para alcanzar el equilibrio. La mezcla de agentes activantes generó sólidos porosos con cinéticas similares a las asociadas a la sal de hierro. Por lo tanto, el cloruro de hierro (III) pareció determinar la cinética del

catalizador bimetálico, haciendo que el tiempo de equilibrio fuera el mismo que para el Industrial-Fe, es decir, 120 min.

Con respecto a la concentración de equilibrio para la dosis de carbón empleada (0,3 g/L), se alcanzaron valores de 30,1, 27,8, 37,9 y 30,2 mg/L para el Urban-Fe, Industrial-Fe, Industrial-Ni e Industrial-FeNi, respectivamente. Por lo tanto, las capacidades de adsorción de ciprofloxacina para los materiales sintetizados fueron 66,3, 73,9, 40,4 y 66,0 mg/g. Estos resultados se encuentran en sintonía con lo reportado en la bibliografía para otros adsorbentes derivados de precursores biomásicos y aplicados a la eliminación tanto de ciprofloxacina como de otros contaminantes emergentes.

El estudio de la matriz acuosa en el proceso de adsorción evidenció un efecto relativamente pequeño en los cuatro materiales. En este sentido, aunque la cinética mantuvo una tendencia similar, las concentraciones de ciprofloxacina en la fase acuosa sufrieron un ligero aumento en el siguiente orden: agua ultrapura < agua superficial < agua EDAR. La menor eliminación del antibiótico en las matrices reales, en comparación con el agua ultrapura, podría deberse a la presencia de otros compuestos orgánicos e inorgánicos que compiten por los sitios activos del sólido. Este hecho también explicaría que la menor capacidad de adsorción fuera la correspondiente a la matriz del efluente de EDAR, cuyos parámetros macroscópicos indicaron una demanda química de oxígeno, carbono orgánico total, y sólidos disueltos totales considerablemente elevados.

4.3.3 Oxidación promovida por peróxido de hidrógeno

La cinética de degradación de la ciprofloxacina utilizando el catalizador Urban-Fe fue considerablemente más lenta que la mostrada para el Industrial-Fe. Es decir, mientras que el primero necesitó tiempos superiores a 180 min para alcanzar una eliminación del 98 %, el catalizador de hierro procedente de lodo industrial lo hizo antes de 30 min. Además, durante los primeros 15 min, el perfil de reacción para el Urban-Fe fue idéntico al mostrado en los blancos de adsorción. Esto podría deberse a la formación de una concentración mínima de radicales hidroxilo para iniciar la reacción de oxidación. Este tiempo se redujo considerablemente para el Industrial-Fe, coincidiendo los perfiles de adsorción y reacción sólo hasta los primeros 5 min. Por otra parte, a pesar de que el contenido de hierro para el

Industrial-Fe (5,1 %) fue considerablemente inferior al Urban-Fe (9,3 %), la actividad catalítica mostró la tendencia opuesta. Este comportamiento evidenció una mayor dispersión y accesibilidad de la fase activa en la superficie del catalizador Industrial-Fe, lo que condujo a una mayor lixiviación del metal. Concretamente, la concentración de hierro en el medio de reacción para una eliminación de ciprofloxacina cercana al 98% fue de 0,48 mg/L (a 180 min) y 0,61 mg/L (a 30 min) para los catalizadores Urban-Fe e Industrial-Fe, respectivamente. Por lo tanto, el origen de los lodos influyó considerablemente en la actividad catalítica de los catalizadores sintetizados.

En cuanto a la influencia del agente activante, el níquel mostró una actividad catalítica significativamente más desfavorable que el hierro. Es decir, mientras que el catalizador Industrial-Fe, con un 5,1 % de hierro, alcanzó una eliminación del 99,7 %, la obtenida para el Industrial-Ni, con un 26,8 % de níquel, fue del 32,5 %. El catalizador bimetálico mostró una cinética de degradación más rápida que el catalizador Industrial-Fe, lo que podría asociarse principalmente a su mayor contenido en hierro (8,7 %), puesto que el níquel (15,8 %) no mostró evidencias de ser catalíticamente activo en el proceso CWPO. De esta forma, mientras que el material Industrial-FeNi únicamente necesitó 15 min para eliminar el antibiótico casi por completo, el Industrial-Fe requirió 15 min más. Sin embargo, aunque se vio favorecida la cinética, la lixiviación de metales en el medio de reacción fue considerablemente mayor, por lo que el catalizador Industrial-Fe podría considerarse como el material óptimo para este proceso.

La cinética y la actividad catalítica dependieron de la matriz acuosa y, al igual que lo observado en los blancos de adsorción, disminuyeron en el siguiente orden: agua ultrapura > agua superficial > agua de EDAR. Este efecto podría estar relacionado con la presencia de contaminantes en las aguas reales que competirían con la ciprofloxacina durante la reacción.

Con respecto al mecanismo de reacción, los radicales hidroxilo procederían de tres vías: de los metales presentes en la superficie del catalizador sólido, de la pequeña cantidad de iones metálicos lixiviados al medio de reacción, y de los grupos funcionales del biocarbón que contienen oxígeno. Como paso final, la molécula de ciprofloxacina reaccionaría con los radicales generados para formar CO_2, H_2O y otros intermedios.

4.4 Publicación 4: Procesos WAO, CWAO y de adsorción para la eliminación de ciprofloxacina

Journal of Environmental Chemical Engineering

"Efficient removal of antibiotic ciprofloxacin by catalytic wet air oxidation using sewage sludge-based catalysts: Degradation mechanism by DFT studies"

Factor de impacto (2021): 7,968

Posición: Primer Cuartil (Q1)

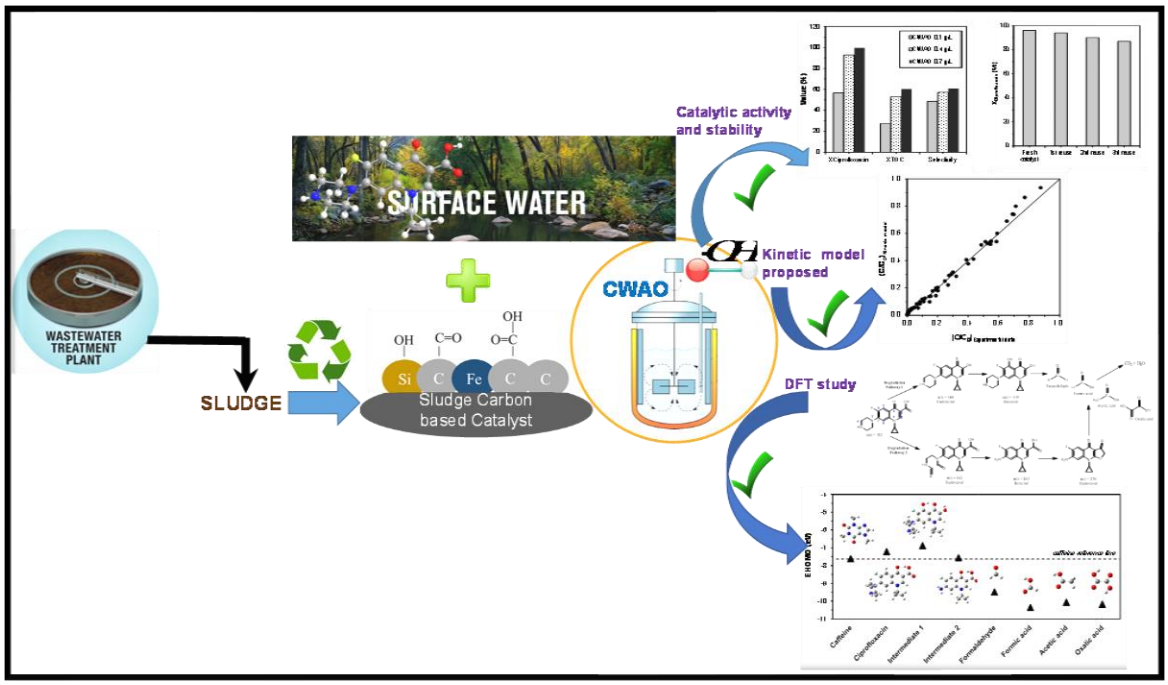

DOI: 10.1016/j.jece.2023.109344

4.4.1 Caracterización de los materiales carbonosos

El análisis elemental del catalizador sintetizado proporcionó el contenido de carbono (70,9 %), nitrógeno (3,8 %) e hidrógeno (1,8 %), mientras que el análisis por fluorescencia de rayos X permitió conocer el contenido de otros elementos principales, como el oxígeno (8,5 %) y el hierro (5,1 %). La etapa de pirólisis aumentó el contenido de carbono presente en el precursor biomásico, hasta aproximadamente el 67 % de su valor inicial. Durante este proceso, el contenido de oxígeno e hidrógeno también se redujo. Aunque el lodo empleado se caracterizó por un elevado contenido en calcio, la concentración en el material resultante fue poco significativa, posiblemente debido al lavado realizado durante la síntesis del catalizador.

Según la clasificación de la Unión Internacional de Química Pura y Aplicada, el material carbonoso mostró una isoterma de tipo IV con un ciclo de histéresis tipo H4, representativa de materiales mesoporosos. La adsorción inicial de nitrógeno, a valores de presión relativa inferiores a 0,05, indicó la presencia de microporos en la estructura. El área superficial BET fue de 582 m^2/g, que se encuentra dentro del intervalo señalado por otros autores para materiales carbonosos sintetizados a partir de lodos. Además, se obtuvo un volumen de microporos de 0,17 cm^3/g, correspondiente al 47,5 % del volumen total de poros. La distribución del tamaño de poro reveló un máximo en la zona mesoporosa, alrededor de 4 nm, y el diámetro medio de poro, calculado a partir del modelo BJH, fue de 7,2 nm. Estos valores justifican la histéresis, ya que ocurre cuando el ancho de los poros excede un valor crítico, que depende del adsorbato, la temperatura y la estructura porosa. Para el nitrógeno a -196 ºC, dicho fenómeno se produce para valores superiores a 4 nm. La microscopía electrónica de barrido confirmó la existencia de una superficie rugosa y porosa, con una estructura heterogénea formada por pequeñas partículas de hierro de diferente forma y tamaño adheridas a la matriz sólida. El agente activante empleado pareció haber generado una red compleja de poros, con cavidades y grietas en su superficie.

El perfil de degradación térmica mostró tres zonas claramente definidas. La primera se encontró a 100 ºC, donde se alcanzó una pérdida de masa del 7 % debido a la evaporación del agua adsorbida. La segunda zona se localizó en el intervalo 150-750 ºC, variando hasta un 12 % el valor de su masa inicial. La temperatura de pirólisis (800 ºC) explicaría esta

variación tan pequeña, asociada a compuestos tanto volátiles como de alto peso molecular que no fueron completamente eliminados durante el proceso. Finalmente, a temperaturas superiores a 800 ºC, la degradación térmica del catalizador aumentó sustancialmente, alcanzando una pérdida de masa cercana al 18 % a 1000 ºC. Esta disminución tan drástica se explicaría por la eliminación de compuestos de alto peso molecular que no tuvieron tiempo de degradarse durante la síntesis del catalizador y aquellos que requirieron una temperatura más elevada para hacerlo.

4.4.2 Blancos de adsorción

Las pruebas iniciales para determinar la contribución de la adsorción de ciprofloxacina a 140 ºC y 20 bar evidenciaron que, durante el acondicionamiento se alcanzó el equilibrio. Es decir, el tiempo requerido para alcanzar la temperatura de operación fue suficiente para saturar el material.

Con respecto a la concentración relativa de equilibrio en la fase acuosa, se alcanzaron valores próximos a 0,55, 0,70 y 0,88 para dosis de adsorbente de 0,70, 0,40 y 0,10 g/L, respectivamente. Por tanto, las capacidades de adsorción de ciprofloxacina en el equilibrio fueron de 32,1, 37,5 y 60,0 mg/g. Estos valores se encuentran dentro del orden de magnitud reportado por otros autores para adsorbentes derivados de precursores biomásicos y aplicados a la eliminación de ciprofloxacina.

4.4.3 Oxidación húmeda catalítica y no catalítica

El ensayo del proceso WAO a 140 °C y 20 bar, mostró una cinética de reacción considerablemente lenta, requiriendo un tiempo de alrededor de 1 h para eliminar menos del 17 % de la concentración inicial de ciprofloxacina. Además, durante los primeros 15 min se observa un periodo de inducción en el que apenas se produce degradación, debido al tiempo requerido para la generación de una concentración mínima de radicales hidroxilo que desencadene la reacción. El uso del catalizador sintetizado permitió la eliminación de esta etapa en todas las reacciones CWAO consideradas, minimizando el tiempo necesario para comenzar a degradar el contaminante.

La temperatura es una de las variables de operación con un efecto más significativo en los procesos de CWAO, ya que la producción de radicales libres, que inician la reacción de oxidación, se incrementa a medida que lo hace la temperatura. Este hecho podría deberse a la contribución de dos factores, la influencia en la constante cinética y la solubilidad del oxígeno en el medio acuoso, es decir, la concentración de uno de los reactivos. Según la bibliografía, la solubilidad del oxígeno en agua por encima de 100 °C y a alta presión muestra una tendencia creciente al aumentar la temperatura. Este comportamiento es cada vez más notable a presiones más elevadas. No obstante, la solubilidad del oxígeno a 20 bar muestra un ligero aumento entre 120 ºC (54,7 mg O_2/L) y 160 ºC (67,4 mg O_2/L), por lo que podría pensarse que el efecto de la temperatura tiene un mayor efecto sobre la constante cinética que sobre la concentración del agente oxidante.

El análisis de este parámetro se realizó variando la temperatura entre 120 y 180 ºC, y manteniendo constantes la presión total (20 bar) y la dosis de catalizador (0,7 g/L). El proceso catalítico mostró una pequeña eliminación a tiempo cero de reacción, lo que podría deberse a la contribución tanto de la degradación térmica como de la adsorción durante el tiempo de acondicionamiento. Sin embargo, el análisis de la muestra a tiempo cero mediante LC-MS no detectó compuestos de degradación térmica por lo que la eliminación del antibiótico en el medio acuoso únicamente se debió a la adsorción. La concentración de antibiótico alcanzó valores cercanos al 20 % de su valor inicial a los 15, 30 y 60 min, para temperaturas de 160, 140 y 120 ºC, respectivamente. Esta diferencia fue más pronunciada a altas conversiones y 120 ºC, alcanzando una eliminación del 95 % a las 3 h de reacción, mientras que a las otras temperaturas ensayadas se alcanzaron valores superiores al 99 % entre 1 y 2 h antes. Aunque un aumento de la temperatura favorece la conversión de ciprofloxacina, ocurre lo contrario con el carbono orgánico total. Por tanto, a pesar de que la concentración a 180 min fue muy similar a las tres temperaturas, un aumento de la concentración de carbono orgánico se tradujo en una menor selectividad hacia CO_2, es decir, una menor mineralización del fármaco. Este comportamiento podría deberse a una modificación de la ruta de reacción o a un aumento de la velocidad de producción de algún intermedio altamente recalcitrante. Después de 180 min, el pH final se mantuvo constante en el intervalo 3,9-4,2. Teniendo en cuenta los aspectos mencionados anteriormente, la temperatura óptima para el proceso fue 140 ºC.

El equilibrio gas-líquido también es función de la presión, por lo que la eliminación de ciprofloxacina podría verse afectada. Concretamente, la solubilidad del oxígeno en agua oscila entre 29,8 y 89,4 mg O_2/L para una presión total de 10 y 30 bar a 140 ºC, respectivamente. La degradación del antibiótico mostró una ligera mejora con el aumento de la presión total, aunque podría considerarse despreciable para el intervalo de presiones evaluado. Es decir, la conversión no parece depender de la concentración de oxígeno disuelto, al menos en el intervalo considerado. Este comportamiento valida lo mencionado en el estudio de la temperatura sobre su influencia mayoritaria en la constante cinética, y no tanto sobre la concentración de oxígeno disuelto, pues la variación de la solubilidad del oxígeno entre 120 y 160 ºC a 20 bar se encuentra dentro de los valores obtenidos entre 10 y 30 bar a 140 ºC. La presión también tuvo un efecto poco significativo sobre la conversión de carbono orgánico total, la selectividad a CO_2, la velocidad de reacción inicial y el pH final. La presión óptima se fijó en 20 bar, ya que un aumento de este parámetro no mejoró sustancialmente la degradación de ciprofloxacina.

La dosis de catalizador se estudió en el intervalo de 0,1-0,7 g/L, mostrando un impacto significativo en la eliminación del antibiótico. El aumento de la dosis generó un incremento tanto en la degradación del fármaco como del carbono orgánico total, siendo más notable para valores superiores a 0,10 g/L. Tras 1 h de reacción, se alcanzaron concentraciones relativas próximas a 0,65, 0,27 y 0,08 empleando dosis de catalizador de 0,1, 0,3 y 0,7 g/L, respectivamente. Según esta tendencia, concentraciones de catalizador por encima de 0,7 g/L no compensarían la ligera mejora en la eliminación del compuesto.

La velocidad inicial de reacción se redujo al aumentar la dosis, lo que podría deberse a la disminución de la concentración de ciprofloxacina en el fluido como resultado de la mayor contribución de adsorción. Además, los procesos CWAO ocurren por vía radicalaria. En este sentido, si la reacción se produjera sólo en la superficie del catalizador, la velocidad de reacción por unidad de masa de catalizador sería independiente de la dosis. La dependencia de la velocidad con la concentración de catalizador, según un orden menor a la unidad, indicaría una combinación de mecanismos radicalarios homogéneos y heterogéneos, como se ha discutido en la bibliografía.

En todos los estudios realizados, el catalizador mostró una lixiviación de hierro inferior a 0,024 mg/L y el pH final del medio de reacción alcanzó valores entre 4 y 5, es decir, ligeramente más ácido que el inicial. Esto evidenciaría la formación de ácidos de cadena corta refractarios a los procesos de oxidación. Los ensayos en agua de río mostraron una adsorción inicial y conversiones ligeramente inferiores, debido a la presencia de otros contaminantes orgánicos que compiten con la ciprofloxacina. Es decir, en el proceso CWAO, los radicales hidroxilo generados intervienen en la oxidación de otros compuestos existentes en la matriz real. Las tres reutilizaciones del catalizador en matrices reales confirmaron su elevada estabilidad. Durante el primer ciclo, se alcanzó una conversión del 94 %, es decir, un 2 % inferior a la obtenida con el catalizador fresco. Para el segundo y el tercero, la eliminación a 120 min fue del 90 y 87 %, respectivamente.

El modelado cinético de la reacción se realizó mediante una expresión de tipo potencial, definiendo también un parámetro denominado “concentración inicial efectiva” que contemplara la contribución de la adsorción durante el tiempo de acondicionamiento. El ajuste obtenido no solo ofreció un valor elevado de R^2, sino que mostró desviaciones pequeñas, aleatorias y no sistemáticas de los datos experimentales con respecto a los predichos. La pequeña influencia de la presión total en el proceso generó un orden parcial próximo a cero ($m = 0,13$). El orden de la dosis de catalizador fue inferior a la unidad ($z = 0,2$), estando dentro de los valores encontrados en la literatura para procesos CWAO similares y teniendo en cuenta tanto las contribuciones heterogéneas como homogéneas en el proceso de reacción. La energía de activación del proceso catalítico (53,8 kJ/mol) se encontró muy próxima a la reportada para otros catalizadores con metales más costosos y tóxicos que el hierro (alrededor de 40 kJ/mol empleando rutenio y platino). Por tanto, el enfoque propuesto en este estudio no sólo permitió la valorización de un residuo como son los lodos de depuradora, sino que el material sintetizado mostró una actividad catalítica y pérdida de la fase activa comparable a la obtenida para catalizadores basados en metales nobles. Asimismo, el uso del catalizador disminuyó la energía de activación del proceso de oxidación húmeda no catalítica de ciprofloxacina (70 kJ/mol).

CAPÍTULO V

Conclusiones

La presente Tesis Doctoral ha contribuido a la elaboración de un marco de procesos de eliminación de contaminantes emergentes en disolución acuosa. De esta forma, se ha propuesto y desarrollado una serie de metodologías técnicamente viables que permiten establecer una ingeniería química básica general, a fin de abordar uno de los problemas medioambientales que más impacto social, político, económico y medioambiental está generando. La estructuración del contenido se ha realizado de la siguiente forma:

- Publicación 1: Extracción líquido-líquido de pesticidas neonicotinoides.
- Publicación 2: Extracción líquido-líquido de antibióticos.
- Publicación 3: Procesos CWPO y de adsorción para la eliminación de ciprofloxacina.
- Publicación 4: Procesos WAO, CWAO y de adsorción para la eliminación de ciprofloxacina.
- Futuras investigaciones.

5.1 Publicación 1: Extracción líquido-líquido de pesticidas neonicotinoides

El crecimiento de la industria de los pesticidas ha promovido la presencia de estos contaminantes emergentes en el medio acuático. Esta investigación se centra en la extracción líquido-líquido de tres pesticidas neonicotinoides (acetamiprid, imidacloprid y tiametoxam) en matrices acuosas mediante el uso de disolventes alternativos, como los terpenoides y disolventes eutécticos, que presentan un menor impacto medioambiental. La selección inicial, se realizó mediante simulación molecular con la metodología COSMO-RS. Las pruebas experimentales de extracción mostraron resultados prometedores, alcanzándose rendimientos de extracción para los terpenos puros considerablemente superiores a los convencionales, mientras que esta diferencia fue ligeramente menor en el caso de los disolventes eutécticos. Concretamente, el carvacrol mostró rendimientos próximos al 95 % para el tiametoxam y superiores al 98 y 99 % para el imidacloprid y el acetamiprid, respectivamente, a una relación S/F de 0,1, una temperatura de 30 ºC y matriz de agua ultrapura. Además, el efecto de la matriz, el pH del alimento y la temperatura no fueron significativos para la extracción de pesticidas con este terpenoide.

5.2 Publicación 2: Extracción líquido-líquido de antibióticos

En este estudio se ha propuesto la extracción líquido-líquido multicomponente de tres de los antibióticos (ciprofloxacino, trimetoprima y sulfametoxazol) incluidos en las Listas de Observación de la Unión Europea, utilizando terpenoides y mezclas eutécticas. A partir de los coeficientes de actividad a dilución infinita, estimados con la metodología COSMO-RS, se realizó un cribado inicial de los disolventes de extracción. Los terpenoides y las mezclas eutécticas presentaron rendimientos globales de extracción considerablemente superiores a los obtenidos con los disolventes convencionales, para cualquier pH y matriz acuosa. Sin embargo, ningún valor de pH permitió alcanzar el óptimo para la extracción simultánea de los tres antibióticos, que varió según sus equilibrios de disociación. Aunque

los disolventes eutécticos mostraron una menor sensibilidad a los cambios de pH en el alimento, el carvacrol se posicionó como el extractante más favorable, ofreciendo rendimientos del 98,9, 99,5 y 97,0 % para la trimetoprima, ciprofloxacina y sulfametoxazol, respectivamente, empleando matrices reales a pH 5,0 y relación S/F 1,00. Además, las pérdidas de disolvente en la fase acuosa fueron sustancialmente inferiores a las encontradas con los compuestos orgánicos convencionales. Los ensayos realizados en columnas de extracción, empleando tiempos de residencia bajos, mostraron que no existe limitación a la transferencia de materia. También se evaluó con éxito la reutilización del carvacrol durante cinco etapas consecutivas y su recuperación mediante un evaporador rotatorio a 164 °C y 20 mbar.

5.3 Publicación 3: Procesos CWPO y de adsorción para la eliminación de ciprofloxacina

En este artículo se abordó la valorización de lodos de depuradora mediante procesos pirolíticos para producir materiales carbonosos con propiedades adsorbentes y/o catalíticas, que pudieran ser aplicados en la eliminación de contaminantes emergentes. En este sentido, el uso de lodos de depuradora como precursor biomásico promovió la generación de una gran variedad de grupos funcionales en su superficie. Todos los materiales exhibieron una combinación de isotermas de adsorción-desorción de nitrógeno tipo I-IV, con ciclos de histéresis tipo H3-H4. El tamaño medio de poro indicó una naturaleza mesoporosa, con una contribución moderada de la microporosidad. Las áreas superficiales BET oscilaron entre 397 y 713 m^2/g.

Los materiales mostraron capacidades de adsorción en el intervalo 40,4-73,9 mg/g, siendo el sintetizado con el haluro de níquel como agente activante el más bajo. Este último, también se caracterizó por una actividad catalítica en procesos CWPO significativamente baja, en comparación con el producido con $FeCl_3$. Aunque el catalizador bimetálico de hierro y níquel presentó un mayor contenido en hierro que el Industrial-Fe y una mayor actividad catalítica, la lixiviación de metales fue considerablemente más elevada.

5.4 Publicación 4: Procesos WAO, CWAO y de adsorción para la eliminación de ciprofloxacina

Esta investigación propone la eliminación de ciprofloxacina empleando materiales carbonosos sintetizados a partir de lodos de depuradora que puedan ser aplicados en procesos CWAO. La síntesis de los biocarbones, mediante activación química con $FeCl_3$, proporcionó materiales con un contenido en hierro y unas propiedades texturales y morfológicas adecuadas para su aplicación en este tipo de procesos. Concretamente, el catalizador de hierro mostró una elevada actividad catalítica, oxidando el contaminante emergente casi por completo tras 2 h de reacción y bajo las siguientes condiciones de operación: 140 °C, 20 bar y 0,7 $g_{Catalizador}$/L. La temperatura de reacción y la dosis de catalizador mostraron una influencia significativa, mientras que la presión total no pareció ser relevante en el intervalo analizado. El hierro lixiviado en el medio de reacción reveló una baja pérdida de la fase activa, mostrando valores inferiores a 0,024 mg/L. La propuesta de un modelo cinético de tipo potencial describió con éxito los resultados experimentales, alcanzándose un valor de R^2 de 0,990. El material sintetizado también presentó una actividad comparable a la reportada en la literatura para otros catalizadores basados en metales nobles. La viabilidad técnica del proceso se verificó a través de su eficacia con matrices reales y en ciclos consecutivos de reutilización del catalizador.

5.5 Futuras investigaciones

Las investigaciones incluidas en esta memoria han puesto de manifiesto la gran eficacia que presentan los procesos de extracción líquido-líquido, adsorción, oxidación húmeda y oxidación promovida por peróxido de hidrógeno para la eliminación de contaminantes emergentes. Sin embargo, todavía queda un largo recorrido en este campo.

En este sentido, y como continuación a los hallazgos discutidos en las publicaciones recogidas en este documento, se encuentran en fase de estudio y/o publicación los siguientes aspectos:

- Aplicación de materiales carbonosos procedentes de biomasa en procesos CWPO para la degradación de pesticidas neonicotinoides, como el acetamiprid, imidacloprid y tiametoxam.
- Empleo de otros adsorbentes, como los materiales arcillosos, para la eliminación de ciprofloxacina en disolución acuosa.
- Evaluación de otros agentes activantes, como el $ZnCl_2$ o el KOH, en la síntesis de materiales carbonosos a partir de lodos de depuradora de diferente procedencia, aplicándolos en procesos de adsorción y catálisis para el tratamiento de contaminantes emergentes.
- Empleo de terpenos y disolventes eutécticos para la extracción multicomponente con múltiples grupos de fármacos (como los analgésicos, antibióticos, antidepresivos o reguladores de presión), analizando otras variables como la extracción en contracorriente y la reutilización y regeneración del disolvente.
- Escalado de los diferentes tratamientos desarrollados y evaluación económica de los mismos.

Capítulo VI

Bibliografía

A. Quiroz, M., R. Bandala, E., & A. Martínez-Huitle, C. (2011). Advanced Oxidation Processes (AOPs) for Removal of Pesticides from Aqueous Media. *Pesticides - Formulations, Effects, Fate*.

Ahel, M., Mikac, N., Cosovic, B., Prohic, E., & Soukup, V. (1998). The impact of contamination from a municipal solid waste landfill (Zagreb, Croatia) on underlying soil. *Water Science and Technology*, *37*(8), 203–210.

Ahmed, M. B., Zhou, J. L., Ngo, H. H., Guo, W., Thomaidis, N. S., & Xu, J. (2017). Progress in the biological and chemical treatment technologies for emerging contaminant removal from wastewater: A critical review. *Journal of Hazardous Materials*, *323*, 274–298. https://doi.org/10.1016/j.jhazmat.2016.04.045

Ahnert, F., Arafat, H. A., & Pinto, N. G. (2003). A study of the influence of hydrophobicity of activated carbon on the adsorption equilibrium of aromatics in non-aqueous media. *Adsorption*, *9*, 311–319.

Alaqarbeh, M. (2021). Adsorption phenomena: Definition, mechanisms, and adsorption types: Short review. *RHAZES: Green and Applied Chemistry*, *13*, 43–51.

American Public Health Association. (2017). Standard methods for the examination of water and wastewater. In R. B. Baird, A. D. Eaton, & E. W. Rice (Eds.), *American Public Health Association, American Water Works Association, Water Environment Federation* (23rd ed.).

Artioli, Y. (2008). Adsorption. In S. E. Jørgensen & B. D. Fath (Eds.), *Encyclopedia of Ecology* (pp. 60–65). Academic Press. https://doi.org/https://doi.org/10.1016/B978-008045405-4.00252-4

Asano, T., Burton, F., & Leverenz, H. (2007). *Water reuse: issues, technologies, and applications*. McGraw-Hill Education.

Baquero, F., Martínez, J.-L., & Cantón, R. (2008). Antibiotics and antibiotic resistance in water environments. *Current Opinion in Biotechnology*, *19*(3), 260–265.

Barbosa, M. O., Moreira, N. F. F., Ribeiro, A. R., Pereira, M. F. R., & Silva, A. M. T. (2016). Occurrence and removal of organic micropollutants: An overview of the watch list of EU Decision 2015/495. *Water Research*, *94*, 257–279. https://doi.org/10.1016/j.watres.2016.02.047

Barceló, D., & Petrovic, M. (2008). *Emerging contaminants from industrial and municipal waste: occurrence, analysis and effects* (Vol. 5). Springer.

Barnes, K. K., Kolpin, D. W., Furlong, E. T., Zaugg, S. D., Meyer, M. T., & Barber, L. B. (2008). A national reconnaissance of pharmaceuticals and other organic wastewater contaminants in the United States—I) Groundwater. *Science of the Total Environment*, *402*(2–3), 192–200.

Bartelt-Hunt, S., Snow, D. D., Damon-Powell, T., & Miesbach, D. (2011). Occurrence of steroid hormones and antibiotics in shallow groundwater impacted by livestock waste control facilities. *Journal of Contaminant Hydrology*, *123*(3–4), 94–103.

Bell, K. Y., Bandy, J., Beck, S., Keen, O., Kolankowsky, N., Parker, A. M., & Linden, K. (2012). Emerging pollutants–part II: treatment. *Water Environment Research*, *84*(10), 1909–1940.

Ben Salha, G., Abderrabba, M., & Labidi, J. (2019). A status review of terpenes and their separation methods. *Reviews in Chemical Engineering*. https://doi.org/10.1515/revce-2018-0066

Benitez, F. J., García, J., Acero, J. L., Real, F. J., & Roldan, G. (2011). Non-catalytic and catalytic wet air oxidation of pharmaceuticals in ultra-pure and natural waters. *Process Safety and Environmental Protection*, *89*(5), 334–341.

Berk, Z. (2018). Extraction. In *Food Process Engineering and Technology* (Issue Chapter 12, pp. 289–310). https://doi.org/10.1016/c2016-0-03186-8

Bhargava, S. K., Tardio, J., Prasad, J., Föger, K., Akolekar, D. B., & Grocott, S. C. (2006). Wet oxidation and catalytic wet oxidation. *Industrial & Engineering Chemistry Research*, *45*(4), 1221–1258.

Boncan, D. A. T., Tsang, S. S. K., Li, C., Lee, I. H. T., Lam, H. M., Chan, T. F., & Hui, J. H. L. (2020). Terpenes and terpenoids in plants: Interactions with environment and insects. *International Journal of Molecular Sciences*, *21*(19), 1–19. https://doi.org/10.3390/ijms21197382

Bonilla-Petriciolet, A., Mendoza-Castillo, D. I., & Reynel-Ávila, H. E. (2017). *Adsorption processes for water treatment and purification* (Vol. 256). Springer.

Bouki, C., Venieri, D., & Diamadopoulos, E. (2013). Detection and fate of antibiotic resistant bacteria in wastewater treatment plants: a review. *Ecotoxicology and Environmental Safety*, *91*, 1–9.

Bound, J. P., & Voulvoulis, N. (2005). Household disposal of pharmaceuticals as a pathway for aquatic contamination in the United Kingdom. *Environmental Health Perspectives*, *113*(12), 1705–1711.

Boutekedjiret, C., Vian, M. A., & Chemat, F. (2014). Terpenes as Green Solvents for Natural Products Extraction. In *Alternative Solvents for Natural Products Extraction* (pp. 205–219). Springer Berlin Heidelberg. https://doi.org/10.1007/978-3-662-43628-8_9

Boxall, A. B. A. (2012a). *New and emerging water pollutants arising from agriculture*.

Boxall, A. B. A. (2012b). *New and emerging water pollutants arising from agriculture*.

Bracamontes-Ruelas, A. R., Ordaz-Díaz, L. A., Bailón-Salas, A. M., Ríos-Saucedo, J. C., Reyes-Vidal, Y., & Reynoso-Cuevas, L. (2022). Emerging Pollutants in Wastewater, Advanced Oxidation Processes as an Alternative Treatment and Perspectives. *Processes*, *10*(5), 1041.

Buszka, P. M., Yeskis, D. J., Kolpin, D. W., Furlong, E. T., Zaugg, S. D., & Meyer, M. T. (2009). Waste-indicator and pharmaceutical compounds in landfill-leachate-affected ground water near Elkhart, Indiana, 2000–2002. *Bulletin of Environmental Contamination and Toxicology*, *82*, 653–659.

Calvo-Flores, F. G., Isac-Garcéa, J., & Dobado, J. A. (2017). Industrial chemicals as emerging pollutant. *Emerging Pollutants: Origin, Structure and Properties, Wiley-VCH Verlag GmbH & Co. KGaA, Weinheim, Germany*, 265–340.

Carey, F. A. (2003). *Organic chemistry*. McGraw-Hill.

Carrara, C., Ptacek, C. J., Robertson, W. D., Blowes, D. W., Moncur, M. C., Sverko, E. D., & Backus, S. (2008). Fate of pharmaceutical and trace organic compounds in three septic system plumes, Ontario, Canada. *Environmental Science & Technology*, *42*(8), 2805–2811.

Carsanba, E., Pintado, M., & Oliveira, C. (2021). Fermentation strategies for production of pharmaceutical terpenoids in engineered yeast. *Pharmaceuticals*, *14*(4), 295.

Cavero, S. G., García-Gil, A., Cruz-Pérez, N., Rodríguez, L. F. M., Laspidou, C., Contreras-Llin, A., Quintana, G., Díaz-Cruz, S., & Santamarta, J. C. (2023). First emerging pollutants profile in groundwater of the volcanic active island of El Hierro (Canary Islands). *Science of the Total Environment*, *872*, 162204.

Chen, R., & Pignatello, J. J. (1997). Role of quinone intermediates as electron shuttles in Fenton and photoassisted Fenton oxidations of aromatic compounds. *Environmental Science & Technology*, *31*(8), 2399–2406.

Cheremisinoff, P. N. (2019). *Handbook of water and wastewater treatment technology*. Routledge.

Chorkendorff, I., & Niemantsverdriet, J. W. (2017). *Concepts of modern catalysis and kinetics*. John Wiley & Sons.

Christianson, D. W. (2017). Structural and chemical biology of terpenoid cyclases. *Chemical Reviews*, *117*(17), 11570–11648.

Chua, P. L. C., Seposo, X. T., & Hashizume, M. (2023). Chapter 9 - Heat exposure and the transmission of infectious diseases. In Y. Guo & S. Li (Eds.), *Heat Exposure and Human Health in the Context of Climate Change* (pp. 189–221). Elsevier. https://doi.org/https://doi.org/10.1016/B978-0-12-819080-7.00003-3

Clarke, B. O., & Smith, S. R. (2011). Review of 'emerging'organic contaminants in biosolids and assessment of international research priorities for the agricultural use of biosolids. *Environment International*, *37*(1), 226–247.

Cooper, E. R., Siewicki, T. C., & Phillips, K. (2008). Preliminary risk assessment database and risk ranking of pharmaceuticals in the environment. *Science of the Total Environment*, *398*(1–3), 26–33.

Cordy, G. E., Duran, N. L., Bouwer, H., Rice, R. C., Furlong, E. T., Zaugg, S. D., Meyer, M. T., Barber, L. B., & Kolpin, D. W. (2004). Do pharmaceuticals, pathogens, and other organic waste water compounds persist when waste water is used for recharge? *Groundwater Monitoring & Remediation*, *24*(2), 58–69.

Croteau, R., Kutchan, T. M., & Lewis, N. G. (2000). Natural products (secondary metabolites). In Bob B. Buchanan, Wilhelm Gruissem, & Russell L. Jones (Eds.), *Biochemistry and Molecular Biology of Plants* (pp. 1250–1319). John Wiley & Sons. https://books.google.es/books?id=yRIWCgAAQBAJ&dq=Biochemistry+and+Molecular+Biology+of+Plants&lr=&hl=es&source=gbs_navlinks_s

Dahuron, L., Holden, B. S., Prince, W. D., Seibert, A. F., Wilson, L. C., & Frank, T. C. (2008). Liquid-liquid extraction and other liquid-liquid operations and equipment. In *Perry's Chemical Engineers' Handbook*. McGraw-Hill Pub.

Díaz-Cruz, M. S., & Barceló, D. (2008). Trace organic chemicals contamination in ground water recharge. *Chemosphere*, *72*(3), 333–342.

Eggen, T., Moeder, M., & Arukwe, A. (2010). Municipal landfill leachates: a significant source for new and emerging pollutants. *Science of the Total Environment*, *408*(21), 5147–5157.

Eggersdorfer, M. (2000). Terpenes. *Ullmann's Encyclopedia of Industrial Chemistry*. https://doi.org/10.1002/14356007.a26_205

Engelbert, E. A., & Scheuring, A. F. (2022). *Water scarcity: Impacts on western agriculture*. Univ of California Press.

Englezos, N., Kartala, X., Koundouri, P., Tsionas, M., & Alamanos, A. (2023). A Novel HydroEconomic-Econometric Approach for Integrated Transboundary Water Management Under Uncertainty. *Environmental and Resource Economics*, *84*(4), 975–1030.

European Centre for Disease Prevention and Control. (n.d.). *Antimicrobial consumption dashboard (ESAC-Net)*. Retrieved May 18, 2023, from https://www.ecdc.europa.eu/en/antimicrobial-consumption/surveillance-and-disease-data/database

Falconer, I. R., Chapman, H. F., Moore, M. R., & Ranmuthugala, G. (2006). Endocrine-disrupting compounds: A review of their challenge to sustainable and safe water supply and water reuse. *Environmental Toxicology: An International Journal*, *21*(2), 181–191.

Furuichi, T., Kannan, K., Suzuki, K., Tanaka, S., Giesy, J. P., & Masunaga, S. (2006). Occurrence of estrogenic compounds in and removal by a swine farm waste treatment plant. *Environmental Science & Technology*, *40*(24), 7896–7902.

Garcia, J., Gomes, H. T., Serp, P., Kalck, P., Figueiredo, J. L., & Faria, J. L. (2005). Platinum catalysts supported on MWNT for catalytic wet air oxidation of nitrogen containing compounds. *Catalysis Today*, *102*, 101–109.

Gezahegn, T., Tegegne, B., Zewge, F., & Chandravanshi, B. S. (2019). Salting-out assisted liquid-liquid extraction for the determination of ciprofloxacin residues in water samples by high performance liquid chromatography-diode array detector. *BMC Chemistry*, *13*(28). https://doi.org/10.1186/s13065-019-0543-5

Glassmeyer, S. T., Hinchey, E. K., Boehme, S. E., Daughton, C. G., Ruhoy, I. S., Conerly, O., Daniels, R. L., Lauer, L., McCarthy, M., & Nettesheim, T. G. (2009). Disposal practices for unwanted residential medications in the United States. *Environment International*, *35*(3), 566–572.

González-González, R. B., Sharma, P., Singh, S. P., Américo-Pinheiro, J. H. P., Parra-Saldívar, R., Bilal, M., & Iqbal, H. M. N. (2022). Persistence, environmental hazards, and mitigation of pharmaceutically active residual contaminants from water matrices. *Science of The Total Environment*, 153329.

Goulson, D. (2013). An overview of the environmental risks posed by neonicotinoid insecticides. *Journal of Applied Ecology*, *50*(4), 977–987. https://doi.org/10.1111/1365-2664.12111

Gupta, V. K., Carrott, P. J. M., Ribeiro Carrott, M. M. L., & Suhas. (2009). Low-Cost Adsorbents: Growing Approach to Wastewater Treatment—a Review. *Critical Reviews in Environmental Science and Technology*, *39*(10), 783–842. https://doi.org/10.1080/10643380801977610

Gurr, C. J., & Reinhard, M. (2006). *Harnessing natural attenuation of pharmaceuticals and hormones in rivers*. ACS Publications.

Hayat, S., Gupta, J., Vegelin, C., & Jamali, H. (2022). A review of hydro-hegemony and transboundary water governance. *Water Policy*, *24*(11), 1723–1740.

Heberer, T., & Adam, M. (2004). Transport and attenuation of pharmaceutical residues during artificial groundwater replenishment. *Environmental Chemistry*, *1*(1), 22–25.

Heberer, T., Mechlinski, A., Fanck, B., Knappe, A., Massmann, G., Pekdeger, A., & Fritz, B. (2004). Field studies on the fate and transport of pharmaceutical residues in bank filtration. *Groundwater Monitoring & Remediation*, *24*(2), 70–77.

Heberer, T., Verstraeten, I. M., Meyer, M. T., Mechlinski, A., & Reddersen, K. (2001). Occurrence and fate of pharmaceuticals during bank filtration–preliminary results from investigations in Germany and the United States. *Journal of Contemporary Water Research and Education*, *120*(1), 2.

Hernando, M. D., Rodríguez, A., Vaquero, J. J., Fernández-Alba, A. R., & García, E. (2011). Environmental risk assessment of emerging pollutants in water: Approaches under horizontal and vertical EU legislation. *Critical Reviews in Environmental Science and Technology*, *41*(7), 699–731.

Holm, J. V, Ruegge, K., Bjerg, P. L., & Christensen, T. H. (1995). Occurrence and distribution of pharmaceutical organic compounds in the groundwater downgradient of a landfill (Grindsted, Denmark). *Environmental Science & Technology*, *29*(5), 1415–1420.

Houtman, C. J. (2010). Emerging contaminants in surface waters and their relevance for the production of drinking water in Europe. *Journal of Integrative Environmental Sciences*, *7*(4), 271–295.

Huang, C. P., Dong, C., & Tang, Z. (1993). Advanced chemical oxidation: its present role and potential future in hazardous waste treatment. *Waste Management*, *13*(5–7), 361–377.

Imamura, S. (1999). Catalytic and noncatalytic wet oxidation. *Industrial & Engineering Chemistry Research*, *38*(5), 1743–1753.

Insecticide Resistance Action Committee (IRAC). (n.d.). *The IRAC Mode of Action Classification*. Retrieved September 30, 2020, from https://irac-online.org/modes-of-action/

Jeschke, P., & Nauen, R. (2008). Neonicotinoids - From zero to hero in insecticide chemistry. In *Pest Management Science* (Vol. 64, Issue 11, pp. 1084–1098). John Wiley & Sons, Ltd. https://doi.org/10.1002/ps.1631

Jing, G., Luan, M., & Chen, T. (2016). Progress of catalytic wet air oxidation technology. *Arabian Journal of Chemistry*, *9*, S1208–S1213.

Jing, Q., & Li, H. (2019). Hierarchical nickel cobalt oxide spinel microspheres catalyze mineralization of humic substances during wet air oxidation at atmospheric pressure. *Applied Catalysis B: Environmental*, *256*, 117858.

Jones, C. W. (1999). *Applications of Hydrogen Peroxide and Derivatives. Royal Society of Chemistry*.

Karungamye, P. N. (2020). Methods used for removal of pharmaceuticals from wastewater: A review. *Applied Journal of Environmental Engineering Science*, *6*(4), 412–428.

Kaur, H., Hippargi, G., Pophali, G. R., & Bansiwal, A. K. (2019). Treatment methods for removal of pharmaceuticals and personal care products from domestic wastewater. In *Pharmaceuticals and Personal Care Products: Waste Management and Treatment Technology Emerging Contaminants and Micro Pollutants* (pp. 129–150). Elsevier. https://doi.org/10.1016/B978-0-12-816189-0.00006-8

Khan, M. Z. K. (2012). Micro-pollutant risks associated with using recycled water. *Journal of Civil Engineering (IEB)*, *40*(1), 11–22.

Kobayashi, M., & Kuzuyama, T. (2019). Structural and mechanistic insight into terpene synthases that catalyze the irregular non-Head-to-tail coupling of prenyl substrates. *ChemBioChem*, *20*(1), 29–33. https://doi.org/10.1002/cbic.201800510

Kolaczkowski, S. T., Plucinski, P., Beltran, F. J., Rivas, F. J., & McLurgh, D. B. (1999). Wet air oxidation: a review of process technologies and aspects in reactor design. *Chemical Engineering Journal*, *73*(2), 143–160.

Kolodziej, E. P., Harter, T., & Sedlak, D. L. (2004). Dairy wastewater, aquaculture, and spawning fish as sources of steroid hormones in the aquatic environment. *Environmental Science & Technology*, *38*(23), 6377–6384.

Kosma, C. I., Lambropoulou, D. A., & Albanis, T. A. (2010). Occurrence and removal of PPCPs in municipal and hospital wastewaters in Greece. *Journal of Hazardous Materials*, *179*(1–3), 804–817.

Kumar, R., Qureshi, M., Vishwakarma, D. K., Al-Ansari, N., Kuriqi, A., Elbeltagi, A., & Saraswat, A. (2022). A review on emerging water contaminants and the application of sustainable removal technologies. *Case Studies in Chemical and Environmental Engineering*, *6*, 100219.

Kümmerer, K. (2008). Pharmaceuticals in the environment–a brief summary. *Pharmaceuticals in the Environment: Sources, Fate, Effects and Risks*, 3–21.

Kümmerer, K. (2009a). Antibiotics in the aquatic environment – A review – Part I. *Chemosphere*, *75*(4), 417–434. https://doi.org/10.1016/J.CHEMOSPHERE.2008.11.086

Kümmerer, K. (2009b). The presence of pharmaceuticals in the environment due to human use–present knowledge and future challenges. *Journal of Environmental Management*, *90*(8), 2354–2366.

Kwon, B. G., Lee, D. S., Kang, N., & Yoon, J. (1999). Characteristics of p-chlorophenol oxidation by Fenton's reagent. *Water Research*, *33*(9), 2110–2118.

LaLonde, R. T. (2005). Terpenes and terpenoids. In *Van Nostrand's Encyclopedia of Chemistry*. John Wiley & Sons, Inc. https://doi.org/10.1002/0471740039.vec2473

Lapworth, D. J., Baran, N., Stuart, M. E., & Ward, R. S. (2012). Emerging organic contaminants in groundwater: a review of sources, fate and occurrence. *Environmental Pollution*, *163*, 287–303.

Largitte, L., & Pasquier, R. (2016). A review of the kinetics adsorption models and their application to the adsorption of lead by an activated carbon. *Chemical Engineering Research and Design*, *109*, 495–504. https://doi.org/10.1016/J.CHERD.2016.02.006

Levec, J., & Pintar, A. (2007). Catalytic wet-air oxidation processes: A review. *Catalysis Today*, *124*(3–4), 172–184.

Levenspiel, O. (1998). *Chemical reaction engineering*. John wiley & sons.

Li, L., Dong, Y., Chen, Y., Jiao, J., & Zou, X. (2022). A New Method for Environmental Risk Assessment of Pollutants Based on Multi-Dimensional Risk Factors. *Toxics*, *10*(11), 659.

Li, Y., Zhu, G., Ng, W. J., & Tan, S. K. (2014). A review on removing pharmaceutical contaminants from wastewater by constructed wetlands: design, performance and mechanism. *Science of the Total Environment*, *468*, 908–932.

Linh, N. S., Ahmed, F., & Loc, H. H. (2023). Applications of Nature-Based Solutions in Urban Water Management in Singapore, Thailand and Vietnam: A Review. *Regional Perspectives of Nature-Based Solutions for Water: Benefits and Challenges*, 101–126.

Liu, J. L., & Wong, M. H. (2013). Pharmaceuticals and personal care products (PPCPs): A review on environmental contamination in China. *Environment International*, *59*, 208–224. https://doi.org/10.1016/j.envint.2013.06.012

Luck, F. (1996). A review of industrial catalytic wet air oxidation processes. *Catalysis Today*, *27*(1–2), 195–202.

Luck, F. (1999). Wet air oxidation: past, present and future. *Catalysis Today*, *53*(1), 81–91.

Mahamuni, N. N., & Adewuyi, Y. G. (2010). Advanced oxidation processes (AOPs) involving ultrasound for waste water treatment: a review with emphasis on cost estimation. *Ultrasonics Sonochemistry*, *17*(6), 990–1003.

Makatsa, T. J., Baloyi, J., Ntho, T., & Masuku, C. M. (2021). Catalytic wet air oxidation of phenol: Review of the reaction mechanism, kinetics, and CFD modeling. *Critical Reviews in Environmental Science and Technology*, *51*(17), 1891–1923.

Mantzavinos, D., Sahibzada, M., Livingston, A. G., Metcalfe, I. S., & Hellgardt, K. (1999). Wastewater treatment: wet air oxidation as a precursor to biological treatment. *Catalysis Today*, *53*(1), 93–106.

Matatov-Meytal, Y. I., & Sheintuch, M. (1998). Catalytic abatement of water pollutants. *Industrial & Engineering Chemistry Research*, *37*(2), 309–326.

Matthews, G. A. (2016). *Pesticides : Health, Safety and the Environment* (Segunda Ed). John Wiley & Sons.

Mehran Anjum, M. (2017). Pesticides and Environmental Health: A Review. *Agricultural Research & Technology: Open Access Journal*, *5*(5). https://doi.org/10.19080/artoaj.2017.05.555671

Mnif, W., Hassine, A. I. H., Bouaziz, A., Bartegi, A., Thomas, O., & Roig, B. (2011). Effect of endocrine disruptor pesticides: a review. *International Journal of Environmental Research and Public Health*, *8*(6), 2265–2303.

Molander, L., Ågerstrand, M., & Rudén, C. (2009). WikiPharma–A freely available, easily accessible, interactive and comprehensive database for environmental effect data for pharmaceuticals. *Regulatory Toxicology and Pharmacology*, *55*(3), 367–371.

Moles, S., Mosteo, R., Gómez, J., Szpunar, J., Gozzo, S., Castillo, J. R., & Ormad, M. P. (2020). Towards the removal of antibiotics detected in wastewaters in the POCTEFA territory: Occurrence and TiO2 photocatalytic pilot-scale plant performance. *Water (Switzerland)*, *12*(5), 1453. https://doi.org/10.3390/w12051453

Monneret, C. (2017). What is an endocrine disruptor? *Comptes Rendus Biologies*, *340*(9–10), 403–405.

Narenderan, S. T., & Meyyanathan, S. N. (2019). Sample Treatment and Determination of Pesticide Residues in Potato Matrices: a Review. *Potato Research*, *62*(1), 47–67. https://doi.org/10.1007/s11540-018-9396-x

Narenderan, S. T., Meyyanathan, S. N., & Karri, V. V. S. R. (2019). Experimental design in pesticide extraction methods: A review. *Food Chemistry*, *289*(November 2018), 384–395. https://doi.org/10.1016/j.foodchem.2019.03.045

Ngo, H. H., Guo, W., Zhang, J., Liang, S., Ton-That, C., & Zhang, X. (2015). Typical low cost biosorbents for adsorptive removal of specific organic pollutants from water. *Bioresource Technology*, *182*, 353–363.

Noguera-Oviedo, K., & Aga, D. S. (2016). Lessons learned from more than two decades of research on emerging contaminants in the environment. *Journal of Hazardous Materials*, *316*, 242–251.

Oller, I., Malato, S., & Sánchez-Pérez, Ja. (2011). Combination of advanced oxidation processes and biological treatments for wastewater decontamination—a review. *Science of the Total Environment*, *409*(20), 4141–4166.

Ortúzar, M., Esterhuizen, M., Olicón-Hernández, D. R., González-López, J., & Aranda, E. (2022). Pharmaceutical pollution in aquatic environments: A concise review of environmental impacts and bioremediation systems. *Frontiers in Microbiology*, *13*.

Otto, B., & Schleifer, L. (2020). *Domestic water use grew 600% over the past 50 years*.

Oturan, M. A., & Aaron, J.-J. (2014). Advanced oxidation processes in water/wastewater treatment: principles and applications. A review. *Critical Reviews in Environmental Science and Technology*, *44*(23), 2577–2641.

Ou, X., Daly, H., Chansai, S., Beaumont, S. K., Fan, X., & Hardacre, C. (2022). Effect of concentrated NaCl on catalytic wet oxidation (CWO) of short chain carboxylic acids. *Catalysis Communications*, *162*, 106395.

Ou, X., Daly, H., Fan, X., Beaumont, S., Chansai, S., Garforth, A., Xu, S., & Hardacre, C. (2022). High-Ionic-Strength Wastewater Treatment via Catalytic Wet Oxidation over a MnCeO x Catalyst. *ACS Catalysis*, *12*(13), 7598–7608.

Pablos, M. V., García-Hortigüela, P., & Fernández, C. (2015). Acute and chronic toxicity of emerging contaminants, alone or in combination, in Chlorella vulgaris and Daphnia magna. *Environmental Science and Pollution Research*, *22*, 5417–5424.

Pal, A., Gin, K. Y.-H., Lin, A. Y.-C., & Reinhard, M. (2010). Impacts of emerging organic contaminants on freshwater resources: review of recent occurrences, sources, fate and effects. *Science of the Total Environment*, *408*(24), 6062–6069.

Pariente, M. I., Segura, Y., Álvarez-Torrellas, S., Casas, J. A., de Pedro, Z. M., Diaz, E., García, J., López-Muñoz, M. J., Marugán, J., & Mohedano, A. F. (2022). Critical review of technologies for the on-site treatment of hospital wastewater: From conventional to combined advanced processes. *Journal of Environmental Management*, *320*, 115769.

Pera-Titus, M., García-Molina, V., Baños, M. A., Giménez, J., & Esplugas, S. (2004). Degradation of chlorophenols by means of advanced oxidation processes: a general review. *Applied Catalysis B: Environmental*, *47*(4), 219–256.

Perveen, S. (2018). Introductory chapter: Terpenes and terpenoids. In *Terpenes and Terpenoids*. IntechOpen. https://doi.org/10.5772/intechopen.79683

Petrović, M., Gonzalez, S., & Barceló, D. (2003). Analysis and removal of emerging contaminants in wastewater and drinking water. *TrAC - Trends in Analytical Chemistry*, *22*(10), 685–696. https://doi.org/10.1016/S0165-9936(03)01105-1

Pignatello, J. J., Oliveros, E., & MacKay, A. (2006). Advanced oxidation processes for organic contaminant destruction based on the Fenton reaction and related chemistry. *Critical Reviews in Environmental Science and Technology*, *36*(1), 1–84.

Pintar, A., & Levec, J. (1992). Catalytic oxidation of organics in aqueous solutions: I. Kinetics of phenol oxidation. *Journal of Catalysis*, *135*(2), 345–357.

Plakas, K. V., & Karabelas, A. J. (2012). Removal of pesticides from water by NF and RO membranes - A review. *Desalination*, *287*, 255–265. https://doi.org/10.1016/j.desal.2011.08.003

Primo Yúfera, E. (2007). *Química orgánica básica y aplicada : de la molécula a la industria*. Reverté.

Programa Mundial de Evaluación de los Recursos Hídricos (WWAP). (2016). *Informe de las Naciones Unidas sobre el Desarrollo de los Recursos Hidricos en el Mundo 2016: Agua y Empleo*. Organización de Naciones Unidas para la Educación, la Ciencia y la Cultura ….

Programa Mundial de Evaluación de los Recursos Hídricos (WWAP). (2017). *Informe Mundial sobre el Desarrollo de los Recursos Hídricos de las Naciones Unidas 2017: Las aguas residuales: el recurso desaprovechado, resumen ejecutivo*. Unesco Paris, France.

Programa Mundial de Evaluación de los Recursos Hídricos (WWAP). (2019). *Informe Mundial de las Naciones Unidas sobre el Desarrollo de los Recursos Hídricos 2019: No dejar a nadie atrás*. Unesco Paris, France.

Programa Mundial de Evaluación de los Recursos Hídricos (WWAP). (2020). *Informe Mundial de las Naciones Unidas sobre el desarrollo de los recursos hídricos 2020: Agua y cambio climático*. Unesco Paris, France.

Programa Mundial de Evaluación de los Recursos Hídricos (WWAP). (2021). *Informe Mundial de las Naciones Unidas sobre el Desarrollo de los Recursos Hídricos 2021: El valor del agua*. Unesco Paris, France.

Rajmohan, K. S., Chandrasekaran, R., & Varjani, S. (2020). A review on occurrence of pesticides in environment and current technologies for their remediation and management. *Indian Journal of Microbiology*, *60*, 125–138.

Rathore, H. Singh., & Nollet, L. M. L. (2012). *Pesticides : Evaluation of Environmental Pollution*. CRC Press.

Riyaz, M., Shah, R. A., & Sivasankaran, K. (2021). Pesticide residues: Impacts on fauna and the environment. *Biodegradation Technology of Organic and Inorganic Pollutants*.

Rodríguez, A., Letón, P., Rosal, R., Dorado, M., Villar, S., & Sanz, J. (2006). Informe de vigilancia tecnológica: Tratamientos avanzados de aguas residuales industriales. *Universidad de Alcalá Del Círculo de Innovación En. Tecnologías Medioambientales y Energía (CITME)*, 1–136.

Rodríguez, A., Ovejero, G., Romero, M. D., Díaz, C., Barreiro, M., & García, J. (2008). Catalytic wet air oxidation of textile industrial wastewater using metal supported on carbon nanofibers. *The Journal of Supercritical Fluids*, *46*(2), 163–172. https://doi.org/https://doi.org/10.1016/j.supflu.2008.04.007

Rodríguez-Llorente, D., Cañada-Barcala, A., Álvarez-Torrellas, S., Águeda, V. I., García, J., & Larriba, M. (2020). A review of the use of eutectic solvents, terpenes and terpenoids in liquid–liquid extraction processes. *Processes*, *8*(10), 1–54. https://doi.org/10.3390/pr8101220

Rodriguez-Narvaez, O. M., Peralta-Hernandez, J. M., Goonetilleke, A., & Bandala, E. R. (2017). Treatment technologies for emerging contaminants in water: A review. In *Chemical Engineering Journal* (Vol. 323, pp. 361–380). Elsevier B.V. https://doi.org/10.1016/j.cej.2017.04.106

Rubino, S., Cappuccinelli, P., & Kelvin, D. J. (2011). Escherichia coli (STEC) serotype O104 outbreak causing haemolytic syndrome (HUS) in Germany and France. *The Journal of Infection in Developing Countries*, *5*(06), 437–440.

Rueda Márquez, J. J., Levchuk, I., & Sillanpää, M. (2018). Application of catalytic wet peroxide oxidation for industrial and urban wastewater treatment: A review. *Catalysts*, *8*(12), 673.

Sacher, F., Lange, F. T., Brauch, H.-J., & Blankenhorn, I. (2001). Pharmaceuticals in groundwaters: analytical methods and results of a monitoring program in Baden-Württemberg, Germany. *Journal of Chromatography A*, *938*(1–2), 199–210.

Sadana, A., & Katzer, J. R. (1974). Involvement of free radicals in the aqueous-phase catalytic oxidation of phenol over copper oxide. *Journal of Catalysis*, *35*(1), 140–152.

Safari, H., Arab, M., Rashidian, A., Kebriaee-Zadeh, A., & Gorji, H. A. (2018). A comparative study on different pharmaceutical industries and proposing a model for the context of Iran. *Iranian Journal of Pharmaceutical Research*, *17*(4), 1593–1603. https://doi.org/10.22037/ijpr.2018.2307

Saleh, I. A., Zouari, N., & Al-Ghouti, M. A. (2020). Removal of pesticides from water and wastewater: Chemical, physical and biological treatment approaches. *Environmental Technology and Innovation*, *19*.

Salem, H., & Olajos, E. J. (1988). Review of pesticides: Chemistry, uses and toxicology. *Toxicology and Industrial Health*, *4*(3), 291–321. https://doi.org/10.1177/074823378800400303

Samsidar, A., Siddiquee, S., & Shaarani, S. M. (2018). A review of extraction, analytical and advanced methods for determination of pesticides in environment and foodstuffs. *Trends in Food Science and Technology*, *71*(July 2017), 188–201. https://doi.org/10.1016/j.tifs.2017.11.011

Sanderson, H., Brain, R. A., Johnson, D. J., Wilson, C. J., & Solomon, K. R. (2004). Toxicity classification and evaluation of four pharmaceuticals classes: antibiotics, antineoplastics, cardiovascular, and sex hormones. *Toxicology*, *203*(1–3), 27–40.

Saravia, F., & Frimmel, F. H. (2008). Role of NOM in the performance of adsorption-membrane hybrid systems applied for the removal of pharmaceuticals. *Desalination*, *224*(1–3), 168–171.

Schulz, M., Löffler, D., Wagner, M., & Ternes, T. A. (2008). Transformation of the X-ray contrast medium iopromide in soil and biological wastewater treatment. *Environmental Science & Technology*, *42*(19), 7207–7217.

Seckler, D., Barker, R., & Amarasinghe, U. (1999). Water scarcity in the twenty-first century. *International Journal of Water Resources Development*, *15*(1–2), 29–42.

Seijger, C., & Hellegers, P. (2023). How do societies reform their agricultural water management towards new priorities for water, agriculture, and the environment? *Agricultural Water Management*, *277*, 108104. https://doi.org/https://doi.org/10.1016/j.agwat.2022.108104

Serra-Pérez, E., Álvarez-Torrellas, S., Águeda, V. I., Delgado, J. A., Ovejero, G., & García, J. (2019). Insights into the removal of Bisphenol A by catalytic wet air oxidation upon carbon nanospheres-based catalysts: Key operating parameters, degradation intermediates and reaction pathway. *Applied Surface Science*, *473*, 726–737.

Shams, A. K., & Muhammad, N. S. (2022). Towards sustainable transboundary water cooperation between Afghanistan and Pakistan: A case study of Kabul River. *Ain Shams Engineering Journal*, 101842.

Sierra, M. A., & Gómez Gallego, M. (2007). *Principios de química medioambiental*. Síntesis.

Sievers, M. (2011). 4.13 - Advanced Oxidation Processes. In P. Wilderer (Ed.), *Treatise on Water Science* (pp. 377–408). Elsevier. https://doi.org/https://doi.org/10.1016/B978-0-444-53199-5.00093-2

Sims, R. A., Harmer, S. L., & Quinton, J. S. (2019). The role of physisorption and chemisorption in the oscillatory adsorption of organosilanes on aluminium oxide. *Polymers*, *11*(3), 410.

Singh, N. B., Nagpal, G., Agrawal, S., & Rachna. (2018). Water purification by using Adsorbents: A Review. *Environmental Technology & Innovation*, *11*, 187–240. https://doi.org/https://doi.org/10.1016/j.eti.2018.05.006

Stefanakis, A., Akratos, C. S., & Tsihrintzis, V. A. (2014). *Vertical flow constructed wetlands: eco-engineering systems for wastewater and sludge treatment*. Newnes.

Stoker, P., Albrecht, T., Follingstad, G., & Carlson, E. (2022). Integrating land use planning and water management in US cities: A literature review. *JAWRA Journal of the American Water Resources Association*, *58*(3), 321–335.

Suzuki, M., & Suzuki, M. (1990). *Adsorption engineering* (Vol. 14). Kodansha Tokyo.

Swartz, C. H., Reddy, S., Benotti, M. J., Yin, H., Barber, L. B., Brownawell, B. J., & Rudel, R. A. (2006). Steroid estrogens, nonylphenol ethoxylate metabolites, and other wastewater contaminants in groundwater affected by a residential septic system on Cape Cod, MA. *Environmental Science & Technology*, *40*(16), 4894–4902.

Taheran, M., Naghdi, M., Brar, S. K., Verma, M., & Surampalli, R. Y. (2018). Emerging contaminants: here today, there tomorrow! *Environmental Nanotechnology, Monitoring & Management*, *10*, 122–126.

Tambosi, J. L., Yamanaka, L. Y., José, H. J., De Fátima Peralta Muniz Moreira, R., & Schröder, H. F. (2010). Recent research data on the removal of pharmaceuticals from sewage treatment plants (STP). *Quimica Nova*, *33*(2), 411–420. https://doi.org/10.1590/S0100-40422010000200032

Tannoury, M., & Attieh, Z. (2017). The Influence of Emerging Markets on the Pharmaceutical Industry. In *Current Therapeutic Research - Clinical and Experimental* (Vol. 86, pp. 19–22). Excerpta Medica Inc. https://doi.org/10.1016/j.curtheres.2017.04.005

Ternes, T. A., & Hirsch, R. (2000). Occurrence and behavior of X-ray contrast media in sewage facilities and the aquatic environment. *Environmental Science & Technology*, *34*(13), 2741–2748.

Thommes, M., Kaneko, K., Neimark, A. V, Olivier, J. P., Rodriguez-Reinoso, F., Rouquerol, J., & Sing, K. S. W. (2015). Physisorption of gases, with special reference to the evaluation of surface area and pore size distribution (IUPAC Technical Report). *Pure and Applied Chemistry*, *87*(9–10), 1051–1069.

Timofeeva, I., Shishov, A., Kanashina, D., Dzema, D., & Bulatov, A. (2017). On-line in-syringe sugaring-out liquid-liquid extraction coupled with HPLC-MS/MS for the determination of pesticides in fruit and berry juices. *Talanta*, *167*, 761–767. https://doi.org/10.1016/j.talanta.2017.01.008

Topp, E., Monteiro, S. C., Beck, A., Coelho, B. B., Boxall, A. B. A., Duenk, P. W., Kleywegt, S., Lapen, D. R., Payne, M., & Sabourin, L. (2008). Runoff of pharmaceuticals and personal care products following application of biosolids to an agricultural field. *Science of the Total Environment*, *396*(1), 52–59.

Tran, N. H., & Gin, K. Y.-H. (2017). Occurrence and removal of pharmaceuticals, hormones, personal care products, and endocrine disrupters in a full-scale water reclamation plant. *Science of the Total Environment*, *599*, 1503–1516.

Unfried, K., Kis-Katos, K., & Poser, T. (2022). Water scarcity and social conflict. *Journal of Environmental Economics and Management*, *113*, 102633.

UNICEF. (2019). *1 de cada 3 personas en el mundo no tiene acceso a agua potable*. https://www.unicef.org/es/comunicados-prensa/1-de-cada-3-personas-en-el-mundo-no-tiene-acceso-a-agua-potable

Vagı, M. C., & Petsas, A. S. (2017). Advanced Oxidation Processes for the Removal of Pesticides from Wastewater: Recent Review and Trends. *15th International Conference on Environmental Science and Technology*. https://cest.gnest.org/sites/default/files/presentation_file_list/cest2017_01225_oral_paper.pdf

Vaschetto, E. G., Sicardi, M. I., Elías, V. R., Ferrero, G. O., Carraro, P. M., Casuscelli, S. G., & Eimer, G. A. (2019). Metal modified silica for catalytic wet air oxidation (CWAO) of glyphosate under atmospheric conditions. *Adsorption*, *25*(7), 1299–1306.

Verlicchi, P., Galletti, A., Petrovic, M., & Barceló, D. (2010). Hospital effluents as a source of emerging pollutants: an overview of micropollutants and sustainable treatment options. *Journal of Hydrology*, *389*(3–4), 416–428.

Vollmer, G. (2010). Disposal of pharmaceutical waste in households–a European survey. *Green and Sustainable Pharmacy*, 165–178.

Wakita, T., Kinoshita, K., Yamada, E., Yasui, N., Kawahara, N., Naoi, A., Nakaya, M., Ebihara, K., Matsuno, H., & Kodaka, K. (2003). The discovery of dinotefuran: A novel neonicotinoid. *Pest Management Science*, *59*(9), 1016–1022. https://doi.org/10.1002/ps.727

Wang, J., & Guo, X. (2020). Adsorption kinetic models: Physical meanings, applications, and solving methods. *Journal of Hazardous Materials*, *390*, 122156. https://doi.org/https://doi.org/10.1016/j.jhazmat.2020.122156

Wang, L., Geng, C., Yu, D., Liu, D., Sun, H., Xiao, K., & Zhao, H. (2023). Catalytic performance and mechanism of PTFE modified NiCo2O4 in high-salt organic wastewater treatment during wet air oxidation at ambient pressure. *Applied Catalysis B: Environmental*, 122786.

Wess, R. A. (2021). Update of EMA's guideline on the environmental risk assessment (ERA) of medicinal products for human use. *Therapeutic Innovation & Regulatory Science*, *55*(2), 309–323.

Williams, S. A., Eden, S., Megdal, S. B., & Joe-Gaddy, V. (2023). Diversity, Equity, Inclusion, and Justice in Water Dialogues: A Review and Conceptualization. *Journal of Contemporary Water Research & Education*, *177*(1), 113–139.

World Health Organization. (2021). *Progress on household drinking water, sanitation and hygiene 2000-2020: five years into the SDGs*.

World Health Organization. (2022). *Agua para consumo humano*. https://www.who.int/es/news-room/fact-sheets/detail/drinking-water

Xiuling, D., Qian, L., Lipeng, L., & Sarkar, A. (2023). The Impact of Technical Training on Farmers Adopting Water-Saving Irrigation Technology: An Empirical Evidence from China. *Agriculture*, *13*(5), 956.

Yadav, N., Yadav, R., & Goyal, A. (2014). Chemistry of terpenoids. *International Journal of Pharmaceutical Sciences Review and Research*, *27*(2), 272–278.

Zainal-Abidin, M. H., Hayyan, M., Hayyan, A., & Jayakumar, N. S. (2017). New horizons in the extraction of bioactive compounds using deep eutectic solvents: A review. In *Analytica Chimica Acta* (Vol. 979, pp. 1–23). Elsevier B.V. https://doi.org/10.1016/j.aca.2017.05.012

Zazo, J. A., Casas, J. A., Mohedano, A. F., Gilarranz, M. A., & Rodríguez, J. J. (2005). Chemical Pathway and Kinetics of Phenol Oxidation by Fenton's Reagent. *Environmental Science & Technology*, *39*(23), 9295–9302. https://doi.org/10.1021/es050452h

Zazo, J. A., Casas, J. A., Mohedano, A. F., & Rodríguez, J. J. (2006). Catalytic wet peroxide oxidation of phenol with a Fe/active carbon catalyst. *Applied Catalysis B: Environmental*, *65*(3), 261–268. https://doi.org/https://doi.org/10.1016/j.apcatb.2006.02.008

Zhang, Y., Nielsen, J., & Liu, Z. (2017). Engineering yeast metabolism for production of terpenoids for use as perfume ingredients, pharmaceuticals and biofuels. *FEMS Yeast Research*, *17*(8), fox080.

Zhou, F., & Pichersky, E. (2020). More is better: the diversity of terpene metabolism in plants. *Current Opinion in Plant Biology*, *55*, 1–10.

Ziganshina, D. R., & de Schutter, J. L. G. (2022). Paving the Way for Evidence-Driven Transboundary Water Cooperation in Central Asia. *JAWRA Journal of the American Water Resources Association*, *58*(6), 1149–1161.

Zwenger, S., & Basu, C. (2008). Plant terpenoids: applications and future potentials. *Biotechnology and Molecular Biology Reviews*, *3*(1), 1–7.

Capítulo VII

Anexos

En este capítulo se recogen los artículos científicos que forman parte del cuerpo de la presente Tesis Doctoral, y que se encuentran publicados en revistas de alto impacto. De esta forma, se valida, no solo la relevancia y la innovación de esta memoria, sino también la calidad de los resultados obtenidos.

El listado de las cuatro publicaciones que se han ido abordando a lo largo del documento, y cuyo acceso se encuentra también disponible a través de las plataformas digitales de las revistas, es el siguiente:

Publicación 1

Gutiérrez-Sánchez, P., Navarro, P., Álvarez-Torrellas, S., García, J., & Larriba, M. (2022). Extraction of neonicotinoid pesticides from aquatic environmental matrices with sustainable terpenoids and eutectic solvents. *Separation and Purification Technology*, *302*, 122148. Factor de impacto: 9.136 (Q1). DOI: 10.1016/J.SEPPUR.2022.122148

Publicación 2

Gutiérrez-Sánchez, P., Rodríguez-Llorente, D., Navarro, P., Águeda, V. I., Álvarez-Torrellas, S., García, J., & Larriba, M. (2022). Extraction of antibiotics identified in the EU Watch List 2020 from hospital wastewater using hydrophobic eutectic solvents and terpenoids. *Separation and Purification Technology*, *282*, 120117. Factor de impacto: 9.136 (Q1). DOI: 10.1016/j.seppur.2021.120117

Publicación 3

Gutiérrez-Sánchez, P., Álvarez-Torrellas, S., Larriba, M., Victoria Gil, M., Garrido-Zoido, J. M., & García, J. (2023). Influence of transition metal-based activating agent on the properties and catalytic activity of sewage sludge-derived catalysts. Insights on mechanism, DFT calculation and degradation pathways. *Journal of Molecular Liquids*, *381*, 121840. Factor de impacto: 6.633 (Q1). DOI: 10.1016/J.MOLLIQ.2023.121840

Publicación 4

Gutiérrez-Sánchez, P., Álvarez-Torrellas, S., Larriba, M., Gil, M. V., Garrido-Zoido, J. M., & García, J. (2023). Efficient removal of antibiotic ciprofloxacin by catalytic wet air oxidation using sewage sludge-based catalysts: Degradation mechanism by DFT studies. *Journal of Environmental Chemical Engineering*, *11*(2), 109344. Factor de impacto: 7.968 (Q1). DOI: 10.1016/J.JECE.2023.109344

7.1 Publicación 1

Separation and Purification Technology 302 (2022) 122148

Contents lists available at ScienceDirect

Separation and Purification Technology

journal homepage: www.elsevier.com/locate/seppur

Extraction of neonicotinoid pesticides from aquatic environmental matrices with sustainable terpenoids and eutectic solvents

Pablo Gutiérrez-Sánchez [a], Pablo Navarro [b], Silvia Álvarez-Torrellas [a], Juan García [a], Marcos Larriba [a,*]

[a] Grupo de Catálisis y Procesos de Separación (CyPS), Departamento de Ingeniería Química y de Materiales, Universidad Complutense de Madrid, Avda. Complutense s/n, 28040 Madrid, Spain
[b] Departamento de Ingeniería Química, Universidad Autónoma de Madrid, C/ Francisco Tomás y Valiente 7, 28049 Madrid, Spain

ARTICLE INFO

Keywords:
Neonicotinoid pesticides
Terpenoids
Eutectic solvents
Liquid-liquid extraction
River water matrix

ABSTRACT

The potential environmental impact and adverse effects of the occurrence of pesticides in the aquatic environment have raised great social and political concern, leading to their control by means of several regulations, such as the European Directive 98/83/EC. In this regard, the three neonicotinoid pesticides analyzed in this work (acetamiprid, imidacloprid, and thiamethoxam) have been included in the surface water European Watch Lists under the Water Framework Directive. This research proposes the use of terpenoid-based solvents for the extraction of the three emerging contaminants previously mentioned. An initial screening of the extraction solvents was carried out through the COSMO-RS methodology, selecting the most favourable pure terpenes, eutectic terpenoid-based and conventional solvents. Furthermore, relevant issues were experimentally analyzed, such as extraction in more realistic multicomponent mixtures together with key parametric studies covering operating temperature and matrix influence. Carvacrol, a pure terpenoid not applied before as an extraction solvent of pesticides, has been revealed as an effective and sustainable substitute for conventional solvents for the first time to the best of our knowledge. Specifically, carvacrol exhibited overall extraction yields of around 97.5 % from a river water matrix at a volumetric S/F ratio of 0.1 and 303.2 K. High extraction yields from river water matrices regardless of temperature pointed to the potential of this solvent for a wide range of industrial application.

1. Introduction

In recent decades, plant protection products have played a key role in sustainable food production and in the elimination of insect-borne diseases. Consequently, the pesticide industry has experienced exceptional growth since the 1980 s and has increased the presence of these pollutants in both surface water and groundwater [1]. According to the literature, the concentration of pesticides in wastewaters ranges from 0.1 to 107 mg/L [2].

The pesticide market has evolved significantly since the first inorganic, botanical or simple aliphatic compounds, reducing crop losses from 42 to 9 %. Despite these benefits, their massive use has led to a major impact on the environment, ranking as one of the main emerging pollutants [1,3,4]. Thus, great efforts have been made over the last few years to develop new plant protection compounds presenting lower application rates, persistence and toxicity to non-target species. In this context, the so-called neonicotinoid or pyrethroid pesticides, whose application rates (0.01 and 0.1 kg/ha) are considerably lower than those of organochlorine compounds (3 kg/ha), have been introduced more recently [5,6]. Their success can also be attributed to their low toxicity to vertebrates, their high toxicity to insects, their flexibility in application methods and their systemic activity [4,7].

The growing social concern about the occurrence of these pollutants, for which information is still scarce, is leading to the development of new regulations. For instance, under Directive 2000/60/EC, contaminants for which limited information is available but suspected to pose a significant risk have been included in the named European Watch Lists. The increasing relevance of neonicotinoid pesticides and their presence on the European Watch Lists have turned the spotlight on them [8].

Neonicotinoid pesticides are a new type of neurotoxic compound whose mode of action is similar to that of nicotine. Based on the pharmacophore of their chemical structure, they are classified into

* Corresponding author. Tel.: +34 91 394 4135.
E-mail address: marcoslarriba@ucm.es (M. Larriba).

https://doi.org/10.1016/j.seppur.2022.122148
Received 29 June 2022; Received in revised form 14 September 2022; Accepted 14 September 2022
Available online 20 September 2022

nitroenamines, *N*-nitroguanidines, and *N*-cyanoamidines. In addition, they are either cyclic or open-chain compounds. Imidacloprid and thiamethoxam, both presenting cyclic structures, belong to the group of *N*-nitroguanidines. Acetamiprid, presenting an open-chain structure, is in the *N*-cyanoamidine group [9,10].

Conventional methods for wastewater treatment are generally ineffective for removing some micropollutants, such as pesticides. However, their potential adverse health effects, even at very low concentrations, impose interest in developing ad hoc water treatments for these compounds. A wide variety of physical, chemical and biological techniques have been proposed in the literature for the removal of pesticides in aqueous solution: advanced oxidation processes, chlorination, membrane bioreactors, adsorption, membrane filtration or extraction processes [2,11–19].

Liquid-liquid extraction is effective for the separation of pesticides in an aqueous solution. However, it presents some drawbacks, such as the use of large doses of solvents, which may cause a severe impact on the environment when they are partially soluble in water [20–23]. For this reason, the search for natural and eco-friendly solvents is essential for the sustainable application of this technique. In this context, the present article proposes the application of terpenes, terpenoids, and their eutectic mixtures, as alternative extraction solvents.

Terpenes and terpenoids are natural products that have a recurrent isoprene skeleton. The difference between both groups of compounds lies in the presence or not of oxygen atoms in their chemical structure. That is, while terpenoids are simple hydrocarbons, terpenoids are their oxygenated derivatives. However, both terms are generally used indistinctly. Terpenoids may be classified according to the number of carbon atoms into hemiterpenoids (C5), monoterpenoids (C10), sesquiterpenoids (C15), diterpenoids (C20), sesterterpenoids (C25), triterpenoids (C30), sesquarterpenoids (C35), tetraterpenoids (C40) and polyterpenoids (C > 40) [24,25].

Terpenes and terpenoids can be considered renewable due to their biomass origin, also presenting a lower hazard and environmental impact. For instance, carvacrol has been used in ships' ballast water management systems, proving its natural degradation and minimising its environmental impact. This terpenoid has also been proposed as a functional agent for a wide range of health benefits, such as food preservative due to its antimicrobial and antioxidant properties. The use of terpenes and terpenoids as solvents in extraction processes is relatively recent, with only 46 articles published in the literature in 2020. Furthermore, although there is a wide variety of terpenes and terpenoids, only a few have been studied in the literature [26–29].

In this research, the experimental application of pure terpenoids, such as carvacrol and thymol, for the extraction of three neonicotinoid pesticides, acetamiprid, imidacloprid, and thiamethoxam, is proposed after their selection by molecular simulation screenings using COSMO-RS. The utilization of pure terpenoids has not been previously reported in the literature for the removal of these types of emerging contaminants. Terpenoid-based eutectic solvents, i.e., mixtures whose melting temperature is lower than that of the pure components, have also been tested experimentally [30–32].

2. Experimental section

2.1. Solvent screening with the COSMO-RS method.

Several solvents were screened using the Conductor-like Screening Model for Real Solvents (COSMO-RS) approach. Turbomole 7.4 software was used to optimize the molecules of the pesticides and terpenoids, selecting COSMO continuum solvation method with a BP86/TZVP computational level using solvent effect by a single point calculation. The full information of the optimized molecule is stored in a *.cosmo file, which makes them available in COSMOtherm software, version 19.0.4, for predicting purposes [33]. The affinity of each extractant was evaluated by calculating the activity coefficients and excess enthalpies by contributions, namely hydrogen bonding, Van der Waals and electrostatic misfit, of acetamiprid, imidacloprid, and thiamethoxam at infinite dilution and 323,15 K in a wide list of terpenoids, hydrophobic eutectic solvents and conventional solvents. The mole fraction of the pesticide in each solvent was 5·10-5 for the simulations, which ensured the infinite dilution region [34]. As previously reported by other authors, the eutectic solvents were simulated as a mixture of two different compounds at the eutectic composition [35–39]. According to the pKa values shown in Table S1 of the Supplementary Material, the pesticides considered are in their neutral form in most of the pH range [40–44]. Therefore, the simulations were carried out considering this fact.

2.2. Chemicals

The compounds selected as suitable extractants with the COSMO-RS approach were two terpenoids (thymol and carvacrol), three eutectic solvents (thymol + octanoic acid, thymol + decanoic acid, and thymol + dodecanoic acid), and two conventional solvents (ethyl acetate and methyl isobutyl ketone). These solvents and the three neonicotinoid pesticides considered (acetamiprid, imidacloprid, and thiamethoxam) are detailed in Table S2 of the Supplementary Material. This includes suppliers, chemical structures, purities, and melting temperatures (Tm).

The aqueous solutions were prepared with both ultrapure water from PURELAB® Flex Water Purification System (Veolia) and a river water sample collected in the Manzanares river (Madrid, Spain). The characterization of the latter, which could be considered an environmentally-relevant aqueous matrix, is summarized in Table 1. The total organic carbon, total carbon and total nitrogen content were measured by a Shimadzu TOC-V CPH analyzer. The conductivity and pH were determined with a Mettler Toledo conductivity meter and a 2002 Crison pH meter. These values are within the range published in the literature for this kind of surface water [45–47].

2.3. Preparation of eutectic solvents and pesticides aqueous solutions.

The three eutectic solvents were prepared at the eutectic composition. For the mixtures thymol + octanoic acid, thymol + decanoic acid, and thymol + dodecanoic acid, the thymol mole fractions are 0.33, 0.44, and 0.56, respectively [39]. These solvents were stirred in a thermostatic bath at 323.2 ± 0.1 K until a homogeneous liquid appeared.

Monocomponent aqueous solutions of acetamiprid, imidacloprid, and thiamethoxam at 50 mg/L were prepared with ultrapure water. Additionally, two multicomponent solutions were prepared at 50 mg/L of each pesticide by using both ultrapure water and river water. The pH value of the pesticide aqueous solutions were around 5.5 and 7.0 for ultrapure water and river water, respectively.

2.4. Liquid-liquid extraction of neonicotinoid pesticides from aqueous solutions.

The liquid–liquid extractions were performed by contacting the aqueous pesticide solutions previously described with the organic solvents selected. The volumetric Solvent/Feed ratios (S/F) were as follows: 0.10, 0.25, 0.50, 1.00, and 2.00. Both phases were stirred for 12 h in glass vials, maintaining the temperature constant by using a C-MAG

Table 1
Macroscopic characterization of a river water sample.

Parameters	Value
pH	7.33
Chemical Oxygen Demand (mg/L)	<15
Total Organic Carbon (mg/L)	3.17
Total Carbon (mg/L)	7.42
Total Nitrogen (mg/L)	0.61
Total Dissolved Solids (mg/L)	64
Conductivity at 20 °C (μS/cm)	38.21

HS 7 dry bath (IKA). To observe the effect of this parameter in the extraction process, two temperatures were considered, 323.2 ± 0.1 K and 303.2 ± 0.1 K. After mixing, the two phases were left to settle for 4 h, and a sample of each was taken for further analyze. The raffinate, aqueous phase, was tested by using an analytical High Performance Liquid Chromatograph VARIAN ProStar with Diode Array Detector, and a Teknokroma chromatographic column (25 × 0,46 cm; 5 μm). The HPLC method developed consisted of a mixture (70 % acetonitrile + 30 % aqueous acetic acid solution 75 mM) as a mobile phase, a volumetric flow rate of 0.85 mL/min, an oven temperature of 303.2 K, an injection volume of 20 μL, and wavelengths of 223 nm and 275 nm. The retention times were 6.8 min, 10.1 min, and 11.6 min for thiamethoxam, imidacloprid and acetamiprid, respectively. The limits of detection were 0.1 mg/L for thiamethoxam and acetamiprid, while for imidacloprid it was 0.05 mg/L.

Finally, the influence of the feed pH value on the extraction process was analyzed. The pH value of the multicomponent aqueous solution with the river water matrix was modified by adding HCl and NaOH and the same procedure for the extraction process was repeated as above. The modified feed pH values were 1.0; 3.0; 5.0; 7.0; and 9.0.

3. Results and discussion

3.1. Solvent screening with the COSMO-RS method.

One of the methods reported in the literature for solvent screening is based on activity coefficients, which might be estimated by using the COSMO-RS method [33,48–51]. In this regard, a lower infinite dilution activity coefficient of the solute would indicate a higher affinity for the extraction solvent. Figs. 1-2 show the infinite dilution activity coefficients of acetamiprid, imidacloprid, and thiamethoxam in a wide range of terpenoids, hydrophobic eutectic solvents and conventional solvents at 323.2 K.

As shown in Fig. 1, thymol and carvacrol exhibit the lowest activity coefficient values in the group of terpenes and terpenoids. In this study, eleven solvents containing no heteroatoms in their hydrocarbon skeleton, i.e. terpenes, have been considered: myrcene, ocimene, sabinene, limonene, phellandrene, terpinene-alfa, 3-carene, pinene-beta, camphene, pinene-alfa and pinane. In general, these compounds seem to have a lower affinity for the three neonicotinoid pesticides, excluding eucalyptol, which has a lower activity coefficient for acetamiprid than myrcene and ocimene. As shown through the excess enthalpy contributions by hydrogen bonding, Van der Waals, and electrostatic interactions, shown in Figures S1-S3 of the Supplementary Material, the lesser influence of hydrogen bonding and dipole–dipole interactions could explain this behaviour for terpenes compared to terpenoids [52–54]. Since the entropic contribution is not governing these mixtures, promoting hydrogen bonding interactions has been concluded as the better strategy to promote low activity coefficients.

Eutectic solvents consisting of two terpenoids exhibit activity coefficients between those of pure terpenoids, as shown in Fig. 2. However,

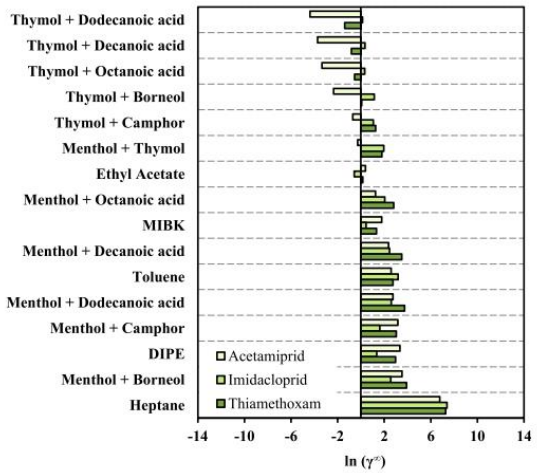

Fig. 2. Infinite dilution activity coefficients of acetamiprid, imidacloprid, and thiamethoxam in several hydrophobic eutectic solvents and conventional solvents at 323.2 K.

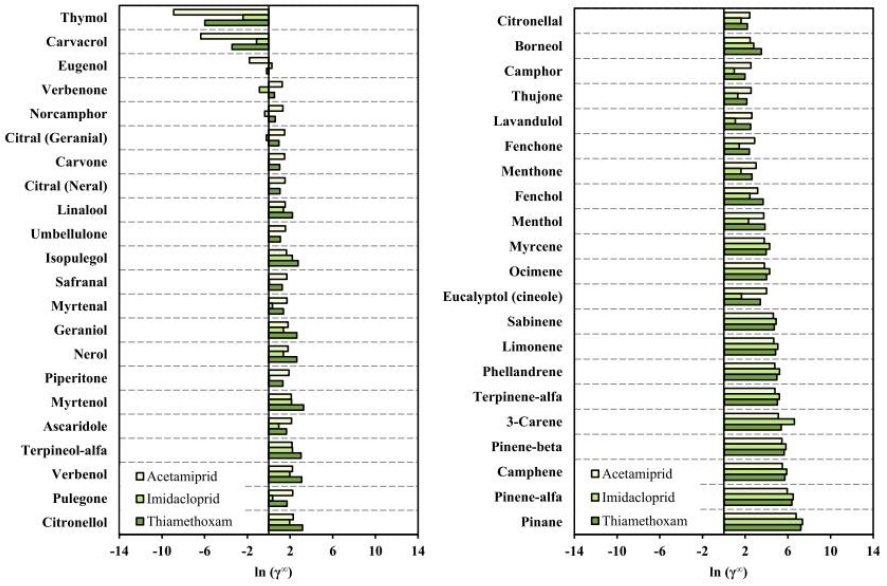

Fig. 1. Infinite dilution activity coefficients of acetamiprid, imidacloprid, and thiamethoxam in several terpenoids at 323.2 K.

it has been reported in the literature that they can show improved experimental results compared to those predicted by molecular simulation [35,37]. The eutectic mixtures with the lowest activity coefficients were those composed of thymol and carboxylic acids: thymol + octanoic acid, thymol + decanoic acid, and thymol + dodecanoic acid.

Among conventional solvents, those with the highest affinity for the three pesticides are ethyl acetate and methyl isobutyl ketone. In both cases, a lower compromise situation is reached compared to terpenes and eutectic solvents.

From the infinite dilution activity coefficients estimated by molecular simulation with COSMO-RS, seven extractants for the removal of neonicotinoid pesticides have been selected: two terpenoids (carvacrol and thymol), three eutectic mixtures (thymol + octanoic acid, thymol + decanoic acid, and thymol + dodecanoic acid) and two conventional solvents (ethyl acetate and methyl isobutyl ketone).

3.2. Extraction of single components from ultrapure water at 323.2 K

The seven solvents selected in the molecular simulation stage were tested to extract each of the three pesticides from single-component aqueous solutions. The temperature was 323.2 K in order to ensure that all of the solvents remained in the liquid state and to be able to compare them under the same operating conditions. The extraction of each pesticide was determined from its concentration in the aqueous phase, in mg/L, before ($C_{i,0}^{aq}$) and after the extraction ($C_{i,f}^{aq}$), as shown in equation (1).

$$Yld_i\,(\%) = \frac{C_{i,0}^{aq} - C_{i,f}^{aq}}{C_{i,0}^{aq}} \bullet 100 \quad (1)$$

Figs. 3-5 show the extraction yields of imidacloprid, acetamiprid and thiamethoxam, respectively, at 323.3 K and different volumetric S/F ratios.

Experimental results revealed that the extraction yields of the three neonicotinoid pesticides are very similar for the two terpenoids. The high extraction yields with thymol and carvacrol could be due to the presence of the hydroxyl group in their molecular structures, which would enhance hydrogen bonding type molecular interactions. The delocalization of electrons as a consequence of resonance in the aromatic ring would increase the acidity of the hydrogen present in this group, favoring, even more, its capacity as hydrogen bond donors. This fact, together with their capacity to behave also as hydrogen-bond acceptors, could explain the high affinity of these two terpenoids for the three pesticides tested.

As predicted by COSMO-RS, pure terpenoids exhibited higher yields than their eutectic mixtures. In addition, an expectable and slight increase in extraction yield was observed as the alkyl chain length increased: (thymol + octanoic acid) < (thymol + decanoic acid) < (thymol + dodecanoic acid). Specifically, thiamethoxam is the pesticide with the most pronounced variation.

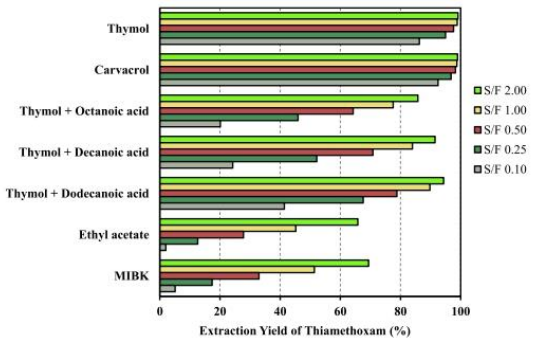

Fig. 3. Extraction yields of thiamethoxam from ultrapure water at 323.2 K and several volumetric S/F ratios.

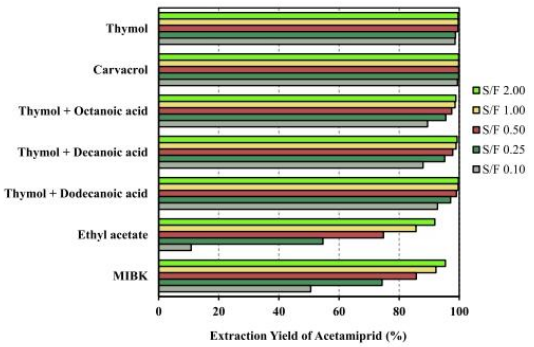

Fig. 4. Extraction yields of acetamiprid from ultrapure water at 323.2 K and several volumetric S/F ratios.

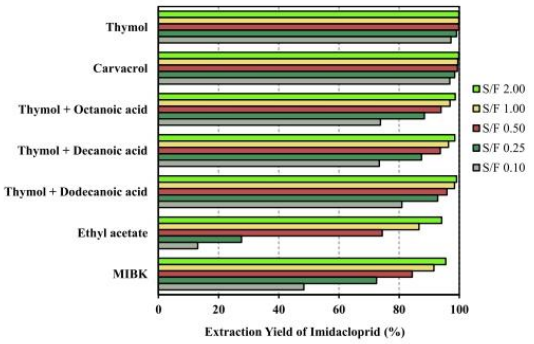

Fig. 5. Extraction yields of imidacloprid from ultrapure water at 323.2 K and several volumetric S/F ratios.

In the literature, only a limited number of terpenes and terpenoids, in the form of eutectic mixtures, have been reported to be used to extract pesticides. However, applying these extraction solvents as pure agents has not been studied so far [29,55–57]. The relatively recent use of these compounds in extraction processes, together with the novel character of neonicotinoid pesticides, highlights the relevance of research in this field.

Florindo et al. (2017) proposed the use of hydrophobic eutectic solvents formed by natural organic acids (octanoic, decanoic and dodecanoic acids) and the terpenoid DL-menthol. In that study, the eutectic solvents that presented the highest extraction yields allowed the removal of 75 %, 70 % and 40 % for acetamiprid, imidacloprid, and thiamethoxam, respectively, using an S/F ratio of 1.00 [57]. However, under the same operating conditions, the eutectic solvents suggested in the present investigation (thymol + carboxylic acids) allow to achieve yields of 98.6–99.6 %, 96.4–98.4 %, and 77.5–89.7 % for acetamiprid, imidacloprid, and thiamethoxam, respectively. Therefore, thymol appears to formulate eutectic solvents capable of extracting a greater amount of pesticide from an aqueous solution. Although the eutectic solvents described in this study achieve higher yields than those reported in the literature so far, the use of pure terpenoids exhibited even more favorable results and avoided the use of a binary solvent. That is, both thymol and carvacrol exhibited extraction yields higher than 99.6 %, 99.4 and 97.6 % for acetamiprid, imidacloprid, and thiamethoxam, respectively.

Conventional solvents seem to be the most unsuitable compounds for

the extraction of neonicotinoid pesticides, as evidenced by their low yields even at high S/F ratios. This could be due to the fact that, unlike terpenoids, MIBK and ethyl acetate are characterized by behaving only as hydrogen-bond acceptors, i. e. they do not possess acidic hydrogens attached to an element of high electronegativity. As shown in the chemical structures of Table S2, all three pesticides act as hydrogen bond acceptors, and only imidacloprid has a hydrogen atom bonded to an element electronegative enough to act as a hydrogen bond donor. This would imply less impact on the intermolecular interactions between these solvents and the neonicotinoid pesticides. Thus, the extraction capacity of conventional solvents would not be due to hydrogen bond formation so much as to other types of intermolecular interactions, such as Van der Waals and electrostatic interactions.

In addition, the influence of the S/F ratio increases in the following order: terpenes < eutectic solvents < conventional solvents. In this regard, pure terpenes seem to present lower solvent requirements compared to their eutectic mixtures to achieve similar yields. This difference is considerably greater for conventional solvents. Although the prices of the terpenoids (carvacrol 10–25 $/kg [58] and thymol 9–11 $/kg [59]) may be higher than those of conventional solvents (MIBK 1.0–1.5 $/kg [37] and ethyl acetate 1.3 $/kg [60]), the very low S/F ratio required to achieve extraction yields above 90 %, coupled with their low toxicity and solvent losses, places them in a more favorable status for the application in terms of both holdup costs and operating costs, respectively.

In fact, the losses of the extraction solvent in the aqueous phase were considerably higher for conventional solvents, reaching values around 1.52 wt% and 10.18 wt% for MIBK and ethyl acetate, respectively. Concerning the pure terpenes, carvacrol showed a solubility in the raffinate of 0.17 wt%, while thymol 0.25 wt%. As reported in the literature, the eutectic solvents comprising thymol + carboxylic acid presented lower thymol losses in water than the pure terpene, obtaining values lower than 0.10 wt% [61].

As previously discussed, both terpenes and eutectic solvents are more suitable than conventional ones. In particular, carvacrol seems to exhibit the most favourable conditions, not only because of its high extraction yields and low losses to water but also because it has a melting temperature that allows extraction at room temperature, see Table S2. The latter would avoid the energy costs associated with heating. Therefore, carvacrol has been selected to be assessed in a multicomponent extraction process, also analyzing the effect of the matrix and the influence of temperature.

3.3. Multicomponent extraction: Matrix effect and temperature influence.

The results from individual extractions led to the study of new issues, which are closely related to the implementation of the process on an industrial scale. One of them is the proof of the extraction efficiency from multicomponent aqueous solutions since more than one type of neonicotinoid pesticide is likely to be present in the real matrices. This was accomplished by calculating the extraction yields of each pesticide according to equation (1), and also the overall extraction yields according to equation (2):

$$Yld_{Overall}\,(\%) = \frac{\sum_{i=1}^{3}(C_{i,0}^{aq} - C_{i,f}^{aq})}{\sum_{i=1}^{3} C_{i,0}^{aq}} \bullet 100 \qquad (2)$$

where $C_{i,0}^{aq}$ and $C_{i,f}^{aq}$ are the concentrations of each pesticide in the aqueous phase, in mg/L, before and after the extraction.

In addition, it is worth studying the effect of the matrix on the extraction process, comparing the feasibility of this technology in aqueous solutions prepared with ultrapure water and with an environmentally relevant resource such as river water, where this type of emerging pollutants can be found. On the other hand, the high extraction yields obtained in extractions of single components at 323.2 K using the carvacrol as solvent highlight the importance of evaluating the extraction process at 303.2 K (a more representative room temperature), which would avoid the possible energy costs associated to heating conditioning.

The multicomponent extraction yields from ultrapure water and from a river water matrix by using carvacrol and MIBK at S/F 0.10 and two temperatures, 323.2 K and 303.2 K are shown in Fig. 6. The results obtained for the S/F ratios 0.25, 0.50, 1.00 and 2.00 are given in Figures S4- S7 in the Supplementary Material.

Concerning the influence of temperature, a slight increase in individual and overall extraction yields was observed with decreasing temperature for both carvacrol and MIBK. This would favor the multicomponent extraction process at a more representative room temperature, i.e., around 303.2 K. This would also avoid the energy requirement associated with heating conditioning and minimize operating costs if the process developed in this article were scaled up.

Moreover, the effect of the matrix showed different trends depending on the pesticide. For imidacloprid and thiamethoxam, the yields in the river water matrix were lower than those obtained for ultrapure water. Therefore, the solutes present in the river water matrix seem to favor the solvation of the two neonicotinoid pesticides in the aqueous phase, decreasing their mass transfer to the organic solvent. On the contrary, the extraction yields of acetamiprid were higher with the river water matrix, indicating that the solutes present in the river water matrix favor their transfer to the organic phase due to a salting-out effect. The behavior previously analyzed for each of the three pesticides is the same for the two solvents analyzed, MIBK and carvacrol. However, the matrix effect seems to be considerably lower for the terpene. In general, the differences associated with the matrix effect appear to decrease with increasing S/F ratio, as evidenced in Figures S4-S7 of the Supplementary Material. It should be noted that the most suitable S/F ratio for carvacrol is 0.10, as it allows to reach overall extraction yields close to 98 %. A higher solvent dosage would not justify the slight rise in the extraction yield, which would increase operating and investment and costs.

Finally, comparing single versus multicomponent extraction from ultrapure water at 323.2 K, see Figs. 3-6, scarcely any differences were observed for carvacrol. However, MIBK achieved higher extraction yields of each of the three pesticides in the multicomponent process compared to single extraction. Specifically, thiamethoxam was the neonicotinoid pesticide that showed the most significant variation when using MIBK.

The feed pH is a further process variable that could lead to a variation in the extraction yield results. Therefore, a thorough study has been carried out using five different feed pH values: 1.0; 3.0; 5.0; 7.0; and 9.0. Carvacrol was selected as the extraction solvent, as it is the most suitable for its potential to be applied on an industrial scale. Fig. 7 shows the influence of feed pH on multicomponent extraction yields from river

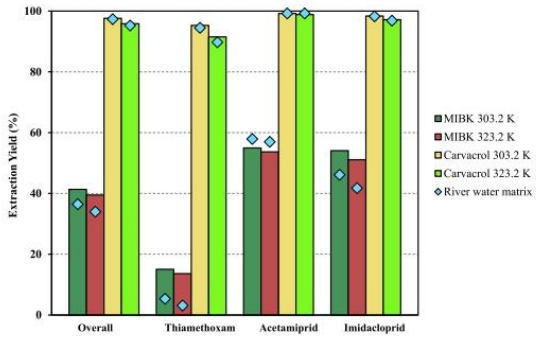

Fig. 6. Multicomponent extraction yields of pesticides from ultrapure water and river water matrix by using carvacrol and MIBK at S/F 0.10 and two temperatures, 323.2 K and 303.2 K.

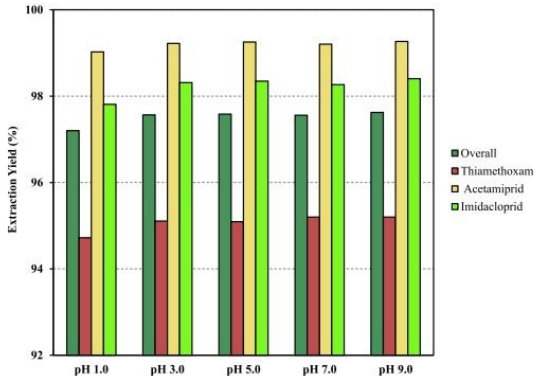

Fig. 7. Feed pH influence on multicomponent extraction yields of pesticides from river water matrix by using carvacrol at S/F 0.10 and 303.2 K.

water matrix at S/F 0.10 and 303.2 K.

The results of this study revealed that the feed pH value has a negligible effect on extraction yields, making carvacrol even more versatile for its industrial-scale application in the extraction of neonicotinoid pesticides, avoiding the need to modify the feed pH to ensure high extraction yields. Moreover, according to the pKa values of the nenonicotinoid pesticides, shown in Table S1, the pesticides are in their neutral form in most of the pH range. However, at pH values around 1, the protonated (cationic) form of the three compounds increases. As reported in the literature, charged solutes generally exhibit a stronger interaction with water, favoring partitioning into the aqueous phase [62–64]. Due to this fact, the extraction yields are slightly lower at feed pH of 1. Despite the latter, carvacrol seems to stabilize both the neutral and cationic forms without almost any variation in the extraction yields. Finally, it should be noted that in the natural feed solution, i.e., without pH modification, the pesticides are in their neutral form. This fact applies to the feed solution with both ultrapure water (natural feed pH ≈ 5.5) and river water matrix (natural feed pH ≈ 7.0).

4. Conclusions

The growth of the pesticide industry has favoured the presence of these emerging pollutants in the aquatic environment, which also present a potential environmental impact. This study focuses on removing neonicotinoid pesticides in an aqueous solution by using ecological and environmentally friendly solvents, such as terpenoid-based solvents. For this purpose, an initial screening was performed by molecular simulation with the COSMO-RS methodology, selecting two pure terpenes and three eutectic solvents as alternatives to conventional solvents.

Experimental extraction tests showed promising results. The pure terpenes achieved considerably higher extraction yields than the conventional ones, whereas this difference was slightly smaller for the eutectic solvents analyzed. Specifically, carvacrol exhibited extraction yields around 95 % for thiamethoxam and above 98 % and 99 % for imidacloprid and acetamiprid, respectively, at a volumetric S/F ratio of 0.1, 303.2 K and ultrapure water. In addition, the matrix, feed pH and temperature effect were practically negligible for the selected terpene, not limiting its competitive S/F ratio for the three pesticides. Carvacrol has not been proposed so far in the literature for the removal of pesticides in wastewater, opening this work a wide range of possibilities regarding the potential of this solvent to extract neonicotinoid pesticides from aqueous streams in an industrial context.

CRediT authorship contribution statement

Pablo Gutiérrez-Sánchez: Investigation, Formal Analysis, Software, Methodology, Writing - original draft, Writing - review & editing. **Pablo Navarro:** Software, Writing - review & editing. **Silvia Álvarez-Torrellas:** Conceptualization, Writing - review & editing. **Juan García:** Conceptualization, Funding acquisition, Project administration, Writing - review & editing. **Marcos Larriba:** Conceptualization, Funding acquisition, Methodology, Project administration, Writing - review & editing.

Declaration of Competing Interest

The authors declare that they have no known competing financial interests or personal relationships that could have appeared to influence the work reported in this paper.

Data availability

No data was used for the research described in the article.

Acknowledgments

The authors are grateful to Comunidad Autónoma de Madrid for financial support of Project S2018/EMT-4341, IND2017/AMB-7720, and PR65/19-22441 and to Ministerio de Ciencia e Innovación for financial support of Project PID2020-116478RB-I00. This work has been supported by the Madrid Government (Comunidad Autónoma de Madrid- Spain) under the Multiannual Agreement with Complutense University in the line Program to Stimulate Research for Young Doctors in the context of the V PRICIT (Regional Programme of Research and Technological Innovation). Finally, we thank Centro de Computación Científica de la Universidad Autónoma de Madrid for computational facilities.

Appendix A. Supplementary material

Supplementary data to this article can be found online at https://doi.org/10.1016/j.seppur.2022.122148.

References

[1] G.A. Matthews, Pesticides : Health, Safety and the Environment, Segunda Ed, John Wiley & Sons, Hoboken, NJ, 2016.
[2] I.A. Saleh, N. Zouari, M.A. Al-Ghouti, Removal of pesticides from water and wastewater: Chemical, physical and biological treatment approaches, Environ. Technol. Innov. 19 (2020).
[3] H. Salem, E.J. Olajos, Review of pesticides: Chemistry, uses and toxicology, Toxicol. Ind. Health. 4 (1988) 291–321, https://doi.org/10.1177/074823378800400303.
[4] M.A. Sierra, M. Gómez Gallego, Principios de química medioambiental, Síntesis, Madrid, 2007.
[5] H.S. Rathore, L.M.L. Nollet, Pesticides : Evaluation of,, Environmental Pollution (2012).
[6] M. Mehran Anjum, Pesticides and Environmental Health: A Review, Agric. Res. Technol. Open Access J. 5 (2017), https://doi.org/10.19080/artoaj.2017.05.555671.
[7] D. Goulson, An overview of the environmental risks posed by neonicotinoid insecticides, J. Appl. Ecol. 50 (2013) 977–987, https://doi.org/10.1111/1365-2664.12111.
[8] A. Lahora, J. Llorca, Sustancias de la lista de observación (Decisión UE 2015/495) en aguas residuales de la Región de Murcia, TECNOAQUA. (2017).
[9] P. Jeschke, R. Nauen, Neonicotinoids - From zero to hero in insecticide chemistry, Pest Manag. Sci. 64 (2008) 1084–1098, https://doi.org/10.1002/ps.1631.
[10] T. Wakita, K. Kinoshita, E. Yamada, N. Yasui, N. Kawahara, A. Naoi, M. Nakaya, K. Ebihara, H. Matsuno, K. Kodaka, The discovery of dinotefuran: A novel neonicotinoid, Pest Manag. Sci. 59 (2003) 1016–1022, https://doi.org/10.1002/ps.727.
[11] M. A. Quiroz, E. R. Bandala, C. A. Martínez-Huitle, Advanced Oxidation Processes (AOPs) for Removal of Pesticides from Aqueous Media, Pestic. - Formul. Eff. Fate. (2011).
[12] M.C. Vagi, A.S. Petsas, Advanced Oxidation Processes for the Removal of Pesticides from Wastewater: Recent Review and Trends, in: 15th Int. Conf. Environ. Sci. Technol., 2017. https://cest.gnest.org/sites/default/files/presentation_file_list/cest2017_01225_oral_paper.pdf (accessed November 10, 2020).
[13] J. Zhao, P. Huang, X. Wang, J. Yang, Z. Zhou, X. Du, X. Lu, Efficient adsorption removal of organic nitrogen pesticides: Insight into a new hollow NiO/Co@C

magnetic nanocomposites derived from metal-organic framework, Sep. Purif. Technol. 287 (2022), 120608, https://doi.org/10.1016/j.seppur.2022.120608.
[14] M. Kida, S. Ziembowicz, P. Koszelnik, Removal of organochlorine pesticides (OCPs) from aqueous solutions using hydrogen peroxide, ultrasonic waves, and a hybrid process, Sep. Purif. Technol. 192 (2018) 457–464, https://doi.org/10.1016/j.seppur.2017.10.046.
[15] M. Mbaye, P.A. Diaw, O.M.A. Mbaye, N. Oturan, M.D. Gaye Seye, C. Trellu, A. Coly, A. Tine, J.-J. Aaron, M.A. Oturan, Rapid removal of fungicide thiram in aqueous medium by electro-Fenton process with Pt and BDD anodes, Sep. Purif. Technol. 281 (2022) 119837. https://doi.org/https://doi.org/10.1016/j.seppur.2021.119837.
[16] Y. Shi, S. Wang, M. Xu, X. Yan, J. Huang, H. Wang, Removal of neonicotinoid pesticides by adsorption on modified Tenebrio molitor frass biochar: Kinetics and mechanism, Sep. Purif. Technol. 297 (2022), 121506, https://doi.org/10.1016/j.seppur.2022.121506.
[17] J. Liu, C. Feng, Y. Li, Y. Zhang, Q. Liang, S. Xu, Z. Li, S. Wang, Photocatalytic detoxification of hazardous pymetrozine pesticide over two-dimensional covalent-organic frameworks coupling with Ag3PO4 nanospheres, Sep. Purif. Technol. 288 (2022), 120644, https://doi.org/10.1016/j.seppur.2022.120644.
[18] E. Serrano, M. Munoz, Z.M. de Pedro, J.A. Casas, Fast oxidation of the neonicotinoid pesticides listed in the EU Decision 2018/840 from aqueous solutions, Sep. Purif. Technol. 235 (2020), 116168, https://doi.org/10.1016/j.seppur.2019.116168.
[19] M.M. Sablas, M.D.G. de Luna, S. Garcia-Segura, C.-W. Chen, C.-F. Chen, C.-D. Dong, Percarbonate mediated advanced oxidation completely degrades recalcitrant pesticide imidacloprid: Role of reactive oxygen species and transformation products, Sep. Purif. Technol. 250 (2020), 117269, https://doi.org/10.1016/j.seppur.2020.117269.
[20] S.T. Narenderan, S.N. Meyyanathan, Sample Treatment and Determination of Pesticide Residues in Potato Matrices: a Review, Potato Res. 62 (2019) 47–67, https://doi.org/10.1007/s11540-018-9396-x.
[21] I. Timofeeva, A. Shishov, D. Kanashina, D. Dzema, A. Bulatov, On-line in-syringe sugaring-out liquid-liquid extraction coupled with HPLC-MS/MS for the determination of pesticides in fruit and berry juices, Talanta. 167 (2017) 761–767, https://doi.org/10.1016/j.talanta.2017.01.008.
[22] A. Samsidar, S. Siddiquee, S.M. Shaarani, A review of extraction, analytical and advanced methods for determination of pesticides in environment and foodstuffs, Trends Food Sci. Technol. 71 (2018) 188–201, https://doi.org/10.1016/j.tifs.2017.11.011.
[23] S.K. Selahle, A. Mpupa, P.N. Nomngongo, A review of extraction, analytical, and advanced methods for the determination of neonicotinoid insecticides in environmental water matrices, Rev. Anal. Chem. 40 (2021) 187–203.
[24] R.T. LaLonde, Terpenes and Terpenoids, in: Van Nostrand's Encycl. Chem., John Wiley & Sons, Inc., Hoboken, NJ, USA, 2005. https://doi.org/10.1002/0471740039.vec2473.
[25] D.A.T. Boncan, S.S.K. Tsang, C. Li, I.H.T. Lee, H.M. Lam, T.F. Chan, J.H.L. Hui, Terpenes and terpenoids in plants: Interactions with environment and insects, Int. J. Mol. Sci. 21 (2020) 1–19. https://doi.org/10.3390/ijms21197382.
[26] H. Kim, S. Lee, B. Son, J. Jeon, D. Kim, H. Youn, J.-M. Lee, B. Youn, Biocidal effect of thymol and carvacrol on aquatic organisms: Possible application in ballast water management systems, Mar. Pollut. Bull. 133 (2018) 734–740.
[27] V. Ghorani, A. Alavinezhad, O. Rajabi, A.H. Mohammadpour, M.H. Boskabady, Safety and tolerability of carvacrol in healthy subjects: a phase I clinical study, Drug Chem. Toxicol. 44 (2) (2021) 177–189.
[28] N.B. Rathod, P. Kulawik, F. Ozogul, J.M. Regenstein, Y. Ozogul, Biological activity of plant-based carvacrol and thymol and their impact on human health and food quality, Trends Food Sci. Technol. 116 (2021) 733–748.
[29] D. Rodríguez-Llorente, A. Cañada-Barcala, S. Álvarez-Torrellas, V.I. Águeda, J. García, M. Larriba, A review of the use of eutectic solvents, terpenes and terpenoids in liquid–liquid extraction processes, Processes. 8 (2020) 1–54, https://doi.org/10.3390/pr8101220.
[30] C. Florindo, F. Lima, L.C. Branco, I.M. Marrucho, Hydrophobic deep eutectic solvents: a circular approach to purify water contaminated with ciprofloxacin, ACS Sustain. Chem. Eng. 7 (2019) 14739–14746.
[31] B.D. Ribeiro, C. Florindo, L.C. Iff, M.A.Z. Coelho, I.M. Marrucho, Menthol-based eutectic mixtures: Hydrophobic low viscosity solvents, ACS Sustain. Chem. Eng. 3 (2015) 2469–2477, https://doi.org/10.1021/acssuschemeng.5b00532.
[32] R. Verma, T. Banerjee, Liquid–liquid extraction of lower alcohols using menthol-based hydrophobic deep eutectic solvent: experiments and COSMO-SAC predictions, Ind. Eng. Chem. Res. 57 (9) (2018) 3371–3381.
[33] F. Eckert, A. Klamt, Fast Solvent Screening via Quantum Chemistry: COSMO-RS Approach, AIChE J. 48 (2002) 369–385, https://doi.org/10.1002/aic.690480220.
[34] K. Kojima, S. Zhang, T. Hiaki, Measuring methods of infinite dilution activity coefficients and a database for systems including water, Fluid Phase Equilib. 131 (1997) 145–179, https://doi.org/10.1016/s0378-3812(96)03210-4.
[35] D. Rodríguez-Llorente, A. Bengoa, G. Pascual-Muñoz, P. Navarro, V.I. Águeda, J. A. Delgado, S. Álvarez-Torrellas, J. García, M. Larriba, Sustainable Recovery of Volatile Fatty Acids from Aqueous Solutions Using Terpenoids and Eutectic Solvents, ACS Sustain. Chem. Eng. 7 (2019) 16786–16794, https://doi.org/10.1021/acssuschemeng.9b04290.
[36] M. Larriba, M. Ayuso, P. Navarro, N. Delgado-Mellado, M. Gonzalez-Miquel, J. García, F. Rodríguez, Choline Chloride-Based Deep Eutectic Solvents in the Dearomatization of Gasolines, ACS Sustain. Chem. Eng. 6 (2018) 1039–1047, https://doi.org/10.1021/acssuschemeng.7b03362.
[37] D. Rodríguez-Llorente, A. Cañada-Barcala, C. Muñoz, G. Pascual-Muñoz, P. Navarro, R. Santiago, V.I. Águeda, S. Álvarez-Torrellas, J. García, M. Larriba, Separation of phenols from aqueous streams using terpenoids and hydrophobic eutectic solvents, Sep. Purif. Technol. 251 (2020), 117379, https://doi.org/10.1016/j.seppur.2020.117379.
[38] M.A.R. Martins, L.P. Silva, N. Schaeffer, D.O. Abranches, G.J. Maximo, S.P. Pinho, J.A.P. Coutinho, Greener Terpene-Terpene Eutectic Mixtures as Hydrophobic Solvents, ACS Sustain. Chem. Eng. 7 (2019) 17414–17423, https://doi.org/10.1021/acssuschemeng.9b04614.
[39] M.A.R. Martins, E.A. Crespo, P.V.A. Pontes, L.P. Silva, M. Bülow, G.J. Maximo, E.A. C. Batista, C. Held, S.P. Pinho, J.A.P. Coutinho, Tunable Hydrophobic Eutectic Solvents Based on Terpenes and Monocarboxylic Acids, ACS Sustain. Chem. Eng. 6 (2018) 8836–8846, https://doi.org/10.1021/acssuschemeng.8b01203.
[40] M.P. Didović, T. Kowalkowski, D. Broznić, Emerging Contaminant Imidacloprid in Mediterranean Soils: The Risk of Accumulation Is Greater than the Risk of Leaching, Toxics. 10 (2022) 358.
[41] M. Tomizawa, J.E. Casida, Neonicotinoid insecticide toxicology: mechanisms of selective action, Annu. Rev. Pharmacol. Toxicol. 45 (1) (2005) 247–268.
[42] L. Cox, W.C. Koskinen, R. Celis, M.C. Hermosin, J. Cornejo, P.Y. Yen, Sorption of imidacloprid on soil clay mineral and organic components, Soil Sci. Soc. Am. J. 62 (4) (1998) 911–915.
[43] M.G. Valverde, M.J.M. Bueno, M.M. Gómez-Ramos, A. Aguilera, M.D.G. García, A. R. Fernández-Alba, Determination study of contaminants of emerging concern at trace levels in agricultural soil. A pilot study, Sci. Total Environ. 782 (2021), 146759.
[44] K. Chamberlain, A.A. Evans, R.H. Bromilow, 1-Octanol/water partition coefficient (Kow) and pKa for ionisable pesticides measured by apH-metric method, Pestic. Sci. 47 (3) (1996) 265–271.
[45] P. Sande-Fouz, J.M. Mirás-Avalos, R. Da Silva Dias, E. Vidal-Vázquez, Concentrations of Three Different Carbon Forms in Surface Waters from an Agroforestry Catchment in Northwest Spain, Commun. Soil Sci. Plant Anal. 44 (1-4) (2013) 404–414.
[46] M. Lorite-Herrera, K. Hiscock, R. Jiménez-Espinosa, Distribution of dissolved inorganic and organic nitrogen in river water and groundwater in an agriculturally-dominated catchment, south-east Spain, Water. Air. Soil Pollut. 198 (1-4) (2009) 335–346.
[47] P. Sobczak, A. Rosińska, Concentration of total organic carbon and its fractions in surface water in Poland and Germany, in, Multidiscip. Digit. Publ. Inst. Proc. (2020) 35.
[48] L. Dahuron, B.S. Holden, W.D. Prince, A.F. Seibert, L.C. Wilson, T.C. Frank, Liquid-Liquid Extraction and Other Liquid-Liquid Operations and Equipment, in, Perry's Chem. Eng. Handb., McGraw-Hill Pub (2008).
[49] L.Y. Garcia-Chavez, A.J. Hermans, B. Schuur, A.B. De Haan, COSMO-RS assisted solvent screening for liquid–liquid extraction of mono ethylene glycol from aqueous streams, Sep. Purif. Technol. 97 (2012) 2–10, https://doi.org/10.1016/J.SEPPUR.2011.11.041.
[50] Y. Chen, S. Zhou, Y. Wang, L. Li, Screening solvents to extract phenol from aqueous solutions by the COSMO-SAC model and extraction process simulation, Fluid Phase Equilib. 451 (2017) 12–24, https://doi.org/10.1016/J.FLUID.2017.08.007.
[51] M. Grabda, M. Zawadzki, S. Oleszek, M. Matsumoto, M. Królikowski, Y. Tahara, Removal of perfluorooctanoic acid from water using a hydrophobic ionic liquid selected using the Conductor-like Screening Model for Realistic Solvents, Environ. Sci. Technol. 56 (10) (2022) 6445–6454.
[52] G. Leeke, F. Gaspar, R. Santos, The effect of water on the solubilities of essential oils in dense CO2, J. Essent. Oil Res. 15 (2003) 172–177, https://doi.org/10.1080/10412905.2003.9712105.
[53] P. Gutiérrez-Sánchez, D. Rodríguez-Llorente, P. Navarro, V.I. Águeda, S. Álvarez-Torrellas, J. García, M. Larriba, Extraction of antibiotics identified in the EU Watch List 2020 from hospital wastewater using hydrophobic eutectic solvents and terpenoids, Sep. Purif. Technol. 282 (2022), 120117, https://doi.org/10.1016/j.seppur.2021.120117.
[54] J.S. Dambolena, M.P. Zunino, J.M. Herrera, R.P. Pizzolitto, V.A. Areco, J. A. Zygadlo, Terpenes: Natural Products for Controlling Insects of Importance to Human Health—A Structure-Activity Relationship Study, Psyche (Stuttg). 2016 (2016) 4595823, https://doi.org/10.1155/2016/4595823.
[55] Y. Wang, N. Li, S. Jiang, X. Chen, Application of extraction and determination based on deep eutectic solvents in different types of environmental samples, Water. 14 (2021) 46.
[56] A. Santana-Mayor, R. Rodriguez-Ramos, A.V. Herrera-Herrera, B. Socas-Rodriguez, M.Á. Rodríguez-Delgado, Deep eutectic solvents. The new generation of green solvents in analytical chemistry, TrAC, Trends Anal. Chem. 134 (2021), 116108.
[57] C. Florindo, L.C. Branco, I.M. Marrucho, Development of hydrophobic deep eutectic solvents for extraction of pesticides from aqueous environments, Fluid Phase Equilib. 448 (2017) 135–142, https://doi.org/10.1016/j.fluid.2017.04.002.
[58] Alibaba, Manufacturers, Suppliers, Exporters & Importers from the world's largest online B2B marketplace, (n.d.). https://www.alibaba.com/ (accessed May 7, 2022).
[59] ICIS, Petrochemicals, Energy, and Fertilizers Market Information, (n.d.). https://www.icis.com (accessed May 10, 2022).
[60] B. Šulgan, J. Labovský, Z. Labovská, Multi-aspect comparison of ethyl acetate production pathways : reactive distillation process integration & intensification via mechanical and chemical approach, Processes. 8 (2020) 1–40, https://doi.org/10.3390/pr8121618.
[61] F. Bergua, M. Castro, J. Muñoz-Embid, C. Lafuente, M. Artal, Hydrophobic eutectic solvents: Thermophysical study and application in removal of pharmaceutical products from water, Chem. Eng. J. 411 (2021), 128472, https://doi.org/10.1016/j.cej.2021.128472.

[62] P.B. Kyle, Toxicology: GCMS, Elsevier Inc., 2017. https://doi.org/10.1016/B978-0-12-800871-3.00007-9.
[63] F.F. Cantwell, M. Losier, Liquid-liquid extraction, Compr. Anal. Chem. 37 (2002) 297–340, https://doi.org/10.1016/S0166-526X(02)80048-4.
[64] Z. Berk, Extraction, in: Food Process Eng. Technol., 2018: pp. 289–310. https://doi.org/10.1016/c2016-0-03186-8.

SUPPLEMENTARY MATERIAL

Extraction of neonicotinoid pesticides from aquatic environmental matrices with sustainable terpenoids and eutectic solvents

Pablo Gutiérrez-Sánchez,[a] Pablo Navarro,[b] Silvia Álvarez-Torrellas,[a] Juan García,[a] Marcos Larriba[a,*]

[a]*Grupo de Catálisis y Procesos de Separación (CyPS), Departamento de Ingeniería Química y de Materiales, Universidad Complutense de Madrid, Avda. Complutense s/n, 28040 Madrid, Spain.*

[b]*Departamento de Ingeniería Química, Universidad Autónoma de Madrid, C/ Francisco Tomás y Valiente 7, 28049 Madrid, Spain.*

Content

Number of pages: 8

Number of tables: 2

Number of figures: 7

Table S1. pKa values of the dissociation equilibria for acetamiprid, imidacloprid, and thiamethoxam [40–44].

Neonicotinoid pesticide	pKa
Acetamiprid	0.8
Imidacloprid	1.56-11.12
Thiamethoxam	0.4

Table S2. Properties of the chemicals used in this research.

Chemical	Structure	Supplier	Purity (wt %)	T_m (K)	T_b (K)
Neonicotinoid pesticides					
Acetamiprid, CAS nº 160430-64-8	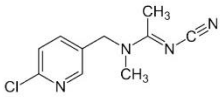	Sigma-Aldrich	≥ 98	372.0	-
Imidacloprid, CAS nº 138261-41-3	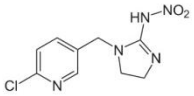	Sigma-Aldrich	≥ 98.0	417.1	-
Thiamethoxam, CAS nº 153719-23-4	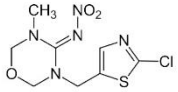	Sigma-Aldrich	≥ 98.0	412.2	-
Extraction solvents					
Carvacrol, CAS nº 499-75-2	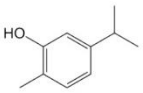	Sigma-Aldrich	≥ 98.0	276.7	509.7
Thymol, CAS nº 89-83-8	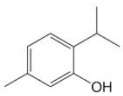	Sigma-Aldrich	≥ 99.0	322.7	505.2
Dodecanoic acid, CAS nº 143-07-7	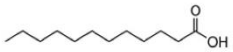	Sigma-Aldrich	98.0	318.2	571.2
Decanoic acid, CAS nº 334-48-5	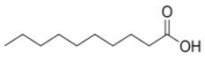	Sigma-Aldrich	≥ 98.0	302.2	542.2
Octanoic acid, CAS nº 124-07-2	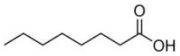	Sigma-Aldrich	≥ 98.0	289.2	510.2
Ethyl acetate, CAS nº 141-78-6		Fluka	> 99.5	189.5	350.1
Methyl isobutyl ketone, CAS nº 108-10-1 (MIBK)	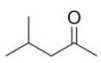	Sigma-Aldrich	99.0	189.1	389.6
Other chemicals					
Acetonitrile, CAS nº 75-05-08	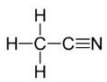	Scharlau	≥ 99.9	227.5	354.8
Acetic acid, CAS nº 64-19-7		PanReac	≥ 99.7	289.9	391.2

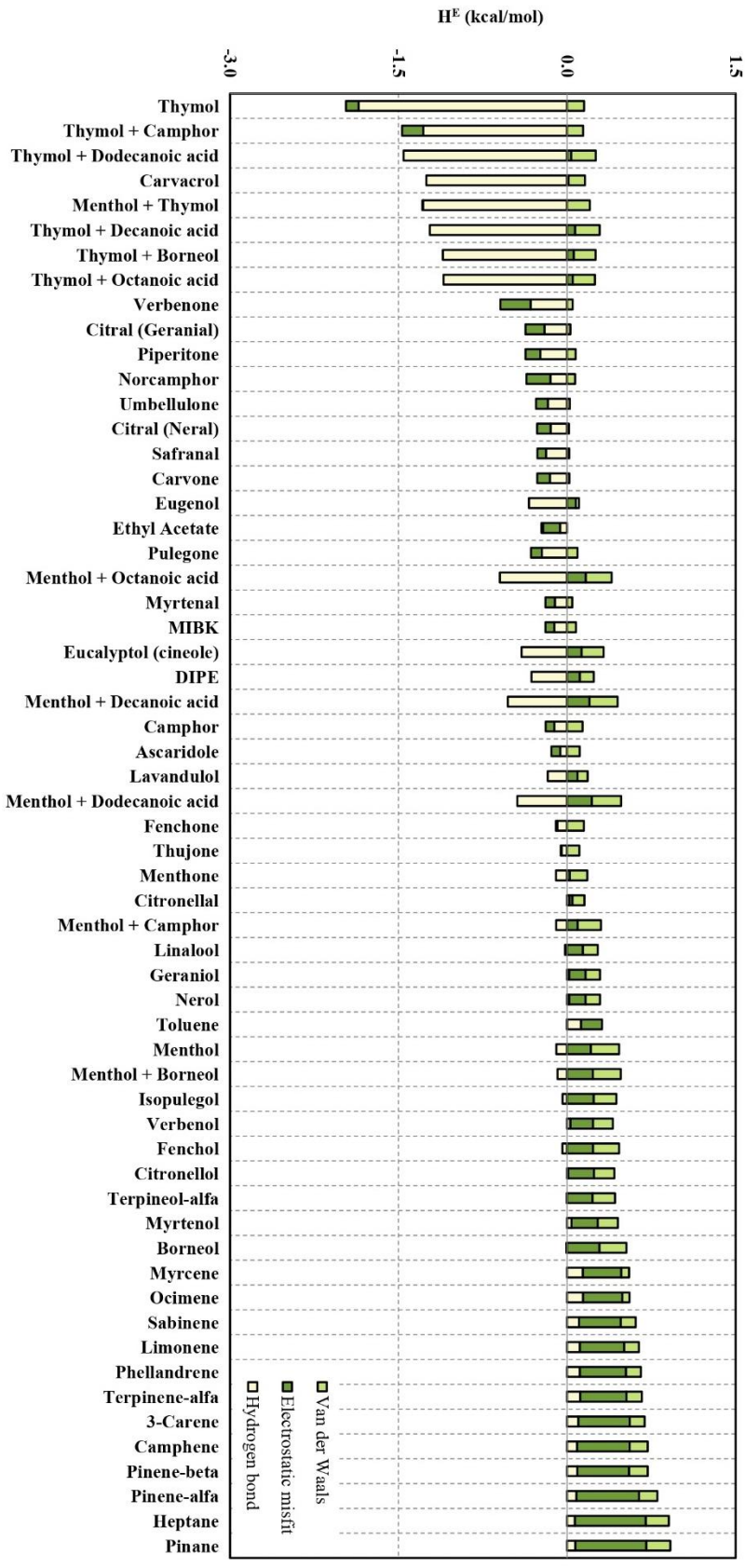

Figure S1. Contributions of excess enthalpies predicted by COSMOtherm for imidacloprid.

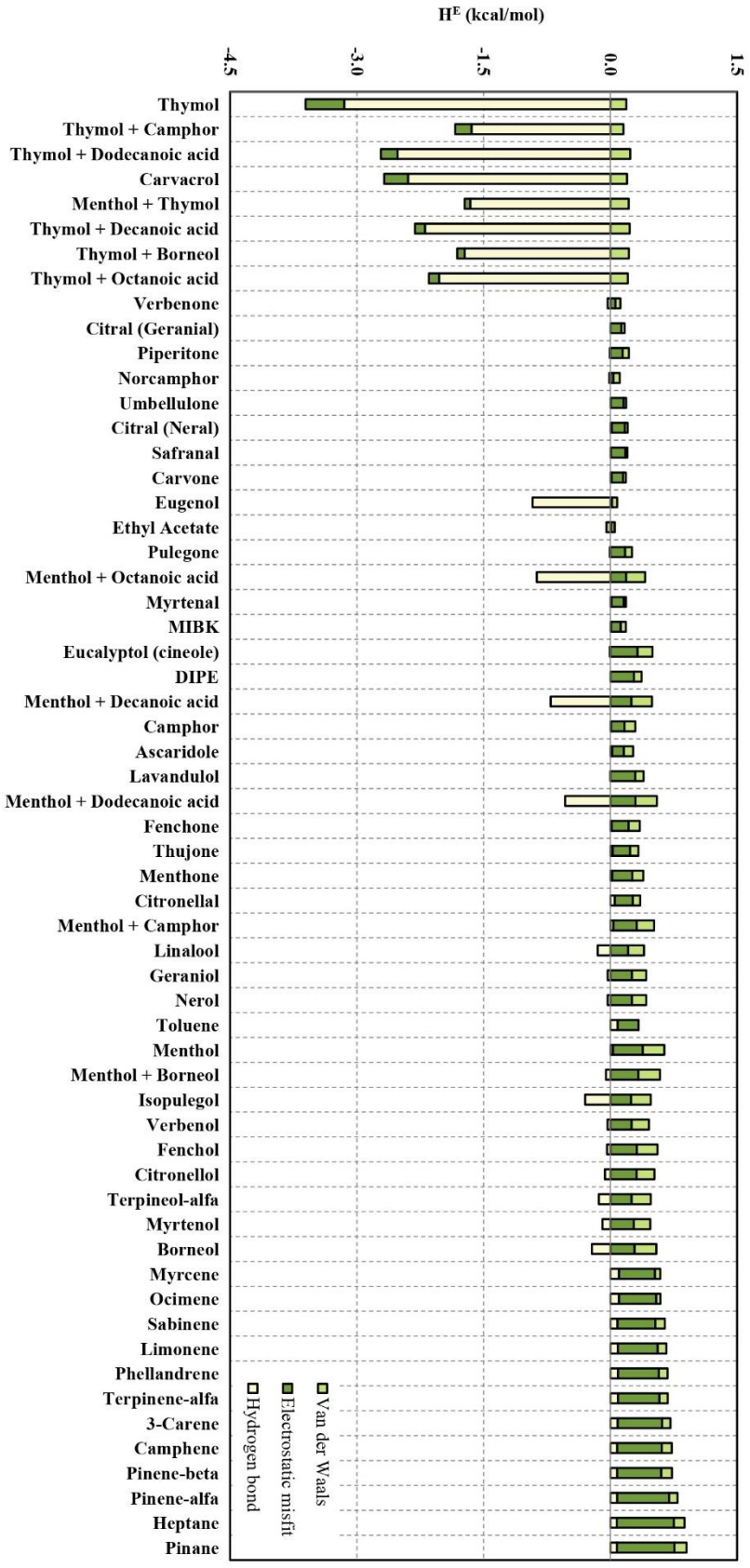

Figure S2. Contributions of excess enthalpies predicted by COSMOtherm for acetamiprid.

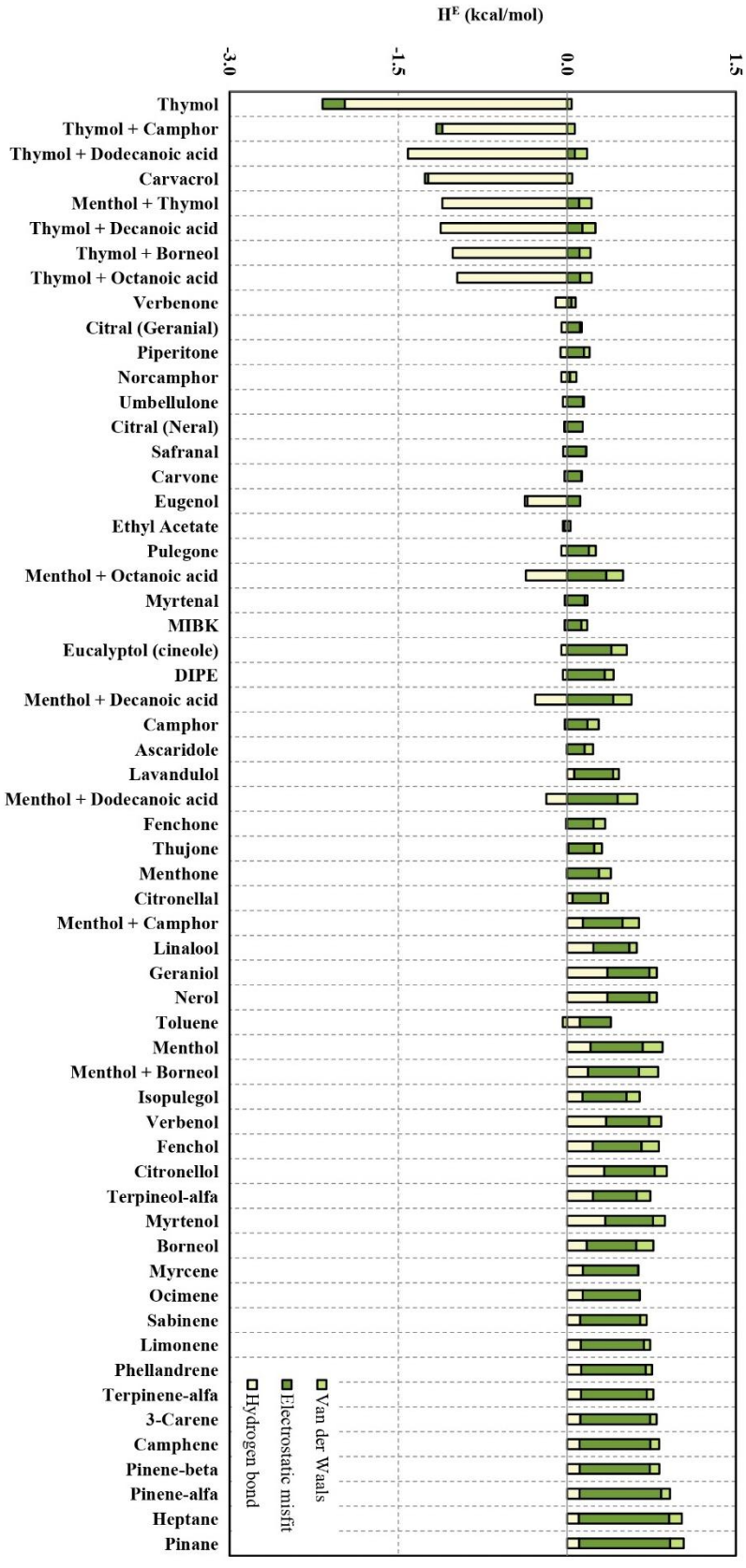

Figure S3. Contributions of excess enthalpies predicted by COSMOtherm for thiamethoxam.

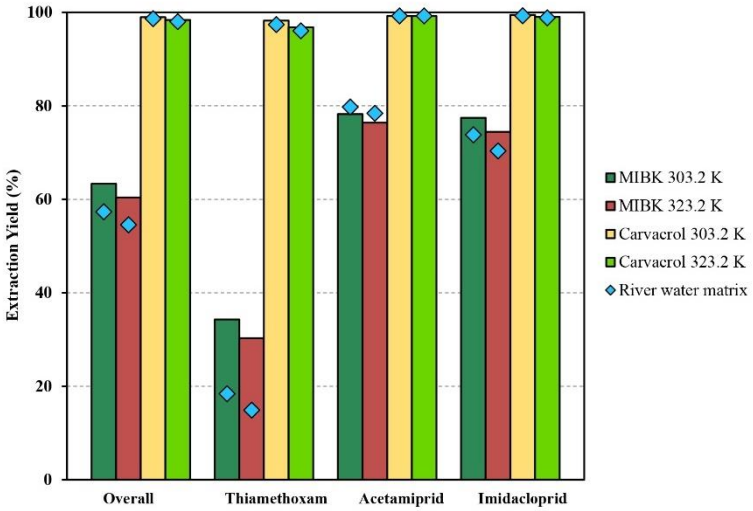

Figure S4. Multicomponent extraction yields of pesticides from ultrapure water and river water matrix by using carvacrol and MIBK at S/F 0.25 and two temperatures, 323.2 K and 303.2 K.

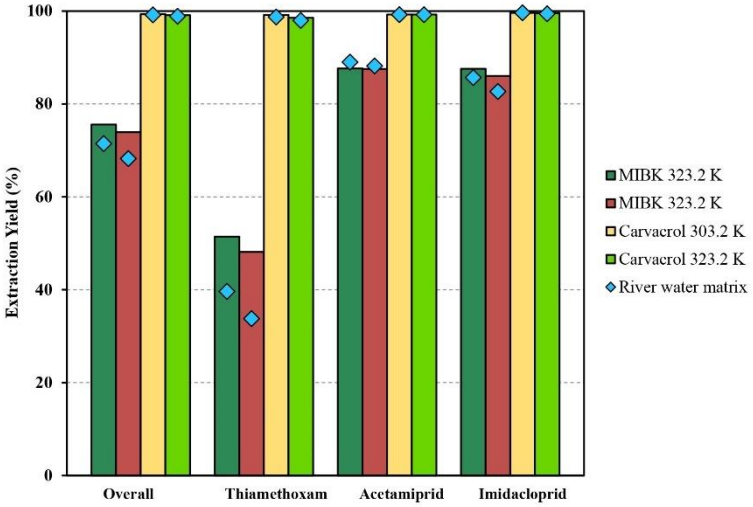

Figure S5. Multicomponent extraction yields of pesticides from ultrapure water and river water matrix by using carvacrol and MIBK at S/F 0.50 and two temperatures, 323.2 K and 303.2 K.

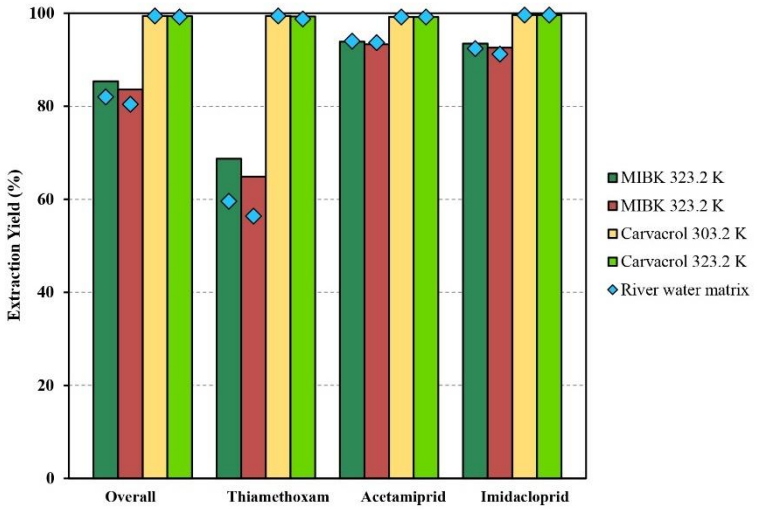

Figure S6. Multicomponent extraction yields of pesticides from ultrapure water and river water matrix by using carvacrol and MIBK at S/F 1.00 and two temperatures, 323.2 K and 303.2 K.

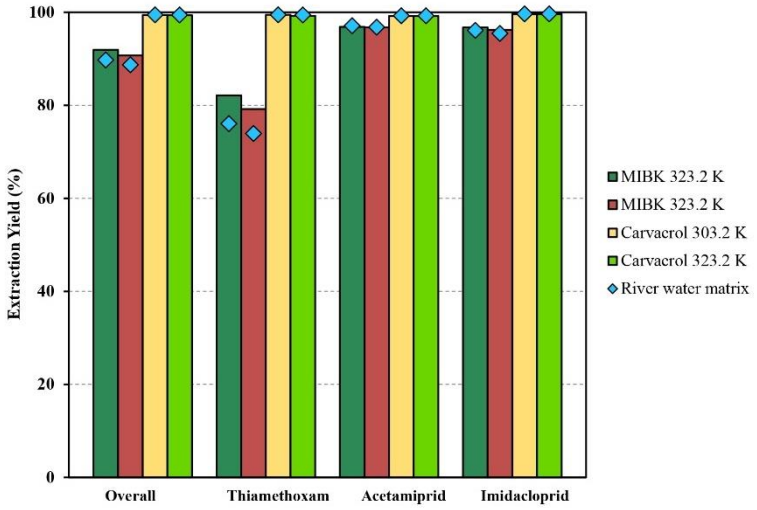

Figure S7. Multicomponent extraction yields of pesticides from ultrapure water and river water matrix by using carvacrol and MIBK at S/F 2.00 and two temperatures, 323.2 K and 303.2 K.

7.2 Publicación 2

Separation and Purification Technology 282 (2022) 120117

Contents lists available at ScienceDirect

Separation and Purification Technology

journal homepage: www.elsevier.com/locate/seppur

Extraction of antibiotics identified in the EU Watch List 2020 from hospital wastewater using hydrophobic eutectic solvents and terpenoids

Pablo Gutiérrez-Sánchez [a], Diego Rodríguez-Llorente [a], Pablo Navarro [b], V. Ismael Águeda [a], Silvia Álvarez-Torrellas [a], Juan García [a], Marcos Larriba [a,*]

[a] Grupo de Catálisis y Procesos de Separación (CyPS), Departamento de Ingeniería Química y de Materiales, Universidad Complutense de Madrid, Avda. Complutense s/n, 28040 Madrid, Spain
[b] Departamento de Ingeniería Química, Universidad Autónoma de Madrid, C/ Francisco Tomás y Valiente 7, 28049 Madrid, Spain

ARTICLE INFO

Keywords:
Antibiotics
Terpenoids
Eutectic solvents
Liquid-liquid extraction
Solvent recovery

ABSTRACT

The increasing consumption of pharmaceuticals, along with the ineffectiveness of conventional wastewater treatment, has resulted in an increased presence of these pollutants in both drinking water supplies and aquatic environments. The potential adverse health effects and environmental impact of these chemicals are drawing the attention of several bodies around the world. For instance, some antibiotics such as ciprofloxacin, trimethoprim, and sulfamethoxazole have been included in the most recent European Surface Water Watch List under the EU Water Framework Directive (Decision 2020/1161). The present work proposes the use of terpenoids and eutectic solvents, as effective and green solvents with low toxicity, for multicomponent liquid–liquid extraction of ciprofloxacin, trimethoprim, and sulfamethoxazole from ultrapure water and hospital wastewater. The COSMO-RS method was used for a predictive initial solvent screening. Thymol, carvacrol, eutectic solvents (thymol + fatty acids), and conventional solvents (methyl isobutyl ketone and ethyl acetate) were selected to be used in the experiments. The influence of the volumetric S/F ratio, aqueous matrix, and pH was analysed. Conventional solvents show significantly lower overall extraction yields than those observed for eutectic solvents and terpenoids at any pH and matrix. Carvacrol presented the most favourable conditions, reaching overall extraction yields above 98.0% (98.9% for trimethoprim, 99.5% for ciprofloxacin, and 97.0% for sulfamethoxazole) with hospital wastewater at pH 5.0 and S/F ratio of 1.00. Carvacrol showed a feasible operation in a continuous extraction column at room temperature, providing effective reuse and regeneration processes in this study.

1. Introduction

The pharmaceutical industry has played a key role in both developed and developing countries, increasing life expectancy and having to adapt to changing policy environments [1–2]. Pharmaceuticals are substances used as medicinal drugs to produce a therapeutic effect, comprising a wide variety of organic compounds: antibiotics, blood lipid regulators, hormones, anti-inflammatory drugs, β-blockers, antiepileptic drugs, contrast media, and cytostatic drugs [3–5].

Nowadays, antibiotics are one of the most widespread pharmaceuticals all over the world, and their global consumption reaches values of around 100,000 and 200,000 tons per year. The United States of America stands out as one of the leading manufacturers, producing more than 20,000 tons of antibiotics annually, 60% for human use and 40% for veterinary applications. These compounds are used to treat bacterial and fungal infections and contain chemical subgroups such as macrolides, sulfonamides, or fluoroquinolones [5–7]. Many of them are derived wholly or partially from certain microorganisms, but some are synthetic [8]. So far, one of the most discussed topics related to the effects induced by pharmaceuticals is the development of antimicrobial resistance in bacterial populations, which is favored by the exposure to low concentrations of antibiotics [6,9–13].

In fact, pharmaceuticals are considered as one of the most critical emerging pollutants. They are released into the environment mainly due to their incomplete removal in Wastewater Treatment Plants (WWTP), in addition to other sources such as hospital effluents, waste from industry and livestock, and the disposal of unused or expired pharmaceutical products [4,14–16]. The average concentration of antibiotics in hospital effluents ranges from 5 to 10 times higher than that measured in WWTP effluents [17].

* Corresponding author.
E-mail address: marcoslarriba@ucm.es (M. Larriba).

https://doi.org/10.1016/j.seppur.2021.120117
Received 14 September 2021; Received in revised form 20 October 2021; Accepted 7 November 2021
Available online 10 November 2021

Table 1
Physicochemical properties of the compounds used in this paper [84–85].

Chemical	Structure	Supplier	Purity (wt %)	T_m (K)	T_b (K)
Antibiotics					
Trimethoprim	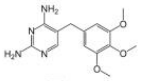	Sigma-Aldrich	≥ 99	474.2	–
Ciprofloxacin	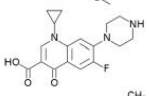	Sigma-Aldrich	≥ 98.0	–	–
Sulfamethoxazole	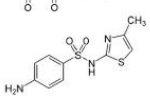	Sigma-Aldrich	≥ 98.0	442.7	–
Extraction solvents					
Carvacrol	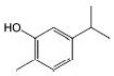	Sigma-Aldrich	≥ 98.0	276.7	509.7
Thymol		Sigma-Aldrich	≥ 99.0	322.7	505.2
Dodecanoic acid		Sigma-Aldrich	98.0	318.2	571.2
Decanoic acid		Sigma-Aldrich	≥ 98.0	302.2	542.2
Octanoic acid	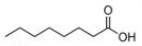	Sigma-Aldrich	≥ 98.0	289.2	510.2
Ethyl acetate		Fluka	> 99.5	189.5	350.1
Methyl isobutyl ketone (MIBK)		Sigma-Aldrich	99.0	189.1	389.6
Other chemicals					
Acetonitrile		Scharlau	≥ 99.9	227.5	354.8
Acetic acid		PanReac	≥ 99.7	289.9	391.2
Hydrochloric acid		Fluka	37	238.2	315.2

Due to the lack of data about the possible chronic health effects associated with the long-term ingestion of pharmaceuticals at low concentrations, these compounds are not either regulated or included in the models for the assessment of water quality index [4,6,18–20]. However, their potential environmental impact and adverse health effects have drawn the attention of health bodies and agencies worldwide. For this reason, antibiotics such as sulfamethoxazole, trimethoprim, and ciprofloxacin have been included in the second and the third versions of the EU Watch List of contaminants of emerging concern under the Water Framework Directive [21–23].

Over the last few years, several techniques have been studied for the removal of pharmaceuticals from wastewater, such as activated sludge treatment [24–27], membrane bioreactor [28–32], constructed wetland [33–37], adsorption [3,38–40], membrane filtration (ultrafiltration, nanofiltration and reverse osmosis) [41–46], and advanced oxidation processes (wet air oxidation; electrochemical oxidation; photolysis; ultrasound irradiation; heterogeneous photocatalysis; ozone and ozone/hydrogen peroxide treatment; and Fenton oxidation) [15,18,47–51].

Liquid-liquid extraction has also been studied in the pharmaceutical industry, although mainly applied to the isolation and purification of pharmaceutical compounds during their production, rather than for wastewater treatment [4,47,52,53]. This technique has traditionally presented drawbacks, such as excessive and unsustainable consumption of non-renewable and environmentally hazardous substances [54,55]. In this regard, terpenes and terpenoids, which are plant products derived from the basic isoprene unit, stand out as a group of renewable solvents [56–59]. They also show less toxicity than conventional petroleum-based solvents [60–64]. On the other hand, eutectic solvents might also be proposed as an emerging class of green solvents. They are a newly discovered sort of mixtures with depression in melting points in comparison to those for pure components, mainly due to hydrogen bonding interactions between the compounds of the mixture [65–74].

The aim of this research is to study the behavior of terpenoids and eutectic solvents as extractants to be used in the multicomponent extraction of ciprofloxacin, trimethoprim, and sulfamethoxazole from ultrapure water and hospital wastewater. As reported in the literature, these three antibiotics are frequently detected in this sort of sewage [75]. Making an initial selection of suitable solvents through molecular simulation with Conductor like Screening Model for Real Solvents (COSMO-RS) methodology, the following solvents were selected to move on to the experimental phase: 2 terpenoids (thymol and carvacrol), 3 hydrophobic eutectic solvents (thymol + dodecanoic acid, thymol + decanoic acid and thymol + octanoic acid) and 2 conventional solvents (ethyl acetate and methyl isobutyl ketone) [76,77]. In addition, the effect of pH and aqueous matrix on the liquid–liquid extraction process was analysed. Several experiments were carried out in vials (batch operation) and in a packed column (continuous operation), also evaluating the solvent reuse and recovery by vacuum distillation.

Table 2
Macroscopic characterization of the raw hospital wastewater [78].

Parameters	Value
pH	8.5
Chemical Oxygen Demand (mg/L)	332
Total Organic Carbon (mg/L)	286
Total Nitrogen (mg/L)	90.1
Total Dissolved Solids (mg/L)	0.5
CO_3^{2-} (mg/L)	365.5[a]
Conductivity at 20 °C (μS/cm)	2360

[a] Calculated from Total Inorganic Carbon measurement.

2. Experimental section

2.1. Materials

Chemical compounds used in this paper are listed in Table 1, also detailing chemical structures, suppliers, purities, melting points (T_m), and boiling temperatures (T_b). Ultrapure water was obtained from PURELAB® Flex Water Purification System (Veolia).

Hospital wastewater effluent was collected from a hospital located in the southern zone of Madrid (Spain), and its characterization is summarized in Table 2 [78]. This sample was used to test the antibiotic extraction from an environmentally-relevant aqueous matrix.

2.2. Screening of solvents using the COSMO-RS method

An initial selection of suitable solvents was performed through molecular simulation with COSMO-RS method using COSMO*therm* software (version 19.0.4). Since terpenoids are not found as conventional compounds in COSMO*therm* database, COSMO continuum solvation model at the BVP86/TZVP calculation theory level was used to optimize their geometry and build the cosmo file, whereas default BP_TZVP_19 parametrization was used to screen the solvents in COSMO*therm* software. For solvent screening, infinite dilution activity coefficients of ciprofloxacin, trimethoprim, and sulfamethoxazole were estimated in 43 terpenoids, 11 hydrophobic eutectic solvents, and 5 conventional solvents at 323.15 K, being the experimental temperature. To ensure working in the infinite dilution region, all simulations were carried out considering an antibiotic mole fraction of $5{\cdot}10^{-5}$ [79]. This approach has been successfully used in the liquid-liquid extraction of phenols and volatile fatty acids with terpenes, terpenoids and eutectic solvents composed by them [80–81]. As reported in the literature, the eutectic solvents were successfully described as a mixture of solvents at the eutectic composition [72,80–83].

2.3. Preparation of eutectic solvents

The three eutectic solvents selected from the screening described previously were prepared at their eutectic composition. The thymol mole fractions used were 0.56, 0.44, and 0.33 in the mixtures (thymol + dodecanoic acid), (thymol + decanoic acid), and (thymol + octanoic acid), respectively. At the eutectic point, melting temperatures for the previous eutectic solvents mentioned are 270.82, 287.00, and 306.30 K [83]. The compounds were weighed in an analytical balance M-420 CBC (Cobos CB-Complet, precision ± 0.001 g). The mixture was melted under stirring in a thermostatic bath at 323.2 ± 0.1 K and, once a homogenous liquid mixture appeared, it was cooled to room temperature.

2.4. Preparation of multicomponent aqueous solutions of antibiotics in ultrapure water and hospital wastewater

Firstly, a multicomponent aqueous solution of ciprofloxacin, trimethoprim, and sulfamethoxazole was prepared at 50 mg/L of each antibiotic in ultrapure water by using an analytical balance TE124S (Sartorius, precision ± 0.0001 g). This range of concentration has been previously reported by other authors [78,86–90]. The pH of the solution prepared in ultrapure water was measured by using a 2002 pH meter (Crison), reaching a value of 6.5.

To test the effect of the matrix, the aqueous solution mentioned above was also prepared using hospital wastewater, resulting in a pH of 8.0. Also, in order to study the effect of pH, two more solutions were prepared in hospital wastewater by adjusting the pH to 6.5 and 5.0 with hydrochloric acid 37 wt%.

2.5. Multicomponent liquid–liquid extraction of antibiotics from water and hospital wastewater in vial

Liquid-liquid extraction of the previously prepared aqueous solutions was carried out with each of the 6 selected solvents: 2 terpenoids (thymol and carvacrol), 3 eutectic solvents (thymol + dodecanoic acid, thymol + decanoic acid and thymol + octanoic acid), and 2 conventional solvents (MIBK and ethyl acetate). Feed and solvent were mixed according to the following volumetric solvent/feed (S/F) ratios: 2.00, 1.00, 0.50, 0.25, and 0.10. Both phases were placed in 8 mL glass vials with magnetic stirring in a C-MAG HS 7 dry bath (IKA) at 323.2 ± 0.1 K for 12 h, time to ensure equilibrium conditions. This temperature was selected to ensure the liquid state of the 6 extraction solvents and to compare the results obtained under the same operating conditions. After 4 h stirring, the two phases were settled and sampled using glass Pasteur pipettes, maintaining a constant temperature of 323.2 ± 0.1 K for all the steps. The concentration of the organic compounds in the raffinate (aqueous phase at the bottom of the vial) was determined by using an analytical High Performance Liquid Chromatograph 1260 Infinity II with Diode Array Detector (Agilent), and a Poroshell 120 EC-C18 chromatographic column (4.6 × 150 mm, 4 μm). Thus, a mobile phase consisting of a mixture of acetonitrile and an aqueous acetic acid solution 75 mM was used. The volumetric flow rate was 0.9 mL/min and the column temperature was set at 313.2 K. The wavelengths to measure the concentration of antibiotics and organic solvents in the raffinate phase were 233 nm and 275 nm.

2.6. Multicomponent liquid–liquid extraction of antibiotics from hospital wastewater in a packed column

In order to study the mass transfer effect and evaluate the scale-up of the liquid–liquid extraction process, continuous parallel extraction was accomplished in a column of 8 mm internal diameter and 80 mm length, filled with a bed of glass spheres of 2 mm diameter. The multicomponent aqueous solution of antibiotics in hospital wastewater at pH 5.0 was used as feed, whereas carvacrol was the solvent selected due to the promising results obtained in the vial extraction tests (batch mode). By using a KDS 100 Legacy (Fisher Scientific) and an Orion Sage M361 (Thermo Orion Sage) syringe pumps, feed and solvent were introduced into the column at 298.2 ± 1 K (room temperature) according to the following volumetric S/F ratios: 2.00, 1.00, and 0.50. This operating temperature was selected due to the low melting point of carvacrol (Table 1), which guarantees the liquid state of the solvent at room temperature and avoids the energy costs associated with heating. The total volumetric flow rate remained constant during the three experiments at 10 mL/h and the residence time in the column was 21 min. After leaving the column, both phases were settled and analyzed using the same procedure previously described in the batch extraction. A scheme of the packed column installation is included in Figure S1 of the Supplementary Material.

2.7. Solvent reuse in consecutive stages of antibiotic extraction from hospital wastewater and solvent recovery

Another key aspect for the implementation of an industrial-scale extraction process is the evaluation of the solvent reuse. For this purpose, multicomponent aqueous solution of ciprofloxacin, trimethoprim,

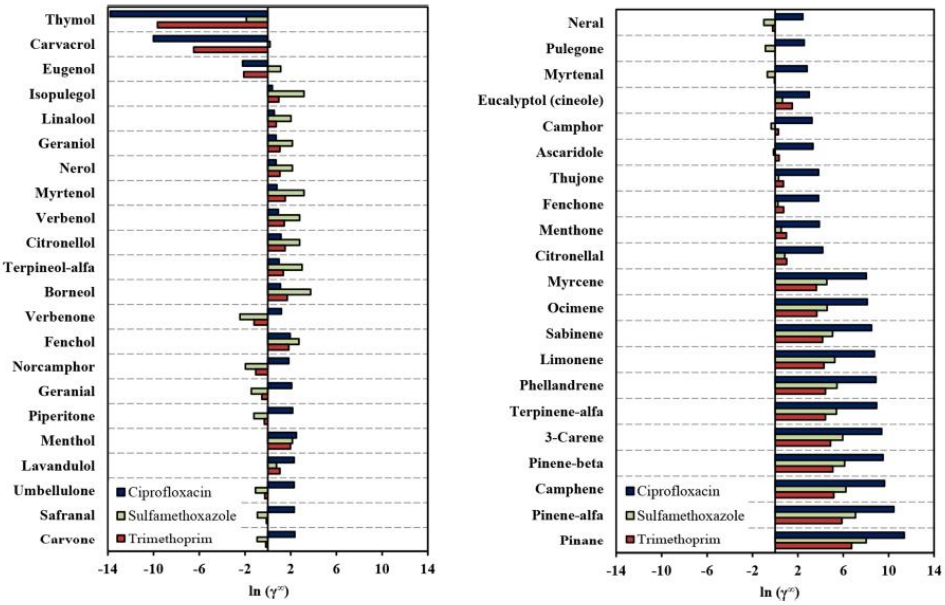

Fig. 1. Activity coefficients at infinite dilution of ciprofloxacin, trimethoprim, and sulfamethoxazole in several terpenoids by using COSMO-RS approach and setting the temperature at 323.2 K.

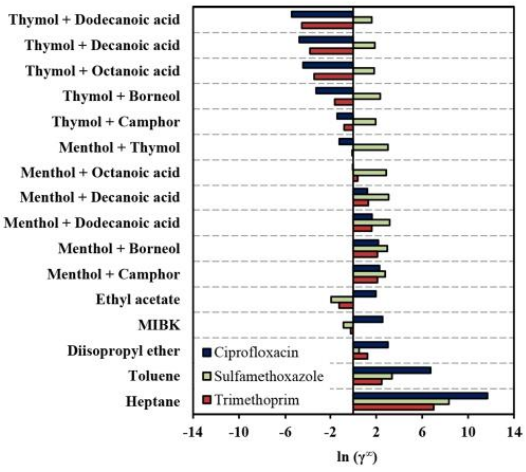

Fig. 2. Activity coefficients at infinite dilution of ciprofloxacin, trimethoprim, and sulfamethoxazole in several eutectic solvents and conventional solvents by using the COSMO-RS approach and setting the temperature at 323.2 K.

and sulfamethoxazole in hospital wastewater with pH adjusted to 5.0 was used as feed. Regarding the solvent, and due to the promising results obtained in the vial extraction experiments, only carvacrol was selected at a volumetric S/F ratio of 1.00. Five consecutive extraction stages were carried out in 500 mL glass bottles with magnetic stirring at 298.2 ± 1 K (room temperature) for 12 h, time to ensure the equilibrium. For the first extraction stage, 125 mL of feed and 125 mL of fresh solvent were brought into contact. For the rest, fresh feed and solvent from the previous stage were used. The volumes of each phase for stages 2 to 5 were 100, 80, 65, and 45 mL. The separation and characterization of the extract and the raffinate were carried out in a similar way as described for the batch process.

On the other hand, the regeneration of the solvent from stage 5 was carried out using an R-200 rotary evaporator (Büchi) at 437.2 K and 20 mbar. To check the extractive properties of the regenerated solvent, the latter was tested by doing an extraction in an 8 mL glass vial with magnetic stirring at 298.2 ± 1 K (room temperature) for 12 h. 2 mL of regenerated carvacrol and 2 mL of multicomponent aqueous solution of antibiotics in hospital wastewater with pH adjusted to 5.0 were mixed. Then, the separation and characterization of the extract and the raffinate were carried out as described previously.

3. Results and discussion

3.1. Screening of solvents using the COSMO-RS approach

As widely reported in the literature, solvent screening can be performed by comparing the magnitude of activity coefficients of the solute in each of the solvents considered. In this regard, the lower the activity coefficient of a solute is, the higher affinity the extractant presents [55,91–93]. By using the COSMO-RS method, infinite dilution activity coefficients of ciprofloxacin, trimethoprim, and sulfamethoxazole in several terpenoids, eutectic solvents, and conventional solvents at 323.2 K were estimated. These values are shown in Figs. 1-2. In this study, as multicomponent extraction is involved, it is essential to select a solvent showing the best compromise situation for the three considered solutes.

Among the terpenoids, the solvents with the lowest activity coefficient values for all three antibiotics are thymol and carvacrol. Furthermore, it is noteworthy that terpenes with no heteroatoms in their hydrocarbon skeleton (from pinene to myrcene in Fig. 1) exhibit the highest activity coefficient values for each of the antibiotics, regardless of whether they are aromatic or not. The higher affinity for antibiotics of solvents with heteroatoms can be explained, among others, due to hydrogen bond or dipole–dipole interactions [94–95].

For conventional solvents, the compounds that seem to present the best situation of compromise for the three antibiotics are ethyl acetate

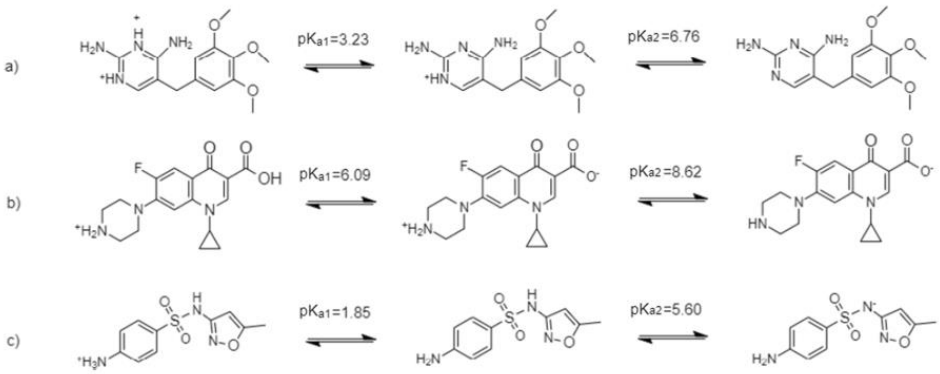

Fig. 3. Dissociation equilibria and pK_a values of trimethoprim (a), ciprofloxacin (b), and sulfamethoxazole (c) [96–97].

and MIBK, as shown in Fig. 2. Compared to the results obtained for thymol and carvacrol, conventional solvents show a lower affinity for both ciprofloxacin and trimethoprim. However, for sulfamethoxazole, this behaviour does not seem to be as noticeable.

Regarding the eutectic solvents, the mixtures with thymol showed the lowest activity coefficients, especially those containing carboxylic acids: thymol + dodecanoic acid, thymol + decanoic acid, and thymol + octanoic acid. Compared to the results for sulfamethoxazole, these three solvents presented notably lower activity coefficients for ciprofloxacin and trimethoprim. It should be noted that, as mentioned in the literature, eutectic solvents can give better experimental extraction results than those predicted by molecular simulation [80–81].

Following the discussion above, solvent screening has been carried out. The compounds selected as the most suitable solvents to be used as extractants of ciprofloxacin, trimethoprim, and sulfamethoxazole are the following: terpenoids (thymol and carvacrol), eutectic solvents (thymol + dodecanoic acid, thymol + decanoic acid, and thymol + octanoic acid) and conventional solvents (ethyl acetate and MIBK). Moreover, sulfamethoxazole shows the lowest affinity for the solvent for both terpenoids and eutectic solvents listed before, while this antibiotic presents the opposite behaviour for organic solvents. Therefore, the compound that would limit the overall extraction yield of the process would be sulfamethoxazole for terpenoids and eutectic solvents. In contrast, for conventional solvents, it would be trimethoprim and ciprofloxacin.

3.2. Multicomponent liquid–liquid extraction of antibiotics from ultrapure water and hospital wastewater in vial

For each of the extraction solvents previously selected, three fundamental aspects will be reviewed here: the influence of the volumetric S/F ratio, the effect of the aqueous matrix, and the pH value.

The extraction yields of each antibiotic (Yld_i) and the overall extraction yields ($Yld_{Overall}$) were calculated from the concentration of antibiotics in the aqueous phase, in mg/L, before ($C_{i,0}^{aq}$) and after the extraction ($C_{i,f}^{aq}$), according to the following equations:

$$Yld_i(\%) = \frac{C_{i,0}^{aq} - C_{i,f}^{aq}}{C_{i,0}^{aq}} \cdot 100 \quad (1)$$

$$Yld_{Overall}(\%) = \frac{\sum_{i=1}^{3}(C_{i,0}^{aq} - C_{i,f}^{aq})}{\sum_{i=1}^{3} C_{i,0}^{aq}} \cdot 100 \quad (2)$$

Firstly, the influence of both the water matrix used for feed preparation and the pH value on the extraction of each of the three antibiotics will be discussed. This fact will be analysed according to the dissociation

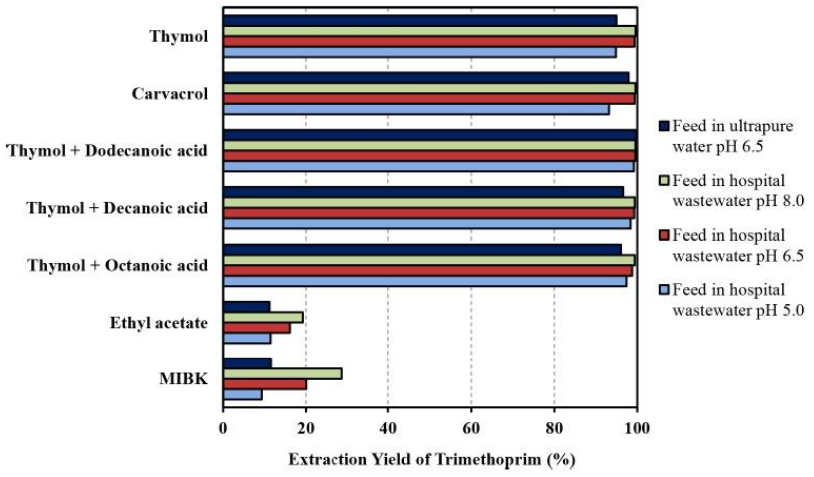

Fig. 4. Extraction yields of trimethoprim from different matrices (ultrapure water and hospital wastewater at different pH) at 323.2 K and S/F 0.25.

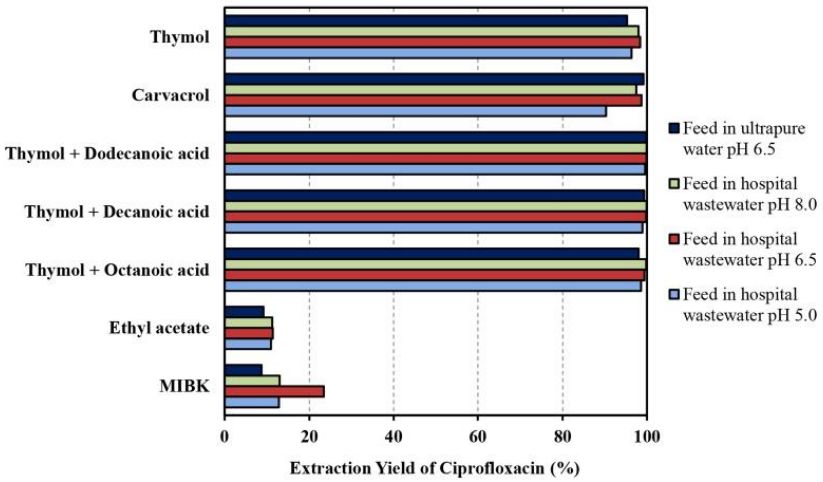

Fig. 5. Extraction yields of ciprofloxacin from different matrices (ultrapure water and hospital wastewater at different pH) at 323.2 K and S/F 0.25.

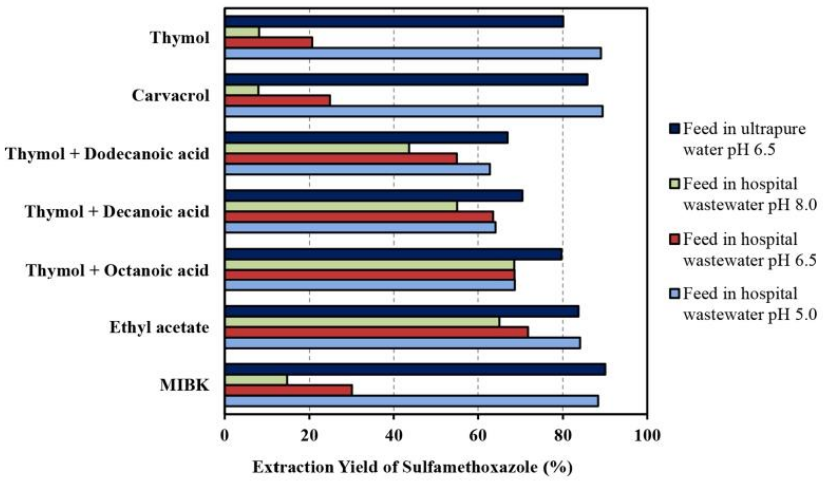

Fig. 6. Extraction yields of sulfamethoxazole from different matrices (ultrapure water and hospital wastewater at different pH) at 323.2 K and S/F 0.25.

equilibria of the pharmaceuticals considered, which are shown together with pK_a values in Fig. 3 [96–97]. Figs. 4-7 show the extraction yields of trimethoprim, ciprofloxacin, sulfamethoxazole, and the overall value, respectively, from two matrices (feed in ultrapure water and in hospital wastewater at three different pH) by using different solvents at 323.15 K and volumetric S/F ratio of 0.25. The experimental results obtained for S/F ratios of 0.10, 0.25, 0.50, 1.00, and 2.00 are included in Tables S1-S5 of the Supplementary Material.

Before comparing different solvents, it should be noted that when the feed is brought into contact with them, a small amount is transferred to the aqueous phase. This fact can modify the pH of the raffinate and the state of the antibiotic (cationic, anionic, or neutral form) in the aqueous phase. For conventional solvents and terpenoids, the pH of the raffinate remained the same as the pH of the feed. However, for the three eutectic solvents considered, formed with dodecanoic acid, decanoic acid, and octanoic acid, the raffinate reached values between 4.9 and 6.5 when using the feed in hospital wastewater at pH 8.0, while it ranged from 3.7 and 4.5 for the feed in hospital wastewater at pH 5.0. Therefore, this will be considered when analyzing the ability of the solvent to solvate an antibiotic in a particular charged or non-charged state.

For trimethoprim, as can be seen in Fig. 4, decreasing the pH value of the feed in the hospital wastewater matrix reduces the extraction yields with all solvents, which can be explained due to the acid-base equilibrium of this diaminopyridine-derived compound (as shown in Fig. 3). As widely discussed in the literature, the partitioning of the solute into one phase or the other depends on whether it is in its neutral or charged ionic state and the ability of both phases to dissolve that form of the solute. Generally, water interacts more strongly with charged solutes, favoring partitioning into the aqueous phase, while the nonionic ones usually favor partitioning into the organic phase [55,98–100].

In this case, increasing the pH increases the concentration of trimethoprim in its neutral form, improving the extraction yields. Conventional solvents show considerably poorer results than terpenoids and eutectic solvents at any pH value and matrix. In the case of eutectic solvents, yields drop when reducing the alkyl chain length of the carboxylic acid. This trend might be caused due to the decrease of

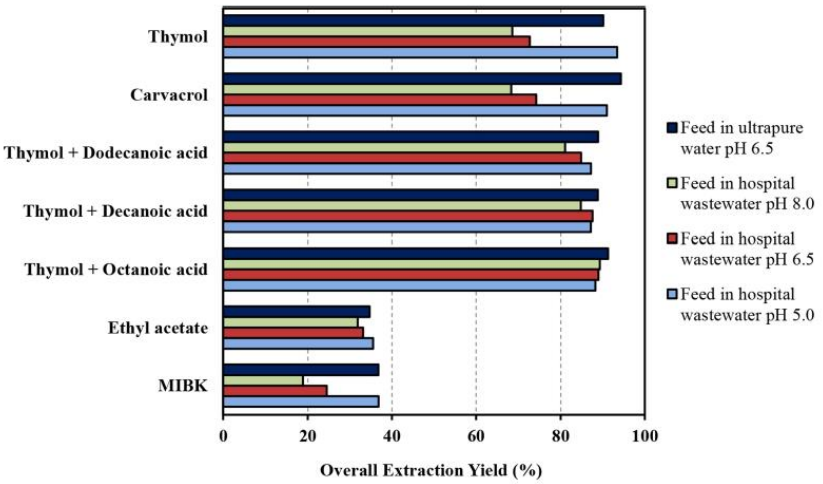

Fig. 7. Overall extraction yields of antibiotics from different matrices (ultrapure water and hospital wastewater at different pH) at 323.2 K and S/F 0.25.

hydrophobicity, which increases the partial solubility of the acid in water, decreasing the pH of the aqueous phase and favouring the presence of the protonated form of this antibiotic. At high pH, as trimethoprim in its neutral state predominates, both terpenoids and eutectic solvents showed similar results. However, when the solute in its ionic state prevails (pH < pK_{a2}), eutectic solvents seem to stabilise the positively charged ion more effectively, and the extraction yields are considerably higher than those for terpenoids, possibly due to the higher influence of hydrogen-bonding interactions [94,101].

Finally, in order to study the effect of the matrix, it is necessary to compare the feeds in ultrapure water and in hospital wastewater at the same pH value, 6.5. This allows to analyse the influence that the compounds in the wastewater matrix have on the extraction process, avoiding the pH effect on trimethoprim extraction. In this regard, for all solvents, higher extraction yields were observed when using the feed in hospital wastewater, indicating that the solutes in the matrix favour the transfer of trimethoprim into the organic phase. This effect might be caused by salting-out mechanism.

In the case of ciprofloxacin, as observed in Fig. 5, the decrease of the pH value of the feed in hospital wastewater matrix shows two different trends, one for eutectic solvents and another for terpenoids and conventional solvents. The former presented higher yields with the feed at pH 8.0, while the latter exhibited better results with the feed at pH 6.5. As shown by the acid-base equilibrium of this quinolone in Fig. 3b, pH 6.5 is approximately as close to the isoelectric point ($pH_{IEP} \approx 7.4$) as pH 8. The isoelectric point is defined as the pH at which the solute concentration as zwitterion is maximum and, therefore, the net charge is zero. As reported in the literature, analytes have their lowest solubility in water at the isoelectric point [102–103]. Therefore, the higher the solute concentration in its electrically neutral state, the larger the mass transfer to the organic phase should be.

For both terpenoids and conventional solvents, the extraction yields of ciprofloxacin can be ordered as follows: pH 6.5 > pH 8.0 > pH 5.0. Despite being approximately at the same distance from the pH_{IEP}, the higher yields obtained at pH 6.5 compared to those obtained at pH 8.0 indicate that these two solvent groups may solvate ciprofloxacin more effectively in its cationic state than in its anionic state. In the case of eutectic solvents, the extraction yields followed this order: pH 8.0 > pH 6.5 > pH 5.0. This might be due to the fact that when the feed is put in contact with the eutectic solvent, part of the carboxylic acid forming the eutectic solvent is transferred to the aqueous phase, lowering the pH considerably. Thus, the feed in hospital wastewater at pH 8.0 approaches the isoelectric point, increasing the extraction yield of ciprofloxacin. As the pH value of the feed decreases below 8.0, the pH of the raffinate moves increasingly away from the isoelectric point, and the concentration of the cationic form increases.

As with trimethoprim, conventional solvents show considerably lower extraction yields of ciprofloxacin than terpenoids and eutectic solvents at any pH value and matrix. With regard to eutectic solvents, for a given feed, the yield drops as the length of the alkyl chain of the carboxylic acid decreases. This can be attributed to the fact that in the pH range tested, the raffinate resulting from extraction with the eutectic solvents showed values below 6.5 (pH < pH_{IEP}). Thus, as the number of carbons of the acid decreases, its solubility in water rises, decreasing the pH of the raffinate and moving further away from the isoelectric point value. In general, the eutectic solvents showed higher extraction yields than those found for the terpenoids. This difference is considerably more significant when the concentration of ciprofloxacin in its charged state increases, i.e., when the pH value of the feed in hospital wastewater is 5.0. Therefore, as observed for trimethoprim, eutectic solvents solvate the charged species of ciprofloxacin more effectively.

Finally, when comparing the results obtained for feeds of ciprofloxacin in ultrapure water and in hospital wastewater at pH 6.5, higher extraction yields are observed in the real wastewater matrix. Therefore, as with trimethoprim, the solutes in the wastewater matrix favour the transfer of ciprofloxacin into the organic phase, which might be caused by salting-out effect.

In the case of sulfamethoxazole, as shown in Fig. 6, reducing the pH value of the feed in the hospital wastewater matrix increases the extraction yields. This is due to the fact that in the pH range of the feed considered, i.e., between 5.0 and 8.0, decreasing the pH value increases the concentration of sulfamethoxazole in its neutral state, as shown in Fig. 3. As previously evidenced and mentioned in the literature, uncharged solutes tend to solvate more efficiently in the organic solvent compared to their ionic forms.

For conventional solvents, MIBK shows similar yields to those for terpenoids at any pH value. However, ethyl acetate presents yields significantly higher than those for terpenoids at feed pH values between 6.5 and 8.0, i.e., when the solute predominates in its anionic state. On the other hand, when sulfamethoxazole predominates in its neutral state, at feed pH of 5.0, terpenoids show slightly higher extraction yields than ethyl acetate.

Among the eutectic solvents, for the same feed pH value and the same matrix, the yields rise as the length of the alkyl chain of the

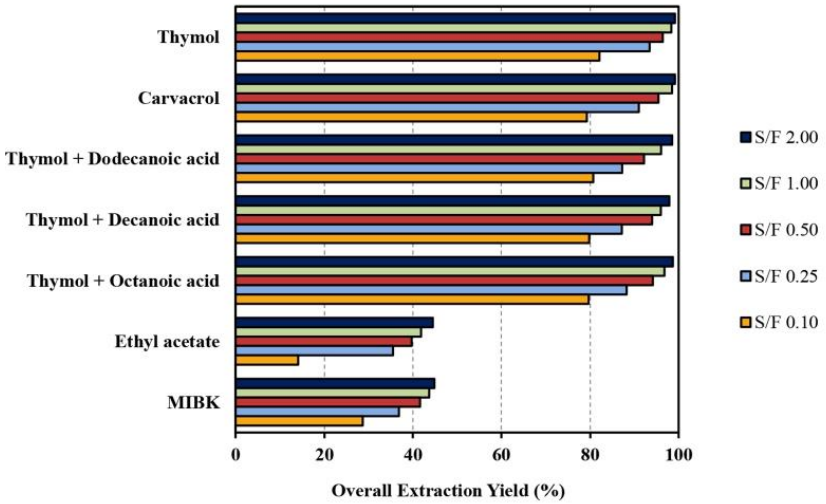

Fig. 8. Influence of the volumetric S/F ratio on the overall extraction yields of antibiotics from hospital wastewater at pH 5.0 and 323.2 K.

carboxylic acid decreases. This could be due to the diminishing hydrophobicity, which increases the solubility of the acid in water and, thus, the pH value and the concentration of the antibiotic in its neutral state. Regarding the feeds in hospital wastewater, at pH values of 8.0 and 6.5, eutectic solvents show better results since, as part of the carboxylic acid is being transferred to the aqueous phase, the pH of the raffinate is considerably lower than that of the fresh feed. In this way, the concentration of sulfamethoxazole in its anionic form decreases, increasing its neutral form and improving the mass transfer of the compound into the organic phase. On the other hand, for the feeds at pH 5.0 ($pH < pK_{a2}$), when the neutral form predominates, terpenoids show higher extraction yields than those with eutectic solvents. In other words, the carboxylic acid of the eutectic solvents decreases the pH value of the aqueous phase when the extraction solvent and the feed are in contact.

Finally, when comparing the results obtained for feeds in ultrapure water and in hospital wastewater at pH 6.5, clearly higher extraction yields are observed in the ultrapure water matrix. Therefore, solutes in the wastewater matrix seem to favour the solvation of sulfamethoxazole in the aqueous phase, decreasing its transfer to the organic phase. Compared to the results observed for trimethoprim and ciprofloxacin, both pH and matrix present a more noticeable influence on sulfamethoxazole extraction.

All the above-mentioned issues highlight the fact that there is no single pH value that presents the best results for the extraction of the three antibiotics. Therefore, as a multicomponent extraction, it is necessary to analyse the overall extraction yield of the three antibiotics, given by Eq. (2). As illustrated in Fig. 7, conventional solvents show significantly lower overall extraction yields than those obtained for eutectic solvents and terpenoids at any pH and matrix.

Eutectic solvents seem to have a lower sensitivity to pH changes in the feed. As previously reported, this is due to the greater ease of solvating solutes in their ionic state and the decrease of the pH value as a consequence of the carboxylic acid transfer to the aqueous phase. However, the operating conditions with the highest antibiotic mass transfer to the organic phase, as an overall value, was with the feed in wastewater at pH 5.0 and using pure terpenoids. At this pH value, terpenoids present the highest compromise situation for the multicomponent extraction of the three antibiotics. For instance, at pH 5.0 and S/F 0.25, carvacrol achieved extraction yields of 93.2%, 90.3%, and 89.4% for trimethoprim, ciprofloxacin, and sulfamethoxazole, respectively, whereas the eutectic solvent thymol + octanoic acid exhibited values of 97.4%, 98.6%, and 68.0%. Therefore, the most adequate pH value of the feed seems to be 5.0.

The third effect studied in this section was the influence of the S/F ratio on the overall extraction yields. According to Fig. 8, the S/F ratio selected as the most suitable value for the extraction process is 1.00, as it allows overall extraction yields above 98% for terpenoids (greater than99% for trimethoprim and ciprofloxacin, and 97% for sulfamethoxazole). Larger amounts of solvent do not justify the slight increase in the extraction yield, raising investment and operating costs.

Concerning organic solvent losses in the aqueous phase, higher solubility of conventional solvents was observed compared to terpenoids. The mass contents of thymol and carvacrol in the raffinate were 0.12–0.15% and 0.12–0.14%, respectively, while those for ethyl acetate and MIBK were 6.84–7.96% and 1.38–1.48 %. Therefore, thymol and carvacrol showed considerably lower losses of solvent in water. Currently, large-scale sales prices of terpenes (thymol 9–11 $/kg [104] and carvacrol 10–25 $/kg [105]) are more expensive than those of conventional solvents (ethyl acetate 1.3 $/kg [106] and MIBK 1.0–1.5 $/kg [81]). However, the low S/F ratio required to accomplish high extraction yields, the small solvent losses in the raffinate, and their low toxicity and high sustainability compared to petroleum-based solvents place terpenes as potential extraction solvents for industrial application.

Generally, the use of pure solvents rather than mixtures is preferable on an industrial scale. This usually increases the simplicity of the extraction process and facilitates solvent recovery. Hence, since the overall extraction yields were comparable for terpenoids and eutectic solvents, it is preferable to use a pure terpenoid. In particular, carvacrol shows the most favourable conditions to be selected as extractant, not only because of all the above-mentioned results for terpenoids but also because it has a low melting point compared to thymol (see Table 1). This allows its use at room temperature, without the need for heating. Therefore, the optimal conditions of the extraction process in this study, and which will be used for the subsequent sections, were: feed in hospital wastewater at pH 5.0, S/F ratio of 1.00, and carvacrol as extractant.

3.3. Multicomponent liquid–liquid extraction of antibiotics from hospital wastewater in a packed column

In order to test the scalability, a continuous parallel extraction process in a packed column has been studied. Carvacrol presents a relatively high viscosity (36.66 mPa s at 20 °C [107]) compared to the feed in

Table 3
Extraction yields of trimethoprim, ciprofloxacin, and sulfamethoxazole in a parallel extraction column at different S/F ratios.

S/F	Extraction Yield (%)			
	Trimethoprim	Ciprofloxacin	Sulfamethoxazole	Overall
0.50	99.30	98.57	95.65	97.84
1.00	99.69	98.85	96.25	98.26
2.00	99.82	99.71	98.71	99.41

hospital wastewater at pH 5.0, which may affect the mass transfer in the liquid–liquid extraction process. Therefore, although it was observed in the vial extraction experiments that the optimum value of S/F ratio is 1.00, the S/F ratios 0.50 and 2.00 have also been analysed. In this way, it can be observed whether the limitations to mass transfer vary considerably with the amount of carvacrol used. Thus, the extraction yields obtained in a packed column at different S/F ratios are shown in Table 3.

The results obtained were comparable to those obtained in the vial tests with carvacrol as extractant and using the feed in hospital wastewater at pH 5.0. This implies that extraction yields for the experiments in vial (prepared under 12 h stirring) and in a packed column (using a residence time of 21 min) were similar, indicating that antibiotics mass transfer is not limited by the amount of carvacrol used in the S/F ratio range considered.

3.4. Solvent reuse in consecutive stages of antibiotic extraction from hospital wastewater and solvent recovery

One of the key aspects to check the feasibility of scaling up an extraction process for industrial purposes is the evaluation of the reuse and recovery of the extractant. Therefore, this fact will be investigated following the optimal operating conditions obtained in the batch process, this is, carvacrol as extraction solvent, feed in hospital wastewater at pH 5.0, and S/F ratio of 1.00.

The process developed to evaluate the solvent reuse and recovery is represented in Fig. 9. The liquid–liquid extraction was performed by reusing the solvent (extract phase) for five consecutive stages without intermediate solvent regeneration, thus using fresh solvent only in stage 1. Finally, the extract from stage 5 was regenerated by using a rotary evaporator at 437.2 K and 20 mbar.

As can be seen in Fig. 10, the decrease of the extraction yields in each stage is most steep for sulfamethoxazole, followed by ciprofloxacin and trimethoprim. Reuse of the solvent, under the operating conditions described above, led to extraction yields higher than 83%, 96%, and

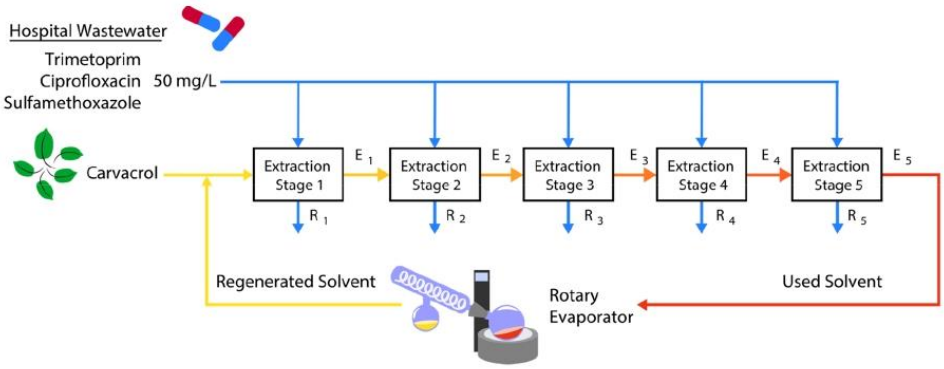

Fig. 9. Scheme of solvent reuse and recovery.

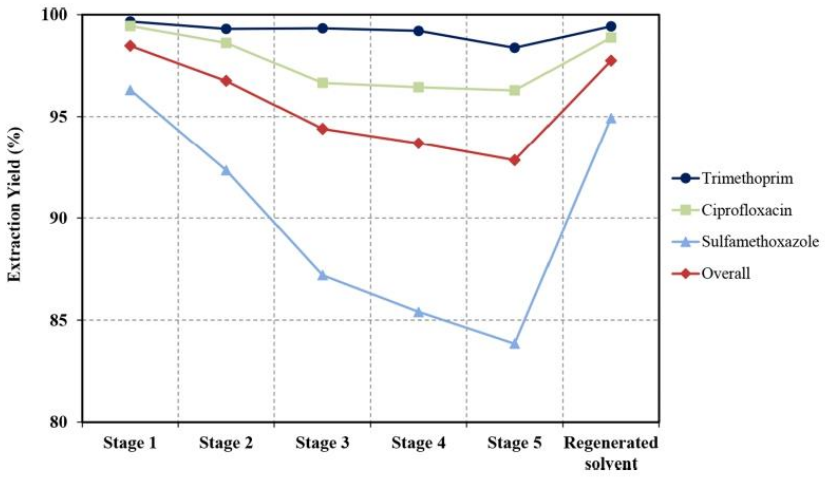

Fig. 10. Evolution of the extraction yield with the number of consecutive extraction stages and after solvent regeneration. Extractions with carvacrol and feed in hospital wastewater at pH 5.0, S/F ratio 1.00, and 323.2 K.

98% for sulfamethoxazole, ciprofloxacin, and trimethoprim, respectively, during the 5 stages. For the regenerated solvent, extraction yields were very close to those obtained with the fresh extractant (stage 1). Therefore, carvacrol not only allows the removal of more than 98% of the overall antibiotic content in a single step but also has been proven to be feasible operating in a continuous extraction column, and it can be regenerated using vacuum distillation.

4. Conclusions

Over the last few years, the demand for quality water has been steadily growing, bringing the importance of water treatment and reuse into focus. In this regard, multicomponent liquid–liquid extraction of three of the antibiotics included in the European Surface Water Watch List (ciprofloxacin, trimethoprim, and sulfamethoxazole) has been proposed using terpenoids and eutectic mixtures.

From the infinite dilution activity coefficient estimated by the COSMO-RS method, the compounds selected to move on to the experimental phase were the following: 2 terpenoids (thymol and carvacrol), 2 eutectic solvents (thymol + dodecanoic acid, thymol + decanoic acid, and thymol + octanoic acid), and 2 conventional solvents (ethyl acetate and MIBK).

Terpenoids and eutectic mixtures exhibited significantly higher overall extraction yields than those obtained for conventional solvents at any pH and aqueous matrix. However, no single pH value presented the best results for the extraction of the three antibiotics simultaneously, depending substantially on the dissociation equilibrium of each compound. Although eutectic solvents showed lower sensitivity to pH changes in the feed, terpenoids provided the operating conditions with the highest overall extraction yield with the feed in wastewater at pH 5.0 and volumetric S/F ratio of 1.00. Carvacrol emerged as the most favourable extractant, reaching extraction yields of 98.9% for trimethoprim, 99.5% for ciprofloxacin, and 97.0% for sulfamethoxazole from hospital wastewater at pH 5.0 and S/F ratio 1.00. In addition, the losses of thymol and carvacrol in the aqueous phase were substantially lower than those of conventional organic compounds.

The scalability of the extraction process was tested by performing a continuous process in a packed column, using low residence times, and obtaining no limitation to mass transfer. For industrial purposes, the reuse of carvacrol for five consecutive stages and its recovery by using a rotary evaporator at 437.2 K and 20 mbar was also successfully evaluated.

Declaration of Competing Interest

The authors declare that they have no known competing financial interests or personal relationships that could have appeared to influence the work reported in this paper.

Acknowledgments

The authors are grateful to Comunidad Autónoma de Madrid for financial support of Project S2018/EMT-4341, IND2017/AMB-7720, and PR65/19-22441 and to Ministerio de Ciencia, Innovación y Universidades for financial support of Project CTM2017-84033-R. This work has been supported by the Madrid Government (Comunidad Autónoma de Madrid- Spain) under the Multiannual Agreement with Complutense University in the line Program to Stimulate Research for Young Doctors in the context of the V PRICIT (Regional Programme of Research and Technological Innovation). Diego Rodríguez-Llorente thanks to Ministerio de Ciencia, Innovación y Universidades for awarding an FPU grant (FPU18/01536). Finally, we thank Centro de Computación Científica de la Universidad Autónoma de Madrid for computational facilities.

Appendix A. Supplementary material

Supplementary data to this article can be found online at https://doi.org/10.1016/j.seppur.2021.120117.

References

[1] H. Safari, M. Arab, A. Rashidian, A. Kebriaee-Zadeh, H.A. Gorji, A comparative study on different pharmaceutical industries and proposing a model for the context of Iran, Iran. J. Pharm. Res. 17 (2018) 1593–1603, https://doi.org/10.22037/ijpr.2018.2307.
[2] S. Marić, A. Jocić, A. Krstić, M. Momčilović, L. Ignjatović, A. Dimitrijević, Poloxamer-based aqueous biphasic systems in designing an integrated extraction platform for the valorization of pharmaceutical waste, Sep. Purif. Technol. 275 (2021) 119101, https://doi.org/10.1016/j.seppur.2021.119101.
[3] J. Ouyang, L. Zhou, Z. Liu, J.Y.Y. Heng, W. Chen, Biomass-derived activated carbons for the removal of pharmaceutical mircopollutants from wastewater: A review, Sep. Purif. Technol. 253 (2020) 117536, https://doi.org/10.1016/j.seppur.2020.117536.
[4] T. Gezahegn, B. Tegegne, F. Zewge, B.S. Chandravanshi, Salting-out assisted liquid-liquid extraction for the determination of ciprofloxacin residues in water samples by high performance liquid chromatography-diode array detector, BMC Chem. 13 (1) (2019), https://doi.org/10.1186/s13065-019-0543-5.
[5] J.L. Liu, M.H. Wong, Pharmaceuticals and personal care products (PPCPs): A review on environmental contamination in China, Environ. Int. 59 (2013) 208–224, https://doi.org/10.1016/j.envint.2013.06.012.
[6] J.L. Tambosi, L.Y. Yamanaka, H.J. José, R. De Fátima Peralta Muniz Moreira, H. F. Schröder, Recent research data on the removal of pharmaceuticals from sewage treatment plants (STP), Quim. Nova. 33 (2010) 411–420, https://doi.org/10.1590/S0100-40422010000200032.
[7] T. Heberer, Occurrence, fate, and removal of pharmaceutical residues in the aquatic environment: A review of recent research data, Toxicol. Lett. 131 (1-2) (2002) 5–17, https://doi.org/10.1016/S0378-4274(02)00041-3.
[8] K. Ikehata, N. Jodeiri Naghashkar, M. Gamal El-Din, Degradation of aqueous pharmaceuticals by ozonation and advanced oxidation processes: A review, Ozone Sci. Eng. 28 (6) (2006) 353–414.
[9] O.M. Rodriguez-Narvaez, J.M. Peralta-Hernandez, A. Goonetilleke, E.R. Bandala, Treatment technologies for emerging contaminants in water: A review, Chem. Eng. J. 323 (2017) 361–380, https://doi.org/10.1016/j.cej.2017.04.106.
[10] K Fent, A Weston, D Caminada, Ecotoxicology of human pharmaceuticals, Aquat. Toxicol. 76 (2) (2006) 122–159, https://doi.org/10.1016/j.aquatox.2005.09.009.
[11] S. Moles, R. Mosteo, J. Gómez, J. Szpunar, S. Gozzo, J.R. Castillo, M.P. Ormad, Towards the removal of antibiotics detected in wastewaters in the POCTEFA territory: Occurrence and TiO2 photocatalytic pilot-scale plant performance, Water (Switzerland). 12 (2020) 1453, https://doi.org/10.3390/w12051453.
[12] S.E. Jørgensen, B. Halling-Sørensen, Drugs in the environment, Chemosphere. 40 (7) (2000) 691–699, https://doi.org/10.1016/S0045-6535(99)00438-5.
[13] J. Zhan, Z. Li, G. Yu, X. Pan, J. Wang, W. Zhu, X. Han, Y. Wang, Enhanced treatment of pharmaceutical wastewater by combining three-dimensional electrochemical process with ozonation to in situ regenerate granular activated carbon particle electrodes, Sep. Purif. Technol. 208 (2019) 12–18, https://doi.org/10.1016/j.seppur.2018.06.030.
[14] A. Mukimin, H. Vistanty, N. Zen, Hybrid advanced oxidation process (HAOP) as highly efficient and powerful treatment for complete demineralization of antibiotics, Sep. Purif. Technol. 241 (2020) 116728, https://doi.org/10.1016/j.seppur.2020.116728.
[15] P.N. Karungamye, Methods used for removal of pharmaceuticals from wastewater: A review, Appl. J. Environ. Eng. Sci. 6 (2020) 412–428.
[16] N. Pathak, V.H. Tran, A. Merenda, M.A.H. Johir, S. Phuntsho, H. Shon, Removal of Organic Micro-Pollutants by Conventional Membrane Bioreactors and High-Retention Membrane Bioreactors, Appl. Sci. 10 (2020) 2969.
[17] P. Verlicchi, A. Galletti, M. Petrovic, D. Barceló, Hospital effluents as a source of emerging pollutants: An overview of micropollutants and sustainable treatment options, J. Hydrol. 389 (3-4) (2010) 416–428, https://doi.org/10.1016/j.jhydrol.2010.06.005.
[18] A.A. Renita, P.S. Kumar, S. Srinivas, S. Priyadharshini, M. Karthika, A review on analytical methods and treatment techniques of pharmaceutical wastewater, Desalin. Water Treat. 87 (2017) 160–178, https://doi.org/10.5004/dwt.2017.21311.
[19] H. Abu Hasan, S.R. Sheikh Abdullah, A.W.N. Al-Attabi, D.A.H. Nash, N. Anuar, N. Abd, H. Rahman, Sulistiyaning Titah, Removal of ibuprofen, ketoprofen, COD and nitrogen compounds from pharmaceutical wastewater using aerobic suspension-sequencing batch reactor (ASSBR), Sep. Purif. Technol. 157 (2016) 215–221, https://doi.org/10.1016/j.seppur.2015.11.017.
[20] X. Xu, R. Lin, X. Deng, J. Liu, In situ synthesis of FeOOH-coated trimanganese tetroxide composites catalyst for enhanced degradation of sulfamethoxazole by peroxymonosulfate activation, Sep. Purif. Technol. 275 (2021) 119184, https://doi.org/10.1016/j.seppur.2021.119184.
[21] E. Commission, Decision (EU) 2020/1161, Off. J. Eur. Union. L 257 (2020).
[22] E. Commission, Decision (EU) 2018/840, Off. J. Eur. Union. L 141 (2018).
[23] D. O'Flynn, J. Lawler, A. Yusuf, A. Parle-McDermott, D. Harold, T. Mc Cloughlin, L. Holland, F. Regan, B. White, A review of pharmaceutical occurrence and pathways in the aquatic environment in the context of a changing climate and the

COVID-19 pandemic, Anal. Methods. 13 (5) (2021) 575–594, https://doi.org/10.1039/D0AY02098B.
[24] D Sponza, P Demirden, Treatability of sulfamerazine in sequential upflow anaerobic sludge blanket reactor (UASB)/completely stirred tank reactor (CSTR) processes, Sep. Purif. Technol. 56 (1) (2007) 108–117, https://doi.org/10.1016/j.seppur.2006.07.013.
[25] Y.N Kanafin, Y. Kakimov, A. Adamov, A. Makhatova, A. Yeshmuratov, S. G Poulopoulos, V.J Inglezakis, E. Arkhangelsky, The effect of caffeine, metronidazole, and ibuprofen on continuous flow activated sludge process, J. Chem. Technol. Biotechnol. 96 (5) (2021) 1370–1380, https://doi.org/10.1002/jctb.v96.510.1002/jctb.6658.
[26] J. Rodrigues Pires da Silva, M. Alves Monteiro, S. de Mendonça Ochs, C. da Silva Moura, F.V. da Fonseca, C. Piacsek Borges, Study of effects of pharmaceuticals on the activated sludge process combining advanced oxidation using ultraviolet/hydrogen peroxide to increase their removal and mineralization of wastewater, J. Environ Chem. Eng. 9 (1) (2021) 104576, https://doi.org/10.1016/j.jece.2020.104576.
[27] F. Çeçen, G. Gül, Biodegradation of five pharmaceuticals: estimation by predictive models and comparison with activated sludge data, Int. J. Environ. Sci. Technol. 18 (2) (2021) 327–340, https://doi.org/10.1007/s13762-020-02820-y.
[28] M. Ahsani, H. Hazrati, M. Javadi, M. Ulbricht, R. Yegani, Preparation of antibiofouling nanocomposite PVDF/Ag-SiO2 membrane and long-term performance evaluation in the MBR system fed by real pharmaceutical wastewater, Sep. Purif. Technol. 249 (2020) 116938, https://doi.org/10.1016/j.seppur.2020.116938.
[29] K.K. Ng, X. Shi, M.K.Y. Tang, H.Y. Ng, A novel application of anaerobic bio-entrapped membrane reactor for the treatment of chemical synthesis-based pharmaceutical wastewater, Sep. Purif. Technol. 132 (2014) 634–643, https://doi.org/10.1016/j.seppur.2014.06.021.
[30] M.C. Martí-Calatayud, R. Heßler, S. Schneider, C. Bohner, S. Yüce, M. Wessling, R. F. de Sena, G.B. Athayde Júnior, Transients of micropollutant removal from high-strength wastewaters in PAC-assisted MBR and MBR coupled with high-retention membranes, Sep. Purif. Technol. 246 (2020) 116863, https://doi.org/10.1016/j.seppur.2020.116863.
[31] P. Cartagena, M. El Kaddouri, V. Cases, A. Trapote, D. Prats, Reduction of emerging micropollutants, organic matter, nutrients and salinity from real wastewater by combined MBR-NF/RO treatment, Sep. Purif. Technol. 110 (2013) 132–143, https://doi.org/10.1016/j.seppur.2013.03.024.
[32] T.T. Nguyen, X.T. Bui, T.D.H. Vo, D.D. Nguyen, P.D. Nguyen, H.L.C. Do, H. H. Ngo, W. Guo, Performance and membrane fouling of two types of laboratory-scale submerged membrane bioreactors for hospital wastewater treatment at low flux condition, Sep. Purif. Technol. 165 (2016) 123–129, https://doi.org/10.1016/j.seppur.2016.03.051.
[33] L.G. Chaves-Barquero, B.W. Humeniuk, K.H. Luong, N. Cicek, C.S. Wong, M. L. Hanson, Crushed recycled glass as a substrate for constructed wetland wastewater treatment: a case study of its potential to facilitate pharmaceutical removal, Environ. Sci. Pollut. Res. 28 (37) (2021) 52306–52318, https://doi.org/10.1007/s11356-021-14483-4.
[34] Y.-X. Cheng, J. Chen, D. Wu, Y.-S. Liu, Y.-Q. Yang, L.-X. He, P. Ye, J.-L. Zhao, S.-S. Liu, B. Yang, G.-G. Ying, Highly enhanced biodegradation of pharmaceutical and personal care products in a novel tidal flow constructed wetland with baffle and plants, Water Res. 193 (2021) 116870, https://doi.org/10.1016/j.watres.2021.116870.
[35] J.P.R. De Vargas, M.C. Bastos, M. Al Badany, R. Gonzalez, D. Wolff, D.R.D. Santos, J. Labanowski, Pharmaceutical compound removal efficiency by a small constructed wetland located in south Brazil, Environ. Sci. Pollut. Res. 28 (24) (2021) 30955–30974, https://doi.org/10.1007/s11356-021-12845-6.
[36] B. Hu, S. Hu, Z. Chen, J. Vymazal, Employ of arbuscular mycorrhizal fungi for pharmaceuticals ibuprofen and diclofenac removal in mesocosm-scale constructed wetlands, J. Hazard. Mater. 409 (2021) 124524, https://doi.org/10.1016/j.jhazmat.2020.124524.
[37] X. Hu, H. Xie, L. Zhuang, J. Zhang, Z. Hu, S. Liang, K. Feng, A review on the role of plant in pharmaceuticals and personal care products (PPCPs) removal in constructed wetlands, Sci. Total Environ. 780 (2021) 146637, https://doi.org/10.1016/j.scitotenv.2021.146637.
[38] S.J. Segovia-Sandoval, L.M. Pastrana-Martínez, R. Ocampo-Pérez, S. Morales-Torres, M.S. Berber-Mendoza, F. Carrasco-Marín, Synthesis and characterization of carbon xerogel/graphene hybrids as adsorbents for metronidazole pharmaceutical removal: Effect of operating parameters, Sep. Purif. Technol. 237 (2020) 116341, https://doi.org/10.1016/j.seppur.2019.116341.
[39] N. Zhuo, Y. Lan, W. Yang, Z. Yang, X. Li, X. Zhou, Y. Liu, J. Shen, X. Zhang, Adsorption of three selected pharmaceuticals and personal care products (PPCPs) onto MIL-101(Cr)/natural polymer composite beads, Sep. Purif. Technol. 177 (2017) 272–280, https://doi.org/10.1016/j.seppur.2016.12.041.
[40] D.J. De Ridder, J.Q.J.C. Verberk, S.G.J. Heijman, G.L. Amy, J.C. Van Dijk, Zeolites for nitrosamine and pharmaceutical removal from demineralised and surface water: Mechanisms and efficacy, Sep. Purif. Technol. 89 (2012) 71–77, https://doi.org/10.1016/j.seppur.2012.01.025.
[41] A. Azaïs, J. Mendret, S. Gassara, E. Petit, A. Deratani, S. Brosillon, Nanofiltration for wastewater reuse: Counteractive effects of fouling and matrice on the rejection of pharmaceutical active compounds, Sep. Purif. Technol. 133 (2014) 313–327, https://doi.org/10.1016/j.seppur.2014.07.007.
[42] Z. Ouyang, Z. Huang, X. Tang, C. Xiong, M. Tang, Y. Lu, A dually charged nanofiltration membrane by pH-responsive polydopamine for pharmaceuticals and personal care products removal, Sep. Purif. Technol. 211 (2019) 90–97, https://doi.org/10.1016/j.seppur.2018.09.059.
[43] A.F.S. Foureaux, E.O. Reis, Y. Lebron, V. Moreira, L.V. Santos, M.S. Amaral, L. C. Lange, Rejection of pharmaceutical compounds from surface water by nanofiltration and reverse osmosis, Sep. Purif. Technol. 212 (2019) 171–179, https://doi.org/10.1016/j.seppur.2018.11.018.
[44] J. García-Ivars, J. Durá-María, C. Moscardó-Carreño, C. Carbonell-Alcaina, M. I. Alcaina-Miranda, M.I. Iborra-Clar, Rejection of trace pharmaceutically active compounds present in municipal wastewaters using ceramic fine ultrafiltration membranes: Effect of feed solution pH and fouling phenomena, Sep. Purif. Technol. 175 (2017) 58–71, https://doi.org/10.1016/j.seppur.2016.11.027.
[45] J. Kuttiani Ali, M. Abi Jaoude, E. Alhseinat, Polyimide ultrafiltration membrane embedded with reline-functionalized nanosilica for the remediation of pharmaceuticals in water, Sep. Purif. Technol. 266 (2021) 118585, https://doi.org/10.1016/j.seppur.2021.118585.
[46] S.O. Ganiyu, E.D. Van Hullebusch, M. Cretin, G. Esposito, M.A. Oturan, Coupling of membrane filtration and advanced oxidation processes for removal of pharmaceutical residues: A critical review, Sep. Purif. Technol. 156 (2015) 891–914, https://doi.org/10.1016/j.seppur.2015.09.059.
[47] C. Gadipelly, A. Pérez-González, G.D. Yadav, I. Ortiz, R. Ibáñez, V.K. Rathod, K. V. Marathe, Pharmaceutical industry wastewater: Review of the technologies for water treatment and reuse, Ind. Eng. Chem. Res. 53 (2014) 11571–11592.
[48] H. Kaur, G. Hippargi, G.R. Pophali, A.K. Bansiwal, Treatment methods for removal of pharmaceuticals and personal care products from domestic wastewater, in, Pharm. Pers. Care Prod. Waste Manag. Treat. Technol. Emerg. Contam. Micro Pollut., Elsevier (2019) 129–150, https://doi.org/10.1016/B978-0-12-816189-0.00006-8.
[49] H. Guo, D. Li, Z. Li, S. Lin, Y. Wang, S. Pan, J. Han, Promoted elimination of antibiotic sulfamethoxazole in water using sodium percarbonate activated by ozone: Mechanism, degradation pathway and toxicity assessment, Sep. Purif. Technol. 266 (2021) 118543, https://doi.org/10.1016/j.seppur.2021.118543.
[50] G. Maniakova, K. Kowalska, S. Murgolo, G. Mascolo, G. Libralato, G. Lofrano, O. Sacco, M. Guida, L. Rizzo, Comparison between heterogeneous and homogeneous solar driven advanced oxidation processes for urban wastewater treatment: Pharmaceuticals removal and toxicity, Sep. Purif. Technol. 236 (2020) 116249, https://doi.org/10.1016/j.seppur.2019.116249.
[51] M.I. Ashraf, M. Ateeb, M.H. Khan, N. Ahmed, Q. Mahmood Zahidullah, Integrated treatment of pharmaceutical effluents by chemical coagulation and ozonation, Sep. Purif. Technol. 158 (2016) 383–386, https://doi.org/10.1016/j.seppur.2015.12.048.
[52] S. Ben Fredj, J. Nobbs, C. Tizaoui, L. Monser, Removal of estrone (E1), 17β-estradiol (E2), and 17α-ethinylestradiol (EE2) from wastewater by liquid-liquid extraction, Chem. Eng. J. 262 (2015) 417–426.
[53] R.C. Assis, A.B. Mageste, L.R. de Lemos, R.M. Orlando, G.D. Rodrigues, Application of aqueous two-phase systems for the extraction of pharmaceutical compounds from water samples, J. Mol. Liq. 301 (2020) 112411, https://doi.org/10.1016/j.molliq.2019.112411.
[54] A. Samsidar, S. Siddiquee, S.M. Shaarani, A review of extraction, analytical and advanced methods for determination of pesticides in environment and foodstuffs, Trends Food Sci. Technol. 71 (2018) 188–201, https://doi.org/10.1016/j.tifs.2017.11.011.
[55] L. Dahuron, B.S. Holden, W.D. Prince, A.F. Seibert, L.C. Wilson, T.C. Frank, Liquid-Liquid Extraction and Other Liquid-Liquid Operations and Equipment, in, Perry's Chem. Eng. Handb., McGraw-Hill Pub (2008).
[56] D. Rodríguez-Llorente, A. Cañada-Barcala, S. Álvarez-Torrellas, V.I. Águeda, J. García, M. Larriba, A review of the use of eutectic solvents, terpenes and terpenoids in liquid–liquid extraction processes, Processes. 8 (2020) 1–54, https://doi.org/10.3390/pr8101220.
[57] R.T. LaLonde, Terpenes and Terpenoids, in: Van Nostrand's Encycl. Chem., John Wiley & Sons, Inc., Hoboken, NJ, USA, 2005. https://doi.org/10.1002/0471740039.vec2473.
[58] R. Croteau, T.M. Kutchan, N.G. Lewis, Natural Products (Secondary Metabolites), in: Bob B. Buchanan, Wilhelm Gruissem, Russell L. Jones (Eds.), Biochem. Mol. Biol. Plants, John Wiley & Sons, 2000: pp. 1250–1319. https://books.google.es/books?id=yRIWCgAAQBAJ&dq=Biochemistry+and+Molecular+Biology+of+Plants&lr=&hl=es&source=gbs_navlinks_s (accessed December 13, 2020).
[59] S. Zwenger Chhandak Basu, S. Zwenger, C. Basu, Plant Terpenoids: Applications and Future Potentials, Biotechnol. Mol. Biol. Rev. 3 (2008) 1–007.
[60] C. Florindo, L.C. Branco, I.M. Marrucho, Development of hydrophobic deep eutectic solvents for extraction of pesticides from aqueous environments, Fluid Phase Equilib. 448 (2017) 135–142, https://doi.org/10.1016/j.fluid.2017.04.002.
[61] M.A.R. Martins, S.P. Pinho, J.A.P. Coutinho, Insights into the Nature of Eutectic and Deep Eutectic Mixtures, J. Solution Chem. 48 (7) (2019) 962–982, https://doi.org/10.1007/s10953-018-0793-1.
[62] T. Křížek, M. Bursová, R. Horsley, M. Kuchař, P. Tůma, R. Čabala, T. Hložek, Menthol-based hydrophobic deep eutectic solvents: Towards greener and efficient extraction of phytocannabinoids, J. Clean. Prod. 193 (2018) 391–396, https://doi.org/10.1016/j.jclepro.2018.05.080.
[63] C. Boutekedjiret, M.A. Vian, F. Chemat, Terpenes as Green Solvents for Natural Products Extraction, in: Altern. Solvents Nat. Prod. Extr., Springer Berlin Heidelberg, 2014: pp. 205–219. https://doi.org/10.1007/978-3-662-43628-8_9.
[64] B.D. Ribeiro, C. Florindo, L.C. Iff, M.A.Z. Coelho, I.M. Marrucho, Menthol-based eutectic mixtures: Hydrophobic low viscosity solvents, ACS Sustain. Chem. Eng. 3 (10) (2015) 2469–2477, https://doi.org/10.1021/acssuschemeng.5b00532.
[65] M.H. Zainal-Abidin, M. Hayyan, A. Hayyan, N.S. Jayakumar, New horizons in the extraction of bioactive compounds using deep eutectic solvents: A review, Anal. Chim. Acta. 979 (2017) 1–23, https://doi.org/10.1016/j.aca.2017.05.012.

[66] B.B. Hansen, S. Spittle, B. Chen, D. Poe, Y. Zhang, J.M. Klein, A. Horton, L. Adhikari, T. Zelovich, B.W. Doherty, B. Gurkan, E.J. Maginn, A. Ragauskas, M. Dadmun, T.A. Zawodzinski, G.A. Baker, M.E. Tuckerman, R.F. Savinell, J. R. Sangoro, Deep Eutectic Solvents: A Review of Fundamentals and Applications, Chem. Rev. 121 (3) (2021) 1232–1285, https://doi.org/10.1021/acs.chemrev.0c00385.

[67] A. Paiva, R. Craveiro, I. Aroso, M. Martins, R.L. Reis, A.R.C. Duarte, Natural Deep Eutectic Solvents – Solvents for the 21st Century, ACS Sustain. Chem. Eng. 2 (5) (2014) 1063–1071, https://doi.org/10.1021/sc500096j.

[68] Y. Liu, J.B. Friesen, J.B. McAlpine, D.C. Lankin, S.-N. Chen, G.F. Pauli, Natural Deep Eutectic Solvents: Properties, Applications, and Perspectives, J. Nat. Prod. 81 (3) (2018) 679–690, https://doi.org/10.1021/acs.jnatprod.7b0094510.1021/acs.jnatprod.7b00945.s001.

[69] C. Florindo, L. Romero, I. Rintoul, L.C. Branco, I.M. Marrucho, From Phase Change Materials to Green Solvents: Hydrophobic Low Viscous Fatty Acid-Based Deep Eutectic Solvents, ACS Sustain. Chem. Eng. 6 (3) (2018) 3888–3895, https://doi.org/10.1021/acssuschemeng.7b0423510.1021/acssuschemeng.7b04235.s001.

[70] T.E. Phelps, N. Bhawawet, S.S. Jurisson, G.A. Baker, Efficient and Selective Extraction of 99mTcO4- from Aqueous Media Using Hydrophobic Deep Eutectic Solvents, ACS Sustain. Chem. Eng. 6 (11) (2018) 13656–13661, https://doi.org/10.1021/acssuschemeng.8b0395010.1021/acssuschemeng.8b03950.s001.

[71] R. Verma, M. Mohan, V.V. Goud, T. Banerjee, Operational Strategies and Comprehensive Evaluation of Menthol Based Deep Eutectic Solvent for the Extraction of Lower Alcohols from Aqueous Media, ACS Sustain. Chem. Eng. 6 (12) (2018) 16920–16932, https://doi.org/10.1021/acssuschemeng.8b0425510.1021/acssuschemeng.8b04255.s001.

[72] M.A.R. Martins, L.P. Silva, N. Schaeffer, D.O. Abranches, G.J. Maximo, S.P. Pinho, J.A.P. Coutinho, Greener Terpene-Terpene Eutectic Mixtures as Hydrophobic Solvents, ACS Sustain. Chem. Eng. 7 (20) (2019) 17414–17423, https://doi.org/10.1021/acssuschemeng.9b0461410.1021/acssuschemeng.9b04614.s001.

[73] F. Bezold, M. Minceva, Liquid-liquid equilibria of n-heptane, methanol and deep eutectic solvents composed of carboxylic acid and monocyclic terpenes, Fluid Phase Equilib. 477 (2018) 98–106, https://doi.org/10.1016/j.fluid.2018.08.020.

[74] E. Riveiro, B. González, Á. Domínguez, Extraction of adipic, levulinic and succinic acids from water using TOPO-based deep eutectic solvents, Sep. Purif. Technol. 241 (2020) 116692, https://doi.org/10.1016/j.seppur.2020.116692.

[75] Y. Segura, A. Cruz del Álamo, M. Munoz, S. Álvarez-Torrellas, J. García, J. A. Casas, Z.M. De Pedro, F. Martínez, A comparative study among catalytic wet air oxidation, Fenton, and Photo-Fenton technologies for the on-site treatment of hospital wastewater, J. Environ. Manage. 290 (2021) 112624, https://doi.org/10.1016/j.jenvman.2021.112624.

[76] A. Klamt, Conductor-like Screening Model for Real Solvents: A New Approach to the Quantitative Calculation of Solvation Phenomena, J. Phys. Chem. 99 (7) (1995) 2224–2235, https://doi.org/10.1021/j100007a062.

[77] A. Klamt, V. Jonas, T. Bürger, J.C.W. Lohrenz, Refinement and Parametrization of COSMO-RS, J. Phys. Chem. A. 102 (26) (1998) 5074–5085, https://doi.org/10.1021/jp980017s.

[78] S. Álvarez-Torrellas, J.A. Peres, V. Gil-Álvarez, G. Ovejero, J. García, Effective adsorption of non-biodegradable pharmaceuticals from hospital wastewater with different carbon materials, Chem. Eng. J. 320 (2017) 319–329, https://doi.org/10.1016/j.cej.2017.03.077.

[79] K. Kojima, S. Zhang, T. Hiaki, Measuring methods of infinite dilution activity coefficients and a database for systems including water, Fluid Phase Equilib. 131 (1-2) (1997) 145–179, https://doi.org/10.1016/S0378-3812(96)03210-4.

[80] D. Rodríguez-Llorente, A. Bengoa, G. Pascual-Muñoz, P. Navarro, V.I. Águeda, J. A. Delgado, S. Álvarez-Torrellas, J. García, M. Larriba, Sustainable Recovery of Volatile Fatty Acids from Aqueous Solutions Using Terpenoids and Eutectic Solvents, ACS Sustain. Chem. Eng. 7 (19) (2019) 16786–16794, https://doi.org/10.1021/acssuschemeng.9b04290.

[81] D. Rodríguez-Llorente, A. Cañada-Barcala, C. Muñoz, G. Pascual-Muñoz, P. Navarro, R. Santiago, V.I. Águeda, S. Álvarez-Torrellas, J. García, M. Larriba, Separation of phenols from aqueous streams using terpenoids and hydrophobic eutectic solvents, Sep. Purif. Technol. 251 (2020) 117379, https://doi.org/10.1016/j.seppur.2020.117379.

[82] M. Larriba, M. Ayuso, P. Navarro, N. Delgado-Mellado, M. Gonzalez-Miquel, J. García, F. Rodríguez, Choline Chloride-Based Deep Eutectic Solvents in the Dearomatization of Gasolines, ACS Sustain. Chem. Eng. 6 (1) (2018) 1039–1047, https://doi.org/10.1021/acssuschemeng.7b0336210.1021/acssuschemeng.7b03362.s001.

[83] M.A.R. Martins, E.A. Crespo, P.V.A. Pontes, L.P. Silva, M. Bülow, G.J. Maximo, E. A.C. Batista, C. Held, S.P. Pinho, J.A.P. Coutinho, Tunable Hydrophobic Eutectic Solvents Based on Terpenes and Monocarboxylic Acids, ACS Sustain. Chem. Eng. 6 (7) (2018) 8836–8846, https://doi.org/10.1021/acssuschemeng.8b01203.

[84] Sigma-Aldrich, Sigma-Aldrich, (n.d.). https://www.sigmaaldrich.com/spain.html (accessed December 27, 2020).

[85] National Institutes of Health (NIH), PubChem, (n.d.). https://pubchem.ncbi.nlm.nih.gov/ (accessed December 27, 2020).

[86] A.G. Gonçalves, J.J.M. Órfão, M.F.R. Pereira, Catalytic ozonation of sulphamethoxazole in the presence of carbon materials: Catalytic performance and reaction pathways, J. Hazard. Mater. 239–240 (2012) 167–174, https://doi.org/10.1016/j.jhazmat.2012.08.057.

[87] F.J. Beltrán, A. Aguinaco, J.F. García-Araya, A. Oropesa, Ozone and photocatalytic processes to remove the antibiotic sulfamethoxazole from water, Water Res. 42 (14) (2008) 3799–3808, https://doi.org/10.1016/j.watres.2008.07.019.

[88] A.G. Trovó, R.F. Pupo Nogueira, A. Agüera, A.R. Fernandez-Alba, S. Malato, Degradation of the antibiotic amoxicillin by photo-Fenton process - Chemical and toxicological assessment, Water Res. 45 (3) (2011) 1394–1402, https://doi.org/10.1016/j.watres.2010.10.029.

[89] A. Ledezma Estrada, Y.-Y. Li, A. Wang, Biodegradability enhancement of wastewater containing cefalexin by means of the electro-Fenton oxidation process, J. Hazard. Mater. 227-228 (2012) 41–48, https://doi.org/10.1016/j.jhazmat.2012.04.079.

[90] T.H. Kim, S.D. Kim, H.Y. Kim, S.J. Lim, M. Lee, S. Yu, Degradation and toxicity assessment of sulfamethoxazole and chlortetracycline using electron beam, ozone and UV, J. Hazard. Mater. 227–228 (2012) 237–242, https://doi.org/10.1016/j.jhazmat.2012.05.038.

[91] F. Eckert, A. Klamt, Fast Solvent Screening via Quantum Chemistry: COSMO-RS Approach, AIChE J. 48 (2) (2002) 369–385, https://doi.org/10.1002/(ISSN)1547-590510.1002/aic.v48:210.1002/aic.690480220.

[92] L.Y. García-Chavez, A.J. Hermans, B. Schuur, A.B. De Haan, COSMO-RS assisted solvent screening for liquid–liquid extraction of mono ethylene glycol from aqueous streams, Sep. Purif. Technol. 97 (2012) 2–10, https://doi.org/10.1016/J.SEPPUR.2011.11.041.

[93] Y. Chen, S. Zhou, Y. Wang, L. Li, Screening solvents to extract phenol from aqueous solutions by the COSMO-SAC model and extraction process simulation, Fluid Phase Equilib. 451 (2017) 12–24, https://doi.org/10.1016/J.FLUID.2017.08.007.

[94] F. Bergua, M. Castro, J. Muñoz-Embid, C. Lafuente, M. Artal, Hydrophobic eutectic solvents: Thermophysical study and application in removal of pharmaceutical products from water, Chem. Eng. J. 411 (2021) 128472, https://doi.org/10.1016/j.cej.2021.128472.

[95] N.S. Anikina, D. V. Schur, S.Y. Zaginaichenko, O.Y. Krivushchenko, O. V. Mil'to, A. Kale, Investigation of mechanism of fullerene dissolution in aromatical hydrocarbons, in: NATO Secur. through Sci. Ser. A Chem. Biol., Springer, Dordrecht, 2007: pp. 19–36. https://doi.org/10.1007/978-1-4020-5514-0_2.

[96] P. Wang, Y.-L. He, C.-H. Huang, Oxidation of Antibiotic Agent Trimethoprim by Chlorine Dioxide: Reaction Kinetics and Pathways, J. Environ. Eng. 138 (3) (2012) 360–366, https://doi.org/10.1061/(ASCE)EE.1943-7870.0000420.

[97] S. Babić, A.J.M. Horvat, D. Mutavdžić Pavlović, M. Kaštelan-Macan, Determination of pKa values of active pharmaceutical ingredients, TrAC -, Trends Anal. Chem. 26 (11) (2007) 1043–1061, https://doi.org/10.1016/j.trac.2007.09.004.

[98] P.B. Kyle, Toxicology: GCMS, Elsevier Inc., 2017. https://doi.org/10.1016/B978-0-12-800871-3.00007-9.

[99] F.F. Cantwell, M. Losier, Liquid-liquid extraction, Compr. Anal. Chem. 37 (2002) 297–340, https://doi.org/10.1016/S0166-526X(02)80048-4.

[100] Z. Berk, Extraction, in: Food Process Eng. Technol., 2018: pp. 289–310. https://doi.org/10.1016/c2016-0-03186-8.

[101] C. Cao, B. Nian, Y. Li, S. Wu, Y. Liu, Multiple Hydrogen-Bonding Interactions Enhance the Solubility of Starch in Natural Deep Eutectic Solvents: Molecule and Macroscopic Scale Insights, J. Agric. Food Chem. 67 (45) (2019) 12366–12373, https://doi.org/10.1021/acs.jafc.9b0450310.1021/acs.jafc.9b04503.s001.

[102] J.F. Zayas, Solubility of proteins, in: Funct. Proteins Food, Springer, Berlin Heidelberg, 1997, pp. 6–75, https://doi.org/10.1007/978-3-642-59116-7_2.

[103] K. Nadendla, S.H. Friedman, Light Control of Protein Solubility Through Isoelectric Point Modulation, J. Am. Chem. Soc. 139 (49) (2017) 17861–17869, https://doi.org/10.1021/jacs.7b0846510.1021/jacs.7b08465.s001.

[104] ICIS, Petrochemicals, Energy, and Fertilizers Market Information, (n.d.). https://www.icis.com (accessed January 7, 2021).

[105] Alibaba, Manufacturers, Suppliers, Exporters & Importers from the world's largest online B2B marketplace, (n.d.). https://www.alibaba.com/ (accessed January 7, 2021).

[106] B. Šulgan, J. Labovský, Z. Labovská, Multi-aspect comparison of ethyl acetate production pathways : reactive distillation process integration & intensification via mechanical and chemical approach, Processes. 8 (2020) 1–40, https://doi.org/10.3390/pr8121618.

[107] E. Mauriello, G. Ferrari, F. Donsì, Effect of formulation on properties, stability, carvacrol release and antimicrobial activity of carvacrol emulsions, Colloids Surfaces B Biointerfaces. 197 (2021) 111424, https://doi.org/10.1016/j.colsurfb.2020.111424.

SUPPLEMENTARY MATERIAL

Extraction of antibiotics identified in the EU Watch List 2020 from hospital wastewater using hydrophobic eutectic solvents and terpenoids

Pablo Gutiérrez-Sánchez,[a] Diego Rodríguez-Llorente,[a] Pablo Navarro,[b] V. Ismael Águeda,[a] Silvia Álvarez-Torrellas,[a] Juan García,[a] Marcos Larriba[a,*]

[a]*Grupo de Catálisis y Procesos de Separación (CyPS), Departamento de Ingeniería Química y de Materiales, Universidad Complutense de Madrid, Avda. Complutense s/n, 28040 Madrid, Spain*
[b]*Departamento de Ingeniería Química, Universidad Autónoma de Madrid, C/ Francisco Tomás y Valiente 7, 28049 Madrid, Spain*

Content

Number of pages: 7

Number of Figures: 1

Number of tables: 5

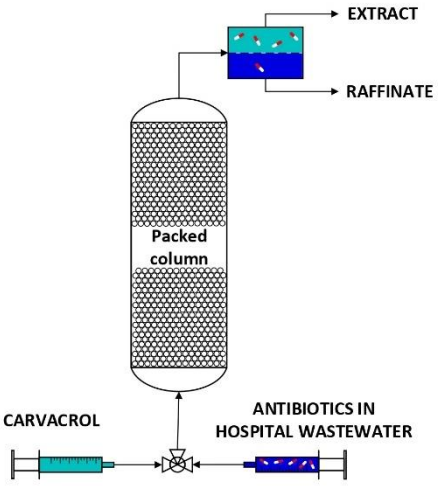

Figure S1. Scheme of the packed column installation.

Table S1. Extraction yields from different matrices (ultrapure water and hospital wastewater at different pH) at 323.2 K and S/F 0.10.

		Thymol	Carvacrol	Thymol + Dodecanoic acid	Thymol + Decanoic acid	Thymol + Octanoic acid	Ethyl acetate	MIBK
$Yld_{Trimethoprim}$ (%)	Feed in ultrapure water pH 6.5	94.05	95.71	99.31	95.60	88.67	10.02	10.67
	Feed in hospital wastewater pH 8.0	99.34	99.05	99.55	99.40	99.16	10.11	13.21
	Feed in hospital wastewater pH 6.5	98.11	98.91	99.45	99.25	98.71	9.90	11.85
	Feed in hospital wastewater pH 5.0	86.87	83.15	98.67	97.65	94.97	9.03	7.26
$Yld_{Ciprofloxacin}$ (%)	Feed in ultrapure water pH 6.5	94.30	98.19	99.79	98.15	90.40	9.15	7.15
	Feed in hospital wastewater pH 8.0	95.73	94.63	99.92	99.83	99.76	9.38	8.10
	Feed in hospital wastewater pH 6.5	95.83	97.38	99.87	98.83	99.35	10.02	8.47
	Feed in hospital wastewater pH 5.0	82.84	79.14	99.55	98.60	96.38	9.31	8.04
$Yld_{Sulfamethoxazole}$ (%)	Feed in ultrapure water pH 6.5	72.08	66.05	45.23	53.20	48.93	29.03	61.27
	Feed in hospital wastewater pH 8.0	0.00	0.00	15.63	22.24	42.72	6.51	9.37
	Feed in hospital wastewater pH 6.5	12.99	15.52	21.92	31.06	46.01	23.48	13.25
	Feed in hospital wastewater pH 5.0	76.50	75.40	43.74	43.02	47.53	23.80	70.70
$Yld_{Overall}$ (%)	Feed in ultrapure water pH 6.5	86.81	86.65	81.44	82.32	76.00	16.07	26.36
	Feed in hospital wastewater pH 8.0	65.03	64.56	71.70	73.82	80.55	8.67	10.23
	Feed in hospital wastewater pH 6.5	68.98	70.60	73.75	76.38	81.36	14.47	11.19
	Feed in hospital wastewater pH 5.0	82.07	79.23	80.66	79.76	79.63	14.05	28.67

Table S2. Extraction yields from different matrices (ultrapure water and hospital wastewater at different pH) at 323.2 K and S/F 0.25.

		Thymol	Carvacrol	Thymol + Dodecanoic acid	Thymol + Decanoic acid	Thymol + Octanoic acid	Ethyl acetate	MIBK
$Yld_{Trimethoprim}$ (%)	Feed in ultrapure water pH 6.5	95.01	97.92	99.81	96.63	96.06	11.17	11.54
	Feed in hospital wastewater pH 8.0	99.63	99.59	99.58	99.43	99.41	19.21	28.86
	Feed in hospital wastewater pH 6.5	99.32	99.40	99.55	99.29	98.81	16.09	20.03
	Feed in hospital wastewater pH 5.0	94.89	93.20	99.20	98.39	97.42	11.46	9.33
$Yld_{Ciprofloxacin}$ (%)	Feed in ultrapure water pH 6.5	95.26	99.17	99.88	99.32	98.04	9.20	8.79
	Feed in hospital wastewater pH 8.0	97.98	97.49	99.92	99.92	99.86	11.30	12.97
	Feed in hospital wastewater pH 6.5	98.41	98.69	99.90	99.87	99.41	11.47	23.42
	Feed in hospital wastewater pH 5.0	96.35	90.31	99.59	98.93	98.60	11.01	12.76
$Yld_{Sulfamethoxazole}$ (%)	Feed in ultrapure water pH 6.5	80.10	85.82	67.00	70.50	79.65	83.72	90.02
	Feed in hospital wastewater pH 8.0	8.17	8.01	43.63	55.01	68.60	65.03	14.70
	Feed in hospital wastewater pH 6.5	20.64	24.88	54.99	63.55	68.62	71.88	30.06
	Feed in hospital wastewater pH 5.0	89.03	89.42	62.82	64.15	68.71	84.08	88.36
$Yld_{Overall}$ (%)	Feed in ultrapure water pH 6.5	90.12	94.30	88.90	88.82	91.25	34.70	36.78
	Feed in hospital wastewater pH 8.0	68.59	68.36	81.04	84.79	89.29	31.85	18.84
	Feed in hospital wastewater pH 6.5	72.79	74.32	84.81	87.57	88.95	33.14	24.50
	Feed in hospital wastewater pH 5.0	93.42	90.98	87.20	87.16	88.24	35.52	36.82

Table S3. Extraction yields from different matrices (ultrapure water and hospital wastewater at different pH) at 323.2 K and S/F 0.50.

		Thymol	Carvacrol	Thymol + Dodecanoic acid	Thymol + Decanoic acid	Thymol + Octanoic acid	Ethyl acetate	MIBK
$Yld_{Trimethoprim}$ (%)	Feed in ultrapure water pH 6.5	99.70	99.44	99.81	98.88	97.80	11.20	22.80
	Feed in hospital wastewater pH 8.0	99.72	99.66	99.59	99.50	99.40	24.89	44.23
	Feed in hospital wastewater pH 6.5	99.48	99.46	99.55	99.49	99.26	23.64	43.25
	Feed in hospital wastewater pH 5.0	97.73	96.75	99.45	98.98	98.79	12.87	11.78
$Yld_{Ciprofloxacin}$ (%)	Feed in ultrapure water pH 6.5	99.92	99.92	99.92	99.91	99.06	9.66	11.15
	Feed in hospital wastewater pH 8.0	98.92	98.67	99.92	99.92	99.92	13.97	22.13
	Feed in hospital wastewater pH 6.5	99.54	99.06	99.91	99.92	99.92	14.48	34.76
	Feed in hospital wastewater pH 5.0	97.45	95.18	99.66	99.65	99.21	13.75	18.82
$Yld_{Sulfamethoxazole}$ (%)	Feed in ultrapure water pH 6.5	86.10	86.81	83.81	83.83	84.70	93.25	95.88
	Feed in hospital wastewater pH 8.0	12.78	13.56	72.51	75.87	82.92	79.83	20.44
	Feed in hospital wastewater pH 6.5	29.60	33.57	76.05	79.24	84.04	86.96	41.81
	Feed in hospital wastewater pH 5.0	94.04	94.39	77.36	83.43	84.55	92.48	94.29
$Yld_{Overall}$ (%)	Feed in ultrapure water pH 6.5	95.24	95.39	94.51	94.21	93.85	38.04	43.28
	Feed in hospital wastewater pH 8.0	70.47	70.63	90.67	91.76	94.08	39.56	28.93
	Feed in hospital wastewater pH 6.5	76.21	77.36	91.84	92.88	94.41	41.69	39.94
	Feed in hospital wastewater pH 5.0	96.40	95.44	92.16	94.02	94.18	39.70	41.63

Table S4. Extraction yields from different matrices (ultrapure water and hospital wastewater at different pH) at 323.2 K and S/F 1.00.

		Thymol	Carvacrol	Thymol + Dodecanoic acid	Thymol + Decanoic acid	Thymol + Octanoic acid	Ethyl acetate	MIBK
$Yld_{Trimethoprim}$ (%)	Feed in ultrapure water pH 6.5	99.82	99.63	99.82	98.99	98.38	11.25	30.26
	Feed in hospital wastewater pH 8.0	99.78	99.82	99.52	99.25	99.36	45.49	61.54
	Feed in hospital wastewater pH 6.5	99.50	99.45	99.52	99.49	99.59	36.56	61.00
	Feed in hospital wastewater pH 5.0	99.20	98.89	99.63	99.04	99.13	14.85	14.16
$Yld_{Ciprofloxacin}$ (%)	Feed in ultrapure water pH 6.5	99.92	99.92	99.92	99.69	99.44	9.88	14.83
	Feed in hospital wastewater pH 8.0	99.47	99.65	99.92	99.92	99.92	14.19	41.36
	Feed in hospital wastewater pH 6.5	99.81	99.76	99.92	99.92	99.92	28.36	61.77
	Feed in hospital wastewater pH 5.0	99.14	99.54	99.77	99.40	99.22	14.11	19.56
$Yld_{Sulfamethoxazole}$ (%)	Feed in ultrapure water pH 6.5	87.72	94.87	93.88	91.84	91.81	96.75	97.85
	Feed in hospital wastewater pH 8.0	22.39	22.67	84.25	87.28	91.07	92.28	35.58
	Feed in hospital wastewater pH 6.5	38.85	45.22	88.76	89.41	91.64	93.83	66.02
	Feed in hospital wastewater pH 5.0	96.72	97.02	88.58	89.43	92.02	96.56	97.29
$Yld_{Overall}$ (%)	Feed in ultrapure water pH 6.5	95.82	98.14	97.87	96.84	96.54	39.29	47.65
	Feed in hospital wastewater pH 8.0	73.88	74.04	94.57	95.48	96.78	50.65	46.16
	Feed in hospital wastewater pH 6.5	79.38	81.48	96.07	96.27	97.05	52.92	62.93
	Feed in hospital wastewater pH 5.0	98.35	98.48	96.00	95.96	96.79	41.84	43.67

Table S5. Extraction yields from different matrices (ultrapure water and hospital wastewater at different pH) at 323.2 K and S/F 2.00.

		Thymol	Carvacrol	Thymol + Dodecanoic acid	Thymol + Decanoic acid	Thymol + Octanoic acid	Ethyl acetate	MIBK
$Yld_{Trimethoprim}$ (%)	Feed in ultrapure water pH 6.5	99.82	99.82	99.82	99.14	98.73	12.34	39.67
	Feed in hospital wastewater pH 8.0	99.78	99.82	99.68	99.49	99.38	62.09	79.55
	Feed in hospital wastewater pH 6.5	99.66	99.53	99.68	99.50	99.64	52.32	68.30
	Feed in hospital wastewater pH 5.0	99.64	99.35	99.82	99.19	99.54	19.64	15.12
$Yld_{Ciprofloxacin}$ (%)	Feed in ultrapure water pH 6.5	99.92	99.92	99.92	99.88	99.81	10.09	19.94
	Feed in hospital wastewater pH 8.0	99.81	99.87	99.92	99.92	99.92	30.57	67.95
	Feed in hospital wastewater pH 6.5	99.92	99.89	99.92	99.92	99.92	32.82	81.34
	Feed in hospital wastewater pH 5.0	99.51	99.77	99.80	99.53	99.59	15.59	20.60
$Yld_{Sulfamethoxazole}$ (%)	Feed in ultrapure water pH 6.5	97.13	97.56	96.16	96.49	97.02	98.44	99.15
	Feed in hospital wastewater pH 8.0	39.29	38.49	94.49	94.55	95.48	96.34	48.29
	Feed in hospital wastewater pH 6.5	70.45	47.63	94.69	94.89	96.56	96.92	90.17
	Feed in hospital wastewater pH 5.0	98.30	98.33	96.02	96.42	96.88	98.31	98.84
$Yld_{Overall}$ (%)	Feed in ultrapure water pH 6.5	98.96	99.10	98.63	98.51	98.52	40.29	52.92
	Feed in hospital wastewater pH 8.0	79.63	79.39	98.03	97.99	98.26	63.00	65.26
	Feed in hospital wastewater pH 6.5	90.01	82.35	98.10	98.10	98.71	60.68	79.94
	Feed in hospital wastewater pH 5.0	99.15	99.15	98.55	98.38	98.67	44.51	44.85

7.3 Publicación 3

Journal of Molecular Liquids 381 (2023) 121840

Contents lists available at ScienceDirect

Journal of Molecular Liquids

journal homepage: www.elsevier.com/locate/molliq

Influence of transition metal-based activating agent on the properties and catalytic activity of sewage sludge-derived catalysts. Insights on mechanism, DFT calculation and degradation pathways

Pablo Gutiérrez-Sánchez [a,*], Silvia Álvarez-Torrellas [a], Marcos Larriba [a], M. Victoria Gil [b], Juan M. Garrido-Zoido [b], Juan García [a,*]

[a] Catalysis and Separation Processes Group, Chemical Engineering and Materials Department, Faculty of Chemistry, Complutense University, Avda. Complutense s/n, 28040 Madrid, Spain
[b] Departamento de Química Orgánica e Inorgánica, Facultad de Ciencias and IACYS Unidad de Química Verde y Desarrollo Sostenible, Universidad de Extremadura, E-06006 Badajoz, Spain

ARTICLE INFO

Keywords:
Activating agents
Catalysts
Density-functional theory
Real wastewater
Sewage sludge

ABSTRACT

Research studies combining the detailed physicochemical properties' analysis, the catalytic activity in different real aqueous matrices, the proposal of degradation mechanisms and the stability of the intermediates/by-products by means of the Density-functional theory (DFT) are scarce. Therefore, this work gives a step forward in the field of circular economy and the removal of emerging pollutants such as the antibiotic ciprofloxacin, covering all the previously aspects mentioned, using four iron and nickel-based catalysts from two different sewage sludge.

Experimental results revealed a significant influence of both the source of the sewage sludge and the activating agent used (iron chloride, nickel chloride and a mixture of both) on the physicochemical properties of the materials and, hence, on their catalytic activity. FTIR studies and chemical composition evidenced that the use of this biomass precursor leads to the generation of a wide variety of functional groups and heteroatoms in the synthesized catalyst structure. Moreover, they showed a combination of Type I-IV isotherms with H3-H4 type hysteresis loops, being mainly mesoporous materials and exhibiting a moderate microporosity except when nickel chloride was used solely as activating agent. The carbonaceous materials reached ciprofloxacin adsorption capacities in the range of 40.4–73.9 mg/g. The use of nickel chloride showed the lowest adsorption contribution and catalytic activity. The bimetallic catalyst (synthesized from a mixture of iron and nickel chloride) showed slightly higher catalytic activity than that found for the iron catalyst, but the metal leaching was also considerably higher. Consequently, the use of iron chloride solely as activating agent seems to be the better alternative, achieving a maximum ciprofloxacin removal around 99.7 % and an iron leaching concentration into the reaction medium of 0.48–0.61 mg/L. The main degradation pathways of ciprofloxacin were proposed according to the detection of LC-MS intermediates and DFT calculation, indicating the most likely areas of attack of reactive species on atoms with a high Fukui index (f^0).

1. Introduction

The demand for water is increasing as the world's population grows. Over the years, the fundamental problem limiting our water availability is the pollution of the various aqueous matrices. In this regard, both human and naturally occurring activities contribute to water pollution. The origin of pollution is mainly due to human activities both in urban and industrial areas, hospitals, veterinary clinics, etc [1–4]. Among all the various pollutants present in water, pharmaceutical residues deserve special attention, organic compounds that are classified as emerging pollutants, mainly due to their persistence in the conventional wastewater treatment plants [5–7].

Pharmaceutical compounds are used every day around the world, either in hospitals for the treatment of human diseases, or in veterinary clinics or farms for the treatment of animal infections. Depending on the chemical characteristics of the pharmaceutical compound, 5 to 90 % are

* Corresponding authors.
E-mail addresses: pgutie03@ucm.es (P. Gutiérrez-Sánchez), jgarciar@ucm.es (J. García).

https://doi.org/10.1016/j.molliq.2023.121840
Received 22 December 2022; Received in revised form 12 February 2023; Accepted 11 April 2023
Available online 15 April 2023

excreted from the body as parent compounds [8–10]. Thus, it can be said that a large amount of pharmaceuticals are consumed in hospitals on a daily basis. In addition, hospitals discharge their wastewater directly into the public sewage system without any pretreatment. It should be noted that several antibiotics are usually present in the natural environment, such as fluoroquinolones, in which ciprofloxacin is included, hold the fourth position in the European market of antibiotics, with a tendency to increase in all countries and been detected in different environmental systems, e.g. soils, sediments, rivers and groundwater, among others [11–14]. Moreover, as antibiotics are highly bioactive compounds, there is high concern about their role in increasing antibiotic resistance among pathogenic bacteria [13]. Thus, numerous studies have been conducted reporting the presence of these pharmaceutical compounds in wastewater treatment plants (WWTPs) as well as into freshwater bodies, where they may be frequently detected at low concentrations [15–18].

On the other hand, activated sludge from a wastewater treatment plant is the main waste from biological treatment [19,20]. It has been estimated that the generation of this waste worldwide (in dry sludge) reached 45 million tons, and its production is expected to continue to grow, predicting a 24 % increase by 2030 and a 51 % increase by 2050 [20,21]. Because these sludges may contain hazardous substances, their adequate treatment is essential [20,22]. In this scenario, it is mandatory to adopt a paradigm shift, in terms of resource consumption by the population to achieve a circular economy. In recent years, several effective sewage sludge treatment technologies have been developed, among which pyrolysis stands out as a promising method, being used to synthesize biochars [23,24]. As these dried sludges contain up to 55–70 % of organic matter, pyrolysis allows reducing carbon by immobilizing it into the biochar [25,26]. Sludge is a bioresidue produced worldwide [20,27], and its valorization is a key issue of the circular economy. It is therefore a strategy to change the consumption pattern of the European population towards a circular, climate-neutral economy that minimizes the impact on the environment.

Activated carbons obtained from sewage sludge are generally characterized by their large surface functional groups, moderate-high specific surface area as well as a developed porosity [28–30]. This allows them to be applied in many applications as adsorbents, catalysts or even as soil amendments [30,31]. In recent years, advanced oxidation processes (AOPs) have been widely applied in the treatment of wastewater containing organic pollutants that are difficult to degrade. In these AOP processes, hydroxyl radicals are used to decompose these organic pollutants into smaller molecules or to remove them completely, obtaining CO_2 and H_2O [32,33]. With reference to the advances made in their application to antibiotics removal, several research papers have been reported that allow the removal of these compounds to be studied from a critical point of view [34–37]. In particular, these reports provide information about the degradation of ciprofloxacin from the aqueous environment. For example, Anjali and Shanthakumar published a review article about several treatments, such as UV/H_2O_2, UV/H_2O_2/Fe^{2+}, and ozonation that have been used for the removal of ciprofloxacin from wastewater [38]. Some reviews on the application of adsorption process for the removal of this pollutants have also been published [39–41].

However, to our knowledge, there are few studies that report a combination of the behavior of iron and nickel-based catalysts from sewage sludge in the removal of an antibiotic, ciprofloxacin, present in real wastewater, with a Density-functional theory (DFT) study of the degradation mechanism of this compound in two real aqueous matrices.

Therefore, the main objectives of this work are: (1) employ a simple method of reusing sewage sludge as a metal–carbon feedstock to synthesize catalysts by a one-step pyrolysis process, studying the activating agent used, as well as the sludge source, urban or industrial; (2) explore the performance of the system oxidation process, catalytic wet peroxide oxidation (CWPO), using the four synthesized catalysts for the degradation of ciprofloxacin in two real aqueous matrices, and (3) elucidate the degradation mechanisms involved in the CWPO system catalyzed by the four synthesized catalysts through a Density-functional theory study.

This study is expected to provide a promising utilization strategy to develop a cost-effective sewage sludge-derived catalyst with high efficiency for the degradation of refractory organic pollutants from aqueous medium.

2. Materials and methods

2.1. Chemicals

The synthesis of the catalysts was carried out by using two chemical activating agents, iron(III) chloride hexahydrate and nickel(II) chloride. Hydrochloric acid was added to acidify the aqueous solutions. In addition, acetonitrile and acetic acid were also employed as mobile phases in the analysis of the samples. Ciprofloxacin was selected as a model antibiotic compound to study the catalytic activity of the various catalysts synthesized. Ultrapure water from Veolia PURELAB® Flex Water Purification System was used for the preparation of the aqueous solutions. The structure, suppliers and purity of the aforementioned compounds are listed in Table 1. The sludge applied as biomass precursor of the carbon catalysts was supplied by an urban and an industrial WWTP, specifically this latter from a pharmaceutical industry.

2.2. Synthesis of the catalysts

Firstly, the biomass precursor was dried in an oven at 105 °C. The dried sludge was ground to a fine powder and stored for later use. The ratio used for the chemical activation was 1 g of activating agent per gram of sludge. For the synthesis of the bimetallic catalyst, this ratio was maintained, so each gram of sludge was impregnated with 0.5 g of each of the two activating agents. Then, an aqueous solution of the chemical activating agent was prepared, and the sludge was treated by incipient wetness impregnation method and placed in an ultrasonic bath at 40 °C for 90 min. The latter stage was carried out to favour the access of the activating agent into the sludge pores and to homogenise the mixture. After impregnation, the mixture was left for 12 h at room temperature and then placed in an oven at 105 °C for 24 h to eliminate moisture. The solid obtained was pyrolyzed for 2 h at 800 °C in a vertical quartz reactor, using a nitrogen flow rate of 100 mL/min and a heating rate of 10 °C/min. After grinding, the obtained carbonaceous material was washed with 1 M hydrochloric acid solution for 1 h under magnetic stirring in order to remove the excess metal from the carbon matrix (100 mL HCl 1 M: 1 g carbonaceous material). Finally, it was filtered and washed with ultrapure water until a neutral pH was reached. The catalyst was dried in an oven at 105 °C for 24 h, and crushed and sieved to a particle size lower than 250 μm.

Table 1
Reagents used in the experiments.

Chemical	Structure	Supplier	Purity (wt %)
Ciprofloxacin, CAS n° 85721-33-1	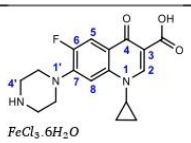	Sigma-Aldrich	≥ 98.0
Ferric chloride hexahydrate, CAS n° 10025-77-1	$FeCl_3.6H_2O$	Sigma-Aldrich	>99.0
Nickel dichloride, CAS n° 7718-54-9	$NiCl_2$	Sigma-Aldrich	98.0
Hydrochloric acid, CAS n° 7647-01-0	HCl	Fluka	37.0
Acetonitrile, CAS n° 75-05-08	CH_3CN	Scharlau	≥ 99.9
Acetic acid, CAS n° 64-19-7	CH_3COOH	PanReac	≥ 99.7

2.3. Characterization of raw sludge and catalysts

Macroscopic characterization of sewage sludge was performed using Standard Methods, determining total (TS), fixed (FS) and volatile (VS) solids, and chemical oxygen demand (COD) [42].

The chemical composition of both the biomass precursor and the synthesized catalysts was quantified by X-ray fluorescence spectroscopy (XRF) and elemental analysis (EA), using a PANalytical Axios spectrometer and a LECO CHNS-932 analyser, respectively.

The porosity of the carbonaceous materials was assessed from nitrogen adsorption–desorption isotherms at −196 °C, using a Micromeritics ASAP 2020 analyser. The surface chemistry was evaluated by Fourier-transformed infrared spectrometry, using a Thermo Nicolet Nexus 670 equipment, in a wavelength range of 400–4000 cm^{-1}.

The structural properties were analysed by the X-ray diffraction (XRD) patterns, collected on a Bruker D8 Advance A25 diffractometer, by scanning electron microscopy (SEM) performed in a JEOL JSM 6335F microscope and Transmission electron microscopy (TEM) performed in a JEOL JEM-2100 microscope equipped with a 200 kV LaB6 electron source and with a high-resolution ORIUS SC1000 CCD camera.

Finally, the thermal stability of the materials was tested by thermogravimetric analysis (TGA), that were accomplished in a PerkinElmer STAR 6000 thermobalance. The analyses were conducted using a heating rate of 10 °C/min, a N_2 flow rate of 30 mL/min, and a temperature range of 30–1000 °C.

2.4. Catalytic activity and adsorption contribution

Aqueous solutions of ciprofloxacin were prepared using three aqueous matrices, e.g., ultrapure water, surface water and an urban WWTP effluent. The macroscopic characterization of the two real matrices is detailed in Table 2. The antibiotic concentration was of 50 mg/L, which is in the range reported in the literature for the study of this type of pollutants [17,43–50]. Then, the pH value was modified until reaching the target point at 3.2 by adding 1 M hydrochloric acid.

For the catalytic reactions, 250 mL of ciprofloxacin solution together with the synthesized catalyst (0.3 g/L) and the required hydrogen peroxide dose (1.1 mL/L) were introduced into the glass reaction vessel. The operating temperature was of 70 °C and the magnetic stirring was set at 300 rpm. Samples were periodically collected for 180 min and then filtered for further analysis using 0.45 μm PTFE filters. Adsorption tests were performed following the same procedure as previously mentioned, but in the absence of hydrogen peroxide in order to avoid the generation of reaction-initiating hydroxyl radicals.

The concentration of ciprofloxacin was determined by an Agilent HPLC 1260 Infinity II with "diode array" detector, using a Poroshell 120 EC-C18 column (4.6 × 150 mm; 4 μm). A mobile phase consisting of 17.5 % acetonitrile and 82.5 % acetic acid 75 mM was used, setting a flow rate of 0.85 mL/min, an injection volume of 50 μL, a column temperature of 30 °C and a wavelength of 275 nm.

The iron leaching was measured by Inductively Coupled Plasma Optical Emission Spectroscopy (ICP-OES), while the reaction intermediates were identified in a Bruker LC-QTOF-MS Impact II equipment.

Table 2
Macroscopic characterization of real aqueous matrices.

Parameters	Surface water	WWTP effluent
pH	7.3	8.8
Chemical Oxygen Demand (mg/L)	< 15.0	23
Total Organic Carbon (mg/L)	3.2	13.2
Total Carbon (mg/L)	7.4	26.0
Total Nitrogen (mg/L)	0.6	4.8
Total Dissolved Solids (mg/L)	64.0	596.0
Conductivity, at 20 °C (μS/cm)	38.2	484.6

2.5. Computational methods

Gaussian 16 software package was used to perform all computations based on the density functional theory (DFT). Geometric optimization was executed using the hybrid M06-2X method at 6–311++G(2df,2pd) basis set level, obtaining the corresponding E_{HOMO} (highest occupied molecular orbital) values and positive frequencies in all the possible conformations evaluated, corresponding to minima energy. Here we show, of all these conformations, those that have turned out to be more stable under the conditions of the study, including Natural Bond Orbitals (NBO) analysis [51,52]. The SMD model (universal solvation model based on solute electron density and a continuum model of the solvent defined by the bulk dielectric constant and atomic surface tensions) was used to address the solvent effects of water [53]. GaussView 6.0 software was used to visualize the computed and optimized structures [54], whose coordinates have been included in the Supplementary Material.

The Fukui function has been widely used for the prediction of reactive sites of electrophilic, nucleophilic and radical attack of organic molecules. In this sense, the Fukui function can be defined as [55]:

$$f(r) = \left(\frac{\partial^2 E}{\partial N.\partial v(r)}\right) = \left[\frac{\partial \mu}{\partial v(r)}\right]_N = \left[\frac{\partial \rho(r)}{\partial N}\right]_{V(r)} \quad (1)$$

where $\rho(r)$ is the electron density at point r in space, N is the electron number in the system, and v in the partial derivative is external potential. In the condensed version of the Fukui function, atomic population number is used to represent the electron density distributed around an atom. The condensed Fukui function can be calculated unambiguously for three situations:

$$\begin{aligned} &\textit{Nucleophilic attack}: && f_k^+ = q_N^k - q_{N+1}^k \\ &\textit{Electrophilic attack}: && f_k^- = q_{N-1}^k - q_N^k \\ &\textit{Radical attack}: && f_k^0 = \left(q_{N-1}^k - q_{N+1}^k\right)/2 \end{aligned} \quad (2)$$

where k is the number of atoms used in the calculation, N is the number of electrons in the current state, and q^k represents the atomic charge population number of the atom k. In this study, free radical reaction is the most important mechanism, so f_k^0 of ciprofloxacin molecule was employed to study the degradation pathway. The greater the value of f_k^0, the more vulnerable the site is to free radical attack.

3. Results and Discussion

3.1. Raw sludge characterization

The properties and origin of the biomass precursor have a significant influence on the final characterization of the synthesised carbonaceous materials. Therefore, this work addresses the valorisation of sewage sludge through the synthesis of carbonaceous catalysts, assessing the technical feasibility using sludge from two different sources: an urban and an industrial WWTP. The most relevant characterization parameters are summarized in Table 3.

Sewage sludge typically has a high organic matter content, which makes it potentially suitable for its use in the synthesis of carbonaceous materials [30]. COD and vS values indirectly indicate the organic matter content of the sewage sludge, being considerably higher for industrial sludge (COD = 34.8 g/L; vS = 29.3 g/L) compared to the urban one (COD = 8.4 g/L; vS = 6.5 g/L). The TS value of the industrial sludge is about 4 times larger than the urban sludge (36.6 *vs* 8.8 g/L), indicating a higher water content in the sludge supplied by the urban WWTP. However, both sludges presented an approximately equal percentage of volatile matter over total solids content, being within the range 74–80 %. In this regard, high values of volatile matter will not only promote the generation of porosity but also increase the efficiency of the carbon synthesis. In the literature, a volatile matter content higher than 70 % is usually recommended, so the two sludges used in this study seem to be

Table 3
Characterization of the raw sludges.

Parameters	Industrial	Urban
Macroscopic characterization (g/L)		
Chemical Oxygen Demand	34.8	8.4
Density	1000.6	955.9
Total Solids	36.6	8.8
Volatile Solids	29.3 (80 %)	6.5 (74 %)
Fixed Solids	7.3 (20 %)	2.3 (26 %)
Chemical composition of the dried sludge (wt.%)		
C	42.4	37.9
O	14.6	18.9
H	5.8	5.6
N	3.7	6.1
Fe	0.7	11.6
Ni	0.4	0.02
Ca	11.7	3.0
S	0.7	0.7
Si	0.73	2.63
Cl	3.5	0.6
Na	2.3	–
P	1.9	4.8
K	1.4	1.9
Al	0.6	1.0

suitable biomass precursors [56]. Finally, the FS content of both urban and industrial sludge is related to the ash content, and is within the values found in the literature for this type of biomass precursor [30,57,58].

The chemical composition of both sludges showed a predominant contribution of carbon (38–42 %) and oxygen (15–19 %), which, together with the hydrogen content, are within the range reported by other authors for this kind of biomass source [30,58–61]. According to the literature, the carbon content required to achieve acceptable carbon yields has to be in the range of 40–90 %, so the industrial sludge would be within it and the urban sludge would be very close to it. Therefore, it seems that both sludges could be potential biomass precursors for the synthesis of carbonaceous materials [62,63].

Sulphur and nitrogen contents in raw sludges were found relatively low. Thus, the emissions of these oxides during the pyrolysis process could be considered as negligible, minimizing the impact of these harmful gases on the environment [56].

The predominant metal concentration found in the urban sludge was iron (11.6 %), while in the industrial sludge it was calcium (11.7 %). A high concentration of these metals in various types of sludge has been reported in the literature [30,64–66]. Other minor elements were potassium, phosphorus, sodium, chlorine, sodium, or silicon. The sludge chemical composition is quite heterogeneous and variable, and its properties can change significantly depending on the sludge source, day or location [66].

3.2. Catalyst characterization

3.2.1. Chemical composition

As can be seen in Table 4, the source of the biomass precursor seems to have a significant influence on the final catalyst composition when the same synthesis conditions and activation agent were used. That is, although the initial carbon content for both precursors was approximately the same, the pyrolysis process generated very different final compositions. While the industrial sludge provided catalysts with a carbon content of more than 70 wt%, the urban sludge only reached to 23 wt%. Therefore, the carbon content of Urban-Fe was lower than that of the biomass precursor, while the carbon content of the industrial-sludge catalyst was higher. This trend evidenced a difference in the pyrolysis mechanisms depending on the composition of the sewage sludge used as precursor, as reported in other studies [30,64].

Also, noteworthy is the high oxygen contribution of the Urban-Fe catalyst (28.3 wt%), compared to the Industrial-Fe sample (8.5 wt%).

Table 4
Influence of the sludge source and activating agent on the final composition of the catalysts.

Parameters	Urban-Fe (wt.%)	Industrial-Fe (wt.%)	Industrial-Ni (wt.%)	Industrial-FeNi (wt.%)
C	23.1	70.9	50.5	52.9
O	28.3	8.5	13.6	14.4
H	2.8	1.8	1.6	1.5
N	4.5	3.8	2.1	2.1
Fe	9.3	5.1	0.1	8.7
Ni	0.08	0.2	26.8	15.8
Ca	0.7	0.6	0.6	0.4
S	0.5	1.2	1.0	0.9
Si	14.9	3.4	0.6	1.0
Cl	4.8	2.4	0.8	0.4
Na	–	–	–	–
P	1.4	0.9	1.7	1.5
K	3.0	0.02	0.01	0.01
Al	3.2	1.0	0.3	0.3

This could be attributed to the high iron content present in the urban sludge, which could favour its combination with the oxygen present in the sample to generate metal oxides, increasing the oxygen content in the carbon material [64]. Moreover, the iron content obtained with the urban sludge precursor was slightly lower than twice that obtained with the industrial sludge. The higher attachment of this metal to the carbonaceous matrix could have been favoured by the high iron content of the raw urban sludge. Silicon was also one of the major elements in the Urban-Fe catalyst (14.9 wt%).

Regarding the influence of the activating agent, the composition of three catalysts obtained from the same biomass precursor, i.e. industrial sludge, was compared. The activating agents applied were iron and nickel salts, and a mixture of both. As can be seen in Table 4, it was observed a considerably higher carbon content for the catalyst synthesized with iron chloride (Industrial-Fe) compared to that obtained using nickel chloride (Industrial-Ni). The bimetallic catalyst (Industrial-FeNi) showed an intermediate value to those obtained for the previous ones, although much closer to the Industrial-Ni catalyst. The oxygen contribution was considerably higher for the two Ni-based catalysts, either pure or as a mixture with the iron salt (13.6 and 14.4 wt%). That is, while the industrial-Fe catalyst reduced the oxygen content to about half of that present in the raw sludge (14.6 wt%), the Ni and bimetallic catalysts showed a negligible variation. The type of chemical activation agent did not seem to have a significant influence on the hydrogen, sulphur or potassium content. However, the nickel salt used in the Industrial-Ni and Industrial-FeNi catalysts led to a slight decrease of the chlorine, nitrogen and silicon content in the final composition of the carbon materials. The potassium content seemed to show the opposite trend, rising as the amount of nickel chloride impregnated in the catalyst increased.

A marked difference in the amount of active phase attached to the carbonaceous matrix was also observed for the Industrial-Fe and Industrial-Ni catalysts. While a 26.8 wt% of nickel was found in the Ni-based catalyst, the Industrial-Fe material only achieved a 5.1 wt% of iron. That is, the activating agent seemed to show a significant influence on the attachment of the active phase, showing a favourable trend in the case of the nickel salt. However, despite having a higher metal content, the Industrial-Ni catalyst may have a lower catalytic activity than the Industrial-Fe material, as will be discussed in the following sections.

Furthermore, it would be expected that, by using a lower relative amount of iron and nickel chloride in the synthesis of the Industrial-FeNi catalyst (1 g dried sludge: 0.5 g iron salt: 0.5 g nickel salt), the content of these metals in the final sample would be between the values for the catalysts obtained from a single metal salt, i.e. Industrial-Fe (1 g dried sludge: 1 g iron salt) and Industrial-Ni (1 g dried sludge: 1 g nickel salt). However, the bimetallic catalyst showed a higher iron concentration than the Industrial-Fe catalyst, while the nickel content was lower than

that found in the Industrial-Ni catalyst. It seems that the use of a bimetallic solution in the incipient wetness impregnation method favoured the iron attachment on the carbonaceous matrix, while nickel attachment was reduced. It should also be noted that the rinsing step during the catalyst synthesis mostly removed the calcium in the industrial sludge-based catalysts, obtaining values lower than 0.6 wt%.

Pyrolysis processes allowed to obtain carbonaceous materials from diverse biomass sources. During this stage, smaller organic molecules condense into conjugated aromatic rings, and organic nitrogen and metals can also be conjugated into the carbonaceous structure. This resulted in metal loading sites, oxygen functionalities, defective edges and nitrogen doping [67]. Compared to other biomass precursors, the use of sewage sludge favoured the generation of functional groups in the carbonaceous materials [64]. For this reason, the chemical composition of the catalysts synthesized with the two sludges and the different chemical activating agents showed carbon content values lower than those found for commercial activated carbons (around 90 %) [58].

3.2.2. Porosity

The porosity of carbonaceous materials is one of the most important properties, since it will determine the feasibility of the materials for applications such as catalysis and/or adsorption. This information has been obtained from the nitrogen adsorption–desorption isotherms at −196 °C.

The behaviour of the synthesized catalysts when exposed to a physisorption process under a nitrogen atmosphere, as shown in Fig. 1a, seems to suggest a combination of Type I-IV isotherms. This pattern has been previously reported in the literature for carbonaceous materials obtained from sewage sludge, and it is characteristic of mesoporous solids, with a moderate contribution of microporosity [30,60,65]. In addition, all four materials showed a hysteresis loop at P/P^0 values close to 0.4, which is often found in micro-mesoporous carbons [68]. This is, H3-H4 Type hysteresis loops, as found for the synthesized catalysts, indicated the occurrence of narrow crack pores and slit-shaped pores in the carbon structure [65,69,70]. A steep nitrogen uptake was observed at low relative pressures, which is related to the microporosity contribution in the analysed samples [68,71].

In addition, the desorption branches showed a step-down at P/P^0 values close to 0.5, which might indicate cavitation induced by the evaporation of the condensed liquid in larger mesopores (capillary condensation effect) [72]. This behaviour seems not to depend on the biomass source, i.e. Urban-Fe and Industrial-Fe catalysts exhibited a similar shape. However, the catalysts in which nickel salt was used as activating agent (Industrial-Ni and Industrial-FeNi) this phenomenon appeared to be increased, showing a sharper step down.

As has been reported in the literature, the BET (Brunauer-Emmett-

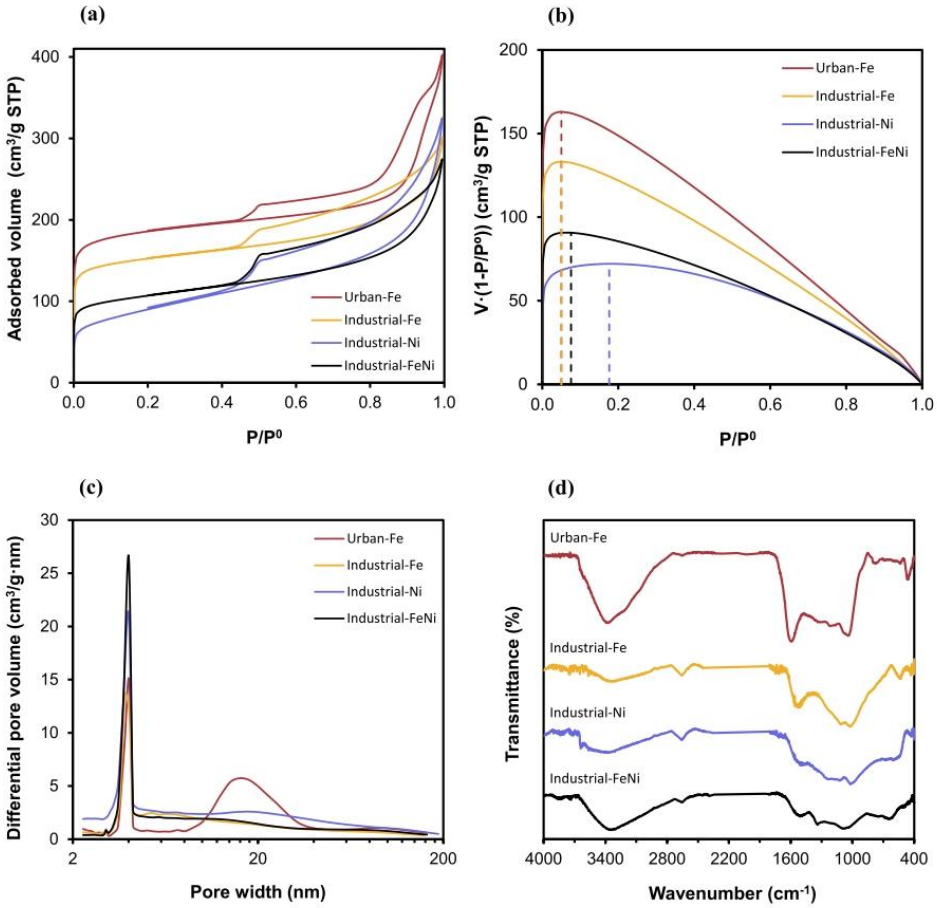

Fig. 1. N_2 adsorption–desorption isotherms (a), BET calculation criteria (b), Pore size distribution calculated with BJH method (c), and FTIR spectra (d) of the synthesized catalysts with different activating agents and sludge source.

Teller) method can be applied to Type IV and II isotherms, where the linearity range of the BET plot is usually found in the relative pressure range of 0.05–0.3. However, the presence of micropores hinders the application of this method, as it may be not possible to separate the micropore filling and monolayer-multilayer adsorption processes, and the standard range of relative pressures is no longer valid. In this case, the linear range of BET plot may be narrow and difficult to locate. To address this issue, Rouquerol et al. proposed a procedure to determine the correct relative pressure range and avoid any subjectivity during the evaluation of the BET monolayer capacity [68,72–74]. Since the catalysts synthesized have a considerable microporosity, these criteria have been used to determine the BET surface area.

The upper relative pressure limit of the BET range, which corresponded to the absolute maximum shown in dashed lines in Fig. 1b, reached values of 0.05 for Urban-Fe and Industrial-Fe catalysts, 0.18 for Industrial-Ni and 0.08 for Industrial-FeNi. Therefore, it seems that a high microporosity in the material increased the narrowing of the applicable relative pressure range. Table 5 shows the calculated values of the apparent BET surface area by applying the previously mentioned procedure for micro-mesoporous materials. The apparent S_{BET} values decreased in the following order: Urban-Fe > Industrial-Fe > Industrial-FeNi > Industrial-Ni. A high apparent BET monolayer capacity was found when urban sludge was used as biomass precursor and when increasing the amount of iron chloride used as chemical activating agent. The resulting BET values are within the range reported in the literature for other carbonaceous materials obtained from sewage sludge by chemical activation with iron chloride (S_{BET} = 468 m^2/g) and zinc chloride (S_{BET} = 266–558 m^2/g) [30,60]. Moreover, the chemical activation agents proposed in this study exhibited apparent S_{BET} higher than those obtained by other authors for chemical activation agents such as iron nitrate (S_{BET} = 240 m^2/g), iron sulphate (S_{BET} = 233 m^2/g), or (ortho)-phosphoric acid (S_{BET} = 230–296 m^2/g) [30,60,71]. According to Álvarez et al., the physical activation of sewage sludge, without any pre-treatment of the raw sludge, allowed to obtain carbonaceous materials with an apparent S_{BET} of 43 m^2/g, values considerably lower than those obtained by chemical activation following the procedure described in this work [75].

On the other hand, nitrogen adsorption–desorption isotherms provided other textural parameters, such as the contribution of microporosity (V_{Micro}) and mesoporosity (V_{Meso}) to the total pore volume (V_{Total}), as well as the average pore width. This information is summarized in Table 5.

The total pore volume, i.e. the maximum amount of N_2 uptake at a relative pressure close to 1.0 decreased in the following order: Urban-Fe > Industrial-Ni > Industrial-Fe > Industrial-FeNi. However, the relative micropore volume showed a different trend: Industrial-Fe > Urban-Fe > Industrial-FeNi > Industrial-Ni. Therefore, while the iron chloride used as activating agent seems to show a slight decrease in the total pore volume, the development of microporosity was considerably favoured. Furthermore, the use of a mixture of iron and nickel chloride as chemical activating agent resulted in a catalyst whose V_{Total} was lower than those values of catalysts synthesized with a single activating agent (Industrial-Fe and Industrial-Ni), but the relative microporosity was found to be in between these two.

Table 5
Porosity-related properties of the synthesized catalysts.

Parameters	Urban-Fe	Industrial-Fe	Industrial-Ni	Industrial-FeNi
S_{BET} (m^2/g)	713	582	319	397
V_{Micro} (cm^3/g) [a]	0.219	0.173	0.030	0.100
V_{Meso} (cm^3/g) [c]	0.404	0.293	0.472	0.325
V_{Total} (cm^3/g) [b]	0.623	0.466	0.502	0.425
V_{Micro}/V_{Total} (%)	35.1	37.1	6.0	23.6
Average pore width (nm)	10.4	7.2	7.1	6.8

[a] Calculated by Dubinin-Radushkevich method.
[b] Volume of pores at P/P^0 = 0.99.
[c] Calculated from V_{Micro} and V_{Total}.

It should be noted that the heterogeneity in the composition depending on the sludge source appeared to have a significant influence on the final porosity of the synthesized carbonaceous materials. In this regard, while the use of urban sludge (Urban-Fe) showed a considerably high total pore volume, the relative contribution of microporosity was slightly lower than that obtained for the Industrial-Fe catalyst. The development of a higher total porosity with the urban sludge could be due to the high iron content found in the dried raw sludge (11.6 wt%). This means that the chemical activation during the catalyst synthesis could have been due to both the contribution of the impregnated iron chloride and the iron content of the raw sludge. The increase in relative micropore volume when industrial sludge was used could be attributed to the high calcium content present in the raw sludge (see Table 3), which was removed during the catalyst rinsing (see Table 4), unblocking the pores that were occupied in the carbonaceous matrix.

According to the literature, the different pore structure generated during the pyrolysis process for the synthesis of carbonaceous materials from sewage sludge is related to the varying inorganic content depending on the source. However, most authors have reported a simultaneous formation of mesopores and micropores in both physical and chemical activation [75].

Pore size distribution is one of the established criteria for the selection of carbonaceous materials in applications such as adsorption, determining the fraction of the volume accessible to molecules of a particular shape or size [76]. The pore size distribution of the catalysts (Fig. 1c) highlights the micro-mesoporous nature of the materials, reaching a maximum around 4 nm for all catalysts. The Urban-Fe catalyst also showed another relative maximum around 16 nm. As shown in Table 5, the chemical activation of sewage sludge with iron and nickel chloride allowed the synthesis of predominantly mesoporous carbonaceous materials, with average pore width values ranging from 6.8 to 10.4 nm. These values justify the loop hysteresis found in the N_2 adsorption–desorption isotherms (see Fig. 1a), since this phenomenon occurs when the pore width exceeds a critical value, which for nitrogen at −196 °C is 4 nm [72].

Iron and nickel salts used as chemical activating agents have been effective in the synthesis of carbonaceous materials, exhibiting high porosity and surface area. These compounds promoted the degradation of the biomass precursor used as carbon source, generating a dehydration of the raw material that resulted in the carbonisation and aromatisation of the carbon skeleton and developing the porous structure [76]. As a result, biochars of a micro-mesoporous nature were obtained, which is in agreement to the data reported by other authors [65].

3.2.3. Surface chemistry

The surface functional moieties of the catalysts are generally assessed from the Fourier-transformed infrared (FTIR) spectra, shown in Fig. 1d.

As can be observed, all catalysts showed a broad band located between 3700 and 2800 cm^{-1}, which could be related to both the presence of O—H bonds on the catalyst surface and the moisture adsorbed by the materials [30,77]. The intensity of this band decreased in the following order: Urban-Fe > Industrial-FeNi > Industrial-Ni > Industrial-Fe, being in agreement with the oxygen content of the materials, shown in Table 4. This band could also be attributed to the N—H stretching vibrations related to amides and amines from the proteins found in the sewage sludge [75]. However, the low nitrogen content compared to oxygen in the final catalysts seemed to suggest a higher contribution of O—H bonds of the synthesized materials.

The synthesized materials also showed a band around 2650 cm^{-1}, which could be attributed to aliphatic C—H stretching vibrations [30].

All four catalysts showed a peak at a wavelength around 1600 cm^{-1}, which could be related to C═O and/or C═C bonds of carbonyl groups

(belonging to functional groups such as ketones, quinones, keto-esters, diketones and ketoenols) and aromatic rings, respectively [78–80]. This peak seemed to be extremely dependent on the biomass source used in the synthesis, reaching considerably higher values for Urban-Fe material compared to Industrial-Fe. This fact could be favoured by the high oxygen content of the Urban-Fe catalyst (see Table 4), being involved in the formation of carbonyl bonds.

The band found between 1000 and 1200 cm^{-1} could be explained by the C—O stretching from alcohols, phenols, acids, ethers or ester functional groups [78,80,81]. In addition, the absorption peaks located from 900 to 1200 cm^{-1} might be related to Si-O-Si and Si—O—C bonds, which could explain the high intensity of this band for the Urban-Fe catalyst due to its higher silicon content (see Table 4) [75].

Finally, the band located in the wavelength range 400–800 cm^{-1} could indicate the out-of-plane bending vibration of O—H bonds or the stretching vibration of C—H (benzene derivatives) bonds. The presence of these aromatic C—H groups would suggest the surface aromatization of these carbonaceous catalysts [30,82].

3.2.4. Structural properties

In order to characterize the crystalline phases present in the sewage sludge-derived catalysts, XRD studies were accomplished. The XRD patterns obtained are shown in Fig. 2. Thus, XRD patterns for the catalysts containing only iron, named as Urban-Fe and Industrial-Fe, exhibited three main wide peaks, characteristic of poor crystalline solids, located at 2θ values of 26 ° and 43 °, which correspond to graphite phase (ICDD PDF File 001–0646) and were assigned to (002), (100)-(101) planes. The XRD graphs of these materials did not show peaks which could origin from iron in metallic form [83]. Moreover, it should be highlighted that if the particle size of iron is very small, it could not be observed in XRD patterns. On the other hand, the XRD patterns of the Ni-based catalysts (Industrial-Ni and Industrial-FeNi) showed three large reflection signals (as illustrated in Fig. 2) at 44.6 ° (111) 51.9 ° (200) and 76.4° (220), typical of metallic nickel with a CFC structure [84]. These peaks are more intense than those observed in the XRD patterns of iron-based catalysts, since the percentage of Ni used in the synthesis was much higher (Table 4).

The SEM micrographs of the synthesized catalysts are shown in Fig. 3a-d. All the micrographs revealed a morphology characteristic of porous materials, where inner porosity has been developed through a thermal treatment. In Fig. 3a, the largely isolated cylindrical units have

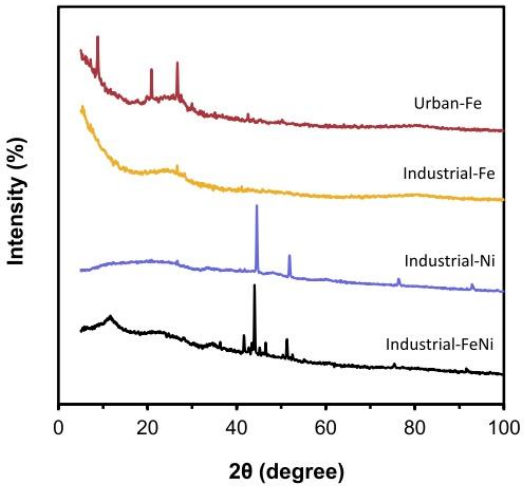

Fig. 2. XRD patterns of the catalysts synthesized with different activating agents and sludge source.

walls formed by layers of thin films. In Fig. 3b, these units seen in Fig. 3a have coalesced at the walls into a singular solid matrix interspersed with pores. The bonding of the walls and the melting of the wall lamellae suggested a deep transformation at molecular level in the sewage sludge during pyrolysis. Generally, all the carbon samples showed a great heterogeneity.

3.2.5. Thermal stability

Thermal stability is a key requirement for the catalysts, and it will limit both the operating conditions under which they can be used and their suitability for thermal regeneration after their application. The thermogravimetric analysis of the four synthesized catalysts are shown in Fig. 4.

Firstly, there is a weight loss of the samples around 100 °C, which could be related to the water adsorbed on the carbonaceous materials. According to the results obtained, both the source of the sludge and the activating agent seemed to have an influence on the sample moisture. That is, while Industrial-Fe material presented moisture values close to 7 %, Urban-Fe reached to 12.2 %. In addition, Industrial-Ni catalyst showed a moisture content close to 5.1 %, which is lower than that observed for Industrial-Fe. However, the use of a mixture of activating agents consisting of iron and nickel chloride seemed to favour water adsorption, reaching values close to 7.9 % for the Industrial-FeNi catalyst. Therefore, the moisture content of the synthesized catalysts decreased in the following order: Urban-Fe > Industrial-FeNi > Industrial-Fe > Industrial-Ni.

All samples showed a slightly decreasing trend in weight at temperatures above 100 °C, which could be associated with the decomposition of compounds that did not have time to degrade during the pyrolysis process in the catalyst synthesis. Moreover, at temperatures close to the pyrolysis temperature, i.e. between 700 and 900 °C, a more steep weight variation was observed, which could be mainly due to the removal of compounds that require a higher pyrolysis temperature or time than the one used in the synthesis. It should be noted that the Industrial-Fe catalyst was the material with the lowest weight variation, i.e. the one with the highest thermal stability.

3.3. Catalytic Wet Peroxide Oxidation of Ciprofloxacin

3.3.1. Adsorption tests

Carbonaceous materials derived from pyrolytic processes using biomass precursors generally exhibit adsorptive properties as a consequence of the porosity generated during their synthesis. In this study, the porous nature of the four synthesized catalysts has been described by their characterization in the previous section. In other words, the information obtained from the N_2 adsorption–desorption isotherms, together with the surface chemistry of the materials, will lead to different kinetics and adsorption capacities depending on the activating agent and the source of the sludge used in the synthesis of the carbon materials.

Therefore, to evaluate the effectiveness of the catalysts in the heterogeneous reaction systems, adsorption blanks are required to assess the contribution of adsorption to the pollutant removal process. This information can be seen in Fig. 5.

With regard to the influence of the source of biomass precursor, the catalyst synthesized from industrial sludge (Fig. 5b) appeared to exhibit considerably slower adsorption kinetics compared to that shown for the material obtained from urban sludge (Fig. 5a). That is, while the Urban-Fe catalyst required times longer than 45 min to reach the equilibrium, an equilibrium time higher than 120 min was needed for the Industrial-Fe catalyst.

On the other hand, the type of activating agent used for the catalyst synthesis also seemed to show some influence on the adsorption kinetics. Zinc chloride allowed obtaining carbons with faster adsorption kinetics than those shown with iron chloride. Specifically, Industrial-Ni catalyst (Fig. 5c) required times longer than 60 min to reach the equilibrium,

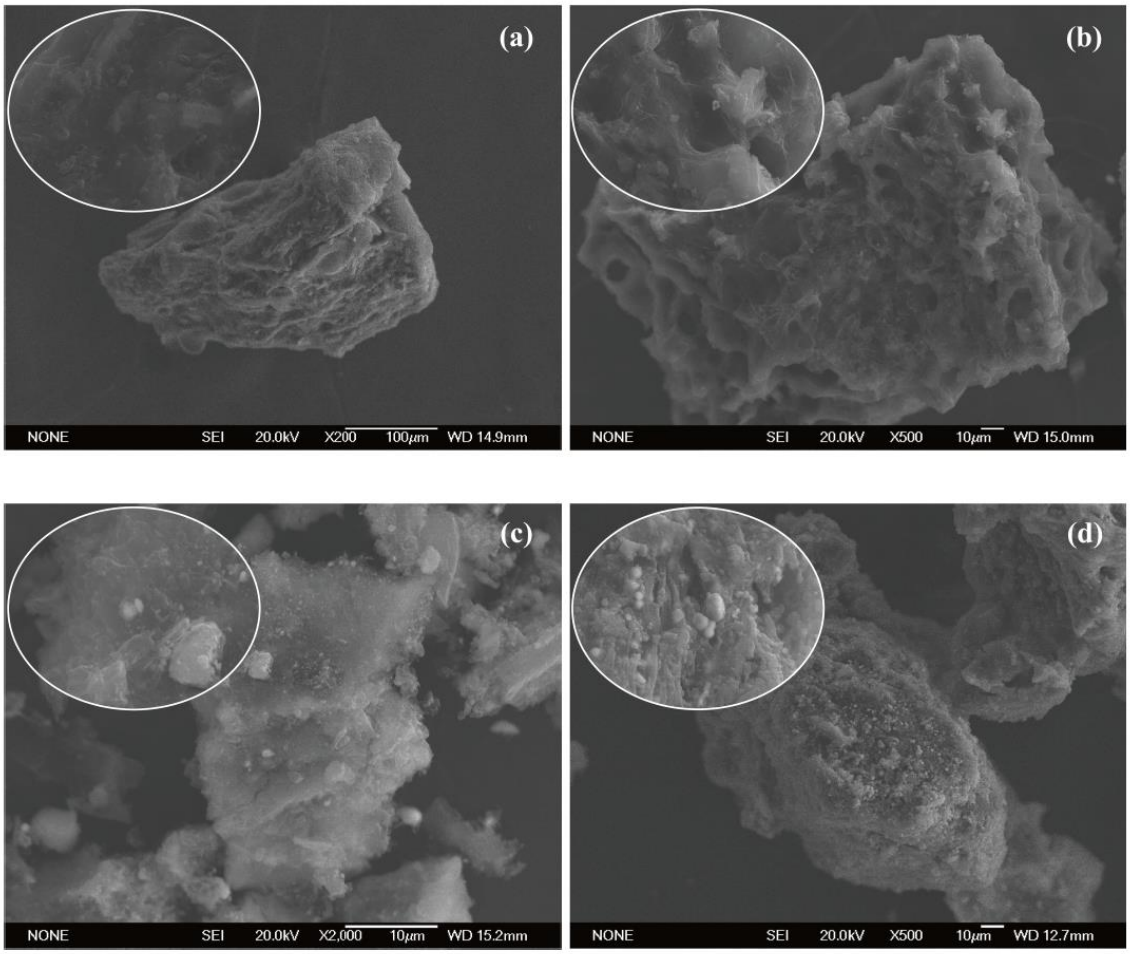

Fig. 3. SEM micrographs of the catalysts synthesized with different activating agents and sludge source: Urban-Fe (a), Industrial-Fe (b), Industrial-Ni (c), Industrial-FeNi (d).

compared to the equilibrium time shown by the previously mentioned Industrial-Fe material. Furthermore, it should be noted that the use of a mixture of activating agents consisting of iron and nickel chloride for the synthesis of the bimetallic Industrial-FeNi catalyst (Fig. 5d) presented similar kinetics to that obtained for the Industrial-Fe catalyst. Therefore, the iron chloride predominantly seemed to determine the kinetics of the bimetallic catalyst, making the time required to reach the equilibrium the same as for the Industrial-Fe, i.e. 120 min.

The adsorption capacity at equilibrium time, defined by Equation 3, is one of the most commonly used parameters to compare the adsorption contribution of different materials.

$$q_e = \frac{C_{Ciprofloxacin,0} - C_{Ciprofloxacin,e}}{C_{Catalyst}} \quad (3)$$

where q_e (mg/g) is the adsorption capacity at equilibrium time; $C_{Ciprofloxacin,0}$ (mg/L) is the initial ciprofloxacin concentration, i.e. 50 mg/L; $C_{Ciprofloxacin,e}$ (mg/L) is the concentration of ciprofloxacin when equilibrium was reached, assuming that the equilibrium time corresponded to the last sample taken at 180 min; and $C_{Catalyst}$ (g/L) is the catalyst dose used, i.e. 0.3 g/L.

As observed, both the biomass source and the activating agent seemed to have an influence on the ciprofloxacin concentration in the aqueous phase at equilibrium time, assuming that equilibrium has been reached at approximately 180 min. In this regard, the equilibrium concentration values were of 30.1, 27.8, 37.9, and 30.2 mg/L for Urban-Fe, Industrial-Fe, Industrial-Ni, and Industrial-FeNi catalysts, respectively. Therefore, the adsorption capacity values of the synthesized materials were 66.3, 73.9, 40.4, and 66.0 mg/g, respectively, in the order previously indicated. The adsorption capacity range of the synthesized materials is in accordance with the one reported in the literature for other biomass-based materials for the removal of ciprofloxacin [85–88] and other emerging contaminants [30,60].

As previously discussed, the sludge source and the activating agent have an influence on the kinetics and adsorption capacity of the catalysts. While the adsorption rate decreased in the following order: Urban-Fe > Industrial-Ni > Industrial-Fe = Industrial-FeNi; the adsorption capacity did so as follows: Industrial-Fe > Urban-Fe ≈ Industrial-FeNi > Industrial-Ni.

Finally, the study of the aqueous matrix effect on the adsorption process evidenced a relatively small effect on the four materials considered. As can be seen, although the kinetics seemed to maintain a

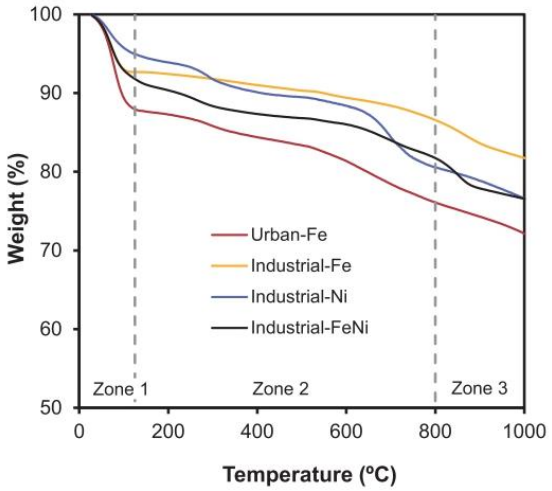

Fig. 4. Thermogravimetric profiles of the synthesized catalysts with different activating agents and sludge source.

similar trend regardless of the matrix, the ciprofloxacin concentrations in the aqueous phase increased in the following order: ultrapure water < surface water < WWTP water. The higher removal of the antibiotic in ultrapure water compared to the real aqueous matrices could be due to the presence of other organic and inorganic compounds competing for the active sites of the solid for the adsorption of ciprofloxacin. Therefore, it seemed that an increase of organic and inorganic matter in the real matrix led to a lower adsorption capacity, i.e. a higher ciprofloxacin equilibrium concentration in the aqueous phase. This could explain the lower ciprofloxacin concentration when using surface water compared to that found in WWTP effluent, since macroscopic parameters, such as the chemical oxygen demand, total organic carbon, total dissolved solids, among others, were considerably higher for the latter (see Table 2).

3.3.2. Catalytic activity

The properties and catalytic activity of the catalysts will determine the removal rate of ciprofloxacin, as well as the formation of different reaction intermediates and by-products. Thus, the evolution of the relative concentration of the tested antibiotic in the reaction tests, using the four synthesized catalysts and the three aqueous matrices, has been illustrated in Fig. 6.

As can be seen, the degradation kinetics of ciprofloxacin using the Urban-Fe catalyst, Fig. 6a, was considerably slower than that shown for the Industrial-Fe, Fig. 6b. That is, while the former needed times longer than 180 min to reach a ciprofloxacin removal of around 98 %, the Industrial-Fe catalyst did so before 30 min. Moreover, the reaction profile for Urban-Fe catalyst before 15 min was identical to that shown in the adsorption profile (see Fig. 5), suggesting that the major contribution in the ciprofloxacin removal up to that time is from adsorption. This could be due to the formation of a minimum concentration of hydroxyl radicals in the oxidation process that initiates the reaction. However, this time seems to be considerably reduced for the Industrial-Fe catalyst, with the adsorption and reaction profiles coinciding only up to the first 5 min.

It should also be noted that the iron content of the Industrial-Fe catalyst (5.1 wt%) was considerably lower than that of the Urban-Fe material (9.3 wt%). However, the catalytic activity showed the opposite trend. This behaviour could indicate a higher dispersion and accessibility of the active phase on the catalyst surface, which could lead to a higher metal leaching. HR-TEM images of the particle size distribution and metallic dispersion of the iron and nickel particles of the catalysts are presented in Fig. S1, the histograms of metals particle size distributions are shown in Fig. S2, supporting information. The average particle size of the iron or nickel particles of the catalysts was obtained by counting using ImageJ software. The results indicated a mean particle size distribution of 46 ± 17.94, 67 ± 23.54, 32 ± 9.63 and 34 ± 16.33 nm, for Urban-Fe, Industrial-Fe, Industrial-Ni and Industrial FeNi catalysts, respectively. In addition, by TEM images, the better dispersion of iron metal on the surface of Industrial-Fe catalyst, with respect to Urban-Fe catalyst, is confirmed. Indeed, the values of the iron leached concentration into the reaction medium were slightly higher for the Industrial-Fe catalyst compared to those observed for the Urban-Fe catalyst. Specifically, the iron concentrations in the reaction medium at near 98 % ciprofloxacin removal were of 0.48 mg/L (at 180 min reaction time) and 0.61 mg/L (at 30 min reaction time) for the Urban-Fe and Industrial-Fe catalysts, respectively. Therefore, the origin of the sludge has a considerable influence on the catalytic activity of the carbonaceous catalyst.

Concerning the influence of the activating agent on the ciprofloxacin removal kinetics, nickel appeared to have a significantly lower catalytic activity than iron. That is, while the Industrial-Fe catalyst achieved a maximum ciprofloxacin removal of 99.7 %, the Industrial-Ni catalyst reached only 32.5 % (Fig. 6c). It is also noteworthy that the concentration of nickel in the Industrial-Ni material (26.8 wt%) was considerably higher than that of iron in the Industrial-Fe catalyst (5.1 wt%), again highlighting the low catalytic activity of nickel in the generation of hydroxyl radicals for the CWPO process.

As previously mentioned, the presence of iron in the catalyst seemed to considerably favour the kinetics of the process. However, the bimetallic Industrial-FeNi catalyst (Fig. 6d) showed faster removal kinetics than the Industrial-Fe catalyst. This behaviour could be due to the high iron (8.7 wt%) and nickel (15.8 wt%) content of the former, although due to the low nickel catalytic activity it is likely to have been caused mainly by iron. That is, while the Industrial-FeNi catalyst required 15 min to remove the antibiotic almost completely, the Industrial-Fe catalyst required 15 min longer. In addition, due to the higher metal content in the Industrial-FeNi catalyst, the leaching into the reaction medium also increased. Specifically, the concentration of iron and nickel in the reaction medium when reaching around 98 % ciprofloxacin removal was 2.0 and 11.4 mg/L, respectively. Therefore, although the reaction kinetics was slightly favoured in the bimetallic catalyst due to the higher iron content, the leaching of metals into the reaction medium was higher, and the Industrial-Fe catalyst could be considered as the optimum material. In other words, the activating agent has a crucial influence on the catalytic activity of the synthesized carbonaceous materials, being preferable the use of iron chloride over nickel chloride.

The initial reaction rates were calculated by numerical derivation from the concentration profile versus time and collected in Table 6. These values evidenced the kinetic behaviour previously discussed. That is, the reaction rate depends on both the origin of the sludge and the active agent, decreasing as follows: Industrial-FeNi > Industrial-Fe > Urban-Fe > Industrial-Ni. Furthermore, the reaction kinetics and the catalytic activity seem to depend on the aqueous matrix and, as observed in the adsorption tests, decrease in the following order: ultrapure water > surface water > WWTP water. This effect could be related to the occurrence of other pollutants in the real aqueous matrices that would compete with ciprofloxacin during the catalytic wet peroxide oxidation. Therefore, as shown in Table 2, the higher pollutant concentration in WWTP water compared to surface water would disfavour the ciprofloxacin reaction rate.

3.3.3. Mechanism and pathways of CWPO degradation of ciprofloxacin. DFT study

The possible mechanism of ciprofloxacin removal on the catalyst (urban or industrial)/hydrogen peroxide could be as follows: When hydrogen peroxide is present, the iron or nickel ions on the catalyst

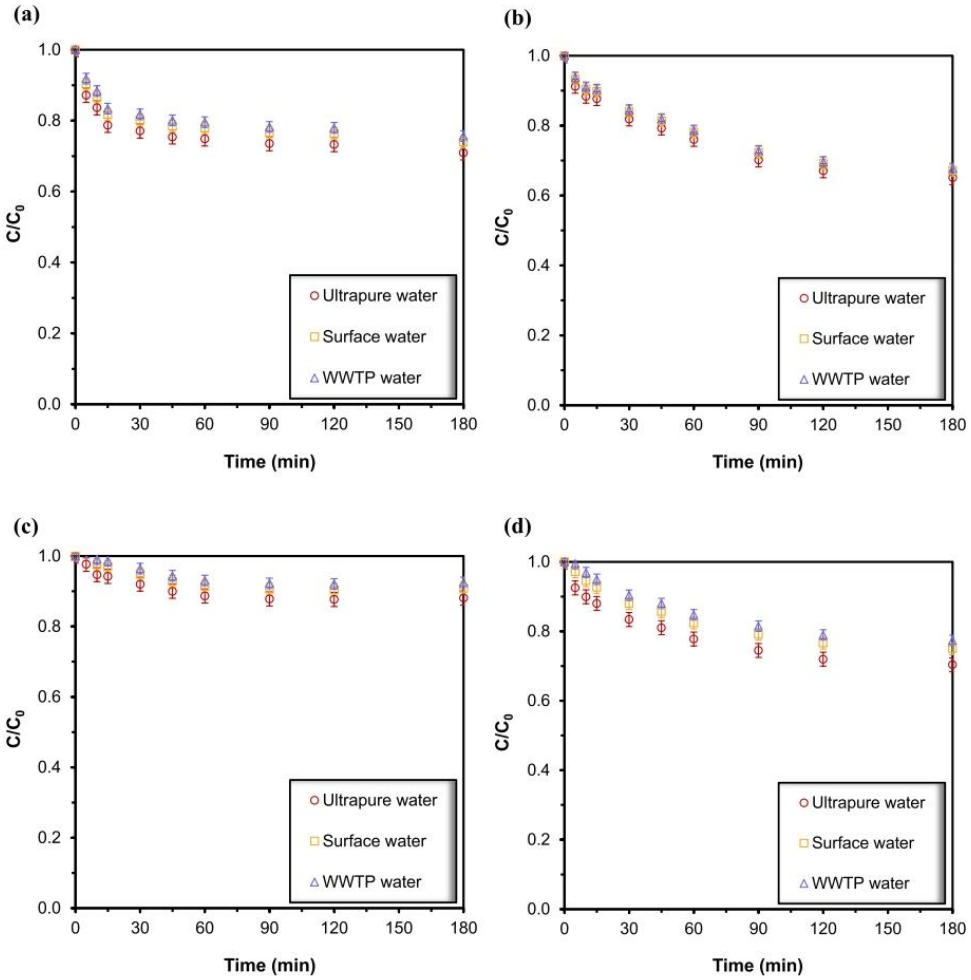

Fig. 5. Adsorption tests of the synthesized catalysts with different activating agents, sludge sources and aqueous matrices: Urban-Fe (a), Industrial-Fe (b), Industrial-Ni (c), Industrial-FeNi (d).

surface could accelerate the generation of $\bullet OH_{surf}$ from hydrogen peroxide through an intermolecular electron transfer process (Equations (3)-(4)). In addition, the oxygen-containing functional groups of the catalyst could react with hydrogen peroxide to form $\bullet OH_{surf}$ via electron transfer (Equation (5)) [89]. On the other hand, a small amount of leached ions could activate hydrogen peroxide to produce $\bullet OH_{surf}$ via chain reaction (Equations (7)-(8)). As a final step, the ciprofloxacin molecule could be degraded by the $\bullet OH_{surf}$ generated on the catalyst surface (Equations (6)) and a small part of $\bullet OH_{free}$ in the solution (Equation (9)). In this sense, the ciprofloxacin can be degraded indirectly through the oxidation of ^{-}OH, and directly mediate electron transfer processes of the oxygen-containing functional groups and the metal of the catalyst. In addition, the carbon base can act as a medium for electron transfer from ciprofloxacin (as electron donor) to hydrogen peroxide (as electron acceptor) [90].

$$Fe^{3+} + H_2O_2 \rightarrow Fe^{2+} + \cdot OH_{surf} + H^+ \quad (3)$$

$$Fe^{2+} + H_2O_2 \rightarrow Fe^{3+} + \cdot OH_{surf} + HO^- \quad (4)$$

$$Catalyst - O - C = O + H_2O_2 \rightarrow Catalyst^+ + HO^- + \cdot OH_{surf} \quad (5)$$

$$Ciprofloxacin + \cdot OH_{surf} \rightarrow Intermediates \rightarrow CO_2 + H_2O \quad (6)$$

$$Fe^{3+} + H_2O_2 \rightarrow Fe^{2+} + HO_{2\cdot free} + H^+ \quad (7)$$

$$Fe^{2+} + H_2O_2 \rightarrow Fe^{3+} + \cdot OH_{free} + HO^- \quad (8)$$

$$Ciprofloxacin + \cdot OH_{free} \rightarrow Intermediates \rightarrow CO_2 + H_2O \quad (9)$$

Ciprofloxacin degradation intermediates were identified by a Bruker LC-QTOF-MS Impact II instrument for each of the four catalysts used in this work. The possible molecular structure was proposed for each intermediate on the basis of MS/MS fragments and their m/z as shown in Tables S1-S4. MS/MS spectra or MS spectra of ciprofloxacin and intermediates are shown in Fig. S3-S6. In addition, energy data and cartesian coordinates for the optimised structure of the organic compounds involved in the reactions are given in Supplementary Material (Table S5-S23). Based on the Fukui index and in conjunction with the identification of the intermediate products of the four catalysts, the different

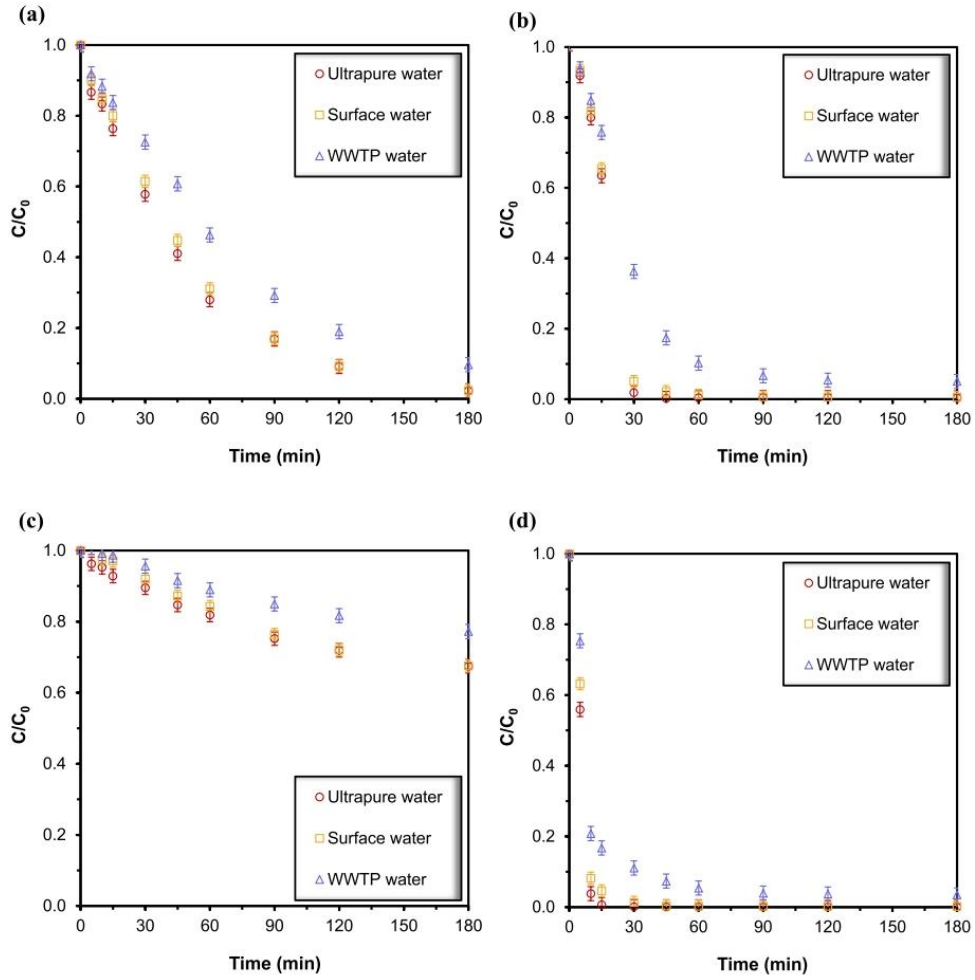

Fig. 6. Catalytic activity of the synthesized catalysts with different activating agents, sludge sources and aqueous matrices: Urban-Fe (a), Industrial-Fe (b), Industrial-Ni (c), Industrial-FeNi (d).

Table 6
Initial reaction rates of the synthesized catalysts with different activating agents, sludge sources and aqueous matrices.

	Urban-Fe	Industrial-Fe	Industrial-Ni	Industrial-FeNi
$r_{0,\ Ultrapure\ water}$ ($mg_{Ciprofloxacin}/g_{Catalyst}\cdot min$)	2.59	3.82	1.07	12.61
$r_{0,\ Surface\ water}$ ($mg_{Ciprofloxacin}/g_{Catalyst}\cdot min$)	2.16	2.79	0.29	10.53
$r_{0,\ WWTP\ water}$ ($mg_{Ciprofloxacin}/g_{Catalyst}\cdot min$)	2.02	2.32	0.16	7.05

possible degradation pathways of ciprofloxacin in each system were proposed (T1-T4), taking into account the integration of the degradation pathways of all catalysts, as shown in Figs. 7-10. The Fukui index (f^0) was computed to identify the vulnerable atomic sites of the ciprofloxacin molecule for radical attack (Fig. 11a,b). According to Fukui function (Eq. 2), a high f^- value suggests that an atom is more like to be attacked by electrophilic reagent (nucleophilic reaction), and a high f^0 value indicates that an atom is likely to be attacked by and •OH. The 1(C), 3(C), 5(C), 11(F), 15(O), 19 (N), 20(C), 35(H) and 41(H) positions exhibited high f^- values, suggesting the potential electrophilic attack. The 6(C), 8 (C), 10(C) and 15(O) positions displayed high positive point charges, and so these positions are expected to undergo preferential nucleophilic attack. High f^0 values were calculated for the 3(C), 6(C), 10(C), 15(O), and 19(N) positions, indicating that these regions tend to lose electrons and be attacked by •OH.

The possible degradation reactions of ciprofloxacin could follow four different degradation pathways (Fig. 7). In the first one, compounds with $m/z = 330$, 346 and 261 are formed by processes of defluorination and hydroxylation, followed by the cleavage of piperazine ring. All these processes have been reported in the degradation of fluoroquinolones [91,92]. In the second pathway, hydroxyl groups are incorporated into the piperazine ring and subsequently oxidised. Successive CO losses could lead to the opening and disappearance of the piperazine ring, resulting in formation of the compound with $m/z = 263$. The third

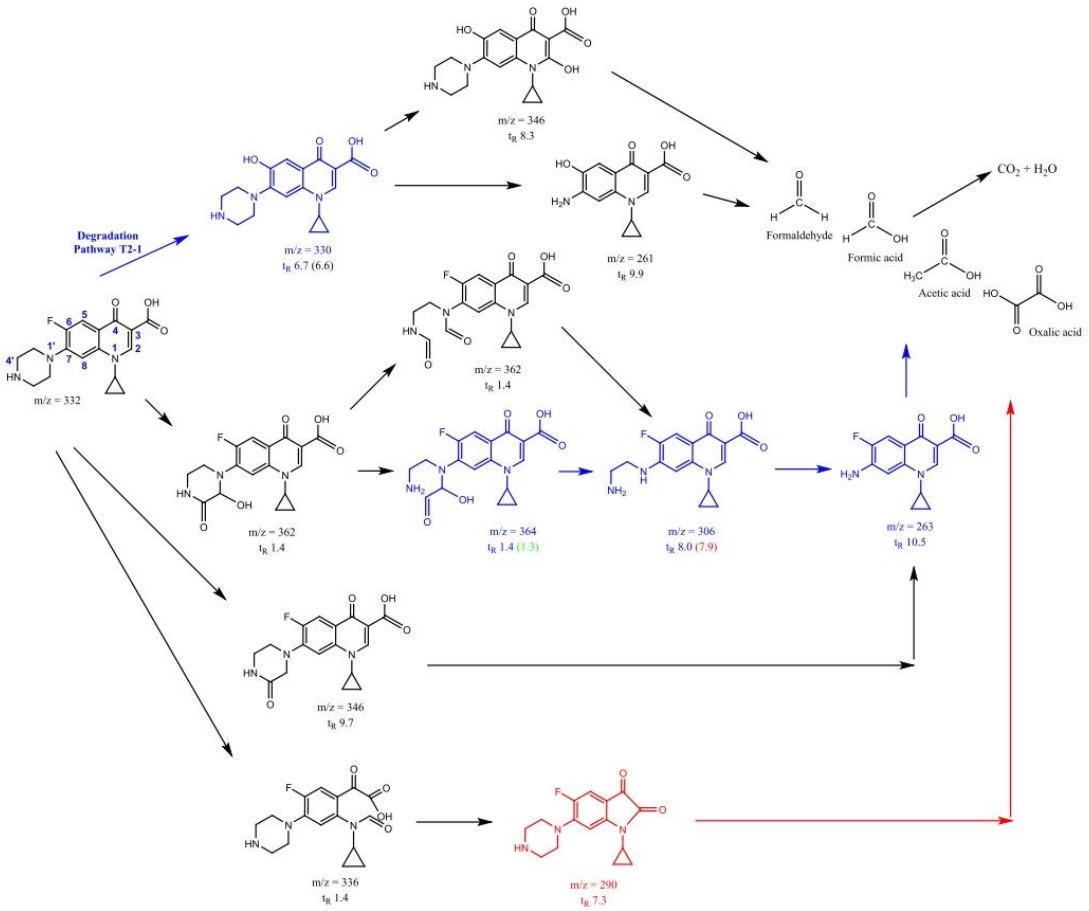

Fig. 7. Degradation pathway of ciprofloxacin by T1 (Urban-Fe) comprising T2 (Industrial-Fe), part of T3 (Industrial-Ni) and part of T4 (Industrial FeNi).

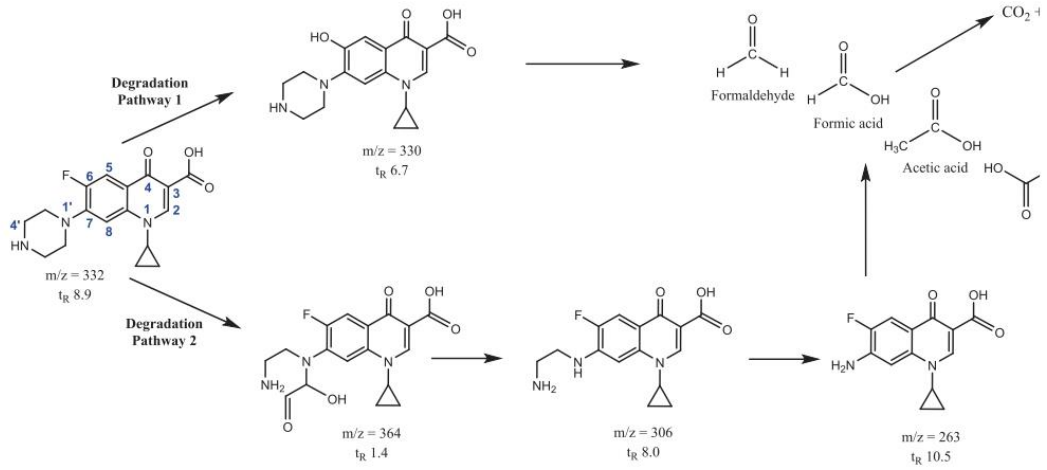

Fig. 8. Degradation pathway of ciprofloxacin by T2 (Industrial-Fe).

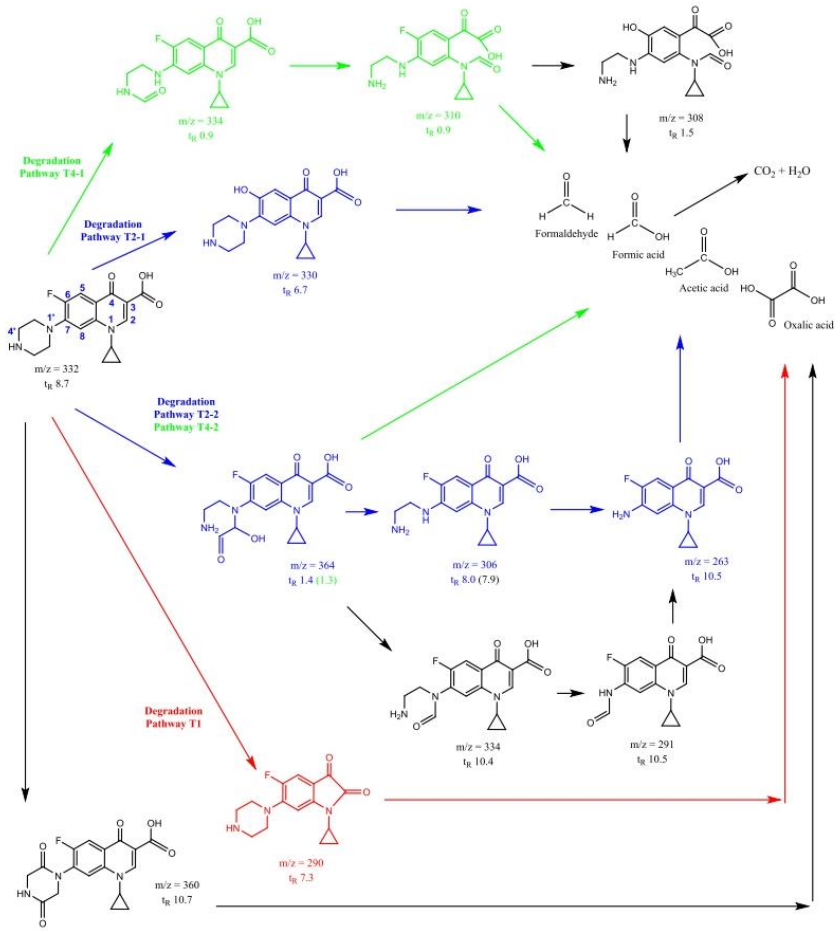

Fig. 9. Degradation pathway of ciprofloxacin by T3 (Industrial-Ni) from T2 (Industrial-Fe) as contained in T1 (Urban-Fe) and T4 (Industrial-FeNi).

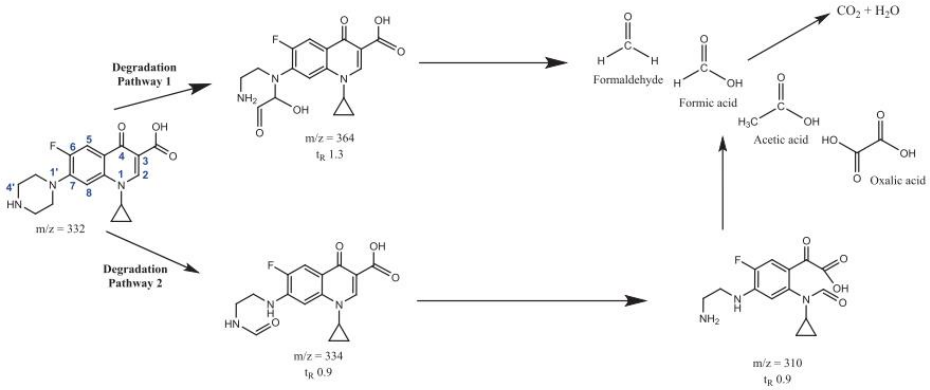

Fig. 10. Degradation pathway of ciprofloxacin by T4 (Industrial-FeNi).

a)

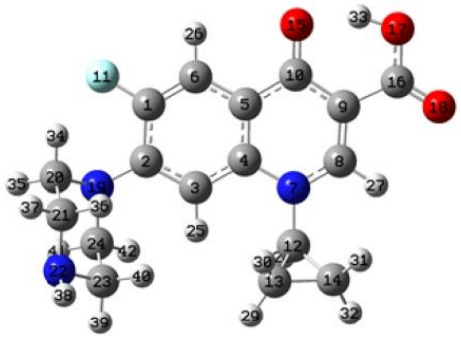

b)

Atom	q(N)	q(N+1)	q(N-1)	f^-	f^+	f^0
1(C)	0,0820	0,0395	0,1287	0,0467	0,0424	0,0446
2(C)	0,0506	-0,0058	0,0820	0,0314	0,0564	0,0439
3(C)	-0,0625	-0,1071	0,0115	0,0740	0,0446	0,0593
4(C)	0,0562	0,0276	0,0778	0,0216	0,0287	0,0251
5(C)	-0,0376	-0,0659	0,0227	0,0603	0,0283	0,0443
6(C)	-0,0449	-0,1206	-0,0154	0,0296	0,0756	0,0526
7(N)	0,0319	-0,0082	0,0384	0,0065	0,0400	0,0233
8(C)	0,0802	-0,0051	0,0974	0,0172	0,0853	0,0512
9(C)	-0,0678	-0,1006	-0,0523	0,0155	0,0328	0,0242
10(C)	0,1133	0,0015	0,1326	0,0192	0,1118	0,0655
11(F)	-0,0987	-0,1198	-0,0729	0,0258	0,0211	0,0234
12(C)	0,0262	0,0190	0,0278	0,0016	0,0072	0,0044
13(C)	-0,0588	-0,0676	-0,0557	0,0031	0,0088	0,0059
14(C)	-0,0557	-0,0640	-0,0516	0,0040	0,0084	0,0062
15(O)	-0,3113	-0,4147	-0,2815	0,0297	0,1035	0,0666
16(C)	0,1831	0,1669	0,1902	0,0071	0,0163	0,0117
17(O)	-0,2278	-0,2443	-0,2204	0,0074	0,0165	0,0120
18(O)	-0,3824	-0,4060	-0,3715	0,0108	0,0236	0,0172
19(N)	-0,0700	-0,0934	0,0960	0,1660	0,0233	0,0947
20(C)	-0,0088	-0,0171	0,0223	0,0311	0,0082	0,0197
21(C)	-0,0155	-0,0199	0,0108	0,0263	0,0044	0,0154
22(N)	-0,1762	-0,1789	-0,1527	0,0235	0,0026	0,0131
23(C)	-0,0136	-0,0175	0,0117	0,0253	0,0039	0,0146
24(C)	-0,0032	-0,0099	0,0265	0,0297	0,0067	0,0182
25(H)	0,0510	0,0334	0,0729	0,0219	0,0176	0,0198
26(H)	0,0598	0,0214	0,0777	0,0180	0,0384	0,0282
27(H)	0,0748	0,0394	0,0831	0,0083	0,0355	0,0219
28(H)	0,0673	0,0524	0,0716	0,0043	0,0149	0,0096
29(H)	0,0588	0,0519	0,0617	0,0030	0,0069	0,0049
30(H)	0,0543	0,0476	0,0573	0,0030	0,0068	0,0049
31(H)	0,0594	0,0520	0,0620	0,0026	0,0074	0,0050
32(H)	0,0599	0,0535	0,0626	0,0028	0,0063	0,0045
33(H)	0,1100	0,0955	0,1148	0,0048	0,0145	0,0096
34(H)	0,0360	0,0297	0,0586	0,0225	0,0064	0,0145
35(H)	0,0378	0,0299	0,0712	0,0334	0,0078	0,0206
36(H)	0,0254	0,0208	0,0439	0,0185	0,0046	0,0115
37(H)	0,0447	0,0397	0,0679	0,0232	0,0050	0,0141
38(H)	0,1100	0,1071	0,1294	0,0193	0,0030	0,0111
39(H)	0,0444	0,0398	0,0665	0,0221	0,0047	0,0134
40(H)	0,0280	0,0241	0,0456	0,0175	0,0039	0,0107
41(H)	0,0397	0,0312	0,0754	0,0357	0,0085	0,0221
42(H)	0,0506	0,0437	0,0762	0,0256	0,0069	0,0162

Fig. 11. Ciprofloxacin chemical structure (a). Hirshfeld charges and condensed Fukui functions of ciprofloxacin (b). Units used are "e" (elementary charge).

pathway involved the oxidation of the piperazine ring ($m/z = 346$), and subsequent loss of this ring generates the compound $m/z = 263$ [93]. Finally, in the fourth pathway, it is proposed that the intermediate with $m/z = 336$ could be generated by the attack of free radicals on C═C followed by the loss of CO. A compound with $m/z = 290$ could be formed through a decarboxylation process, where later an intramolecular nucleophilic substitution reaction takes place.

4. Conclusions

This work addressed the valorisation of sewage sludge by pyrolytic processes to produce iron and nickel carbonaceous catalysts that may be applied in the removal of emerging pollutants, such as the antibiotic ciprofloxacin. In this regard, the use of sewage sludge as a biomass precursor promoted the generation of functional groups, as evidenced by both the chemical composition and the FTIR spectra. All materials exhibited a combination of Type I-IV N_2 adsorption–desorption isotherms, showing H3-H4 Type hysteresis loops. The average pore width of the materials was found in the mesopore zone, although they also presented a high microporosity, except for the catalyst obtained with nickel chloride as activating agent. S_{BET} values of the synthesized catalysts ranged from 397 to 713 m^2/g.

The adsorption blanks showed adsorption capacity values in the range of 40.4–73.9 mg/g, with the Industrial-Ni catalyst exhibiting the lowest value. Nickel, as active phase, also showed significantly low catalytic activity compared to iron. Although the bimetallic catalyst Industrial-FeNi had a higher iron content than Industrial-Fe and therefore a higher catalytic activity, the measured metal leaching into the reaction medium was higher. Consequently, the use of iron chloride as activating agent was preferable.

The experiments performed, as well as the DFT calculations developed, show that the active atoms of the ciprofloxacin molecule with high Fukui index indicate C-F bond cleavage, ring hydroxylation, nucleophilic addition and aldehydic reaction under radical attack.

5. Data availability

Data will be made available on request.

CRediT authorship contribution statement

Pablo Gutiérrez-Sánchez: Conceptualization, Investigation, Formal analysis, Software, Methodology, Writing – original draft, Writing – review & editing. **Silvia Álvarez-Torrellas:** Writing – review & editing. **Marcos Larriba:** Writing – review & editing. **M. Victoria Gil:** Software, Writing – review & editing. **Juan M. Garrido-Zoido:** Software, Writing – review & editing. **Juan García:** Conceptualization, Funding acquisition, Project administration, Writing – review & editing.

Declaration of Competing Interest

The authors declare that they have no known competing financial interests or personal relationships that could have appeared to influence the work reported in this paper.

Data availability

Data will be made available on request.

Acknowledgments

This work has been supported by the Spanish MICINN through the project CATAD3.0 PID2020-116478RB-I00. In addition, the authors thank the financial support from the Comunidad de Madrid (Spain) through the Industrial PhD projects (IND2017/AMB-7720 and IND2019/AMB-17114), REMTAVARES Network (S2018/EMT-4341) and the European Social Fund. MVG also thanks Grant PID2021-125295OB-I00 funded by MCIN/AEI/ 10.13039/501100011033 and by "ERDF A way of making Europe" and the Junta de Extremadura and the European Regional Development Fund (ERDF/FEDER), through Grant No. GR21039. The authors are grateful for the Supercomputer facility LUSITANIA funded by CenitS and the Computaex Foundation.

Appendix A. Supplementary material

Supplementary data to this article can be found online at https://doi.org/10.1016/j.molliq.2023.121840.

References

[1] Y. Chen, J. Zhang, H. Xu, Exploration of the degradation mechanism of ciprofloxacin in water by nano zero-valent iron combined with activated carbon and nickel, J. Mol. Liq. 345 (2022), 118212, https://doi.org/10.1016/J.MOLLIQ.2021.118212.

[2] Y. Qin, K. Wang, Q. Xia, S. Yu, M. Zhang, Y. An, X. Zhao, Z. Zhou, Up-concentration of nitrogen from domestic wastewater: A sustainable strategy from removal to recovery, Chem. Eng. J. 451 (2023), 138789, https://doi.org/10.1016/J.CEJ.2022.138789.

[3] S.A. Afolalu, O.M. Ikumapayi, T.S. Ogedengbe, R.A. Kazeem, A.T. Ogundipe, Waste pollution, wastewater and effluent treatment methods - An overview, Mater. Today:. Proc. 62 (2022) 3282–3288, https://doi.org/10.1016/J.MATPR.2022.04.231.

[4] P. Gutiérrez-Sánchez, P. Navarro, S. Álvarez-Torrellas, J. García, M. Larriba, Extraction of neonicotinoid pesticides from aquatic environmental matrices with sustainable terpenoids and eutectic solvents, Sep. Purif. Technol. 302 (2022), 122148, https://doi.org/10.1016/J.SEPPUR.2022.122148.

[5] O.J. Ajala, J.O. Tijani, R.B. Salau, A.S. Abdulkareem, O.S. Aremu, A review of emerging micro-pollutants in hospital wastewater: Environmental fate and remediation options, Results Eng. 16 (2022), 100671, https://doi.org/10.1016/J.RINENG.2022.100671.

[6] J. Wilkinson, P.S. Hooda, J. Barker, S. Barton, J. Swinden, Occurrence, fate and transformation of emerging contaminants in water: An overarching review of the field, Environ. Pollut. 231 (2017) 954–970, https://doi.org/10.1016/J.ENVPOL.2017.08.032.

[7] A. Pal, K.Y.H. Gin, A.Y.C. Lin, M. Reinhard, Impacts of emerging organic contaminants on freshwater resources: Review of recent occurrences, sources, fate and effects, Sci. Total Environ. 408 (2010) 6062–6069, https://doi.org/10.1016/J.SCITOTENV.2010.09.026.

[8] K. Kümmerer, Antibiotics in the aquatic environment - A review - Part I, Chemosphere 75 (2009) 417–434, https://doi.org/10.1016/J.CHEMOSPHERE.2008.11.086.

[9] F.S. Souza, L.A. Féris, Consumption-based approach for pharmaceutical compounds in a large hospital, Doi.: 10.1080/09593330.2016.1255262. 38 (2016) 2217-2223. Doi: 10.1080/09593330.2016.1255262.

[10] M. Ibáñez, L. Bijlsma, E. Pitarch, F.J. López, F. Hernández, Occurrence of pharmaceutical metabolites and transformation products in the aquatic environment of the Mediterranean area, Trends Environ. Anal. Chem. 29 (2021) e00118.

[11] P. Sukul, M. Spiteller, Fluoroquinolone antibiotics in the environment, Rev. Environ. Contam. Toxicol. 191 (2007) 131–162, https://doi.org/10.1007/978-0-387-69163-3_5.

[12] M.S. Gaballah, J. Guo, H. Sun, D. Aboagye, M. Sobhi, A. Muhmood, R. Dong, A review targeting veterinary antibiotics removal from livestock manure management systems and future outlook, Bioresour. Technol. 333 (2021), 125069, https://doi.org/10.1016/J.BIORTECH.2021.125069.

[13] C.F. Nnadozie, S. Kumari, F. Bux, Status of pathogens, antibiotic resistance genes and antibiotic residues in wastewater treatment systems, Rev. Environ. Sci. Bio/Technol. 2017 16:3. 16 (2017) 491-515. Doi: 10.1007/S11157-017-9438-X.

[14] D. Cheng, H.H. Ngo, W. Guo, S.W. Chang, D.D. Nguyen, Y. Liu, Q. Wei, D. Wei, A critical review on antibiotics and hormones in swine wastewater: Water pollution problems and control approaches, J. Hazard. Mater. 387 (2020), 121682, https://doi.org/10.1016/J.JHAZMAT.2019.121682.

[15] L.J.M. Githinji, M.K. Musey, R.O. Ankumah, Evaluation of the fate of ciprofloxacin and amoxicillin in domestic wastewater, Water Air Soil Pollut. 219 (2011) 191–201, https://doi.org/10.1007/S11270-010-0697-1/FIGURES/10.

[16] S. Aleksić, A.Ž. Gotvajn, K. Premzl, M. Kolar, S.Š. Turk, Ozonation of amoxicillin and ciprofloxacin in model hospital wastewater to increase biotreatability, Antibiotics (Basel). 10 (2021), https://doi.org/10.3390/ANTIBIOTICS10111407.

[17] S. Álvarez-Torrellas, J.A. Peres, V. Gil-Álvarez, G. Ovejero, J. García, Effective adsorption of non-biodegradable pharmaceuticals from hospital wastewater with different carbon materials, Chem. Eng. J. 320 (2017) 319–329, https://doi.org/10.1016/j.cej.2017.03.077.

[18] Y. Segura, A. Cruz del Álamo, M. Munoz, S. Álvarez-Torrellas, J. García, J.A. Casas, Z.M. de Pedro, F. Martínez, A comparative study among catalytic wet air oxidation, Fenton, and Photo-Fenton technologies for the on-site treatment of hospital wastewater, J. Environ. Manage. 290 (2021), 112624, https://doi.org/10.1016/J.JENVMAN.2021.112624.

[19] G. di Giacomo, P. Romano, Evolution and prospects in managing sewage sludge resulting from municipal wastewater purification, Energies 2022, Vol. 15, Page 5633. 15 (2022) 5633. Doi: 10.3390/EN15155633.

[20] J.C. Jiménez, J.G. Rodríguez, B.H. Mendioroz, V. Ismael Águeda Maté, S. Álvarez-Torrellas, Revision of the Most Harmful Organic Compounds Present in Sewage and Sludge, in: The Handbook of Environmental Chemistry, Springer, 2022: pp. 1-20. Doi: 10.1007/698_2022_855.

[21] K. Shanmugam, V. Gadhamshetty, M. Tysklind, D. Bhattacharyya, V.K. K. Upadhyayula, A sustainable performance assessment framework for circular management of municipal wastewater treatment plants, J. Clean. Prod. 339 (2022), 130657, https://doi.org/10.1016/J.JCLEPRO.2022.130657.

[22] Z. He, X. Cheng, G.Z. Kyzas, J. Fu, Pharmaceuticals pollution of aquaculture and its management in China, J. Mol. Liq. 223 (2016) 781–789, https://doi.org/10.1016/J.MOLLIQ.2016.09.005.

[23] H. Zhang, F. Chen, J. Zhang, Y. Han, Supercritical water gasification of fuel gas production from waste lignin: The effect mechanism of different oxidized iron-based catalysts, Int. J. Hydrogen Energy 46 (2021) 30288–30299, https://doi.org/10.1016/J.IJHYDENE.2021.06.169.

[24] H. Zhang, F. Chen, J. Xu, J. Zhang, Y. Han, Chemical reactions of oily sludge catalyzed by iron oxide under supercritical water gasification condition, Front. Chem. Sci. Eng. 16 (2022) 886–896, https://doi.org/10.1007/S11705-021-2125-Z/METRICS.

[25] Z. Li, Y. Huang, Z. Zhu, H. Cheng, J. Zhao, M. Yu, W. Xu, Q. Yuan, T. He, S. Wang, Co-pyrolysis of sewage sludge with polyvinyl chloride (PVC)/CaO: Effects on heavy metals behavior and ecological risk, Fuel 333 (2023), 126281, https://doi.org/10.1016/J.FUEL.2022.126281.

[26] J. Racek, J. Sevcik, T. Chorazy, J. Kucerik, P. Hlavinek, Biochar - recovery material from pyrolysis of sewage sludge: A review, Waste Biomass Valoriz. 11 (2020) 3677–3709, https://doi.org/10.1007/S12649-019-00679-W/TABLES/16.

[27] I.B.S. Poblete, O. de Q.F. Araujo, J.L. de Medeiros, Sewage-water treatment and sewage-sludge management with power production as bioenergy with carbon capture system: A review, Processes 2022, Vol. 10, Page 788. 10 (2022) 788. Doi: 10.3390/PR10040788.

[28] X. Chen, S. Jeyaseelan, N. Graham, Physical and chemical properties study of the activated carbon made from sewage sludge, Waste Manag. 22 (2002) 755–760, https://doi.org/10.1016/S0956-053X(02)00057-0.

[29] E. Sanz-Santos, S. Álvarez-Torrellas, M. Larriba, J. García, Activated carbons derived from biomass for the removal by adsorption of several pesticides from water, Advanced Materials for Sustainable Environmental Remediation: Terrestrial and Aquatic Environments. (2022) 565-583. Doi: 10.1016/B978-0-323-90485-8.00020-5.

[30] E. Sanz-Santos, S. Álvarez-Torrellas, M. Larriba, D. Calleja-Cascajero, J. García, Enhanced removal of neonicotinoid pesticides present in the Decision 2018/840/EU by new sewage sludge-based carbon materials, J. Environ. Manage. 313 (2022), 115020.

[31] N. Graham, X.G. Chen, S. Jayaseelan, The potential application of activated carbon from sewage sludge to organic dyes removal, Water Sci. Technol. 43 (2001) 245–252, https://doi.org/10.2166/WST.2001.0096.

[32] Y. Huaccallo-Aguilar, S. Álvarez-Torrellas, M.v. Gil, M. Larriba, J. García, Insights of emerging contaminants removal in real water matrices by CWPO using a magnetic catalyst, J. Environ. Chem. Eng. 9 (2021), 106321, https://doi.org/10.1016/J.JECE.2021.106321.

[33] A. Pieczyńska, A.F. Borzyszkowska, A. Ofiarska, E.M. Siedlecka, Removal of cytostatic drugs by AOPs: A review of applied processes in the context of green, technology 47 (2017) 1282–1335, https://doi.org/10.1080/10643389.2017.1370990.

[34] N. Nasrollahi, V. Vatanpour, A. Khataee, Removal of antibiotics from wastewaters by membrane technology: Limitations, successes, and future improvements, Sci. Total Environ. 838 (2022), 156010, https://doi.org/10.1016/J.SCITOTENV.2022.156010.

[35] V. Homem, L. Santos, Degradation and removal methods of antibiotics from aqueous matrices - A review, J. Environ. Manage. 92 (2011) 2304–2347, https://doi.org/10.1016/J.JENVMAN.2011.05.023.

[36] G. Lofrano, R. Pedrazzani, G. Libralato, M. Carotenuto, Advanced oxidation processes for antibiotics removal: a review, Curr. Org. Chem. 21 (2017) 1054–1067.

[37] M. Verma, A.K. Haritash, Review of advanced oxidation processes (AOPs) for treatment of pharmaceutical wastewater, Adv. Environ. Res. 9 (2020) 1–17.

[38] R. Anjali, S. Shanthakumar, Insights on the current status of occurrence and removal of antibiotics in wastewater by advanced oxidation processes, J. Environ. Manage. 246 (2019) 51–62, https://doi.org/10.1016/J.JENVMAN.2019.05.090.

[39] M. Malakootian, M. Faraji, M. Malakootian, M. Nozari, M. Malakootian, Ciprofloxacin removal from aqueous media by adsorption process: A systematic review and meta-analysis, Desalin. Water Treat. 229 (2021) 252–282.

[40] C.E. Enyoh, Q. Wang, Adsorption of ciprofloxacin from aqueous solution by plastic-based adsorbents: a review, International Journal of Environmental Analytical Chemistry 1-21 (2022), https://doi.org/10.1080/03067319.2022.2106432.

[41] M. Malakootian, M. Yaseri, M. Faraji, Removal of antibiotics from aqueous solutions by nanoparticles: a systematic review and meta-analysis, Environ. Sci. Pollut. Res. 2019 26:9. 26 (2019) 8444-8458. Doi: 10.1007/S11356-019-04227-W.

[42] American Public Health Association, Standard methods for the examination of water and wastewater, 23rd ed., 2017.

[43] A.G. Gonçalves, J.J.M. Órfão, M.F.R. Pereira, Catalytic ozonation of sulphamethoxazole in the presence of carbon materials: Catalytic performance and reaction pathways, J. Hazard. Mater. 239–240 (2012) 167–174, https://doi.org/10.1016/j.jhazmat.2012.08.057.

[44] F.J. Beltrán, A. Aguinaco, J.F. García-Araya, A. Oropesa, Ozone and photocatalytic processes to remove the antibiotic sulfamethoxazole from water, Water Res. 42 (2008) 3799–3808, https://doi.org/10.1016/j.watres.2008.07.019.

[45] A.G. Trovó, R.F. Pupo Nogueira, A. Agüera, A.R. Fernandez-Alba, S. Malato, Degradation of the antibiotic amoxicillin by photo-Fenton process - Chemical and toxicological assessment, Water Res. 45 (2011) 1394–1402, https://doi.org/10.1016/j.watres.2010.10.029.

[46] A. Ledezma Estrada, Y.Y. Li, A. Wang, Biodegradability enhancement of wastewater containing cefalexin by means of the electro-Fenton oxidation process,

J. Hazard. Mater. 227-228 (2012) 41–48, https://doi.org/10.1016/j.jhazmat.2012.04.079.
[47] T.H. Kim, S.D. Kim, H.Y. Kim, S.J. Lim, M. Lee, S. Yu, Degradation and toxicity assessment of sulfamethoxazole and chlortetracycline using electron beam, ozone and UV, J. Hazard. Mater. 227–228 (2012) 237–242, https://doi.org/10.1016/j.jhazmat.2012.05.038.
[48] D. Rodríguez-Llorente, E. Hernández, P. Gutiérrez-Sánchez, P. Navarro, V. Ismael Águeda, S. Álvarez-Torrellas, J. García, M. Larriba, Extraction of pharmaceuticals from hospital wastewater with eutectic solvents and terpenoids: Computational, experimental, and simulation studies, Chem. Eng. J. 451 (2023), 138544, https://doi.org/10.1016/J.CEJ.2022.138544.
[49] P. Gutiérrez-Sánchez, D. Rodríguez-Llorente, P. Navarro, V.I. Águeda, S. Álvarez-Torrellas, J. García, M. Larriba, Extraction of antibiotics identified in the EU Watch List 2020 from hospital wastewater using hydrophobic eutectic solvents and terpenoids, Sep. Purif. Technol. 282 (2022), 120117, https://doi.org/10.1016/j.seppur.2021.120117.
[50] P. Gutiérrez-Sánchez, S. Álvarez-Torrellas, M. Larriba, M.V. Gil, J.M. Garrido-Zoido, J. García, Efficient removal of antibiotic ciprofloxacin by catalytic wet air oxidation using sewage sludge-based catalysts: Degradation mechanism by DFT studies, J. Environ. Chem. Eng. 11 (2023), 109344, https://doi.org/10.1016/J.JECE.2023.109344.
[51] F. Weinhold, C.R. Landis, Discovering chemistry with natural bond orbitals, Discovering Chem. with Nat. Bond Orbitals (2012), https://doi.org/10.1002/9781118229101.
[52] E.D. Glendening, A.E. Reed, J.E. Carpenter, F. Weinhold, NBO Version 3.1, TCI, University of Wisconsin. 65 (1998).
[53] A.V. Marenich, C.J. Cramer, D.G. Truhlar, Universal solvation model based on solute electron density and on a continuum model of the solvent defined by the bulk dielectric constant and atomic surface tensions, J. Phys. Chem. B. 113 (2009) 6378-6396. Doi: 10.1021/JP810292N/SUPPL_FILE/JP810292N_SI_003.PDF.
[54] R. Dennington, T. Keith, J. Millam, GaussView, Version 6, Semichem Inc., Shawnee Mission, KS. (2016).
[55] R.G. Parr, W. Yang, Density Functional Approach to the Frontier-Electron Theory of Chemical Reactivity, J. Am. Chem. Soc. 106 (1984) 4049–4050, https://doi.org/10.1021/JA00326A036/ASSET/JA00326A036.FP.PNG_V03.
[56] J. Jjagwe, P.W. Olupot, E. Menya, H.M. Kalibbala, Synthesis and application of granular activated carbon from biomass waste materials for water treatment: A review, J. Bioresour. Bioproducts 6 (2021) 292–322, https://doi.org/10.1016/J.JOBAB.2021.03.003.
[57] G. Gascó, C.G. Blanco, F. Guerrero, A.M.M. Lázaro, The influence of organic matter on sewage sludge pyrolysis, J. Anal. Appl. Pyrol. 74 (2005) 413–420, https://doi.org/10.1016/J.JAAP.2004.08.007.
[58] M.J. Martin, E. Serra, A. Ros, M.D. Balaguer, M. Rigola, Carbonaceous adsorbents from sewage sludge and their application in a combined activated sludge-powdered activated carbon (AS-PAC) treatment, Carbon N Y. 42 (2004) 1389–1394, https://doi.org/10.1016/J.CARBON.2004.01.011.
[59] K.H. Lin, N. Lai, J.Y. Zeng, H.L. Chiang, Residue characteristics of sludge from a chemical industrial plant by microwave heating pyrolysis, Environmental Science and Pollution, Research 25 (2018) 6487–6496, https://doi.org/10.1007/S11356-017-1003-1/TABLES/4.
[60] E. Sanz-Santos, S. Álvarez-Torrellas, L. Ceballos, M. Larriba, V.I. Águeda, J. García, Application of sludge-based activated carbons for the effective adsorption of neonicotinoid pesticides, Appl. Sci. 11 (2021) 3087.
[61] C. Huang, B.A. Mohamed, L.Y. Li, Comparative life-cycle assessment of pyrolysis processes for producing bio-oil, biochar, and activated carbon from sewage sludge, Resour. Conserv. Recycl. 181 (2022), 106273, https://doi.org/10.1016/J.RESCONREC.2022.106273.
[62] C. Nieto-Delgado, M. Terrones, J.R. Rangel-Mendez, Development of highly microporous activated carbon from the alcoholic beverage industry organic by-products, Biomass Bioenergy 35 (2011) 103–112, https://doi.org/10.1016/J.BIOMBIOE.2010.08.025.
[63] B. Janković, N. Manić, V. Dodevski, I. Radović, M. Pijović, Đ. Katnić, G. Tasić, Physico-chemical characterization of carbonized apricot kernel shell as precursor for activated carbon preparation in clean technology utilization, J. Clean. Prod. 236 (2019), 117614, https://doi.org/10.1016/J.JCLEPRO.2019.117614.
[64] Q. Yin, M. Liu, H. Ren, Biochar produced from the co-pyrolysis of sewage sludge and walnut shell for ammonium and phosphate adsorption from water, J. Environ. Manage. 249 (2019), 109410, https://doi.org/10.1016/J.JENVMAN.2019.109410.
[65] A. Gopinath, G. Divyapriya, V. Srivastava, A.R. Laiju P. v. Nidheesh, M.S. Kumar, Conversion of sewage sludge into biochar: A potential resource in water and wastewater treatment, Environ. Res. 194 (2021), 110656, https://doi.org/10.1016/J.ENVRES.2020.110656.
[66] S. Jerez, M. Ventura, R. Molina, M.I. Pariente, F. Martínez, J.A. Melero, Comprehensive characterization of an oily sludge from a petrol refinery: A step forward for its valorization within the circular economy strategy, J. Environ. Manage. 285 (2021), 112124, https://doi.org/10.1016/J.JENVMAN.2021.112124.
[67] R. Yin, W. Guo, H. Wang, J. Du, Q. Wu, J.S. Chang, N. Ren, Singlet oxygen-dominated peroxydisulfate activation by sludge-derived biochar for sulfamethoxazole degradation through a nonradical oxidation pathway: Performance and mechanism, Chem. Eng. J. 357 (2019) 589–599, https://doi.org/10.1016/J.CEJ.2018.09.184.
[68] M. Thommes, K. Kaneko, A. v Neimark, J.P. Olivier, F. Rodriguez-Reinoso, J. Rouquerol, K.S.W. Sing, Physisorption of gases, with special reference to the evaluation of surface area and pore size distribution (IUPAC Technical Report), Pure Appl. Chem. 87 (2015) 1051-1069.
[69] Q. Chen, H. Liu, J.H. Ko, H. Wu, Q. Xu, Structure characteristics of bio-char generated from co-pyrolysis of wooden waste and wet municipal sewage sludge, Fuel Process. Technol. 183 (2019) 48–54, https://doi.org/10.1016/J.FUPROC.2018.11.005.
[70] M. Kończak, P. Oleszczuk, K. Różyło, Application of different carrying gases and ratio between sewage sludge and willow for engineered (smart) biochar production, J. CO2 Util. 29 (2019) 20–28, https://doi.org/10.1016/J.JCOU.2018.10.019.
[71] T. Boualem, A. Debab, A. Martínez de Yuso, M.T. Izquierdo, Activated carbons obtained from sewage sludge by chemical activation: Gas-phase environmental applications, J. Environ. Manage. 140 (2014) 145–151, https://doi.org/10.1016/J.JENVMAN.2014.03.016.
[72] C. Schlumberger, M. Thommes, Characterization of hierarchically ordered porous materials by physisorption and mercury porosimetry—A tutorial review, Adv. Mater. Interfaces 8 (2021) 2002181.
[73] P. Maziarka, C. Wurzer, P.J. Arauzo, A. Dieguez-Alonso, O. Mašek, F. Ronsse, Do you BET on routine? The reliability of N2 physisorption for the quantitative assessment of biochar's surface area, Chem. Eng. J. 418 (2021), 129234, https://doi.org/10.1016/J.CEJ.2021.129234.
[74] J. Rouquerol, P. Llewellyn, F. Rouquerol, Is the bet equation applicable to microporous adsorbents? Stud. Surf. Sci. Catal. 160 (2007) 49–56, https://doi.org/10.1016/S0167-2991(07)80008-5.
[75] J. Alvarez, G. Lopez, M. Amutio, J. Bilbao, M. Olazar, Preparation of adsorbents from sewage sludge pyrolytic char by carbon dioxide activation, Process Saf. Environ. Prot. 103 (2016) 76–86.
[76] H. Saygılı, F. Güzel, Y. Önal, Conversion of grape industrial processing waste to activated carbon sorbent and its performance in cationic and anionic dyes adsorption, J. Clean. Prod. 93 (2015) 84–93, https://doi.org/10.1016/j.jclepro.2015.01.009.
[77] A. Kumar, P. Kumar, C. Joshi, M. Manchanda, R. Boukherroub, S.L. Jain, Nickel Decorated on Phosphorous-Doped Carbon Nitride as an Efficient Photocatalyst for Reduction of Nitrobenzenes, Nanomaterials 2016, Vol. 6, Page 59. 6 (2016) 59. Doi: 10.3390/NANO6040059.
[78] A.F.M. Streit, L.N. Côrtes, S.P. Druzian, M. Godinho, G.C. Collazzo, D. Perondi, G. L. Dotto, Development of high quality activated carbon from biological sludge and its application for dyes removal from aqueous solutions, Sci. Total Environ. 660 (2019) 277–287, https://doi.org/10.1016/J.SCITOTENV.2019.01.027.
[79] L. Li, J. Ai, W. Zhang, S. Peng, T. Dong, Y. Deng, Y. Cui, D. Wang, Relationship between the physicochemical properties of sludge-based carbons and the adsorption capacity of dissolved organic matter in advanced wastewater treatment: Effects of chemical conditioning, Chemosphere 243 (2020), 125333, https://doi.org/10.1016/J.CHEMOSPHERE.2019.125333.
[80] Q.H. Lin, H. Cheng, G.Y. Chen, Preparation and characterization of carbonaceous adsorbents from sewage sludge using a pilot-scale microwave heating equipment, J. Anal. Appl. Pyrol. 93 (2012) 113–119, https://doi.org/10.1016/J.JAAP.2011.10.006.
[81] R. Ali, Z. Aslam, R.A. Shawabkeh, A. Asghar, I.A. Hussein Bet, FTIR, and RAMAN characterizations of activated carbon from waste oil fly ash, Turk. J. Chem. 44 (2020) 279–295, https://doi.org/10.3906/kim-1909-20.
[82] L. Liu, Y. Lin, Y. Liu, H. Zhu, Q. He, Removal of methylene blue from aqueous solutions by sewage sludge based granular activated carbon: Adsorption equilibrium, kinetics, and thermodynamics, J. Chem. Eng. Data 58 (2013) 2248–2253, https://doi.org/10.1021/JE4003543/ASSET/IMAGES/LARGE/JE-2013-003543_0006.JPEG.
[83] K. Fang, J. Chen, X. Zhou, C. Mei, Q. Tian, J. Xu, C.P. Wong, Decorating biomass-derived porous carbon with Fe2O3 ultrathin film for high-performance supercapacitors, Electrochim. Acta 261 (2018) 198–205, https://doi.org/10.1016/J.ELECTACTA.2017.12.140.
[84] R. Fernández, J. Estelle, Y. Cesteros, P. Salagre, F. Medina, J.E. Sueiras, J.L. Garcia Fierro, Structural characterization of NiO doped with several caesium loadings, J. Mol. Catal. A Chem. 119 (1997) 77–85, https://doi.org/10.1016/S1381-1169(96)00471-2.
[85] W.K. Wakejo, B.T. Meshasha, J.W. Kang, Y. Chebude, Enhanced ciprofloxacin removal from aqueous solution using a chemically modified biochar derived from bamboo sawdust: Adsorption process optimization with response surface methodology, Adsorpt. Sci. Technol. 2022 (2022), https://doi.org/10.1155/2022/2699530.
[86] Y. Fu, Z. Yang, Y. Xia, Y. Xing, X. Gui, Adsorption of ciprofloxacin pollutants in aqueous solution using modified waste grapefruit peel, Doi: 10.1080/15567036.2019.1624877. 43 (2019) 225-234. Doi: 10.1080/15567036.2019.1624877.
[87] Q.T. Tran, T.H. Do, X.L. Ha, H.P. Nguyen, A.T. Nguyen, T.C.Q. Ngo, H.D. Chau, Study of the ciprofloxacin adsorption of activated carbon prepared from mangosteen peel, Appl. Sci. 2022, Vol. 12, Page 8770. 12 (2022) 8770. Doi: 10.3390/APP12178770.
[88] M. N, A. Renita A, S. Kumar P, S. Abraham L, Adsorption of ciprofloxacin from aqueous solution using surface improved tamarind shell as an economical and effective adsorbent, Doi: 10.1080/15226514.2021.1932730. 24 (2021) 224-234. Doi: 10.1080/15226514.2021.1932730.
[89] M. Munoz, P. Domínguez, Z.M. de Pedro, J.A. Casas, J.J. Rodriguez, Naturally-occurring iron minerals as inexpensive catalysts for CWPO, Appl Catal B 203 (2017) 166–173, https://doi.org/10.1016/J.APCATB.2016.10.015.
[90] R.S. Ribeiro, A.M.T. Silva, J.L. Figueiredo, J.L. Faria, H.T. Gomes, Catalytic wet peroxide oxidation: a route towards the application of hybrid magnetic carbon

nanocomposites for the degradation of organic pollutants. A review, Appl Catal B. 187 (2016) 428–460, https://doi.org/10.1016/J.APCATB.2016.01.033.
[91] E. Serra-Pérez, C. Ferronato, A. Giroir-Fendler, S. Alvarez-Torrellas, G. Ovejero, J. García, Highly efficient Ru supported on carbon nanosphere nanoparticles for ciprofloxacin removal: Effects of operating parameters, degradation pathways, and kinetic study, Ind. Eng. Chem. Res. 59 (2020) 15515–15530.
[92] Z. Fang, Z. Zhou, G. Xue, Y. Yu, Q. Wang, B. Cheng, Y. Ge, Y. Qian, Application of sludge biochar combined with peroxydisulfate to degrade fluoroquinolones: Efficiency, mechanisms and implication for ISCO, J. Hazard. Mater. 426 (2022), 128081, https://doi.org/10.1016/J.JHAZMAT.2021.128081.
[93] Y. Zhao, H. Wang, J. Ji, X. Li, X. Yuan, L. Jiang, J. Yang, Y. Shao, X. Guan, Degradation of ciprofloxacin by peroxymonosulfate activation using catalyst derived from spent lithium-ion batteries, J. Clean. Prod. 362 (2022), 132442, https://doi.org/10.1016/J.JCLEPRO.2022.132442.

Supplementary Material

for

Influence of transition metal-based activating agent on the properties and catalytic activity of sewage sludge-derived catalysts. Insights on mechanism, DFT calculation and degradation pathways.

Pablo Gutiérrez-Sánchez[1*], Silvia Álvarez-Torrellas[1], Marcos Larriba[1], M. Victoria Gil[2], Juan M. Garrido-Zoido[2], Juan García[1*]

[1]Catalysis and Separation Processes Group, Chemical Engineering and Materials Department, Faculty of Chemistry, Complutense University, Avda. Complutense s/n, 28040, Madrid, Spain.
[2]Departamento de Química Orgánica e Inorgánica, Facultad de Ciencias and IACYS Unidad de Química Verde y Desarrollo Sostenible, Universidad de Extremadura, E-06006 Badajoz, Spain.

Corresponding author
E-mail address: pgutie03@ucm.es; jgarciar@ucm.es; +34 91394.5207

Tables: 23

Figures: 6

Table S1. Retention Time, Relative Intensity at 4.5 kV Interface Voltage, Mass Spectra, Molecular Formula, Name and Proposed Structure of CPF Products in Degradation Pathway (T1), Homo and Lumo Energies, Optimised structure. Urban-Fe Catalyst.

Compound	t_R (min)	$[M+H]^+$ (m/z)	Molecular Formula	Name	Structure	E_{HOMO} (eV)	E_{LUMO} (eV)	Optimization
1	1.4	336	$C_{16}H_{18}FN_3O_4$	2-[2-(N-cyclopropylformamido)-5-fluoro-4-(piperazin-1-yl)phenyl]-2-oxoacetic acid	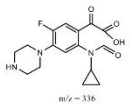	-7,44232	-1,75078	
2		362	$C_{17}H_{16}FN_3O_5$	1-cyclopropyl-6-fluoro-7-(2-hydroxy-3-oxopiperazin-1-yl)-4-oxo-1,4-dihydroquinoline-3-carboxylic acid	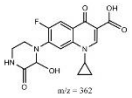	-7,88858	-1,10505	
3		362	$C_{17}H_{16}FN_3O_5$	1-cyclopropyl-6-fluoro-7-[N-(2-formamidoethyl)formamido]-4-oxo-1,4-dihydroquinoline-3-carboxylic acid	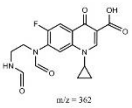	-7,97321	-1,28030	
4 (T2-1, T3-4, T4-4)		364	$C_{17}H_{18}FN_3O_5$	7-[(2-aminoethyl)(1-hydroxy-2-oxoethyl)amino]-1-cyclopropyl-6-fluoro-4-oxo-1,4-dihydroquinoline-3-carboxylic acid	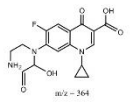	-7,56640	-1,02016	
5 (T2-2, T3-6)	6.6	330	$C_{17}H_{19}N_3O_4$	1-cyclopropyl-6-hydroxy-4-oxo-7-(piperazin-1-yl)-1,4-dihydroquinoline-3-carboxylic acid	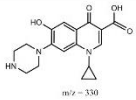	-7,46109	-0,97145	
6 (T3-7)	7.3	290	$C_{15}H_{16}FN_3O_2$	1-cyclopropyl-5-fluoro-6-(piperazin-1-yl)indoline-2,3-dione	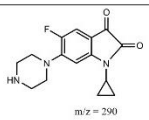	-7,30490	-1,95323	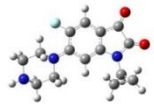
7 (T2-3, T3-8)	8.0	306	$C_{15}H_{16}FN_3O_3$	7-[(2-aminoethyl)amino]-1-cyclopropyl-6-fluoro-4-oxo-1,4-dihydroquinoline-3-carboxylic acid	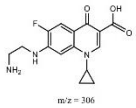	-7,28885	-0,89526	
8	8.3	346	$C_{17}H_{19}N_3O_5$	1-cyclopropyl-2,6-dihydroxy-4-oxo-7-(piperazin-1-yl)-1,4-dihydroquinoline-3-carboxylic acid	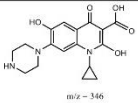	-7,38735	-0,91675	
Ciprofloxacin	8.9	332	$C_{17}H_{18}FN_3O_3$	ciprofloxacin	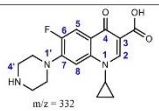	-7,21619	-0,98070	
9	9.7	346	$C_{17}H_{16}FN_3O_4$	1-cyclopropyl-6-fluoro-4-oxo-7-(3-oxopiperazin-1-yl)-1,4-dihydroquinoline-3-carboxylic acid	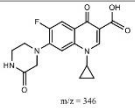	-7,33102	-0,96192	
10	9.9	261	$C_{13}H_{12}N_2O_4$	7-amino-1-cyclopropyl-6-hydroxy-4-oxo-1,4-dihydroquinoline-3-carboxylic acid	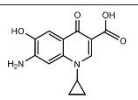	-7,28068	-0,83267	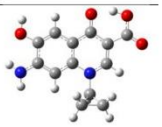
11 (T2-4)	10.5	263	$C_{13}H_{11}FN_2O_3$	7-amino-1-cyclopropyl-6-fluoro-4-oxo-1,4-dihydroquinoline-3-carboxylic acid	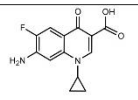	-7,55633	-0,93662	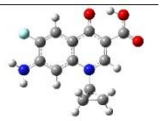

Table S2. Retention Time, Relative Intensity at 4.5 kV Interface Voltage, Mass Spectra, Molecular Formula, Name and Proposed Structure of CPF Products in Degradation Pathway (T2), Homo and Lumo Energies, Optimised structure. Industrial-Fe Catalyst.

Compound	t_R (min)	$[M+H]^+$ (m/z)	Molecular Formula	Name	Structure	E_{HOMO} (eV)	E_{LUMO} (eV)	Optimization
1	1.4	364	$C_{17}H_{18}FN_3O_5$	7-[(2-aminoethyl)(1-hydroxy-2-oxoethyl)amino]-1-cyclopropyl-6-fluoro-4-oxo-1,4-dihydroquinoline-3-carboxylic acid	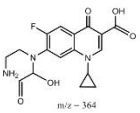	-7,56640	1,02016	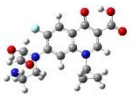
2	6.7	330	$C_{17}H_{19}N_3O_4$	1-cyclopropyl-6-hydroxy-4-oxo-7-(piperazin-1-yl)-1,4-dihydroquinoline-3-carboxylic acid	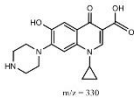	-7,46109	0,97145	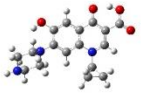
3	8.0	306	$C_{15}H_{16}FN_3O_3$	7-[(2-aminoethyl)amino]-1-cyclopropyl-6-fluoro-4-oxo-1,4-dihydroquinoline-3-carboxylic acid	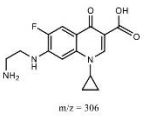	-7,28885	0,89526	
Ciprofloxacin	8.9	332	$C_{17}H_{18}FN_3O_3$	Ciprofloxacin	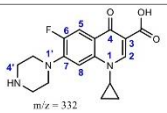	-7,21619	0,98070	
4	10.5	263	$C_{13}H_{11}FN_2O_3$	7-amino-1-cyclopropyl-6-fluoro-4-oxo-1,4-dihydroquinoline-3-carboxylic acid	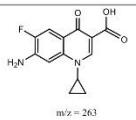	-7,55633	0,93662	

Table S3. Retention Time, Relative Intensity at 4.5 kV Interface Voltage, Mass Spectra, Molecular Formula, Name and Proposed Structure of CPF Products in Degradation Pathway (T3), Homo and Lumo Energies, Optimised structure. Industrial-Ni Catalyst.

Compound	t_R (min)	$[M+H]^+$ (m/z)	Molecular Formula	Name	Structure	E_{HOMO} (eV)	E_{LUMO} (eV)	Optimization
2 (T4-2)	0.9	334	$C_{16}H_{16}FN_3O_4$	1-cyclopropyl-6-fluoro-7-[(2-formamidoethyl)amino]-4-oxo-1,4-dihydroquinoline-3-carboxylic acid	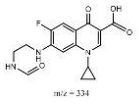	-7,26327	-0,85389	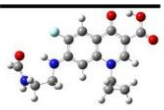
3 (T4-3)		310	$C_{14}H_{16}FN_3O_4$	2-{4-[(2-aminoethyl)amino]-2-(N-cyclopropylformamido)-5-fluorophenyl}-2-oxoacetic acid	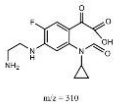	-7,23687	-1,66452	
4 (T4-4, T2-1, T1-4)	1.4	364	$C_{17}H_{18}FN_3O_5$	7-[(2-aminoethyl)(1-hydroxy-2-oxoethyl)amino]-1-cyclopropyl-6-fluoro-4-oxo-1,4-dihydroquinoline-3-carboxylic acid	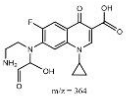	-7,56640	-1,02016	

Table S3. Retention Time, Relative Intensity at 4.5 kV Interface Voltage, Mass Spectra, Molecular Formula, Name and Proposed Structure of CPF Products in Degradation Pathway (T3), Homo and Lumo Energies, Optimised structure. Industrial-Ni Catalyst.

5	1.5	308	$C_{14}H_{17}N_3O_5$	2-{4-[(2-aminoethyl)amino]-2-(N-cyclopropylformamido)-5-hydroxyphenyl}-2-oxoacetic acid	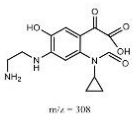	-7,01592	-1,24002	
6 (T2-2, T1-5)	6.7	330	$C_{17}H_{19}N_3O_4$	1-cyclopropyl-6-hydroxy-4-oxo-7-(piperazin-1-yl)-1,4-dihydroquinoline-3-carboxylic acid	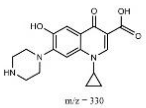	-7,46109	-0,97145	
7 (T1-6)	7.3	290	$C_{15}H_{16}FN_3O_2$	1-cyclopropyl-5-fluoro-6-(piperazin-1-yl)indoline-2,3-dione	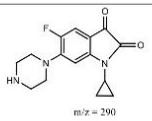	-7,30490	-1,95323	
8 (T2-3, T1-7)	7.9	306	$C_{15}H_{16}FN_3O_3$	7-[(2-aminoethyl)amino]-1-cyclopropyl-6-fluoro-4-oxo-1,4-dihydroquinoline-3-carboxylic acid	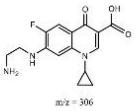	-7,28885	-0,89526	
Ciprofloxacin	8.7	332	$C_{17}H_{18}FN_3O_3$	Ciprofloxacin	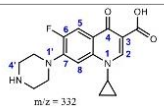	-7,21619	-0,98070	
9	10.4	334	$C_{16}H_{16}FN_3O_4$	7-[N-(2-aminoethyl)formamido]-1-cyclopropyl-6-fluoro-4-oxo-1,4-dihydroquinoline-3-carboxylic acid	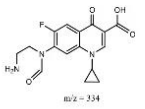	-7,98301	-1,29118	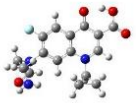
10	10.5	291	$C_{14}H_{11}FN_2O_4$	1-cyclopropyl-6-fluoro-7-formamido-4-oxo-1,4-dihydroquinoline-3-carboxylic acid	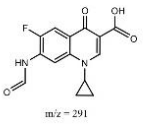	-7,95226	-1,23757	
11 (T2-4 y T1-11)	10.5	263	$C_{13}H_{11}FN_2O_3$	7-amino-1-cyclopropyl-6-fluoro-4-oxo-1,4-dihydroquinoline-3-carboxylic acid	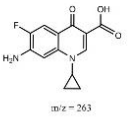	-7,55633	-0,93662	
12	10.7	360	$C_{17}H_{14}FN_3O_5$	1-cyclopropyl-7-(2,5-dioxopiperazin-1-yl)-6-fluoro-4-oxo-1,4-dihydroquinoline-3-carboxylic acid	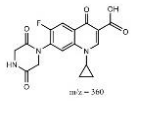	-7,96940	-1,29907	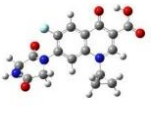

Table S4. Retention Time, Relative Intensity at 4.5 kV Interface Voltage, Mass Spectra, Molecular Formula, Name and Proposed Structure of CPF Products in Degradation Pathway (T4), Homo and Lumo Energies, Optimised structure. Industrial-FeNi Catalyst.

Compound	t_R (min)	$[M+H]^+$ (m/z)	Molecular Formula	Name	Structure	E_{HOMO} (eV)	E_{LUMO} (eV)	Optimization
2	0.9	334	$C_{16}H_{16}FN_3O_4$	1-cyclopropyl-6-fluoro-7-[(2-formamidoethyl)amino]-4-oxo-1,4-dihydroquinoline-3-carboxylic acid	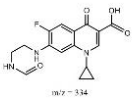	-7,26327	0,85389	
3		310	$C_{14}H_{16}FN_3O_4$	2-{4-[(2-aminoethyl)amino]-2-(N-cyclopropylformamido)-5-fluorophenyl}-2-oxoacetic acid	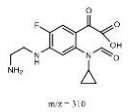	-7,23687	1,66452	
4	1.3	364	$C_{17}H_{18}FN_3O_5$	7-[(2-aminoethyl)(1-hydroxy-2-oxoethyl)amino]-1-cyclopropyl-6-fluoro-4-oxo-1,4-dihydroquinoline-3-carboxylic acid	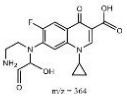	-7,56640	1,02016	

Table S5. Energetic data of organic compounds involved in the reactions.

Compound	Electronic energy (kcal/mol)	Free energy (kcal/mol)	Entropy (cal/(mol·K))	Enthalpy (kcal/mol)	E_{HOMO} (eV)	E_{LUMO} (eV)
Ciprofloxacin	-720626,1580	-720458,3633	168,549	-720388,7273	-7,21619	-0,98070
MZ-261	-572933,3070	-572823,3736	144,238	-572763,7822	-7,28068	-0,83267
MZ-263	-587998,3775	-587896,0157	142,956	-587836,9532	-7,55633	-0,93662
MZ-290	-624815,3143	-624669,9436	155,211	-624605,8184	-7,30490	-1,95323
MZ-291	-659117,5457	-659010,9940	153,614	-658947,5283	-7,95226	-1,23757
MZ-306	-672060,7186	-671916,6587	167,219	-671847,5724	-7,28885	-0,89526
MZ-308	-680265,8094	-680120,6671	182,498	-680045,2680	-7,01592	-1,24002
MZ-310	-695331,8425	-695193,4917	179,015	-695119,5315	-7,23687	-1,66452
MZ-330	-705561,2815	-705385,9904	169,911	-705315,7916	-7,46109	-0,97145
MZ-334A	-743189,7223	-743042,8701	179,860	-742968,5610	-7,26327	-0,85389
MZ-334B	-743178,6913	-743030,1209	176,186	-742957,3298	-7,98301	-1,29118
MZ-336	-743898,6029	-743736,2091	179,840	-743661,9082	-7,44232	-1,75078
MZ-346A	-752778,2388	-752601,0477	173,136	-752529,5166	-7,38735	-0,91675
MZ-346B	-767095,0557	-766941,6340	175,516	-766869,1196	-7,33102	-0,96192
MZ-360	-813559,8444	-813420,1463	180,819	-813345,4407	-7,96940	-1,29907
MZ-362A	-814305,3771	-814149,9361	181,615	-814074,9017	-7,88858	-1,10505
MZ-362B	-814307,5439	-814155,4293	187,446	-814077,9859	-7,97321	-1,28030
MZ-364	-815035,2077	-814868,3893	187,753	-814790,8185	-7,56640	-1,02016

Table S6. Cartesian coordinates for optimized structure of ciprofloxacin.

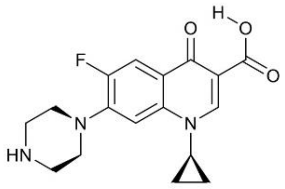

ATOM TYPE	x	y	z
C	1.16925600	-2.03831100	-0.26296700
C	1.75749000	-0.76374200	-0.47890100
C	0.87998700	0.31577300	-0.51864800
C	-0.49212900	0.15086700	-0.31653400
C	-1.03204200	-1.12043400	-0.07685900
C	-0.16029100	-2.22005900	-0.06067400
N	-1.34375100	1.25777000	-0.33905500
C	-2.65729100	1.09457900	-0.18713000
C	-3.25161800	-0.12269300	0.03177100
C	-2.45308500	-1.30839200	0.11247600
F	1.95403100	-3.12726200	-0.33012100
C	-0.79725400	2.58229400	-0.57850700
C	0.03892900	3.21753500	0.48298700
C	-1.33521100	3.74142800	0.18790700
O	-2.95126500	-2.44343900	0.32749200
C	-4.71699500	-0.17185700	0.19026300
O	-5.22297900	-1.37802100	0.41269800
O	-5.43846600	0.80595300	0.12587300
N	3.11448300	-0.65341600	-0.72171600
C	4.04515700	-1.28070100	0.23641900
C	4.32906400	-0.34967600	1.40247400
N	4.90591400	0.90404800	0.91601500
C	3.95024300	1.56535400	0.02455700
C	3.64441200	0.64523800	-1.14729400
H	1.26456800	1.30477900	-0.69267400
H	-0.54831100	-3.21933300	0.07844000
H	-3.25844300	1.99067100	-0.24377100
H	-0.50883200	2.73477400	-1.60879300
H	0.90045200	3.78059200	0.15683600
H	0.16300100	2.66027500	1.40063000
H	-2.10061500	3.54878400	0.92511900
H	-1.43473600	4.67144200	-0.34983500
H	-4.45300900	-2.03276400	0.42691900
H	3.64037700	-2.21481200	0.60500500
H	4.97108600	-1.49576300	-0.29842100
H	3.39091100	-0.17993800	1.94947200
H	5.03065200	-0.83263600	2.08067700
H	5.07192900	1.50957800	1.71114500
H	4.38359600	2.48992900	-0.35314200
H	3.02215000	1.81907400	0.55234400
H	4.57353300	0.44161100	-1.68183000
H	2.95883800	1.11110400	-1.85028500

Table S7. Cartesian coordinates for optimized structure of MZ-261.

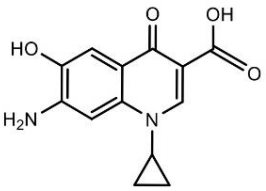

ATOM TYPE	x	y	z
C	-3.44391500	-0.85362000	-0.06290700
C	-2.01958200	-0.47336300	-0.07707500
C	-1.69615700	0.85228000	-0.22488700
N	-0.44367200	1.30359300	-0.24163000
C	-0.18186500	2.72115300	-0.41626600
C	0.35656300	3.49965900	0.73775000
C	-1.05400200	3.71276900	0.27319000
C	0.62796100	0.41314800	-0.14468900
C	0.36813500	-0.95776900	0.01625800
C	1.45472000	-1.84681300	0.11512500
C	2.73841200	-1.39177000	0.05277600
O	3.83940000	-2.19259200	0.14096700
C	3.00592000	-0.00690400	-0.12051100
N	4.30294600	0.41624900	-0.13926300
C	1.94285700	0.87581000	-0.21901000
C	-0.98549600	-1.45409100	0.06522500
O	-1.24339900	-2.68048700	0.21662900
O	-4.35981100	-0.06048900	-0.18622200
O	-3.68237600	-2.14850500	0.09794400
H	-2.47183100	1.59567600	-0.33627400
H	0.18795300	2.95876200	-1.40356500
H	0.48876400	2.96163600	1.66544700
H	1.10272400	4.24851400	0.51978500
H	-1.84075000	3.33658100	0.91025800
H	-1.29306500	4.61059500	-0.27532200
H	1.26479900	-2.90490300	0.23882100
H	3.57332900	-3.11435200	0.24556300
H	5.00994800	-0.27127700	-0.34677700
H	4.47835100	1.34192500	-0.49781800
H	2.15704900	1.92457700	-0.35674800
H	-2.78401300	-2.61298300	0.17845000

Table S8. Cartesian coordinates for optimized structure of MZ-263.

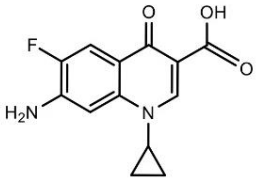

ATOM TYPE	x	y	z
C	2.70226700	-1.41067100	0.05050300
C	3.01535100	-0.04551300	-0.12659700
C	1.95833900	0.84982200	-0.21872000
C	0.64048300	0.39816700	-0.14474500
C	0.35810900	-0.96994700	0.01865800
C	1.43062900	-1.87306200	0.12130500
N	-0.42092100	1.30052400	-0.24036200
C	-1.67948600	0.86245000	-0.22341400
C	-2.02279300	-0.45694500	-0.07526700
C	-1.00232100	-1.45221900	0.06895700
F	3.74046000	-2.26015700	0.14405200
C	-0.14487600	2.71523500	-0.41861500
C	-1.00494100	3.71666400	0.27197000
C	0.40483000	3.49080700	0.73222400
O	-1.27192100	-2.67274500	0.22084000
C	-3.45323300	-0.81561400	-0.06232400
O	-3.71257800	-2.10680800	0.09832500
O	-4.35590000	-0.00866300	-0.18662800
N	4.31523100	0.33812100	-0.24624000
H	2.18237600	1.89674200	-0.35331800
H	1.24267500	-2.92926700	0.25236200
H	-2.44549000	1.61586000	-0.33547700
H	0.22378000	2.94694300	-1.40774700
H	-1.23778600	4.61543200	-0.27765500
H	-1.79268300	3.34931200	0.91299500
H	0.53463000	2.95366900	1.66075000
H	1.15759500	4.23161400	0.50971300
H	-2.82660200	-2.58706300	0.17996700
H	4.51894500	1.32012900	-0.14381700
H	5.02728900	-0.29180100	0.08805700

Table S9. Cartesian coordinates for optimized structure of MZ-290.

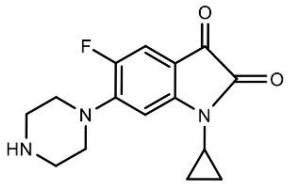

ATOM TYPE	x	y	z
N	2.46331500	0.65793300	0.20877100
C	2.52671600	2.08226100	0.34786100
C	1.91661900	2.91992100	-0.73341800
C	3.40512300	2.84055000	-0.59461000
C	1.26367200	-0.08849000	0.15607400
C	1.52790700	-1.45407500	0.02889600
C	0.47712200	-2.36310100	-0.03485400
C	-0.79655800	-1.86947000	0.02050500
F	-1.81477900	-2.75073500	0.04328200
C	-1.09749800	-0.49045000	0.12977100
N	-2.41019300	-0.06905000	0.20378600
C	-2.64075100	1.33304500	0.55661300
C	-4.10052500	1.55453900	0.89678500
N	-4.94682000	1.18095000	-0.23399000
C	-4.75168700	-0.23776700	-0.52471700
C	-3.30623300	-0.49394900	-0.88962000
C	-0.01612400	0.40933600	0.21315000
C	2.96207300	-1.61944200	0.02461700
O	3.66851900	-2.59645300	-0.06138900
C	3.53335500	-0.17892600	0.17309300
O	4.70830500	0.10234200	0.24949600
H	2.44568000	2.43490200	1.36669500
H	1.41192100	3.82262300	-0.42518500
H	1.46659000	2.39139800	-1.56130700
H	3.94201700	2.26401500	-1.33278300
H	3.93408700	3.68960700	-0.19033100
H	0.64422300	-3.43003900	-0.09600200
H	-2.03375800	1.58389300	1.42405500
H	-2.35048300	1.99011300	-0.27270500
H	-4.34402900	0.97266200	1.79476900
H	-4.24636700	2.60763600	1.12909800
H	-5.91478800	1.32648500	0.02746400
H	-5.37947000	-0.52746600	-1.36525200
H	-5.01766600	-0.86938700	0.33244700
H	-3.04960300	0.07671500	-1.79007000
H	-3.16442100	-1.54639200	-1.10293700
H	-0.18889400	1.47001500	0.29679600

Table S10. Cartesian coordinates for optimized structure of MZ-291.

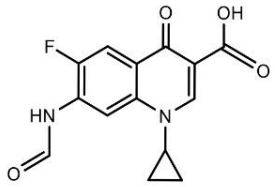

ATOM TYPE	x	y	z
C	-4.01444200	-0.20537200	-0.08771500
C	-2.53964000	-0.14806300	-0.08427000
C	-1.93386600	1.07642500	-0.22028300
N	-0.61395000	1.25113400	-0.22304500
C	-0.05401400	2.58217000	-0.38801900
C	0.64640900	3.21384800	0.76901400
C	-0.68843300	3.72956800	0.31901300
C	0.23793800	0.15118800	-0.12117900
C	-0.30916500	-1.13009300	0.02439100
C	0.55244100	-2.23187800	0.12640500
C	1.89359200	-2.02997000	0.08069600
F	2.73636100	-3.06906000	0.17535600
C	2.46607800	-0.75257200	-0.06945700
N	3.85495600	-0.68671100	-0.10582300
C	1.62501600	0.33705300	-0.17558100
C	-1.74818300	-1.33052600	0.05739200
O	-2.25041300	-2.47174200	0.19396200
O	-4.72766000	0.77167200	-0.21159200
O	-4.53747300	-1.41630800	0.05564800
C	4.64018900	0.42050700	-0.13994500
O	4.24288900	1.57033700	-0.15553900
H	-2.53190000	1.96912600	-0.33277900
H	0.35026500	2.74408600	-1.37698000
H	0.66607400	2.64897600	1.69001100
H	1.53591600	3.78503200	0.55013000
H	-0.73277000	4.66300700	-0.22013200
H	-1.53373700	3.52367000	0.95889200
H	0.15447300	-3.23016700	0.23876200
H	4.34853200	-1.56904000	-0.07107000
H	2.04040100	1.31831500	-0.30522200
H	-3.77804600	-2.07171000	0.13956300
H	5.70422300	0.16390400	-0.14991900

Table S11. Cartesian coordinates for optimized structure of MZ-306.

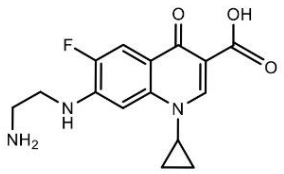

ATOM TYPE	x	y	z
C	1.49934500	-2.10716800	-0.20355500
C	2.10192100	-0.85685200	-0.48903100
C	1.26489800	0.25234700	-0.54897900
C	-0.10767900	0.11636700	-0.33330900
C	-0.67740900	-1.14074700	-0.06936700
C	0.17044000	-2.26327500	-0.00521100
N	-0.93722800	1.23867300	-0.37818900
C	-2.25493600	1.10773600	-0.22422000
C	-2.87377600	-0.09090400	0.02045900
C	-2.09839700	-1.29167800	0.12412700
F	2.32401700	-3.16816400	-0.14225300
C	-0.36060300	2.54560000	-0.64028500
C	-0.87338700	3.73134000	0.10219900
C	0.48621000	3.17902800	0.41350700
O	-2.62547300	-2.41125200	0.36256300
C	-4.33948200	-0.10743400	0.18109900
O	-4.86860400	-1.29870100	0.42690600
O	-5.04142700	0.88360200	0.09886100
N	3.43810000	-0.80926200	-0.72665700
H	1.68458600	1.22024900	-0.76398600
H	-0.23781800	-3.24267900	0.20057700
H	-2.83570000	2.01560800	-0.30146400
H	-0.06395700	2.67252500	-1.67174300
H	-0.94747800	4.65344600	-0.45301200
H	-1.64671500	3.57117500	0.83887400
H	0.59131200	2.63518900	1.34149200
H	1.36334900	3.71460800	0.08270200
H	-4.10856600	-1.96782400	0.45308200
H	3.95826700	-1.62894600	-0.45164500
C	4.18115900	0.44164000	-0.75006500
C	4.27494500	1.12620000	0.61010300
H	3.72979300	1.11522600	-1.47965100
H	5.18339200	0.20615600	-1.10512000
H	4.82636500	2.05654100	0.47635200
H	3.27853800	1.39602300	0.96097100
N	4.92665300	0.33262300	1.64904700
H	4.39897900	-0.52215700	1.79415900
H	5.84136100	0.04169900	1.31781700

Table S12. Cartesian coordinates for optimized structure of MZ-308.

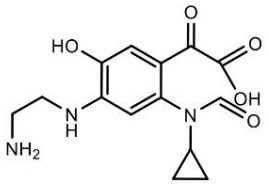

ATOM TYPE	x	y	z
C	3.29939700	0.86123200	-0.60705900
C	1.61375700	-1.75428100	-1.32215600
N	1.43437100	-1.14652100	-0.12961800
C	2.09288400	-1.62402700	1.06956100
C	2.17229100	-3.09537200	1.32280500
C	1.25413600	-2.24002400	2.14342800
C	0.46711900	-0.09839800	0.01262000
C	0.86976800	1.22207200	0.22927800
C	-0.11967300	2.18813600	0.50026100
C	-1.44310900	1.85729600	0.50052200
O	-2.45045900	2.75197400	0.72406000
C	-1.86069700	0.52279600	0.24891700
N	-3.17559400	0.23623500	0.24222400
C	-3.70448800	-1.09650500	0.02395400
C	-5.22214300	-1.07814600	-0.00347300
N	-5.82353600	-0.33924800	-1.11117100
C	-0.87073100	-0.44451300	0.02768600
C	2.25339600	1.66801000	0.17332400
O	2.66023500	2.70821900	0.65894200
O	1.02683100	-1.45405300	-2.35196100
O	4.30293700	0.42700800	-0.10507000
O	3.00416100	0.80751100	-1.89606800
H	2.36320300	-2.55194900	-1.28901100
H	2.93026600	-1.01862800	1.38731300
H	3.08154600	-3.46551400	1.77095100
H	1.71329500	-3.75116400	0.59794600
H	0.19573900	-2.32831500	1.94493800
H	1.52206200	-2.01716100	3.16462400
H	0.17353600	3.21521500	0.67716600
H	-2.08222400	3.63161200	0.87193700
H	-3.81925400	0.98121500	0.46433800
H	-3.32842700	-1.48751300	-0.92577000
H	-3.36224000	-1.77014100	0.81508500
H	-5.59361800	-0.66046000	0.93298000
H	-5.56149800	-2.11145500	-0.04798600
H	-5.57188400	0.64106900	-1.04754600
H	-5.42912600	-0.67417600	-1.98439100
H	-1.14463900	-1.47892400	-0.12101700
H	3.70548700	0.33809200	-2.37884500

Table S13. Cartesian coordinates for optimized structure of MZ-310.

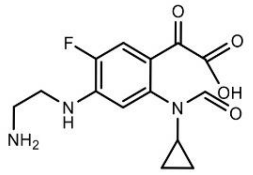

ATOM TYPE	x	y	z
C	3.05018000	-0.88432100	-1.12164000
C	1.14784900	2.25272700	-0.98599000
N	1.27364200	1.29321200	-0.04075500
C	2.46389000	1.31545100	0.77924500
C	2.48752200	2.18524800	1.99870700
C	2.43043500	0.69292500	2.13495800
C	0.33212800	0.22925600	0.01418500
C	0.74462000	-1.10880000	0.05583500
C	-0.22765300	-2.10444000	0.24133600
C	-1.54305000	-1.76558800	0.29549500
F	-2.48217200	-2.72164600	0.42869100
C	-1.99617800	-0.43599000	0.21423400
N	-3.31640900	-0.16501100	0.30089700
C	-3.86467200	1.14531700	-0.00039600
C	-5.37395600	1.11148800	0.10576200
N	-5.93412700	0.12740800	-0.82193100
C	-1.01098100	0.55638200	0.10214000
C	2.12827700	-1.55954400	-0.07940800
O	2.58749800	-2.52632300	0.49255800
O	1.93874400	3.17485200	-1.12034100
O	2.63814800	-0.23619300	-2.04469400
O	4.33576300	-1.14845300	-0.95911700
H	0.27869700	2.12619200	-1.63933100
H	3.38359100	1.26173700	0.21178600
H	3.41263600	2.69448200	2.22177300
H	1.58273900	2.73284100	2.21846200
H	1.49404200	0.26190200	2.45927800
H	3.31702900	0.16343900	2.44979300
H	0.06058500	-3.14553600	0.29486900
H	-3.95269700	-0.93943300	0.17225300
H	-3.47209900	1.88054500	0.70256700
H	-3.56806800	1.45891500	-1.00760500
H	-5.74269000	2.12577300	-0.06388700
H	-5.65601200	0.82590100	1.11911700
H	-6.93535100	0.06500400	-0.68156000
H	-5.79867700	0.45571600	-1.77255700
H	-1.29720300	1.59777800	0.12224200
H	4.45959500	-1.75143600	-0.20691300

Table S14. Cartesian coordinates for optimized structure of MZ-330.

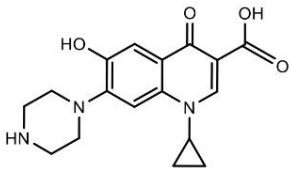

ATOM TYPE	x	y	z
C	-1.16598000	-1.87473400	0.08235400
C	-1.64541200	-0.54043700	0.17378900
C	-0.73518300	0.49640600	0.22752400
C	0.64037600	0.24199800	0.15419700
C	1.10260200	-1.07460000	0.03310900
C	0.17594500	-2.12645600	0.00292400
N	1.55919500	1.29330800	0.19887500
C	2.86438300	1.04202300	0.16927700
C	3.39037400	-0.22352000	0.06387400
C	2.52528300	-1.35804300	-0.02041500
C	1.08016000	2.65858300	0.32839000
C	0.40768400	3.29786500	-0.84107800
C	1.77388000	3.74740600	-0.41455100
O	2.96108200	-2.53311100	-0.12732800
C	4.85715200	-0.37377900	0.03653600
O	5.29863900	-1.62044400	-0.07147100
O	5.63563000	0.55928800	0.10635700
N	-3.03613800	-0.35746100	0.25210400
C	-3.48954000	0.92484500	0.79269100
C	-4.98859900	0.88291300	1.01053200
N	-5.66921700	0.62169700	-0.25740600
C	-5.22751600	-0.66350700	-0.79691700
C	-3.73144700	-0.63599500	-1.02225100
H	-1.08760300	1.51078100	0.31579400
H	0.52874400	-3.14670500	-0.04852800
H	3.51860300	1.89921800	0.23384700
H	0.69351200	2.87221700	1.31461800
H	-0.44412200	3.92751800	-0.63335800
H	0.34765400	2.71005300	-1.74578400
H	2.60061200	3.47579900	-1.05398000
H	1.87626400	4.69163300	0.09725900
H	4.49099100	-2.22593300	-0.11539000
H	-2.98057900	1.10844800	1.73783200
H	-3.24967400	1.74554400	0.10453600
H	-5.21470300	0.11421300	1.76006800
H	-5.31579400	1.84334900	1.40417300
H	-6.66611000	0.57312200	-0.08356000
H	-5.72715700	-0.84933600	-1.74585300
H	-5.46317500	-1.49498200	-0.11971800
H	-3.47648800	0.14645500	-1.74810200
H	-3.39703600	-1.58849600	-1.42733100
O	-2.03413000	-2.92298600	0.10918700
H	-2.90554200	-2.60347100	0.38459400

Table S15. Cartesian coordinates for optimized structure of MZ-334A.

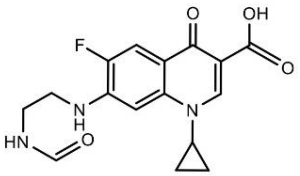

ATOM TYPE	x	y	z
C	4.90241200	-0.63256300	0.31694100
C	3.45671600	-0.37057300	0.19013400
C	3.01155300	0.92101000	0.29762700
N	1.72862900	1.26968700	0.19136200
C	1.33976400	2.66130200	0.33621600
C	0.84688200	3.39921900	-0.86427100
C	2.18834100	3.72192900	-0.27578900
C	0.74668900	0.29614600	-0.00207900
C	1.13906800	-1.04779900	-0.12873300
C	0.14330100	-2.02610800	-0.32838900
C	-1.15402700	-1.65394700	-0.38679900
F	-2.12150200	-2.57005000	-0.57183400
C	-1.58218100	-0.30823800	-0.25241900
N	-2.89807800	-0.03036100	-0.32397300
C	-3.43349800	1.30072700	-0.12062100
C	-4.94786600	1.27745600	-0.17815600
N	-5.56060600	0.51550600	0.90101900
C	-0.60070100	0.66039600	-0.05701600
C	2.52384100	-1.43377100	-0.04206800
O	2.89267200	-2.63467600	-0.15500100
O	5.73424300	0.23379400	0.51619600
O	5.25849300	-1.90467400	0.19897900
C	-5.79688500	-0.79393100	0.83746900
O	-5.48004500	-1.51764500	-0.10855800
H	3.70945300	1.72516500	0.47946300
H	0.86504600	2.86537200	1.28550300
H	0.02666000	4.08521400	-0.71622500
H	0.84153100	2.85572500	-1.79813600
H	3.05647200	3.41271600	-0.83889500
H	2.30465200	4.63362000	0.28930900
H	0.41646800	-3.06697200	-0.42890100
H	-3.55350700	-0.79490800	-0.42016300
H	-3.06811700	1.97796900	-0.89667500
H	-3.10406700	1.69650800	0.84416600
H	-5.27906100	0.85539700	-1.12623900
H	-5.31512100	2.29765600	-0.11522700
H	-5.84942300	1.00140900	1.73659100
H	-0.89117700	1.69210000	0.05041600
H	4.41286200	-2.44131500	0.03949000
H	-6.31211400	-1.19095900	1.71795800

Table S16. Cartesian coordinates for optimized structure of MZ-334B.

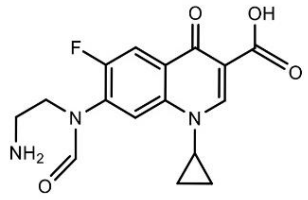

ATOM TYPE	x	y	z
C	-4.68858000	-0.20462100	0.04016900
C	-3.21601200	-0.14389600	-0.04606800
C	-2.62644100	1.07956800	-0.25246300
N	-1.31111300	1.25823000	-0.34670500
C	-0.76381200	2.58647900	-0.56847200
C	0.02685500	3.22463700	0.52586200
C	-1.33781100	3.74070200	0.17835700
C	-0.45199700	0.16343100	-0.27301900
C	-0.97444800	-1.11518800	-0.03933300
C	-0.10659500	-2.20939100	0.05687500
C	1.23453500	-2.01524500	-0.08811600
F	2.06513700	-3.06078100	-0.02401700
C	1.77768600	-0.74537200	-0.33386000
N	3.17698000	-0.58571700	-0.47203400
C	4.01810600	-0.85529900	0.70173900
C	3.75012500	0.14395800	1.82154800
N	3.94545300	1.54558700	1.46402900
C	0.92937500	0.33616600	-0.42036000
C	-2.41303700	-1.31853000	0.08862600
O	-2.89631200	-2.45478800	0.29477500
O	-5.41078900	0.76672300	-0.07106100
O	-5.19859100	-1.41166000	0.24963600
C	3.66173000	0.11229400	-1.52713700
O	4.82532500	0.46089300	-1.65408000
H	-3.23547800	1.96728800	-0.34666800
H	-0.43866800	2.73859900	-1.58764900
H	0.11832900	2.66653100	1.44693500
H	0.89751400	3.79214700	0.23372100
H	-1.42200100	4.67039000	-0.36246800
H	-2.13080400	3.54153500	0.88405800
H	-0.49814500	-3.20205200	0.22739300
H	3.82710500	-1.86936600	1.04838800
H	5.05208500	-0.79427300	0.37192100
H	2.72919800	0.02041100	2.18446600
H	4.41199400	-0.11157600	2.64827900
H	4.85729000	1.65543300	1.03142300
H	3.26838900	1.81227100	0.75537800
H	1.35061000	1.31531200	-0.59094200
H	-4.43607300	-2.06323200	0.31143400
H	2.90804000	0.31341800	-2.29677600

Table S17. Cartesian coordinates for optimized structure of MZ-336.

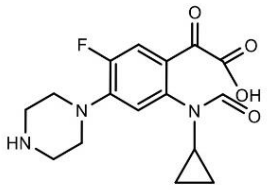

ATOM TYPE	x	y	z
O	-2.85473800	-2.74016100	0.99543600
C	-3.36561600	-2.13515000	0.09280100
C	-1.22667100	2.82557500	-0.96976600
N	-1.53141100	1.72363200	-0.24334200
C	-0.70908200	0.56913900	-0.32165600
C	-1.26145700	-0.71406800	-0.40239300
C	-0.40027900	-1.81543000	-0.38253800
C	0.95299600	-1.62884400	-0.34231800
F	1.74221300	-2.71318800	-0.43382500
C	1.54551200	-0.35934600	-0.25592300
N	2.92531400	-0.21720500	-0.21933800
C	3.61680900	-0.93566200	0.86828500
C	5.11236000	-0.93241500	0.63895500
N	5.60000300	0.44261200	0.55082400
C	4.94419200	1.11043300	-0.57152100
C	3.44522800	1.14420800	-0.35486300
C	0.66566200	0.72884100	-0.22736500
C	-2.69373400	-0.93960800	-0.62474500
O	-3.40694700	-0.25643700	-1.32317000
O	-1.86788700	3.86478800	-0.92496100
C	-2.70732600	1.77028600	0.59683000
C	-2.63062100	2.50319100	1.89779900
C	-2.71534700	1.00308100	1.87540500
O	-4.58452900	-2.39790300	-0.34285500
H	-0.36064600	2.70305300	-1.62786100
H	-0.78078400	-2.82350600	-0.46823100
H	3.39031300	-0.43856800	1.81951900
H	3.25952100	-1.95749000	0.92549600
H	5.59502500	-1.43700200	1.47382500
H	5.33096400	-1.50070100	-0.27411500
H	6.59713300	0.42018100	0.37260700
H	5.15117400	0.60326000	-1.52241200
H	5.30840400	2.13294000	-0.64974800
H	2.97056000	1.62052100	-1.21082000
H	3.21859700	1.73609100	0.54102300
H	1.05695300	1.72390200	-0.08046900
H	-3.63323600	1.83851300	0.04447700
H	-3.49953700	3.06996000	2.19588400
H	-1.67559200	2.93544200	2.15868500
H	-3.64405400	0.52781600	2.15469800
H	-1.82048100	0.45704100	2.13801800
H	-4.82452200	-1.76372800	-1.04067500

Table S18. Cartesian coordinates for optimized structure of MZ-346A.

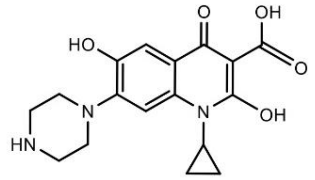

ATOM TYPE	x	y	z
C	-4.63475500	-0.70341500	-0.28523200
C	-3.20899500	-0.44504700	-0.13711400
C	-2.74118000	0.86487800	-0.31222800
N	-1.44631600	1.18309000	-0.16524800
C	-1.03319000	2.57305400	-0.24309600
C	-0.27631700	3.15209300	0.90990100
C	-1.68830200	3.56887500	0.65638100
C	-0.49231300	0.16794000	0.02440200
C	-0.89956500	-1.15364600	0.22388900
C	0.06132500	-2.14648200	0.45464600
C	1.39472500	-1.83809400	0.45547400
O	2.30150400	-2.81381700	0.74644300
C	1.82200700	-0.51725800	0.17272600
N	3.20553900	-0.27256900	0.14629300
C	3.88352900	-0.87255800	-1.02200700
C	5.38415400	-0.78583000	-0.84772500
N	5.78448600	0.61279200	-0.70098700
C	5.12277000	1.19328800	0.46730400
C	3.61860800	1.12367300	0.29595500
C	0.87221100	0.46920600	-0.02104900
C	-2.30940100	-1.49955800	0.17401800
O	-2.70577900	-2.68015500	0.36389800
O	-5.44968600	0.17861400	-0.57494500
O	-5.03473700	-1.94096100	-0.09457400
O	-3.55878400	1.83788700	-0.63123700
H	-0.75844200	2.88592000	-1.24025100
H	0.52943700	3.82946500	0.66980100
H	-0.09944400	2.49962500	1.75280700
H	-1.88401000	4.54391200	0.23713200
H	-2.43972400	3.19524600	1.33547600
H	-0.25680600	-3.15975300	0.65552600
H	3.16037200	-2.40076900	0.91616800
H	3.58029800	-1.91113200	-1.13405800
H	3.58061300	-0.33379900	-1.92873600
H	5.66942500	-1.38703100	0.02556900
H	5.86943000	-1.21190900	-1.72385100
H	6.78618300	0.64785000	-0.55346100
H	5.41934200	2.23552500	0.56887700
H	5.39728700	0.67061900	1.39214400
H	3.33081200	1.71287700	-0.58419100
H	3.12368100	1.54642800	1.16943600
H	1.19140800	1.47495900	-0.23498400
H	-4.20298000	-2.48664800	0.12996800
H	-4.47485500	1.42616000	-0.68792300

Table S19. Cartesian coordinates for optimized structure of MZ-346B.

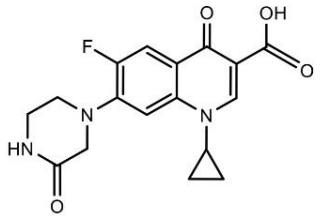

ATOM TYPE	x	y	z
C	-5.04572500	-0.23026800	-0.16975500
C	-3.57416500	-0.14521100	-0.12096800
C	-2.98406200	1.07909000	-0.30624100
N	-1.66674300	1.27649200	-0.27118300
C	-1.12534500	2.60731500	-0.48465700
C	-0.47758300	3.31011000	0.66208900
C	-1.80489700	3.77615800	0.14138000
C	-0.80032600	0.19884800	-0.07762400
C	-1.33796200	-1.08102200	0.12146200
C	-0.45247500	-2.14927400	0.33721700
C	0.88675800	-1.93550900	0.33230900
F	1.70312800	-2.96100100	0.62915300
C	1.46610900	-0.66347800	0.08404200
N	2.82758400	-0.49712700	0.08490800
C	3.70002600	-1.55852700	-0.45193900
C	4.86153300	-0.94760200	-1.20714700
N	5.53304600	0.02825300	-0.36349300
C	4.82302900	0.96750700	0.26090600
C	3.32863900	0.87352400	0.04757600
C	0.58200500	0.39564600	-0.10655100
C	-2.76621600	-1.30413400	0.11660400
O	-3.26278200	-2.44523800	0.30142000
O	-5.77282000	0.72330400	-0.37682800
O	-5.55155500	-1.44047800	0.03076900
O	5.31674900	1.87833800	0.92753000
H	-3.59092200	1.95335300	-0.49226500
H	-0.68938500	2.72902600	-1.46601900
H	-0.47931000	2.79264600	1.61068900
H	0.40744500	3.88909400	0.44558000
H	-1.84702600	4.68107700	-0.44459600
H	-2.66841100	3.58510900	0.76130300
H	-0.83488600	-3.14072300	0.53529200
H	4.08425400	-2.18026600	0.35567700
H	3.13548800	-2.18599200	-1.13785500
H	5.56840500	-1.72812300	-1.46894200
H	4.51445000	-0.47549400	-2.12762300
H	6.54113800	0.06406500	-0.30980100
H	2.85130800	1.45893200	0.82958600
H	3.12016300	1.35966200	-0.91526800
H	0.96814600	1.38046900	-0.30281000
H	-4.77899700	-2.07361600	0.17770400

Table S20. Cartesian coordinates for optimized structure of MZ-360.

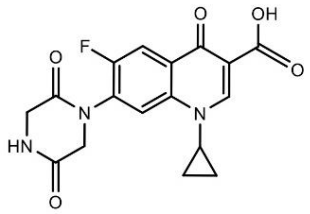

ATOM TYPE	x	y	z
C	-5.14140700	-0.39640200	0.01266200
C	-3.67457900	-0.23148700	-0.02152900
C	-3.16485200	1.00400600	-0.33815300
N	-1.86280200	1.27420800	-0.39140600
C	-1.40689300	2.61062900	-0.73613400
C	-0.72833800	3.42606700	0.31421400
C	-2.10874600	3.78603900	-0.14849300
C	-0.93006400	0.26445700	-0.15944600
C	-1.37180300	-1.02032500	0.18240100
C	-0.43373700	-2.02633100	0.43947700
C	0.89617100	-1.74631800	0.33974400
F	1.79206700	-2.68583500	0.64891500
C	1.35512600	-0.47813600	-0.04737000
N	2.74350700	-0.22862600	-0.14379400
C	3.50988700	-1.00890100	-0.95546900
C	4.97658000	-0.66936200	-1.00827500
N	5.43854300	0.07846500	0.14294900
C	4.69453900	0.99387300	0.76659300
C	3.24717000	1.05813000	0.34424000
C	0.43995400	0.52198600	-0.28602800
C	-2.79573100	-1.31863100	0.27608300
O	-3.20505700	-2.45988700	0.58934000
O	-5.92682000	0.49636900	-0.24012600
O	-5.57089500	-1.60764900	0.34303000
O	5.12643400	1.75587800	1.62789900
O	3.05764800	-1.91854000	-1.63047900
H	-3.83015700	1.82632500	-0.55928600
H	-1.04144300	2.67902600	-1.75067900
H	-0.64260300	2.97998900	1.29480800
H	0.10859900	4.03079700	-0.00044600
H	-2.23693000	4.64247600	-0.79188600
H	-2.92013300	3.59688100	0.53878700
H	-0.76072600	-3.01358200	0.73290000
H	5.14439900	-0.11992400	-1.93844600
H	5.52128200	-1.60638100	-1.07173000
H	6.42261500	0.04142100	0.37341500
H	2.66179500	1.35555800	1.20915200
H	3.15635200	1.83451300	-0.42057000
H	0.78954500	1.49828900	-0.58383200
H	-4.76607400	-2.18633200	0.50892700

Table S21. Cartesian coordinates for optimized structure of MZ-362A.

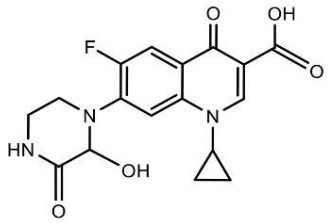

ATOM TYPE	x	y	z
C	5.15476100	-0.57160500	0.26999300
C	3.70281100	-0.33765600	0.14661700
C	3.22674500	0.93428500	0.34786700
N	1.93985500	1.26359500	0.25565000
C	1.51769400	2.63362100	0.49350100
C	0.99747500	3.43250600	-0.65540200
C	2.33533800	3.75080300	-0.05655300
C	0.98523400	0.28495400	-0.02166100
C	1.39822300	-1.03442700	-0.24419100
C	0.43151800	-2.00679000	-0.53558700
C	-0.88092700	-1.65682600	-0.58851400
F	-1.78732500	-2.58843300	-0.91985600
C	-1.33066000	-0.34251800	-0.33933300
N	-2.70202900	-0.04920400	-0.41841800
C	-3.06521800	1.36786000	-0.46450700
C	-4.47065400	1.48548500	-1.00022000
N	-5.36869400	0.59722500	-0.27427600
C	-4.99839800	-0.47015100	0.42609300
C	-3.50719300	-0.77271000	0.55748500
C	-0.37517300	0.61445500	-0.05330100
C	2.80200000	-1.40061300	-0.17620400
O	3.18650500	-2.57770600	-0.38010300
O	5.95846700	0.29828000	0.54657700
O	5.54926400	-1.82008700	0.05588100
O	-3.17187400	-0.44771200	1.89265400
O	-5.79512900	-1.21615000	0.99780700
H	3.90699300	1.73602200	0.59637900
H	1.04695000	2.76392200	1.45742800
H	0.99749700	2.94895900	-1.62177500
H	0.16168000	4.08662100	-0.45823100
H	2.43369900	4.62760900	0.56433000
H	3.20667300	3.49762800	-0.64227700
H	0.72755300	-3.02637800	-0.73742900
H	-2.39475100	1.88721400	-1.14403700
H	-2.98665700	1.83262900	0.52312500
H	-4.48984200	1.23705900	-2.06145700
H	-4.82271700	2.50711600	-0.88051800
H	-6.36557000	0.74315000	-0.36789300
H	-3.39563200	-1.84110300	0.39576000
H	-0.68383600	1.62315600	0.16331500
H	4.73060800	-2.36804000	-0.15627400
H	-2.42997200	-0.99802500	2.16853400

Table S22. Cartesian coordinates for optimized structure of MZ-362B.

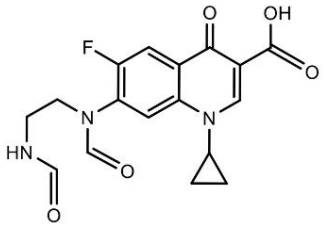

ATOM TYPE	x	y	z
C	4.79292400	-0.32861500	0.37342100
C	3.33989700	-0.23768200	0.12745500
C	2.76762300	1.00910000	0.06077200
N	1.47136800	1.21537100	-0.16023400
C	0.93873800	2.56760100	-0.19651400
C	0.43364100	3.10085900	-1.49623000
C	1.70723000	3.62862000	-0.90536200
C	0.60653900	0.13155800	-0.29933700
C	1.11476500	-1.17275100	-0.24623600
C	0.24198200	-2.25848500	-0.38570100
C	-1.08983200	-2.03045100	-0.55692200
F	-1.91992900	-3.06423900	-0.73529100
C	-1.62610800	-0.73246400	-0.57328500
N	-3.01707700	-0.53993300	-0.72454200
C	-3.95898400	-1.17012900	0.20840400
C	-4.34983400	-0.22005300	1.33353100
N	-3.20898900	0.17192100	2.13917000
C	-2.55241400	1.32022100	1.96533800
C	-3.47867600	0.39131900	-1.59596300
C	-0.76908300	0.33969300	-0.45119700
C	2.53772400	-1.40947000	-0.03840500
O	3.00896800	-2.56901500	0.00050100
O	5.51267900	0.63868700	0.52789400
O	5.28739100	-1.55927700	0.41945000
O	-4.65521800	0.69939600	-1.69251500
O	-1.50139600	1.61796900	2.52962500
H	3.37458400	1.89373400	0.19015000
H	0.40253500	2.82785300	0.70521000
H	0.52569700	2.45210300	-2.35566700
H	-0.45654800	3.71044700	-1.46228800
H	2.62763500	3.34433000	-1.39378900
H	1.70625900	4.60831300	-0.45367000
H	0.62343600	-3.26942400	-0.37181600
H	-3.49287700	-2.05920900	0.62274100
H	-4.84724300	-1.47042600	-0.34322200
H	-5.08680400	-0.71314500	1.96428100
H	-4.80287300	0.68196100	0.92729100
H	-2.77134000	-0.52715500	2.72739800
H	-3.04621600	2.00875300	1.26665100
H	-2.70217900	0.82770400	-2.23355800
H	-1.17828200	1.33832200	-0.44384400
H	4.53029200	-2.20282800	0.26874200

Table S23. Cartesian coordinates for optimized structure of MZ-364.

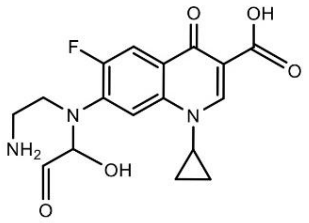

ATOM TYPE	x	y	z
C	-5.17847700	-0.47774700	-0.11758400
C	-3.71632700	-0.28441700	-0.07616800
C	-3.21928600	0.98356800	-0.24453800
N	-1.91999700	1.27643900	-0.21662300
C	-1.47640200	2.64452200	-0.42263800
C	-0.86748200	3.38098900	0.72412400
C	-2.22963600	3.75688500	0.22121700
C	-0.97610800	0.26311300	-0.04303500
C	-1.41386500	-1.05586700	0.13660200
C	-0.45508300	-2.06219300	0.33070200
C	0.86499900	-1.74784700	0.32583600
F	1.76269700	-2.71120700	0.58988200
C	1.34212400	-0.43354300	0.09940000
N	2.70093300	-0.16260400	0.12379100
C	3.10569400	1.23751400	0.30137200
C	4.57956800	1.40880100	0.62146600
N	4.99775700	0.57470600	1.75241200
C	4.18462000	-0.34776600	-1.83393600
C	3.60141800	-1.04175300	-0.60356000
C	0.39009800	0.56065900	-0.07207600
C	-2.82435300	-1.38451800	0.13141300
O	-3.23052300	-2.56301700	0.29179000
O	-5.97589000	0.42434000	-0.29197800
O	-5.59084900	-1.72754500	0.05095400
O	4.61483400	-1.59229000	0.19302500
O	3.51414500	0.33266500	-2.56715700
H	-3.89129000	1.81291200	-0.41164300
H	-1.06033600	2.80426600	-1.40713900
H	-0.02764000	4.02247900	0.50379800
H	-0.82247800	2.85644400	1.66778800
H	-3.07083300	3.49906300	0.84751700
H	-2.34179300	4.66166600	-0.35561600
H	-0.76540700	-3.08156900	0.51174100
H	2.51911700	1.63448200	1.13083700
H	2.87961800	1.83966000	-0.58309000
H	5.20509300	1.14640200	-0.23555600
H	4.73426000	2.47470200	0.79820800
H	5.94229500	0.82117100	2.02517800
H	4.39960100	0.75648300	2.55199200
H	5.24804100	-0.55292000	-2.03706900
H	3.02558900	-1.86427500	-1.02983000
H	0.70997700	1.57278100	-0.25040500
H	-4.77277400	-2.30469200	0.17596900
H	4.85110300	-0.91358900	0.88666100

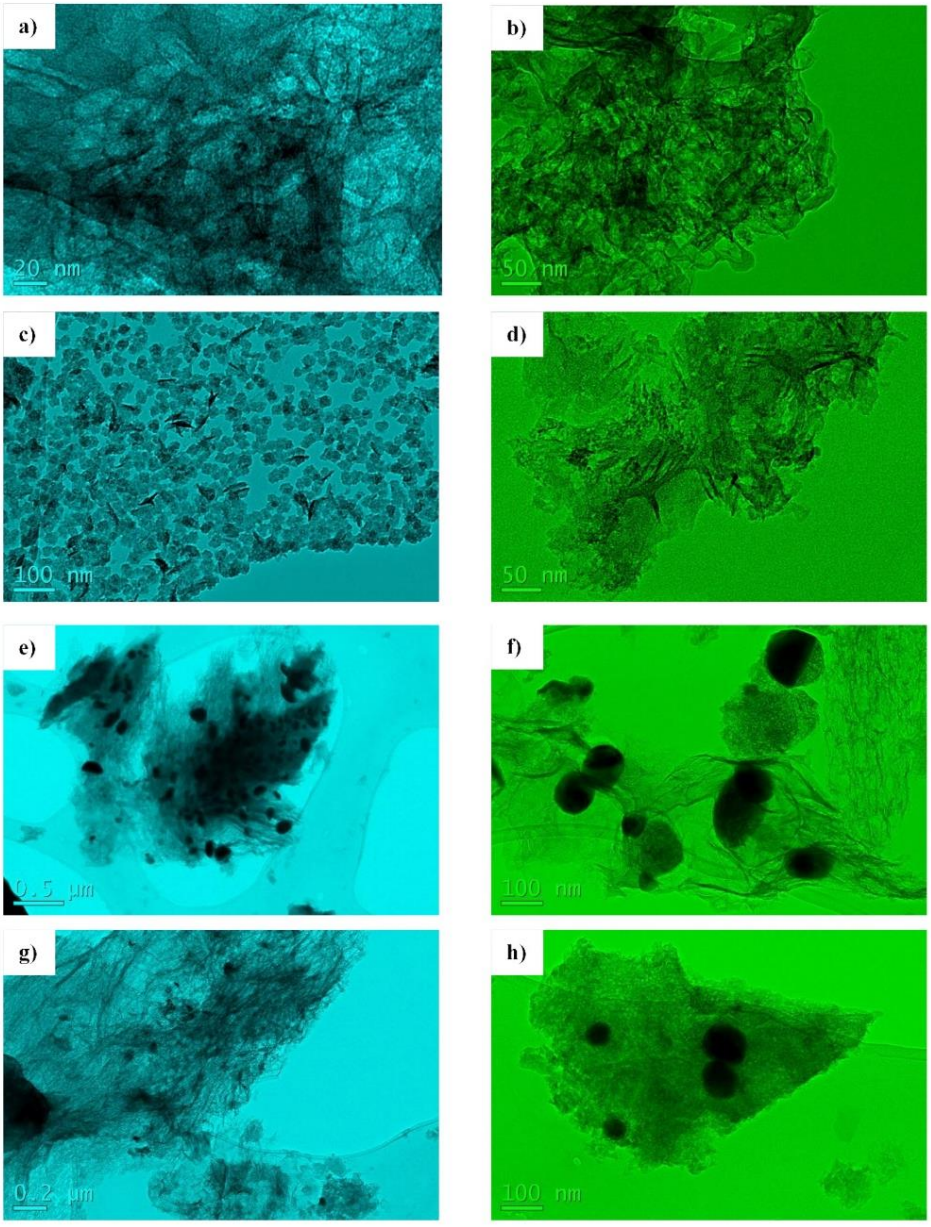

Figure S1. HR-TEM images of the metal dispersion of the active phase on the catalyst surface. (a,b) Urban-Fe catalyst, (c,d) Industrial-Fe Catalyst, (e,f) Industrial-Ni catalyst, (g,h) Industrial FeNi catalyst. Metallic particles are seen as dark spots.

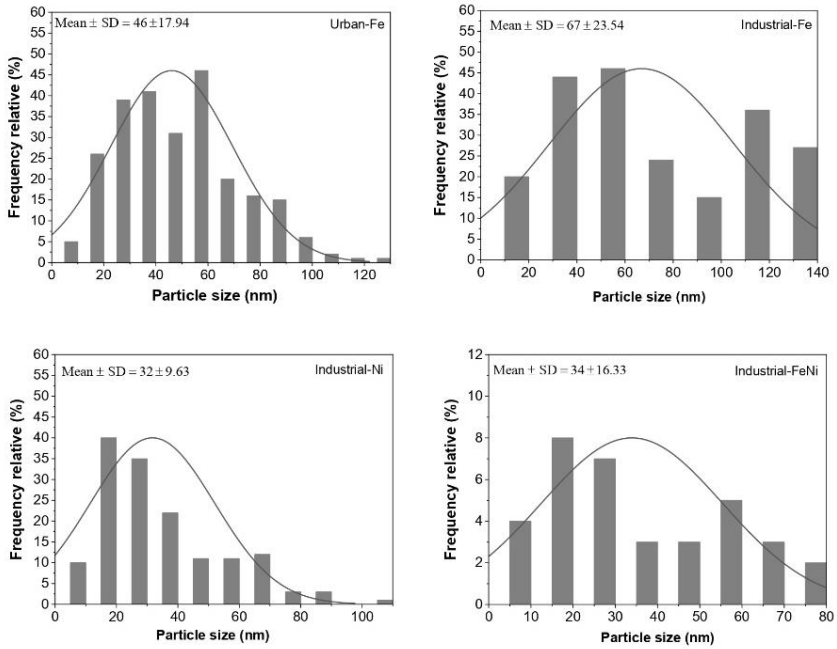

Figure S2. The histograms of iron and nickel particle size distributions.

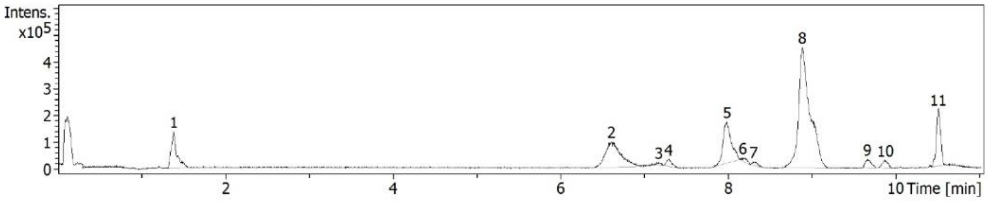

Figure S3. LC-MS chromatogram for the liquid sample of Urban-Fe catalyst.

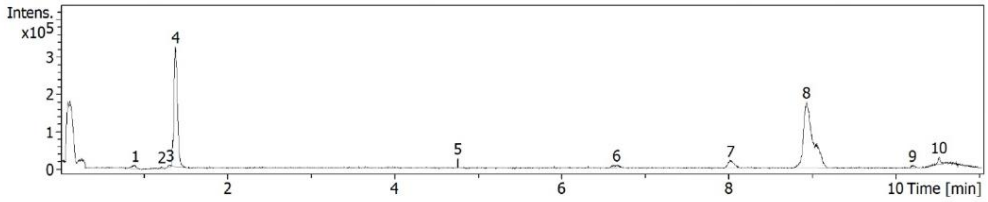

Figure S4. LC-MS chromatogram for the liquid sample of Industrial-Fe catalyst.

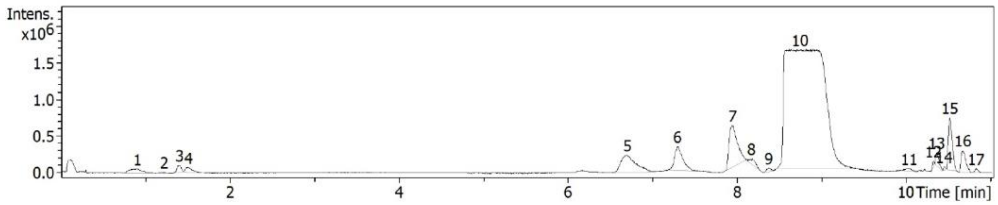

Figure S5. LC-MS chromatogram for the liquid sample of Industrial-Ni catalyst.

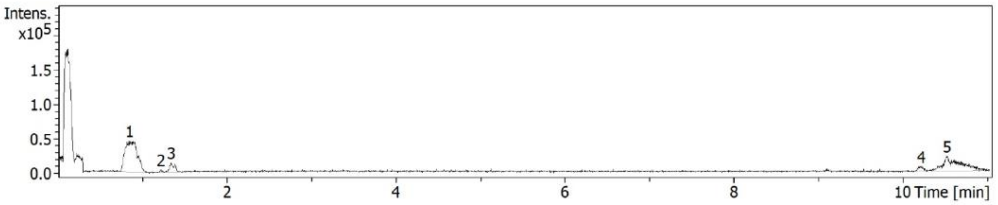

Figure S6. LC-MS chromatogram for the liquid sample of Industrial-FeNi catalyst.

References:

[1] Z.-j. Liu, J-q. Wan, Z-C. Yan, Y. Wang, Y.W. Ma, Efficient removal of ciprofloxacin by heterogeneous electro-Fenton using natural air–cathode, Chem, Eng. J. 433 (2022) 133767.

[2] S. Li, T. Huang, P. Du, W. Liu, J. Hu, Photocatalytic transformation fate and toxicity of ciprofloxacin related to dissociation species: Experimental and theoretical evidences, Water Res. 185 (2020) 116286.

7.4 Publicación 4

Journal of Environmental Chemical Engineering 11 (2023) 109344

Contents lists available at ScienceDirect

Journal of Environmental Chemical Engineering

journal homepage: www.elsevier.com/locate/jece

Efficient removal of antibiotic ciprofloxacin by catalytic wet air oxidation using sewage sludge-based catalysts: Degradation mechanism by DFT studies

Pablo Gutiérrez-Sánchez [a,*], Silvia Álvarez-Torrellas [a], Marcos Larriba [a], M. Victoria Gil [b], Juan M. Garrido-Zoido [b], Juan García [a,*]

[a] Catalysis and Separation Processes Group, Chemical Engineering and Materials Department, Faculty of Chemistry, Complutense University, Avda. Complutense s/n, 28040 Madrid, Spain
[b] Departamento de Química Orgánica e Inorgánica, Facultad de Ciencias and IACYS Unidad de Química Verde y Desarrollo Sostenible, Universidad de Extremadura, E-06006 Badajoz, Spain

ARTICLE INFO

Editor: V. Victor

Keywords:
Catalytic wet air oxidation
Ciprofloxacin
Computational study
Iron catalysts
Sewage sludge valorization

ABSTRACT

In this work, the sewage sludge-derived activated carbon (SAC) loaded with iron nanoparticles (FeSAC) showed a highly effective catalytic activity in the degradation of the antibiotic ciprofloxacin by the CWAO reaction. The properties of FeSAC catalyst were studied by using N_2 adsorption-desorption measurements at 77 K, scanning electron microscopy, X-ray fluorescence spectroscopy, X-ray photoelectron spectroscopy and thermogravimetric analysis. The CWAO reaction was evaluated at different temperatures (120–140 °C), total pressure (10–30 bar) and catalyst doses (0.1–0.7 g/L) in a batch reactor. In this regard, temperature and catalyst dosage showed a significant impact on the removal of the tested antibiotic. By using a catalyst dose of 0.7 g/L, ciprofloxacin degradation and CO_2 selectivity were higher than 99 % and 60 %, respectively, and were achieved within two hours at 140 °C and 20 bar. The loss of the active phase (Fe) of the catalyst in the reaction medium was measured, obtaining negligible values (less than 24 ppb). This catalyst showed high stability under the tested reaction conditions. In addition, a potential equation was proposed to correctly describe the evolution of ciprofloxacin degradation. The calculated activation energy of the CWAO process was 53.8 kJ/mol. Additionally, Density Functional Theory (DFT) calculations were performed to illustrate the degradation mechanism of ciprofloxacin, where the electronic energies indicated the compounds that are most difficult to degrade by CWAO. Finally, a proof of concept using an environmentally-relevant matrix was carried out, verifying the technical feasibility of the synthesized catalyst for its application with more complex matrices, consecutive reaction cycles and at a low treatment cost.

1. Introduction

In 2021 alone, a total of 8.7 million tons of dry sewage sludge were generated in Europe [1]. The amount and characteristics of sludge generated in a WWTP is largely depended on the influent and type of used treatment processes. It has been estimated that sewage sludge production will increase rapidly annually in the coming years [2].

The traditional methods for sewage sludge management include landfill, incineration, composting, anaerobic digestion (biogas production) and agricultural applications, among others [3,4]. One alternative method gaining particular attention in recent years is the pyrolysis. Pyrolysis of sewage sludge can substantially reduce the waste volume, carbonize organic compounds, fix heavy metals, as well as destruct pathogens [4]. The carbon material derived from this process could be sustainably used to produce carbonaceous materials such as adsorbents or catalytic supports for potential environmental applications used in the degradation of many pollutants [5,6].

Emerging pollutants are usually defined as natural and synthetic chemicals that are not commonly monitored in the WWTPs effluents and therefore have the potential to enter the aqueous environment. These pollutants are not new in our environments, but they can stay for a long time in the aqueous medium because of their biotransformation,

* Corresponding authors.
E-mail addresses: pgutie03@ucm.es (P. Gutiérrez-Sánchez), jgarciar@ucm.es (J. García).

https://doi.org/10.1016/j.jece.2023.109344
Received 28 October 2022; Received in revised form 16 December 2022; Accepted 18 January 2023
Available online 20 January 2023

formation of metabolites and by-products. This group of compounds includes pharmaceuticals and personal care products, among many other substances used daily [7,8].

In recent years, the use of pharmaceutical products has grown exponentially. Consequently, there has been an increase of these compounds in groundwater, surface water and wastewater [9–11]. Some of these contaminants belong to the fluoroquinolones group, antibacterial drugs firstly used in the 1970 s [12]. Among them, ciprofloxacin is one of the most widely used. Unfortunately, since these types of antibiotics are characterised by their low biodegradability, the conventional biological wastewater treatment processes are not able to successfully remove these compounds from wastewater [13,14]. Therefore, the development of effective treatment methods is of great importance. In this sense, the advanced oxidation processes (AOPs) constitute a promising group of technologies for the treatment of wastewater containing organic refractory compounds, as an additional stage to the conventional biological treatment [15]. Among AOPs, wet air oxidation (WAO) process has already been successfully applied to treat effluents from printing and dye industry. A wide range of products have been treated efficiently due to the capacity of this process to degrade compounds that show low solubility, such as polymers or fatty acids [16]. The main disadvantages of WAO technique are the high requirements of temperature (200–320 °C) and pressure (20–200 bar), which results in high operation costs. The use of a catalyst strongly improves the degradation of organic pollutants by using milder operating conditions. Soluble transition metal salts (such as iron or copper) have been reported as efficient enhancers of the reaction rate [17]. Therefore, the use of a solid catalyst offers a further advantage compared to the homogeneous catalysts, since the solid can be easily recovered, regenerated and reused, after reaction. Besides, in the catalytic wet air oxidation (CWAO) process, the stability and durability of the catalyst under operating conditions must be strictly tested [18].

To our knowledge, there is only one previous study about the treatment of ciprofloxacin-containing waters by CWAO using ruthenium-based catalysts [12]. Therefore, there is a significant knowledge gap in the application of cheaper iron-based catalysts supported on sewage sludge-derived carbon materials for the removal of emerging pharmaceutical compounds from wastewater effluents by CWAO at moderate pressure and temperatures, which would allow the process to be economically viable. This study aims to step into the gap of existing research.

Ciprofloxacin was considered as model compound because it is hardly biodegradable by the conventional biological processes, but it is widely used to treat serious infections, or infections when other antibiotics have not worked. This pollutant showed the highest concentration among more than 200 pharmaceuticals in surface waters worldwide [19,20]. In addition, it has been included in the European Surface Water Watch List under the EU Water Framework Directive (Decision 2020/1161) [21]. Several studies about the removal of ciprofloxacin by other advanced oxidation processes have been reported in the literature. This information is summarized in Table S1 (Supplementary material).

In the present study, iron catalysts were synthesized from sewage sludge in order to contribute valorization of wastewater treatment plants (WWTPs) wastes and the development of environmentally friendly and low cost catalysts. Reaction tests were carried out in a batch reactor with iron supported on sewage sludge-derived activated carbon (FeSAC). The catalyst efficiency was determined by the ciprofloxacin degradation, mineralization rate, TOC removal and iron leaching. Not only was the effect of operating conditions such as temperature, total pressure and catalyst dosage tested, but a conversion rate equation was proposed for the experimental findings. Furthermore, the degradation intermediates of ciprofloxacin were identified by LC-MS technique. Based on experimental and theoretical results (Density Functional Theory calculations), a reaction pathway was proposed for the ciprofloxacin degradation. Finally, a proof of concept using surface water as an environmentally-relevant water matrix, has been accomplished.

2. Materials and methods

2.1. Materials

Ciprofloxacin (≥98 wt. %) was purchased from Sigma-Aldrich and the chemical activating agent ferric chloride hexahydrate ($FeCl_3{\cdot}6H_2O$, ≥98 wt. %) was provided by Panreac. Hydrochloric acid (HCl, 37 wt. %), acetonitrile (≥99.9 wt. %), and acetic acid glacial (≥99.7 wt. %), were supplied by Fluka, Fisher Chemical and Fluorochem, respectively. Aqueous solutions were prepared with ultrapure water from PURELAB® Flex Water Purification System (Veolia). A proof of concept was also carried out using a surface water matrix collected in the Manzanares river (Madrid, Spain), whose physico-chemical properties were measured following the Standard Methods [22]. These parameters are summarized in Table 1.

2.2. Synthesis of FeSAC catalyst

The industrial sewage sludge was kindly supplied by a local pharmaceutical company located in Spain. This biomass precursor was firstly characterized in terms of Chemical Oxygen Demand (COD), and total (TS), fixed (FS), and volatile (VS) solids content measured according to the Standard Methods [22]. The solid fraction was also undergone to elemental analysis (EA) and X-ray fluorescence spectroscopy (XRF) by using a LECO CHNS-932 analyzer and a PANalytical Axios spectrometer, respectively.

For the catalyst synthesis, the sewage sludge was dried in an oven for 24 h at 105 °C. After a grinding step, the dried sludge powder was chemically activated by using an incipient wetness impregnation technique with $FeCl_3{\cdot}6\ H_2O$, in a ratio of 1 mg $FeCl_3{\cdot}6H_2O$: 1 mg dried sludge. The activation was performed for 24 h at room temperature, followed by drying for 24 h at 105 °C. Next, the impregnated sludge was pyrolyzed in a vertical quartz reactor for 2 h at 800 °C, maintaining a constant N_2 flow rate of 100 mL/min and a heating rate of 10 °C/min. To remove the iron excess (i.e. iron compounds, in any of their oxidation states, which are weakly bound to the carbonaceous matrix and can be released into the aqueous phase leading to high iron leaching), the catalyst was washed with HCl 1 M solution for 1 h under magnetic stirring, and then filtered and rinsed with ultrapure water until neutral pH was reached. The solid was dried in an oven for 24 h at 105 °C, and finally, was ground and sieved to a particle size under 250 μm range.

2.3. Catalyst characterization

Elemental analysis and X-ray fluorescence spectroscopy were performed in order to determine the chemical composition of the synthesized catalyst, using the same equipment mentioned for the characterization of the raw industrial sludge. The textural properties of the material were explored by N_2 adsorption-desorption isotherms at 77 K in an ASAP 2020 equipment. Before measurement, the samples were outgassed for 3 h at 250 °C. The specific surface area of the solids (S_{BET}) was calculated using the Brunauer–Emmett–Teller (BET) equation and micropore volume (V_{Mic}) was estimated using the Dubinin–Radushkevich equation. The morphology and elemental analysis of the solid was studied by scanning electron microscopy with energy

Table 1
Physico-chemical characterization of the surface water.

Parameters	Value
pH	6.9
Chemical Oxygen Demand (mg/L)	<15
Total Organic Carbon (mg/L)	3.2
Total Carbon (mg/L)	7.4
Total Nitrogen (mg/L)	0.6
Total Dissolved Solids (mg/L)	64
Conductivity at 20 °C (ΩS/cm)	38.1

dispersion X-ray spectrometry (SEM-EDX) on a JEOL JSM 6335 F microscope. The binding energies of the elements in the catalyst were determined by X-ray photoelectron spectroscopy (XPS) in a SPECS GmbH electron spectroscopy system with a PHOIBOS 150 9MCD energy analyzer, and Mg X-ray source. Thermogravimetric analysis (TGA) was carried out in a Perkin Elmer STAR 6000 analyzer. The measurements were accomplished in a temperature range between 30 and 1000 °C, under nitrogen flow rate of 30 mL/min and a constant heating rate of 10 °C/min.

2.4. Catalytic wet air oxidation tests of ciprofloxacin in aqueous solution

CWAO experiments were performed using ciprofloxacin solutions with an initial concentration of 50 mg/L, in a Hastelloy autoclave reactor equipped with a heating jacket and a mechanically controlled paddle stirrer. This range of concentration has been previously reported in the literature [14,23–28]. The measured pH of ciprofloxacin aqueous solutions in ultrapure water was found around 6.8. In order to ensure no mass transfer limitations in the liquid phase, the stirring speed was set at 700 rpm. The experiments were performed by loading 100 mL of ciprofloxacin solution and the selected catalyst dose into the reactor. The reactor was then purged with nitrogen to remove any traces of air and to prevent the reaction from initiating before the operating conditions were reached. Subsequently, the stirring was started, and the heating jacket was switched on. Once the reaction temperature was reached, the reactor was pressurized with air up to the operating pressure, considering this step as zero reaction time. Liquid samples were collected periodically for 3 h and immediately filtered through 0.45 μm PTFE filters for further analysis. The influence of different reaction conditions, such as catalyst dose (0.1–0.7 g/L), temperature (120–160 °C) and total pressure (10–30 bar) was investigated. In addition, a proof of concept with a surface water matrix, which can be considered a real and environmentally-relevant aqueous matrix, was accomplished. In this latter case, the measured pH of the initial ciprofloxacin aqueous solution was of 7.0.

2.5. Analytical methods

Ciprofloxacin concentration was analyzed using a High Pressure Liquid Chromatograph 1260 Infinity II coupled with a diode array detector (Agilent) using a Poroshell 120 EC-C18 column (4.6 × 150 mm; 4 μm). The mobile phase was a mixture of acetonitrile (17.5 %) and a 75 mM acetic acid solution (82.5 %) at a flow rate of 0.85 mL/min, using an injection volume of 50 μL. The column temperature and the detection wavelength were set at 30 °C and 275 nm, respectively.

Inductively Coupled Plasma Optical Emission Spectroscopy (ICP-OES) was used to analyze the iron leaching into the reaction medium. The total organic carbon (TOC) content was measured by a Shimadzu TOC-V CPH analyzer. Finally, the reaction intermediates and by-products were identified in a Bruker LC-QTOF-MS Impact II spectrophotometer.

2.6. Computational studies

The molecular structure of the reactants and the observed intermediates were optimized by the Density Functional Theory (DFT)/M06–2X method with a 6–311 + +G(2df,2pd) basis set level, obtaining the corresponding E_{HOMO} values and positive frequencies in all the possible conformations evaluated, corresponding to minima energy. Here we show, of all these conformations, those that have turned out to be more stable under the conditions of the study. The calculations have been carried out using the Gaussian 16 program [29], including Natural Bond Orbitals (NBO) analysis [30,31]. The experimental conditions considered were 20 bar and 140 °C. The SMD model (universal solvation model based on solute electron density and a continuum model of the solvent defined by the bulk dielectric constant and atomic surface tensions) was used to address the solvent effects of water [32]. GaussView 6.0 software was used to visualize the computed and optimized structures [33].

3. Results and discussion

3.1. Sewage sludge characterization

Regarding to the main macroscopic properties of the industrial sewage sludge, a TS concentration of 36.6 g/L was found. The high COD (34.8 g/L) and VS (80 % of TS) values indicated the presence of a relevant organic matter content in the sewage sludge. Generally, this aspect is convenient for the synthesis of biomass-derived catalysts as the more organic matter in the precursor, the higher the efficiency in the production of biomass-based catalyst [34].

Chemical characterization of the sewage sludge solid fraction showed a carbon content of 42.4 wt. %, which is within the carbon concentration range reported in the literature for high char yields [35]. Other elements detected in higher proportions were oxygen (14.6 wt. %), calcium (11.6 wt. %), or hydrogen (5.8 wt. %). Furthermore, the raw sludge presented a low iron content (0.7 wt. %).

3.2. Catalyst characterization

Elemental analysis of the synthesized catalyst provided the content of carbon (70.9 wt. %), nitrogen (3.8 wt. %) and hydrogen (1.8 wt. %). From the results of XRF analysis, other main elements, such as oxygen (8.5 wt. %) and iron (5.1 wt. %) were identified. As expected, the pyrolysis step increased the carbon content of the raw sewage sludge to around 67 % from its initial value. During this process, the oxygen and hydrogen content was also considerably reduced compared to the biomass precursor values. The synthesis of the carbonaceous material by chemical activation required the application of an iron-based activating agent. The use of this metal salt allowed a sufficiently high iron content to act as the active phase of the catalyst in the CWAO process. Although the initial calcium content in the biomass precursor was high, the concentration in the resulting material was practically negligible, possibly due to the catalyst rinsing. Finally, it should be noted that the product yield, after the rinsing step, was found about 61 %.

The textural properties of the FeSAC catalyst were determined by the N_2 adsorption-desorption isotherms at 77 K (Fig. 1a). According to the International Union of Pure and Applied Chemistry (IUPAC) classification, the carbonaceous material showed a type IV isotherm, which is representative of mesoporous materials. In addition, the large initial adsorption of nitrogen at low relative pressure values ($P/P^0 < 0.05$) indicates the occurrence of a considerable amount of micropores in the solid structure. At relative pressure values above 0.4, the isotherm also exhibits an H4-type hysteresis loop, indicating capillary condensation in the mesopores [36]. As has been reported in the literature, hysteresis occurs when the pore width exceeds a critical value (which depends on adsorbate, temperature, and pore networks); and it has been determined that nitrogen at 77 K exhibits this phenomenon when the pores are larger than 4 nm [37].

The measured BET surface area of FeSAC catalyst was of 582 m^2/g, which is within the range reported in the literature for similar carbonaceous materials synthesized from sewage sludge [38]. Furthermore, a micropore volume value of 0.17 cm^3/g was obtained, corresponding to 47.5 % of the total pore volume. As can be seen in the pore size distribution (Fig. 1b), the maximum value was found in the narrow mesopore zone, i.e. around 4 nm. Thus, the mean pore diameter, calculated from the BJH model, was of 7.2 nm.

The thermal stability of the synthesized catalyst was evaluated by TGA, as illustrated in Fig. 2a. The degradation pattern showed three clearly defined zones. The first one was found at 100 °C, where a weight loss of about 7 % was reached due to the evaporation of the adsorbed water in the sample. The second degradation zone could be found in the

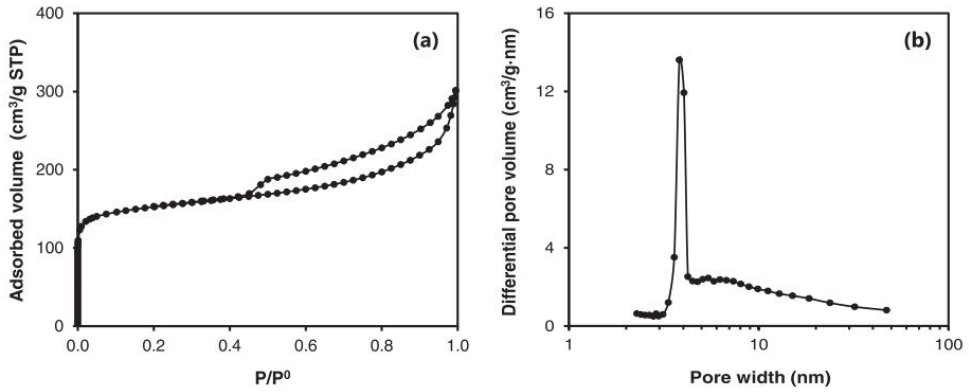

Fig. 1. N_2 adsorption–desorption isotherms at 77 K (a) and pore size distribution (b) of the FeSAC catalyst.

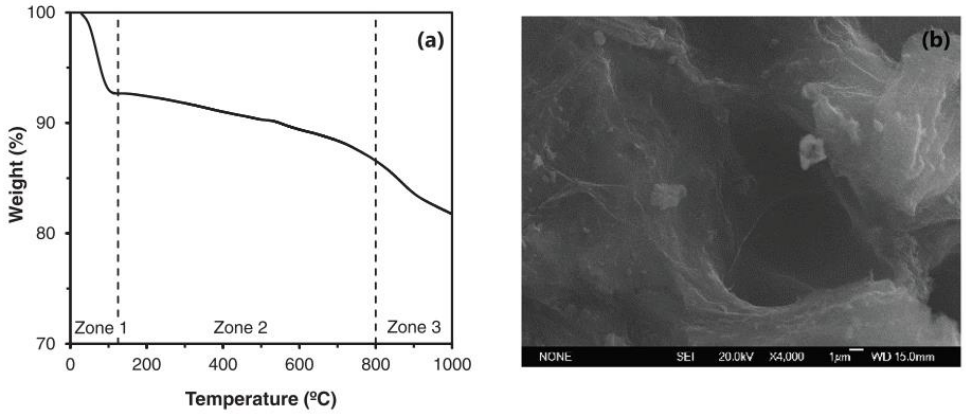

Fig. 2. Thermogravimetric analysis (a) and SEM micrograph (b) of the FeSAC catalyst.

range 150–750 °C, obtaining a weight loss between 7 % and 12 %. The pyrolysis temperature during the catalyst synthesis was of 800 °C, which could explain the narrow weight loss in the previously mentioned temperature range, associated with both volatile and high molecular weight compounds that were not completely eliminated during pyrolysis process. Finally, at temperatures above 800 °C, the thermal degradation of the catalyst increased substantially, reaching a weight loss of around 18 % at 1000 °C. This increase in the thermal degradation compared to the second zone might be related to the removal of high molecular weight compounds that had no time to be degraded during the catalyst synthesis and those that required a higher temperature to do so. The thermal study demonstrated that the synthesized iron-based catalyst could be heated up to 750 °C without significant decomposition.

The morphological properties of the FeSAC catalyst were determined by scanning electron microscopy. Thus, a SEM micrograph of the sample is shown in Fig. 2b, and further information with different magnifications has been included in Fig. S1 (Supplementary material). As can be observed, the carbonaceous material presents a rough and porous surface, with a heterogeneous structure consisting of small iron particles of different size and shape adhered to the carbon matrix. Furthermore, the activating agent, $FeCl_3{\cdot}6H_2O$, appears to have formed a complex network of pores in the catalyst, presenting cavities and crevices on its surface. Fig. S2 (Supplementary material) shows the EDX spectrum of the catalyst. The presence of iron, silicon, oxygen, and carbon elements clearly confirmed the synthesis of the carbon-based catalyst.

The oxidation state of surface iron was determined by X-ray photoelectron spectroscopy (XPS) analysis by deconvolution of the Fe2p spectra of fresh and spent catalyst. Fig. S3 (Supplementary material) represents the deconvoluted Fe2p spectra of the fresh and after used catalyst in the oxidation experiment. A main band is observed centered at approximately 712 eV accompanied by a secondary band at higher binding energy (725 eV). These bands correspond to the characteristic values of Fe^{3+}, in addition to two satellite peaks located around 717 and 728 eV confirming the presence of Fe^{3+} species on the catalyst surface [39]. XPS analysis also detected C and O as major surface components.

3.3. Catalytic performance

3.3.1. Preliminary tests

Initially, preliminary tests were conducted to determine the adsorption contribution of ciprofloxacin onto the synthesized catalyst. Three catalyst doses, between 0.10 and 0.70 g/L, were tested under an inert nitrogen atmosphere to avoid the compound oxidation. Fig. 3 illustrates the adsorption blanks of ciprofloxacin at 140 °C and 20 bar. As can be seen, during conditioning time until the operating temperature is reached, the equilibrium concentration is already attained. Therefore, the concentration of ciprofloxacin remains constant from zero time onwards.

On the other hand, the effectiveness of the synthesized catalyst requires not only to assess the adsorption contribution in the process, but

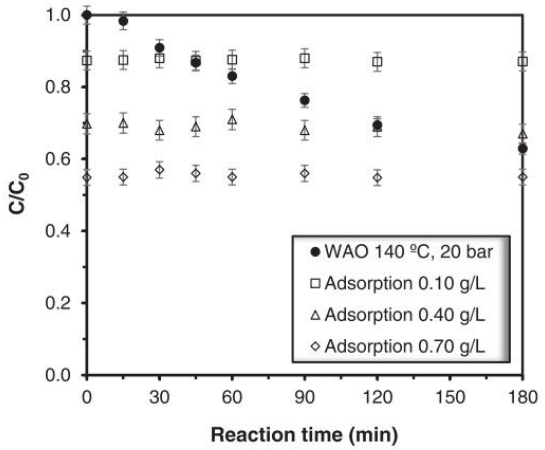

Fig. 3. WAO process and adsorption blanks for different FeSAC catalyst doses at 140 °C and 20 bar (under inert atmosphere).

also to evaluate the degradation reaction without the use of the catalyst and using air as the oxidizing atmosphere. For this purpose, a non-catalytic WAO test was carried out at 140 °C and 20 bar, as shown in Fig. 3. The results revealed considerably slow reaction kinetics, requiring a reaction time of around 1 h to remove less than 17 % of the initial concentration of ciprofloxacin.

During the first 15 min, an initial induction period in which hardly any contaminant degradation occurs can be observed. This pattern has been previously reported in the literature for non-catalytic wet air oxidation reactions, where the generation of a minimum concentration of hydroxyl radicals is necessary for the reaction to occur [40–43]. In addition, as will be mentioned hereafter, the use of catalyst in the reaction eliminates this induction period.

3.3.2. Influence of temperature on the catalytic activity

Temperature is one of the operating variables with the most significant effect on the CWAO processes [44]. The analysis of this parameter was carried out by varying the temperature from 120 to 180 °C, and maintaining the rest of the operating conditions constant, i.e. total pressure (20 bar) and catalyst dose (0.7 g/L). In addition, the TOC degradation efficiency was analyzed to evaluate the mineralization of ciprofloxacin. The TOC degradation efficiency was slower than that of ciprofloxacin, suggesting a prolonged time to achieve a complete mineralization [45]. Selectivity towards non-organic compounds was also evaluated, being defined as ($X_{TOC}/X_{Ciprofloxacin}$). The evolution of the normalized ciprofloxacin concentration, as well as the TOC removal and selectivity to CO_2 at 180 min can be seen in Fig. 4b.

The CWAO reactions exhibited some removal of ciprofloxacin at zero time reaction, which might be due to the contribution between thermal degradation and adsorption effects of the pharmaceutical during the time the reactor reached the operating temperature. According to the blank tests conducted at 140 °C and 20 bar (Fig. 3), the WAO reaction showed a ciprofloxacin removal below 1 % at zero time reaction, thus non-catalytic thermal degradation appears to be negligible. The liquid sample at zero time from CWAO reaction was also analysed by LC-MS to identify thermal degradation compounds in the catalytic process (Fig. S4). In this regard, no other compounds were detected that were not already in the 50 mg/L initial ciprofloxacin solution (Fig. S5), so the removal at this time in the catalytic process can only be attributed to the adsorption contribution. In addition, it should be noted that the use of the catalyst eliminates the induction period observed in the WAO tests, minimizing the time required to start degrading the pollutant.

The experimental results revealed that the degradation of ciprofloxacin is notably temperature-dependent. This is consistent with the results found in the literature, since the production of free radicals, which initiate the oxidation reaction, is enhanced as the temperature increases [44]. In this regard, the antibiotic concentration reached values around 20 % of its initial value at 15, 30 and 60 min, for temperatures of 160, 140 and 120 °C, respectively. This difference was particularly pronounced at high ciprofloxacin conversions when operating at 120 °C, reaching a removal around 95 % at 3 h, while the other temperatures (140 °C and 160 °C) reached yields above 99 % between 1 and 2 h earlier.

However, although an increase in temperature favors ciprofloxacin degradation, this trend seems to be the opposite for TOC removal. Consequently, since the concentration of ciprofloxacin at 180 min is very similar at the three temperatures, an increase in the final TOC concentration would lead to a lower selectivity to CO_2, i.e. a lower drug mineralization. This might be due to a modification of the reaction pathway or to an enhancement of the production rate of some intermediate which is highly recalcitrant to oxidation [45].

The variation in the removal rate of ciprofloxacin as the operating temperature changes could be due to the contribution of two factors, the influence on the kinetic constant and the solubility of oxygen in the aqueous medium, i.e. the concentration of one of the reagents. According to the literature, the solubility of oxygen in water above 100 °C and at high pressure exhibits an increasing trend when the temperature

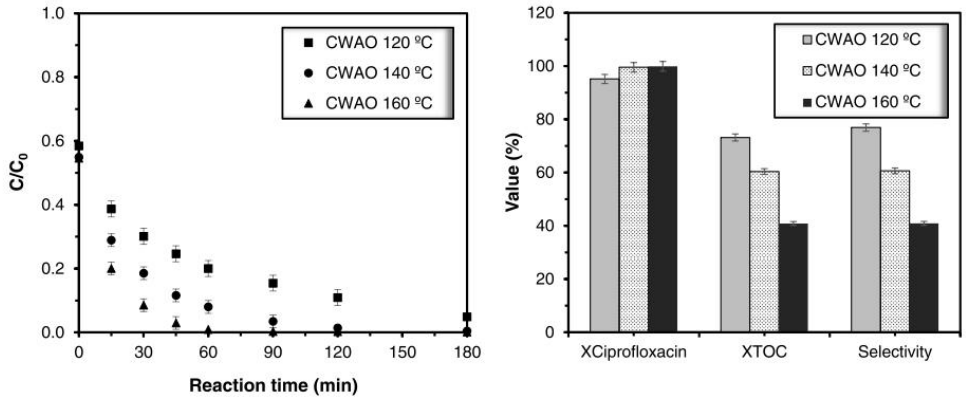

Fig. 4. Temperature effect on ciprofloxacin removal versus time (a); and ciprofloxacin conversion, TOC conversion and selectivity to CO_2 at 180 min (b). Experiments performed at P = 20 bar, $C_{Ciprofloxacin,0}$ = 50 mg/L and $C_{Catalyst}$ = 0.7 g/L.

rises. This behavior is increasingly noticeable at higher pressures. However, oxygen solubility at a total air pressure around 20 bar shows a slight increase between 120 °C (54.7 mg O_2/L) and 160 °C (67.4 mg O_2/L) [46]. Therefore, it seems that the effect of temperature has a greater contribution on the kinetic constant than on the concentration of the oxidizing agent.

The initial reaction rate was determined by numerical derivation from the concentration profile of ciprofloxacin versus reaction time. As shown in Table 2, the initial reaction rate rises as the temperature increases, keeping constant all the other variables. As previously mentioned, this fact could be due to the temperature effect on the kinetic constant. In addition, after 180 min the catalyst showed negligible iron leaching, less than 24 ppb in all reactions, and the final pH remained constant in the range 3.9–4.2. Considering the aspects mentioned above, a temperature of 140 °C has been stablished as the optimum for this study.

3.3.3. Influence of total pressure on the catalytic activity

The hydroxyl radicals generation in CWAO processes depends on the amount of dissolved oxygen, i.e., on the concentration of the oxidizing agent in the reaction medium [44,47]. As previously mentioned, the gas-liquid equilibrium depends, besides the temperature, on the pressure value. Therefore, the ciprofloxacin removal could be affected by this variable. In this study, the total pressure has been evaluated from 10 to 30 bar.

As shown in Fig. 5a, ciprofloxacin degradation appears to be slightly improved with increasing the total pressure, but this variation might be considered negligible for the pressure range evaluated. According to the literature, the oxygen solubility in water ranges from 29.8 to 89.4 mg O_2/L for a total pressure of 10 and 30 bar at 140 °C, respectively [46]. Therefore, the ciprofloxacin conversion did not seem to depend on the dissolved oxygen concentration (Fig. 5b). Furthermore, these results are consistent with what was mentioned in the analysis of the temperature influence. In this regard, the variation of oxygen solubility between 120 and 160 °C at 20 bar is within the values obtained between 10 and 30 bar at 140 °C, confirming the previously discussed idea that the increase in the ciprofloxacin removal rate with rising temperature is mainly due to the kinetic constant, and not to the concentration of the dissolved oxidizing agent. As observed with ciprofloxacin conversion values, the pressure seems to have a negligible effect on TOC conversion and selectivity.

As has been reported in Table 3, the initial reaction rate of ciprofloxacin, calculated by numerical differentiation, could be considered constant for the pressure range analyzed. This is consistent with the overlap of the concentration profiles versus time shown in Fig. 5a. In addition, the catalyst showed a very low concentration of leached active phase and a roughly constant pH at 180 min. For the results mentioned above, the optimum pressure was set at 20 bar, since an increase of this parameter did not substantially improve the ciprofloxacin degradation.

3.3.4. Influence of catalyst dose on the catalytic activity

The catalyst dose was studied in the range of 0.1–0.7 g/L, and all other parameters, i.e., temperature and total pressure, being maintained constant. As illustrated in Fig. 6a, the catalyst dose has a significant impact on the removal of ciprofloxacin, even at relatively low values. In this regard, a higher catalyst dosage in the reaction medium resulted in a greater degradation of the antibiotic. Moreover, this variation seems to be more noticeable for a catalyst dose under 0.40 g/L. After 1 h of reaction, normalized concentrations around 65 %, 27 % and 8 % were reached using catalyst doses of 0.1, 0.3 and 0.7 g/L, respectively. According to this trend, increasing the dose above 0.7 g/L may not compensate for the slight enhancement in the ciprofloxacin removal.

As expected, increasing the catalyst dose not only reduces the final concentration of ciprofloxacin in the reaction medium, but also results in a lower TOC content. This fact indicates a higher antibiotic mineralization when operating at a catalyst concentration of 0.7 g/L.

Regarding the initial reaction rates, given in Table 4, a drop in these values was observed with increasing catalyst loading. This behavior could be explained due to the decrease of ciprofloxacin concentration in the bulk fluid at zero reaction time as a result of the higher adsorption contribution. That is, a concentration drop of the reagent would lead to a decline in the initial reaction rate. In the literature, it has been reported that the oxidation processes occur by a radical pathway, generating hydroxyl radicals on the catalyst surface. However, if the reaction occurred only on the catalyst surface, the reaction rate per unit mass of catalyst would be independent of the dosage. As will be determined in Section 3.3.5, the reaction rate depends on the catalyst concentration according to an order smaller than unity. Thus, this behavior would imply that a combination of homogeneous and heterogeneous free radical mechanism is involved in the reaction [48–51].

Finally, as previously observed for temperature and pressure, the leached iron concentration, and the pH of the reaction medium at 180 min remained practically constant for the catalyst dosage range evaluated.

Table 2
Temperature influence on initial reaction rate, iron leached and pH of the reaction medium after 180 min. Experiments performed at P = 20 bar, $C_{Ciprofloxacin,0}$ = 50 mg/L and $C_{Catalyst}$ = 0.7 g/L.

	CWAO 120 °C	CWAO 140 °C	CWAO 160 °C
$r_{Ciprofloxacin,0}$ (mg/$g_{catalyst}$·min)	951	1259	1590
$Fe_{Leached}$ (mg/L)	< 0.024	< 0.024	< 0.024
pH	3.9	4.1	4.2

3.3.5. Kinetic modelling for ciprofloxacin degradation

The reaction rate for heterogeneous catalytic systems, such as the CWAO process in this study, is usually expressed in terms of the amount of catalyst, and therefore the material balance in the batch reactor would be as follows:

$$\left(-r_{Ciprofloxacin}\right) = \frac{1}{W_{Catalyst}}\cdot\left(-\frac{dn_{Ciprofloxacin}}{dt}\right) = \frac{1}{C_{Catalyst}}\cdot\left(-\frac{dC_{Ciprofloxacin}}{dt}\right) \quad (1)$$

where $r_{Ciprofloxacin}$ is the removal rate of ciprofloxacin ($mg_{Ciprofloxacin}$/$g_{catalyst}$·min), $W_{Catalyst}$ is the mass of catalyst ($g_{Catalyst}$), $C_{Catalyst}$ is the concentration of catalyst in the reaction medium ($g_{Catalyst}$/L), $n_{Ciprofloxacin}$ is the mass of ciprofloxacin ($mg_{Ciprofloxacin}$), $C_{Ciprofloxacin}$ is the concentration of ciprofloxacin ($mg_{Ciprofloxacin}$/L), and t is the reaction time (min).

On the other hand, potential kinetic models have been widely proposed in the literature for CWAO processes. Considering the influence of variables such as temperature, pressure and catalyst dosage, the following conversion rate equation has been proposed:

$$\left(-r_{Ciprofloxacin}\right) = k\cdot C^{n}_{Ciprofloxacin}\cdot P^{m}_{Total}\cdot C^{z}_{Catalyst} \quad (2)$$

where, k is the kinetic constant ($mg_{Ciprofloxacin}{}^{(1-n)}\cdot L^{(n+z)}\cdot bar^{(-m)}\cdot g_{catalyst}{}^{(-z-1)}\cdot min^{(-1)}$), P_{Total} is the total pressure (bar), and the parameters n, m and z represent the reaction orders.

Combining Eqs. (1) and (2), and replacing the kinetic constant as a function of temperature according to the Arrhenius equation results in the following expression:

$$\left(-\frac{dC_{Ciprofloxacin}}{dt}\right) = k_0\cdot e^{\left(\frac{E_a}{R\cdot T}\right)}\cdot C^{n}_{Ciprofloxacin}\cdot P^{m}_{Total}\cdot C^{z+1}_{Catalyst} \quad (3)$$

where, k_0 is the pre-exponential factor ($mg_{Ciprofloxacin}{}^{(1-n)}\cdot L^{(n+z)}\cdot bar^{(-m)}\cdot g_{catalyst}{}^{(-z-1)}\cdot min^{(-1)}$), E_a is the activation energy (kJ/mol), R is the gas constant ($8.314\cdot10^{-3}$ kJ/mol·K), and T is the reaction temperature (K).

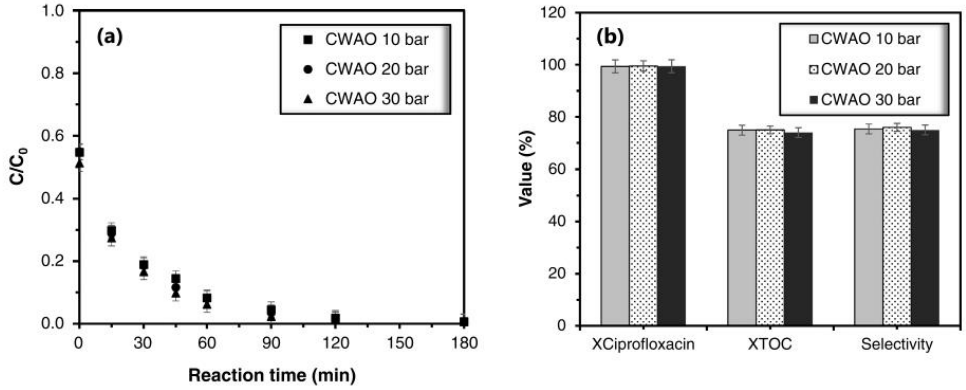

Fig. 5. Pressure effect on ciprofloxacin removal versus time (a); and ciprofloxacin conversion, TOC conversion and selectivity to CO_2 at 180 min (b). Experiments performed at T = 140 °C, $C_{Ciprofloxacin,0}$ = 50 mg/L and $C_{Catalyst}$ = 0.7 g/L.

Table 3
Pressure influence on initial reaction rate, iron leached and pH of the reaction medium after 180 min. Experiments performed at T = 140 °C, $C_{Ciprofloxacin,0}$ = 50 mg/L and $C_{Catalyst}$ = 0.7 g/L.

	CWAO 10 bar	CWAO 20 bar	CWAO 30 bar
$r_{Ciprofloxacin,0}$ ($mg/g_{catalyst}$·min)	1193	1259	1146
$Fe_{Leached}$ (mg/L)	< 0.024	< 0.024	< 0.024
pH	3.9	4.1	3.9

Furthermore, a parameter named as *effective initial concentration* ($C_{0,eff}$) has been defined to consider the decrease of ciprofloxacin concentration at zero reaction time due to the pollutant adsorption until the operating conditions are reached. Thus, ($C_{0,eff}$) is the concentration of ciprofloxacin in the bulk fluid at zero reaction time. As observed in Figs. 4–6, the pharmaceutical concentration at zero reaction time seems to depend predominantly on the catalyst dosage, with negligible influence of temperature and total pressure. Therefore, the initial condition for Eq. (3) could be expressed as indicated in Eq. (4):

$$C_{0,\,eff} = C_{Ciprofloxacin}\big|_{t=0} = C_{0,\,real} - a{\cdot}C_{catalyst} \quad (4)$$

where, a is a model parameter ($mg_{Ciprofloxacin}/g_{catalyst}$), $C_{0,eff}$ is the effective initial concentration ($mg_{Ciprofloxacin}$/L), and $C_{0,real}$ is the initial ciprofloxacin concentration ($mg_{Ciprofloxacin}$/L), i.e. 50 mg/L.

The parameters of the mathematical model consisting of Eqs. (3) and (4) were determined using a mathematical subroutine with Matlab for the nonlinear multiparameter estimation and the integration of the differential equations. To minimize the error between the experimental data ($C_{Ciprofloxacin,\,exp}$) and the model outputs ($C_{Ciprofloxacin,\,model}$), the residual sum of squares indicated in Eq. (5) was applied. This objective function is a statistical technique in regression analysis that allows to determine the function that best fits a set of experimental data. In this regard, the function indicates the level of variance in the residuals of a regression model, so the lower the value, the better the model will fit the experimental data. The above mentioned justifies the selection of the residual sum of squares as the optimality criterion.

Table 4
Catalyst dose influence on initial reaction rate, iron leached and pH of the reaction medium after 180 min. Experiments performed at T = 140 °C, P = 20 bar and $C_{Ciprofloxacin,0}$ = 50 mg/L.

	CWAO 0.1 g/L	CWAO 0.4 g/L	CWAO 0.7 g/L
$r_{Ciprofloxacin,0}$ ($mg/g_{catalyst}$·min)	3578	1806	1259
$Fe_{Leached}$ (mg/L)	< 0.024	< 0.024	< 0.024
pH	5.3	5.3	4.1

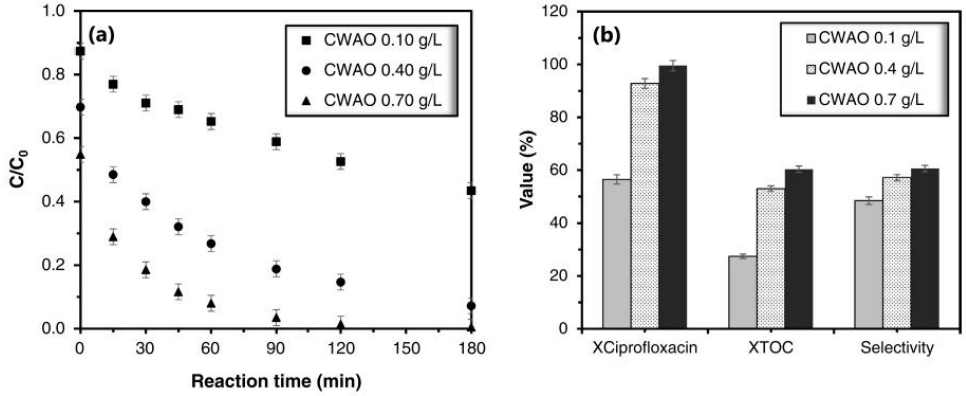

Fig. 6. Catalyst dose effect on ciprofloxacin removal versus time (a); and ciprofloxacin conversion, TOC conversion and selectivity to CO_2 at 180 min (b). Experiments performed at T = 140 °C, P = 20 bar and $C_{Ciprofloxacin,0}$ = 50 mg/L.

$$f_{obj} = \sum \left(C_{Ciprofloxacin,\ exp} - C_{Ciprofloxacin,model} \right)^2 \quad (5)$$

The calculated parameters of the proposed conversion rate equation are summarized in Table 5. The small influence of the total pressure on the kinetics of the ciprofloxacin degradation process, as shown in Fig. 5, results in an order with respect to pressure close to zero (m = 0.13). The order of catalyst dose obtained (z = 0.2) was less than unity, being within the values found in the literature for similar CWAO processes and taking into account both heterogeneous and homogeneous contributions to the pollutant removal rate [12,49–51].

On the other hand, the activation energy of the catalytic process considered in this study (53.8 kJ/mol) is relatively close to that found by other authors using catalysts with more expensive metals as active phase. Specifically, Serra-Perez et al. (2020) studied the degradation of ciprofloxacin using ruthenium and platinum catalysts supported on carbon nanospheres, whose activation energy was around 40 kJ/mol [12]. Besides requiring more costly and toxic metals than the one proposed in this study, i.e. iron, the ruthenium catalysts exhibited a higher metal leaching in the reaction medium. Therefore, the approach suggested in this study not only allows the valorization of a biomass waste such as sewage sludge, but also seems to present a catalytic activity and a loss of the active phase that is comparable to that obtained for catalysts based on more expensive and toxic metals than iron. Finally, it is worth to highlight that the use of the iron sludge-based catalyst employed in this study allowed to decrease the activation energy of the ciprofloxacin degradation process compared to the non-catalytic WAO process of this pollutant, whose value reported in the literature was around of 70 kJ/mol [12].

The parity plot of the experimental ciprofloxacin concentration values versus those obtained with the conversion rate equation (Table 5) is shown in Fig. 7. As can be seen, the experimental data exhibited small, random and non-systematic deviations from the model prediction. Moreover, the high R^2 value obtained indicated a good fit of the experimental data. In general, it could be concluded that the proposed conversion rate equation described the entire measured data set under the tested operating conditions.

3.3.6. Possible degradation pathway of ciprofloxacin removal by CWAO

The identification of reaction intermediates and by-products was accomplished after a reaction time of 180 min by LC-MS analysis. The molecular ion peak of ciprofloxacin (m/z = 332) showed a retention time of 9.4 min. In addition, two reaction intermediates, intermediate 1 and intermediate 2, with m/z values of 319 and 263, respectively, were detected. The degradation compounds identified in the analyzed sample are summarized in Table 6. LC-MS chromatogram and mass spectra of ciprofloxacin solution after 180 min of reaction time and at t_R 9.4, 0.9 and 10.5 min are shown in Figs. S6, S7, S8 and S9 (Supplementary Material).

In the first degradation pathway proposed, m/z 319 can be formed by

Table 5
Conversion rate equation and calculated parameters for ciprofloxacin removal by CWAO using the iron sludge-based catalyst.

Conversion rate equation	$\left(-\frac{dC_{Ciprofloxacin}}{dt}\right) = k_0 \cdot e^{\left(-\frac{E_a}{R \cdot T}\right)} \cdot C^{n}_{Ciprofloxacin} \cdot P^{m}_{Total} \cdot C^{z+1}_{Catalyst}$ $C_{0,\ eff} = C_{Ciprofloxacin}\big\vert_{t=0} = C_{0,\ real} - a \cdot C_{Catalyst}$
$k_0 \left(\frac{L^{n+z}}{mg^{n-1}_{Ciprofloxacin} \cdot bar^{m} \cdot g^{z+1}_{Catalyst} \cdot min} \right)$	$7.8 \cdot 10^4$
E_a (kJ/mol)	53.8
n	1.40
m	0.13
z	0.20
a ($mg_{Ciprotioxacin}/g_{catalyst}$)	33.2
R^2	0.990

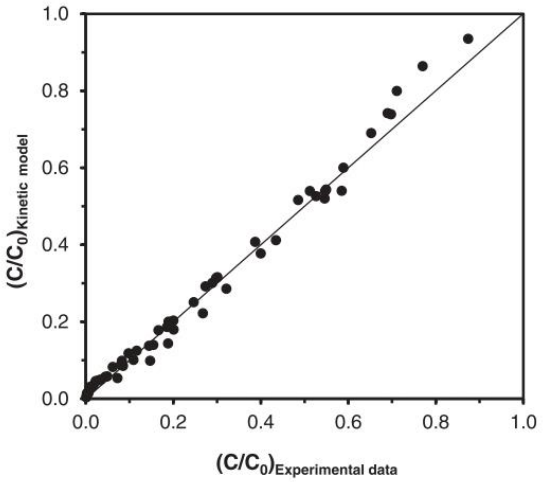

Fig. 7. Parity plot for the tests using the proposed conversion rate equation.

the decarboxylation and hydroxylation of the ciprofloxacin molecule in other pathway. The oxidation process can lead to nitrates, and then continue until mineralization into CO_2 and H_2O [52]. Similar results have been reported by Serra-P é rez et al. for the catalytic degradation of ciprofloxacin [12]. On the other hand, the cleavage of the piperazine ring caused by the attack of •OH groups on the carbons between the 1′ and 4′ position producing stepwise oxidative degradation. This is consistent with the order of oxidability of the functional groups (piperazine ring > benzo ring > pyridine ring). After this, the compound with m/z 263, could be formed after the loss of both formaldehydes and the secondary nitrogen, as well as the subsequent oxidation and loss of formaldehyde from amine side chain from ciprofloxacin [12,53]. A defluorination process could be produced in m/z 263, and further oxidation would lead to low molecular weight carboxylic acids (LMWC), i.e., oxalic, formic and acetic acid. Fig. 8 illustrates, for the first time, the proposed reaction pathway of ciprofloxacin degradation by CWAO process using the synthesized sewage sludge-based catalyst.

It should be noted that, from the molecular point of view, several studies based on Density Functional Theory (DFT) have been carried out with various functional groups. In the case of experimental studies, DFT investigations accurately predicted chemical bonding, band structures, surface character, and the effect of doping, among others.

The calculations showed, both in the reactants and the intermediates, a planar structure from which the substituents at positions 1 and 7 protrude. This plane generates a symmetry that gives rise to some conformations with equivalent energy minima. The different conformations optimized for these substituents have very similar energies, with differences of the order about 0.2 kcal/mol, practically negligible (Fig. 9a).

Considering the carboxylic group, calculations have shown that the most favorable conformations are those in which the OH group is directed towards the oxygen at C4 to interact through hydrogen bridging, being favored by about 8–9 kcal/mol over those that do not contemplate that possibility. This fact is supported by NBO (Natural Bond Orbitals) analysis, which shows stabilizing interactions between the orbitals of the oxygen lone pairs and the anti-bonding orbital of the O-H bond. In addition, electrostatic repulsions between oxygen atoms are reduced in this way. The most representative optimized structures can be seen in Fig. 9b, and their coordinates are collected in Tables S2, S3 and S4 (Supplementary material).

The E_{HOMO} values of the electronic energies corresponding to ciprofloxacin and the reaction intermediates, as well as the HOMO orbital

Table 6
Properties of some identified intermediate compounds during the ciprofloxacin degradation by LC-MS.

Compound	t_R (min)	$[M+H]^+$ (m/z)	Molecular Formula	Name	Structure
1	9.4	332	$C_{17}H_{18}FN_3O_3$	Ciprofloxacin	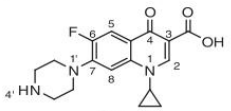
Intermediate 1	0.9	319	$C_{16}H_{16}FN_3O_3$	1-cyclopropyl-6-fluoro-3,5-dihydroxy-7-(piperazin-1-yl)quinolin-4 (1 H)-one	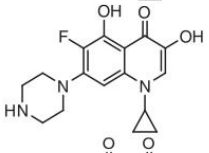
Intermediate 2	10.5	263	$C_{13}H_{11}FN_2O_3$	7-amino-1-cyclopropyl-6-fluoro-4-oxo-1,4-dihydroquinoline-3-carboxilic acid	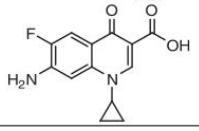

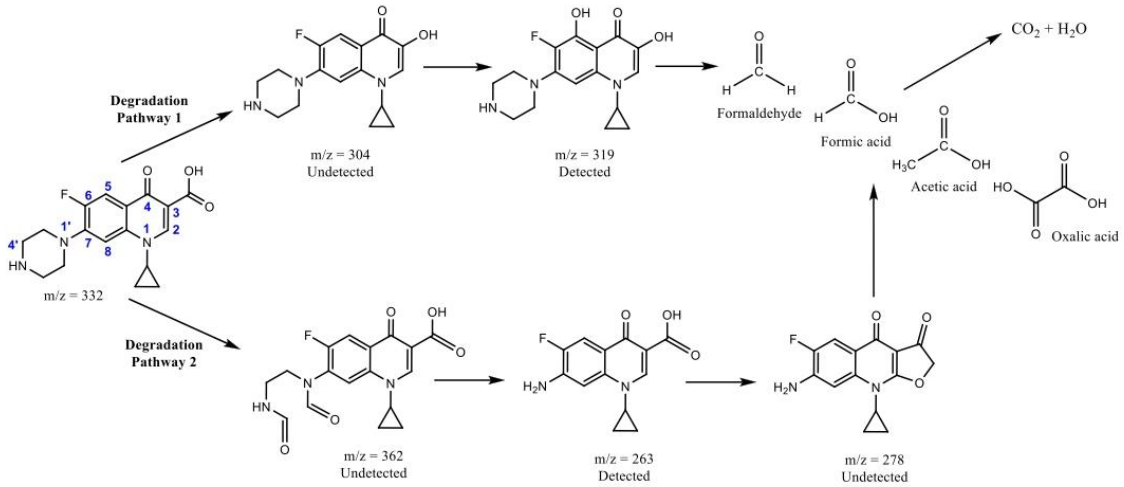

Fig. 8. Proposed reaction pathway of ciprofloxacin degradation by CWAO process.

energies (Table 7) and the optimized geometrical configuration of the organic intermediates calculated using the DFT method are shown in Fig. S8. For comparison purposes, caffeine was used, since it is a typical emerging organic contaminant that has been studied by many researchers in catalytic oxidation [54,55]. Therefore, caffeine was also evaluated using the DFT method for comparison with ciprofloxacin intermediates. Further details are collected in Table S5 (Supplementary material).

From the diagram of E_{HOMO} values, the acidic compounds, i.e., formaldehyde, formic, acetic, and oxalic acids have the lowest E_{HOMO} values among all the organic compounds, with values as low as −10.0 eV. This fact demonstrate the difficulty of oxidizing this type of low molecular weight compounds (that are refractory to oxidation), due to their characteristics, rather than to the oxidation conditions [56]. The organic intermediate 2 showed a lower E_{HOMO} value (−7.56 eV) than intermediate 1 (−6.88 eV). This suggests that intermediate 1 would be easier to degrade, which would be consistent with the mass spectrum data where, being intermediate 1 the major compound after 0.9 min (Fig. S9), it has completely disappeared at 10.5 min, remaining intermediate 2 (Fig. S10). Assuming a faster disappearance of intermediate 1, the fact that at 0.9 min it is the major compound suggests that the reaction would proceed mainly (although not exclusively) by pathway 1.

3.3.7. Proof of concept and catalyst stability

In the literature, CWAO processes of aqueous solutions prepared in ultrapure water have been widely reported. Effectively, this should be the initial study to evaluate the kinetics of the process. However, it is essential to assess the effect that an environmentally-relevant matrix may have on the oxidation reaction [12,57], verifying the feasibility of this technology with the synthesized iron sludge-based catalyst. In this regard, a real surface water matrix fortified with ciprofloxacin (C_0 = 50 mg/L) has been tested. Thus, the evolution of ciprofloxacin concentration for ultrapure water and surface water at 20 bar, 140 °C and a catalyst dosage of 0.70 g/L can be seen in Fig. 10a.

The surface water matrix does not seem to have a significant influence on the degradation of ciprofloxacin. As expected, the conversion of the antibiotic is slightly lower with the surface water matrix compared to ultrapure water, possibly due to the presence of other organic contaminants that compete with ciprofloxacin during the CWAO process. That is, the hydroxyl radicals generated are involved in the oxidation of

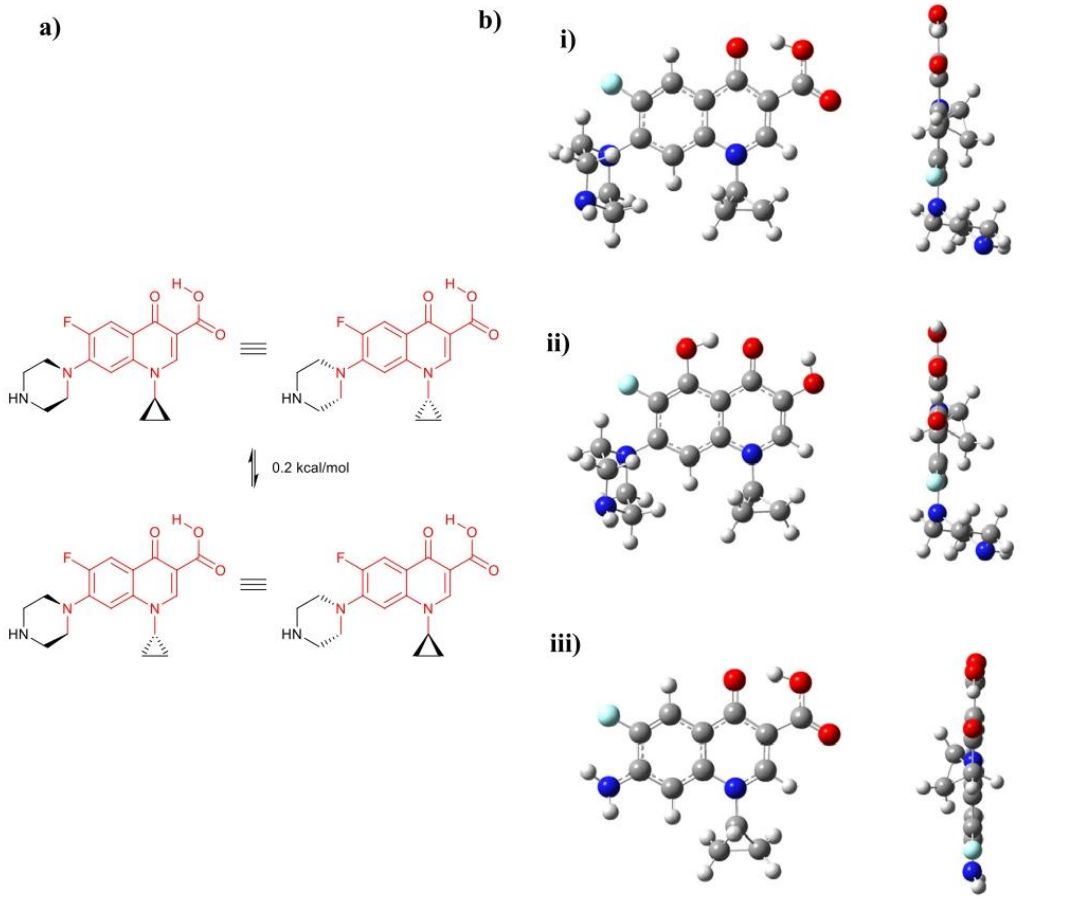

Fig. 9. Most stable conformations of ciprofloxacin (a) and most stable conformations of ciprofloxacin (i); intermediate 1 (ii); and intermediate 2 (iii) (b).

Table 7
Electronic energies and E_{HOMO} values of ciprofloxacin and intermediates.

Compound	Electronic energies (kcal/mol)	E_{HOMO} (eV)
Ciprofloxacin	-720626.16	-7.22
Intermediate 1	-696697.04	-6.88
Intermediate 2	-587998.39	-7.56

other compounds existing in the surface water matrix. It should also be highlighted that the matrix has a small influence on pollutant adsorption, showing a small increase of ciprofloxacin concentration in the bulk fluid at zero reaction time.

On the other hand, the leaching of the active phase in the reaction medium was the same regardless of the matrix, i.e., leached iron concentrations lower than 0.024 mg/L were measured. This iron concentration is significantly lower than the limit value set by the European Directive 2020/2184 for water intended for human consumption, which is 0.2 mg/L [58]. Supported iron catalysts generally exhibit a high metal leaching, so there is a large background in the literature related to the use of noble metal-based catalysts, which are more costly and toxic but present lower losses of active phase [59–63]. Therefore, it seems that the synthesis procedure of the catalyst proposed in this study enables the correct attachment of the active phase to the carbonaceous matrix, ensuring a concentration of leached iron in the aqueous phase that does not pose an environmental risk.

Catalyst deactivation is considered one of the most critical issues in heterogeneous catalytic processes, determining in most cases the technical and economical feasibility. In this research, the stability of the catalyst was assessed by three consecutive reuse cycles for the removal of ciprofloxacin in surface water matrices, as shown in Fig. 10b. As can be seen, the synthesized catalyst exhibited high stability, appreciating a slight decrease in ciprofloxacin conversion over the three cycles. During the first reuse, a removal value close to 94 % was achieved, i.e. 2 % less than the one obtained with the fresh catalyst. Then, for the second and third reuse cycles, the conversions obtained after a reaction time of 120 min were 90 % and 87 %, respectively.

All the aforementioned evidences the potential of the catalyst proposed in this study to be applied in CWAO processes for the removal of several emerging contaminants, such as ciprofloxacin, from aqueous medium.

4. Conclusions

The research described in this work proposes a feasible technique for the valorization of a solid waste, i.e., sewage sludge, contributing to the circular economy in wastewater treatment plants and to the removal of emerging pollutants, such as ciprofloxacin. In this regard, the catalyst

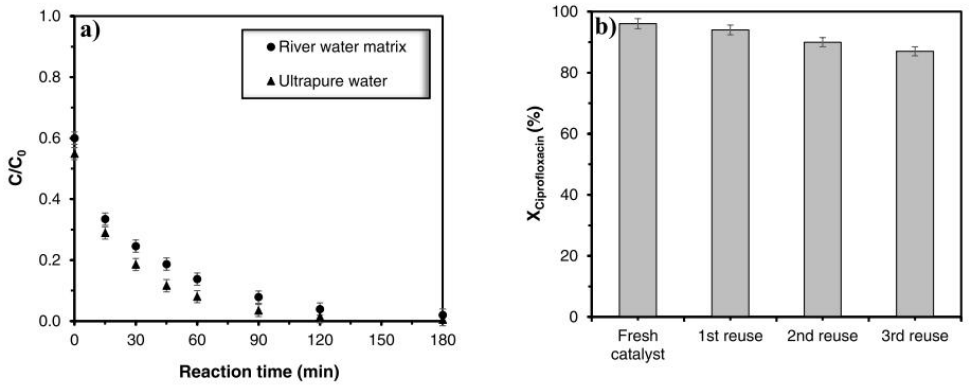

Fig. 10. Matrix effect on ciprofloxacin removal by CWAO experiments at T = 140 °C, P = 20 bar and $C_{Ciprofloxacin,0}$ = 50 mg/L (a) and Influence of catalyst reuse on ciprofloxacin conversion for CWAO experiments at T = 140 °C, P = 20 bar, $C_{Ciprofloxacin,0}$ = 50 mg/L, reaction times of 120 min, and using a surface water as aqueous matrix (b).

synthesized from sewage sludge exhibited an iron content and textural and morphological properties suitable for its application in CWAO processes. The iron-based catalyst showed high catalytic activity, oxidizing the emerging pollutant almost completely within 2 h at the following operating conditions: 140 °C, 20 bar and 0.7 $g_{Catalyst}$/L. The reaction temperature and catalyst dose showed a significant influence on the ciprofloxacin removal from aqueous solution, while total pressure did not play such an important role. In addition, the TOC degradation did not always show the same trend as the ciprofloxacin removal, which may be due to a modification of the reaction pathway. The measurement of leached iron in the reaction medium revealed a low loss of the active phase which does not pose an environmental risk, reaching values of less than 0.024 mg/L. In this way, a longer catalyst lifetime is ensured by increasing the deactivation time. The oxidation state of surface iron on the catalyst, determined by XPS analysis confirmed the presence of Fe^{3+} species on the surface of the fresh and reused catalyst. Regarding the conversion rate equation, a potential model was used to describe the experimental results accurately, with a coefficient of determination (R^2) of 0.990. A Density Functional Theory (DFT) method-based study has been accomplished in order to estimate the stability of the originated intermediates and to elucidate the degree of oxidation by the CWAO process. Furthermore, the synthesized FeSAC catalyst presented a catalytic activity comparable to that reported in the literature for noble metal-based catalysts. Finally, the technical feasibility of the process in environmentally-relevant matrices, such as surface water, was verified, obtaining an almost negligible decreasing in the catalytic activity after three consecutive reaction cycles.

CRediT authorship contribution statement

Pablo Gutiérrez-Sánchez: Conceptualization, Investigation, Formal Analysis, Software, Methodology, Writing - original draft, Writing - review & editing. **Silvia Álvarez-Torrellas:** Writing - review & editing. **Marcos Larriba:** Writing - review & editing. **M. Victoria Gil:** Software, Writing - review & editing. Juan M. Garrido-Zoido: Software, Writing - review & editing. Juan Garcia: Conceptualization, Funding acquisition, Project administration, Writing - review & editing.

Declaration of Competing Interest

The authors declare that they have no known competing financial interests or personal relationships that could have appeared to influence the work reported in this paper.

Acknowledgements

This work has been supported by the Spanish MICINN through the project CATAD3.0 PID2020–116478RB-I00. In addition, the authors thank the financial support from the Comunidad de Madrid (Spain) through the Industrial PhD projects (IND2017/AMB-7720 and IND2019/AMB-17114), REMTAVARES Network (S2018/EMT-4341) and the European Social Fund. MVG also thanks Grant PID2021-125295OB-I00 funded by MCIN/AEI/ 10.13039/501100011033 and by "ERDF A way of making Europe" and the Junta de Extremadura and the European Regional Development Fund (ERDF/FEDER), through Grant No. GR21039. The authors are grateful for the Supercomputer facility LUSITANIA funded by CenitS and the Computaex Foundation.

Appendix A. Supporting information

Supplementary data associated with this article can be found in the online version at doi:10.1016/j.jece.2023.109344.

References

[1] EurEau, Waste water treatment - sludge management, Brief. Note (2021) 1–32.
[2] B. Wu, X. Dai, X. Chai, Critical review on dewatering of sewage sludge: Influential mechanism, conditioning technologies and implications to sludge re-utilizations, Water Res. 180 (2020), 115912.
[3] J. Cañas, J. Garcia, B. Hermana, V.I. Águeda, S. Álvarez-Torrellas, Revision of the most harmful organic compounds present in sewage and sludge. The Handbook of Environmental Chemistry (HEC)-Emerging Pollutants in Sewage Sludge and Soils, eds. by Dr. Avelino Núñez-Delgado & Dr. Manuel Arias-Estévez, Springer, 2022, pp. 1–20.
[4] J. Ji, X. Yuan, Y. Zhao, L. Jiang, H. Wang, Mechanistic insights of removing pollutant in adsorption and advanced oxidation processes by sludge biochar, J. Hazard. Mater. 430 (2022), 128375.
[5] S. Álvarez-Torrellas, J.A. Peres, V. Gil-Álvarez, G. Ovejero, J. García, Effective adsorption of non-biodegradable pharmaceuticals from hospital wastewater with different carbon materials, Chem. Eng. J. 320 (2017) 319–329.
[6] E. Pérez-Mayoral, V. Calvino-Casildaa, E. Soriano, Metal-supported carbon-based materials: opportunities and challenges in the synthesis of valuable products, Catal. Sci. Technol. 6 (2016) 1265–1291.
[7] J.L. Liu, M.H. Wong, Pharmaceuticals and personal care products (PPCPs): a review on environmental contamination in China, Environ. Int. 59 (2013) 208–224.
[8] M. Carballa, F. Omil, J. Lema, Removal of pharmaceuticals and personal care products (PPCPS) from municipal wastewaters by physico-chemical processes, Elec. J. Env. Agric. Food Chem. 2 (2003) 309–313.
[9] E. Sanz-Santos, S. Álvarez-Torrellas, M. Larriba, D. Calleja-Cascajero, J. García, Enhanced removal of neonicotinoid pesticides present in the Decision 2018/840/EU by new sewage sludge-based carbon materials, J. Environ. Manag. 313 (2022), 115020.
[10] P. Gutiérrez-Sánchez, P. Navarro, S. Álvarez-Torrellas, J. García, M. Larriba, Extraction of neonicotinoid pesticides from aquatic environmental matrices with sustainable terpenoids and eutectic solvents, Sep. Purif. Technol. 302 (2022), 122148.

[11] J.L. Tambosi, L. Yamanaka, H.J. José, R. de Fátima Peralta Muniz Moreira, H. F. Schröder, Recent research data on the removal of pharmaceuticals from sewage treatment plants (STP), Quim. Nova 33 (2010) 411–420.

[12] E. Serra-Pérez, C. Ferroato, A. Giroir-Fendler, S. Álvarez-Torrellas, G. Ovejero, J. García, Highly efficient Ru supported on carbon nanosphere nanoparticles for ciprofloxacin removal: Effects of operating parameters, degradation pathways, and kinetic study, Ind. Eng. Chem. Res. 59 (2020) 15515–15530.

[13] P. Gutiérrez-Sánchez, D. Rodríguez-Llorente, P. Navarro, V.I. Águeda, S. Álvarez-Torrellas, J. García, M. Larriba, Extraction of antibiotics identified in the EU Watch List 2020 from hospital wastewater using hydrophobic eutectic solvents and terpenoids, Sep. Purif. Technol. 282 (2022), 120117.

[14] D. Rodríguez-Llorente, E. Hernández, P. Gutiérrez-Sánchez, P. Navarro, V. I. Águeda, S. Álvarez-Torrellas, J. García, M. Larriba, Extraction of pharmaceuticals from hospital wastewater with eutectic solvents and terpenoids: Computational, experimental, and simulation studies, Chem. Eng. J. 451 (2023), 138544.

[15] Y. Segura, A. Cruz Del Álamo, M. Munoz, S. Álvarez-Torrellas, J. García, J.A. Casas, Z.M. De Pedro, F. Martínez, A comparative study among catalytic wet air oxidation, Fenton, and Photo-Fenton technologies for the on-site treatment of hospital wastewater, J. Environ. Manag. 290 (2021), 112624.

[16] M.T. Reza, A. Freitas, X. Yang, C.J. Coronella, Wet air oxidation of hydrothermal carbonization (HTC) process liquid, ACS Sustain. Chem. Eng. 4 (2016) 3250–3254.

[17] M. Kumari, A. Saroha, Performance of various catalysts on treatment of refractory pollutants in industrial wastewater by catalytic wet air oxidation: a review, J. Environ. Manag. 228 (2018) 169–188.

[18] F.J. Benítez, J. García, J.L. Acero, F.J. Real, G. Roldan, Non-catalytic and catalytic wet air oxidation of pharmaceuticals in ultra-pure and natural waters, Process Saf. Environ. Prot. 89 (2011) 334–341.

[19] N. Pathak, V. Huy Tran, A. Merenda, M.A.H. Johir, S. Phuntsho, H. Shon, Removal of organic micro-pollutants by conventional membrane bioreactors and high-retention membrane bioreactors, Appl. Sci. 10 (2020) 2969.

[20] A.K. Al-Buriahi, Muhanna, M.M. Al-shaibani, R.M.S.R. Mohamed, A.A. Al-Gheethi, A. Sharma, N. Ismail, Ciprofloxacin removal from non-clinical environment: a critical review of current methods and future trend prospects, J. Water Process. Eng. 47 (2022), 102725.

[21] European Commission. Decision (EU) 2020/1161. Official Journal of the European Union L 257 (2020).

[22] American Public Health Association, Standard Methods for the Examination of Water and Wastewater. American Public Health Association, American Water Works Association, Water Environment Federation, 2017.

[23] F. Du, Z. Lai, H. Tang, H. Wang, C. Zhao, Construction and application of BiOCl/Cu-doped Bi_2S_3 composites for highly efficient photocatalytic degradation of ciprofloxacin, Chemosphere 287 (2022), 132391.

[24] A.G. Gonçalves, J.J.M. Órfão, M.F.R. Pereira, Catalytic ozonation of sulphamethoxazole in the presence of carbon materials: catalytic performance and reaction pathways, J. Hazard. Mater. 239–240 (2012) 167–174.

[25] F.J. Beltrán, A. Aguinaco, J.F. García-Araya, A. Oropesa, Ozone and photocatalytic processes to remove the antibiotic sulfamethoxazole from water, Water Res. 42 (2008) 3799–3808.

[26] A.G. Trovó, R.F. Pupo Nogueira, A. Agüera, A.R. Fernandez-Alba, S. Malato, Degradation of the antibiotic amoxicillin by photo-fenton process - chemical and toxicological assessment, Water Res. 45 (2011) 1394–1402.

[27] A. Ledezma Estrada, Y.Y. Li, A. Wang, Biodegradability enhancement of wastewater containing cefalexin by means of the electro-Fenton oxidation process, J. Hazard. Mater. 227–228 (2012) 41–48.

[28] T.H. Kim, S.D. Kim, H.Y. Kim, S.J. Lim, M. Lee, S. Yu, Degradation and toxicity assessment of sulfamethoxazole and chlortetracycline using electron beam, ozone and UV, J. Hazard. Mater. 227–228 (2012) 237–242.

[29] M.J. Frisch, G.W. Trucks, H.B. Schlegel, G.E. Scuseria, M.A. Robb, J.R. Cheeseman, et al., Gaussian 16, Revision C.01, Gaussian, Inc., Wallingford CT, 2016.

[30] E.D. Glendening, A.E. Reed, J.E. Carpenter, F. Weinhold, NBO Version 3.1.

[31] F. Weinhold, C.R. Landis, Discovering Chemistry with Natural Bond Orbitals, John Wiley and Sons, Inc, Hoboken, New Jersey, 2012.

[32] A.V. Marenich, C.J. Cramer, D.G. Truhlar, Universal solvation model based on solute electron density and a continuum model of the solvent defined by the bulk dielectric constant and atomic surface tensions, J. Phys. Chem. B 113 (2009) 6378–6396.

[33] R. Dennington, T.A. Keith, J.M. GaussView, Version 6, Millam, Semichem Inc., Shawnee Mission, KS, (2016).

[34] J. Jjagwe, P.W. Olupot, E. Menya, H.M. Kalibbala, Synthesis and application of granular activated carbon from biomass waste materials for water treatment: a review, J. Bioresour. Bioprod. 6 (2021) 292–322.

[35] C. Nieto-Delgado, M. Terrones, J.R. Rangel-Mendez, Development of highly microporous activated carbon from the alcoholic beverage industry organic by-products, Biomass. Bioenerg. 35 (2011) 103–112.

[36] M. Thommes, K. Kaneko, A.V. Neimark, J.P. Olivier, F. Rodriguez-Reinoso, J. Rouquerol, K.S.W. Sing, Physisorption of gases, with special reference to the evaluation of surface area and pore size distribution (IUPAC Technical Report), Pure Appl. Chem. 87 (2015), 1051–106.

[37] C. Schlumberger, M. Thommes, Characterization of hierarchically ordered porous materials by physisorption and mercury porosimetry-a tutorial review, Adv. Mater. Interfaces 8 (2021) 2002181.

[38] E. Sanz-Santos, S. Álvarez-Torrellas, L. Ceballos, M. Larriba, V.I. Águeda, J. García, Application of sludge-based activated carbons for the effective adsorption of neonicotinoid pesticides, Appl. Sci. 11 (2021) 3087.

[39] J.A. Zazo, J. Bedia, C.M. Fierro, G. Pliego, J.A. Casas, J.J. Rodriguez, Highly stable Fe on activated carbon catalysts for CWPO upon $FeCl_3$ activation of lignin from black liquors, Catal. Today 187 (2012) 115–121.

[40] S. Yang, W. Zhu, J. Wang, Z. Chen, Catalytic wet air oxidation of phenol over CeO_2-TiO_2 catalyst in the batch reactor and the packed-bed reactor, J. Hazard. Mater. 153 (2008) 1248–1253.

[41] A. Tungler, E. Szabados, A.M. Hosseini, Wet air oxidation of aqueous wastes, in: M. Samer (Ed.), Wastewater Treatment Engineering, InTech, 2015.

[42] H.S. Joglekar, S.D. Samant, J.B. Joshi, Kinetics of wet air oxidation of phenol and substituted phenols, Water Res. 25 (1991) 135–145.

[43] Q. Wu, X. Hu, P.L. Yue, Kinetics study on catalytic wet air oxidation of phenol, Chem. Eng. Sci. 58 (2003) 923–928.

[44] J. Levec, A. Pintar, Catalytic wet-air oxidation processes: a review, Catal. Today 124 (2007) 172–184.

[45] H. Guo, T. Ke, N. Gao, Y. Liu, X. Cheng, Enhanced degradation of aqueous norfloxacin and enrofloxacin by UV-activated persulfate: kinetics, pathways and deactivation, Chem. Eng. J. 316 (2017) 471–480.

[46] D. Tromans, Temperature and pressure dependent solubility of oxygen in water: a thermodynamic analysis, Hydrometallurgy 48 (1998) 327–342.

[47] M. Besson, J.-C. Beziat, B. Blanc, S. Durecu, P. Gallezot, Treatment of aqueous solutions of organic pollutants by heterogeneous catalytic wet air oxidation (CWAO), Stud. Surf. Sci. Catal. 130 (2000) 1553–1558.

[48] M.E. Suárez-Ojeda, A. Fabregat, F. Stüber, A. Fortuny, J. Carrera, J. Font, Catalytic wet air oxidation of substituted phenols: temperature and pressure effect on the pollutant removal, the catalyst preservation and the biodegradability enhancement, Chem. Eng. J. 132 (2007) 105–115.

[49] P.A. Massa, M.A. Ayude, R.J. Fenoglio, J.F. Gonzalez, P.M. Haure, Catalyst systems for the oxidation of phenol in water, Lat. Am. Appl. Res. 34 (2004) 133–140.

[50] A. Santos, P. Yustos, et al., Catalytic wet oxidation of phenol: kinetics of the mineralization rate, Ind. Eng. Chem. Res. 40 (2001) 2773–2781.

[51] H. Ohta, S. Goto, H. Teshima, Liquid-phase oxidation of phenol in a rotating catalytic basket reactor, Ind. Eng. Chem. Fundam. 19 (1980) 180–185.

[52] L. Oliviero, J. Barbier Jr, D. Duprez, Wet air oxidation of nitrogen-containing organic compounds and ammonia in aqueous media, Appl. Catal. B 40 (2003) 163–184.

[53] A. Sadana, An analysis of the heterogeneously catalyzed free-radical oxidation of phenol in aqueous solution, Ind. Eng. Chem. Process. Des. Dev. 18 (1979) 50–56.

[54] V.O. Ndabankulu, S. Maddila, S.B. Jonnalagadda, Ozone facilitated degradation of caffeine using Ce-TiO_2, Catal., J. Environ. Eng. Sci. B 54 (2019) 138–146.

[55] S. Sathish, S. Supriya, J. Aravind kumar, D. Prabu, D. Marshiana, M. Rajasimman, Yasser Vasseghian, Enhanced photocatalytic degradation of caffeine using Co–Zn/Al_2O_3 nanocomposite, Chemosphere 307 (2022), 135773.

[56] A. Santos, E. Barroso, F. García-Ochoa, Overall rate of aqueous-phase catalytic oxidation of phenol: pH and catalyst loading influences, Catal. Today 48 (1999) 109–117.

[57] J. Deng, G. Wu, S. Yuan, X. Zhan, W. Wang, Z.-H. Hu, Ciprofloxacin degradation in UV/chlorine advanced oxidation process: Influencing factors, mechanisms and degradation pathways, J. Photochem. Photobiol. A Chem. 371 (2019) 151–158.

[58] European Commission. Directive (UE) 2020/2184. Official Journal of the European Union L 435, (2020).

[59] F. Moccia, L. Rigamonti, A. Messori, V. Zanotti, R. Mazzoni, Bringing homogeneous iron catalysts on the heterogeneous side: solutions for immobilization, Molecules 26 (2021) 2728.

[60] A. Fürstner, Iron catalysis in organic synthesis: a critical assessment of what it takes to make this base metal a multitasking champion, ACS Cent. Sci. 2 (2016) 778–789.

[61] A. Vallet, G. Ovejero, A. Rodríguez, J.A. Peres, J. García, Ni/MgAlO regeneration for catalytic wet air oxidation of an azo-dye in trickle-bed reaction, J. Hazard. Mater. 244–245 (2013) 46–53.

[62] M. Munoz, F.J. Mora, Z.M. de Pedro, S. Alvarez-Torrellas, J.A. Casas, J. J. Rodríguez, Application of CWPO to the treatment of pharmaceutical emerging pollutants in different water matrices with a ferromagnetic catalyst, J. Hazard. Mater. 331 (2017) 45–54.

[63] A. Cybulski, Catalytic wet air oxidation: are monolithic catalysts and reactors feasible? Ind. Eng. Chem. Res. 46 (2007) 4007–4033.

Supplementary Material

for

Efficient removal of antibiotic ciprofloxacin by catalytic wet air oxidation using sewage sludge-based catalysts. Degradation mechanism by DFT studies.

Pablo Gutiérrez-Sánchez[1*], Silvia Álvarez-Torrellas[1], Marcos Larriba[1], M. Victoria Gil[2], Juan M. Garrido-Zoido[2], Juan García[1*]

[1]Catalysis and Separation Processes Group, Chemical Engineering and Materials Department, Faculty of Chemistry, Complutense University, Avda. Complutense s/n, 28040, Madrid, Spain.
[2]Departamento de Química Orgánica e Inorgánica, Facultad de Ciencias and IACYS Unidad de Química Verde y Desarrollo Sostenible, Universidad de Extremadura, E-06006 Badajoz, Spain.

Corresponding author
E-mail address: pgutie03@ucm.es; jgarciar@ucm.es; +34 91394.5207

Tables: 5

Figures: 10

Table S1. Comparison of several advanced oxidation processes in the ciprofloxacin removal.

Process	Reference	Year	$C_{0\ Ciprofloxacin}$ (mg/L)	Degradation (%)	t (min)	Conditions
Photocatalysis	[1]	2022	10	93.5	60	Light intensity = 100 mW/cm^2 , power of 300 W, Co_3O_4/SiNWs-30/PMS, C_{PMS} = 0.52 mM, pH = 7
Cavitation	[2]	2022	10-100	79-95	180	ΔP = 0.5, 1, 1.5, and 2 bar, CIP: H_2O_2= 1:100, 1:300, 1:500, 1:700, 1:1000, and 1:1500, pH = 6.6–7.8
Photocatalysis	[3]	2022	20-40	96.1	30	Cu-doped Bi_2S_3, Xc lamp, light intensity = 50 mW/cm^2, 5.0 < pH < 9.0
Heterogeneous Fenton	[4]	2019	10	80-90	20-4h	[sludge biochar catalyst] = 0.2 g·L^{-1}, pH = 4, [H_2O_2] = 10mM
Fenton´s oxidation	[5]	2018	100	70	60	[H_2O_2]:[Fe^{2+}] = 10, stoichiometric [H_2O_2] = 14.2 mM and initial wastewater pH = 3
Fenton	[6]	2013	50	90	30	pH = 2, [H_2O_2]:[Fe^{2+}] = 2.7
This work		2022	50	99	180	T = 140ºC, P = 20 bar, m_{cat} = 0.7 g/L, pH_0=7

Table S2. Cartesian coordinates for optimized structure of ciprofloxacin.

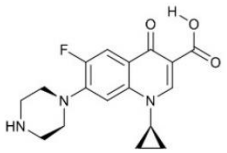

ATOM TYPE	x	y	z
C	1.16925600	-2.03831100	-0.26296700
C	1.75749000	-0.76374200	-0.47890100
C	0.87998700	0.31577300	-0.51864800
C	-0.49212900	0.15086700	-0.31653400
C	-1.03204200	-1.12043400	-0.07685900
C	-0.16029100	-2.22005900	-0.06067400
N	-1.34375100	1.25777000	-0.33905500
C	-2.65729100	1.09457900	-0.18713000
C	-3.25161800	-0.12269300	0.03177100
C	-2.45308500	-1.30839200	0.11247600
F	1.95403100	-3.12726200	-0.33012100
C	-0.79725400	2.58229400	-0.57850700
C	0.03892900	3.21753500	0.48298700
C	-1.33521100	3.74142800	0.18790700
O	-2.95126500	-2.44343900	0.32749200
C	-4.71699500	-0.17185700	0.19026300
O	-5.22297900	-1.37802100	0.41269800
O	-5.43846600	0.80595300	0.12587300
N	3.11448300	-0.65341600	-0.72171600
C	4.04515700	-1.28070100	0.23641900
C	4.32906400	-0.34967600	1.40247400
N	4.90591400	0.90404800	0.91601500
C	3.95024300	1.56535400	0.02455700
C	3.64441200	0.64523800	-1.14729400
H	1.26456800	1.30477900	-0.69267400
H	-0.54831100	-3.21933300	0.07844000
H	-3.25844300	1.99067100	-0.24377100
H	-0.50883200	2.73477400	-1.60879300
H	0.90045200	3.78059200	0.15683600
H	0.16300100	2.66027500	1.40063000
H	-2.10061500	3.54878400	0.92511900
H	-1.43473600	4.67144200	-0.34983500
H	-4.45300900	-2.03276400	0.42691900
H	3.64037700	-2.21481200	0.60500500
H	4.97108600	-1.49576300	-0.29842100
H	3.39091100	-0.17993800	1.94947200
H	5.03065200	-0.83263600	2.08067700
H	5.07192900	1.50957800	1.71114500
H	4.38359600	2.48992900	-0.35314200
H	3.02215000	1.81907400	0.55234400
H	4.57353300	0.44161100	-1.68183000
H	2.95883800	1.11110400	-1.85028500

Table S3. Cartesian coordinates for optimized structure of intermediate 1.

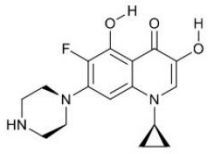

ATOM TYPE	x	y	z
C	0.73348600	-1.90742900	-0.26252700
C	1.31937500	-0.64034400	-0.49130300
C	0.46978700	0.46070800	-0.51492800
C	-0.90435000	0.31943100	-0.28524800
C	-1.46502400	-0.94949800	-0.03562800
C	-0.60411900	-2.07535100	-0.03390600
N	-1.73930900	1.41675000	-0.28393400
C	-3.07720200	1.26986300	-0.10162400
C	-3.65611400	0.06430100	0.12113400
C	-2.86990000	-1.12269900	0.17443000
F	1.48581200	-3.02112700	-0.34820500
C	-1.20012400	2.73643400	-0.54396600
C	-0.31645400	3.37102900	0.48012400
C	-1.70201900	3.89564600	0.24825000
O	-3.41567900	-2.24547400	0.38964600
N	2.68018000	-0.55943300	-0.75585000
C	3.60236900	-1.19230600	0.20649500
C	3.90754100	-0.25838700	1.36456200
N	4.50870400	0.97920500	0.86573900
C	3.56218800	1.65204700	-0.02730600
C	3.22932700	0.72838800	-1.18935700
H	0.87135400	1.44149200	-0.69138800
H	-3.66864500	2.17226800	-0.14234200
H	-0.95609300	2.89838000	-1.58498500
H	0.52900400	3.93656200	0.11783500
H	-0.14996200	2.81142300	1.38955800
H	-2.43477700	3.69914700	1.01698200
H	-1.82470900	4.82838900	-0.28009100
H	3.18283900	-2.11670900	0.58350300
H	4.52380300	-1.42857300	-0.32766900
H	2.97448100	-0.06443000	1.91240900
H	4.60072500	-0.74941300	2.04571000
H	4.68970200	1.58784400	1.65520500
H	4.01360500	2.56330900	-0.41639100
H	2.64355400	1.93107800	0.50357800
H	4.15069600	0.50687900	-1.73065200
H	2.54604600	1.20313100	-1.88863700
O	-5.00671700	-0.03736700	0.30524600
H	-5.19929000	-0.97540800	0.45307200
O	-1.09193400	-3.31864600	0.15415200
H	-2.06962400	-3.20998900	0.28890300

Table S4. Cartesian coordinates for optimized structure of intermediate 2.

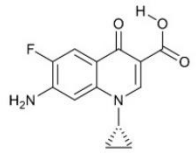

ATOM TYPE	x	y	z
C	-2.70244000	-1.41001800	0.05153800
C	-3.01505200	-0.04384100	-0.11678400
C	-1.95805200	0.85040000	-0.21631000
C	-0.64030400	0.39823100	-0.14318900
C	-0.35825400	-0.97024800	0.01808700
C	-1.43102300	-1.87379500	0.11656300
N	0.42106700	1.30015000	-0.24170000
C	1.67953300	0.86198600	-0.22561600
C	2.02268300	-0.45735500	-0.07655900
C	1.00213200	-1.45262600	0.06703300
F	-3.74207900	-2.25817300	0.14064300
C	0.14493600	2.71484200	-0.42018100
C	-0.40365800	3.49064200	0.73096400
C	1.00574000	3.71621100	0.26947400
O	1.27185100	-2.67324600	0.21872000
C	3.45315300	-0.81597000	-0.06208000
O	3.71244900	-2.10684700	0.10057300
O	4.35584400	-0.00897700	-0.18623900
N	-4.31671100	0.35184000	-0.13073700
H	-2.18207900	1.89705600	-0.35302100
H	-1.24325000	-2.93106600	0.23898800
H	2.44560200	1.61518100	-0.33888600
H	-0.22441400	2.94605900	-1.40916100
H	-1.15664800	4.23143300	0.50899900
H	-0.53300200	2.95358200	1.65961500
H	1.79424700	3.34854800	0.90937400
H	1.23798600	4.61478000	-0.28069700
H	2.82622400	-2.58739200	0.18097700
H	-4.51415200	1.27807900	-0.47622600
H	-5.01980200	-0.34481800	-0.32075300

Table S5. Energetic data of organic compounds involved in the reaction and caffeine as reference.

Compound	Electronic energies (kcal/mol)	Sum of electronic and thermal free energies (kcal/mol)	Entropy (cal/(mol·K))	Electronic energies (Hartrees)	Energies HOMO (eV)	Energies LUMO (eV)
Ciprofloxacin	-720626.16	-720458.36	168.55	-1148.39	-7.22	-0.98
Intermediate 1	-696697.04	-696532.03	164.74	-1110.26	-6.88	-0.75
Intermediate 2	-587998.39	-587895.96	142.78	-937.03	-7.56	-0.94
Formaldehyde	-71848.12	-71848.53	50.54	-114.50	-9.48	-0.10
Formic acid	-119082.05	-119080.54	57.32	-189.77	-10.35	0.39
Acetic acid	-143755.36	-143739.38	68.55	-229.09	-10.06	0.14
Oxalic acid	-237418.40	-237412.27	75.94	-378.35	-10.17	-1.02
Caffeine	-426934.64	-426851.11	123.26	-680.36	-7.61	-0.15

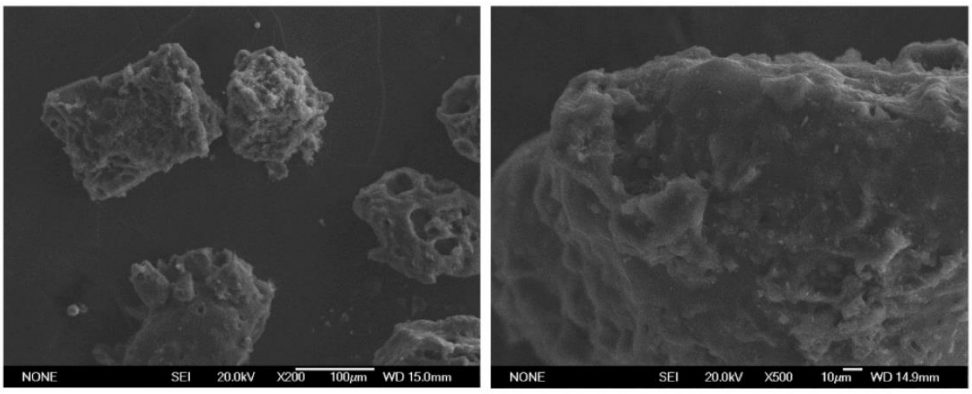

Figure S1. SEM micrographs of the FeSAC catalyst with different magnification.

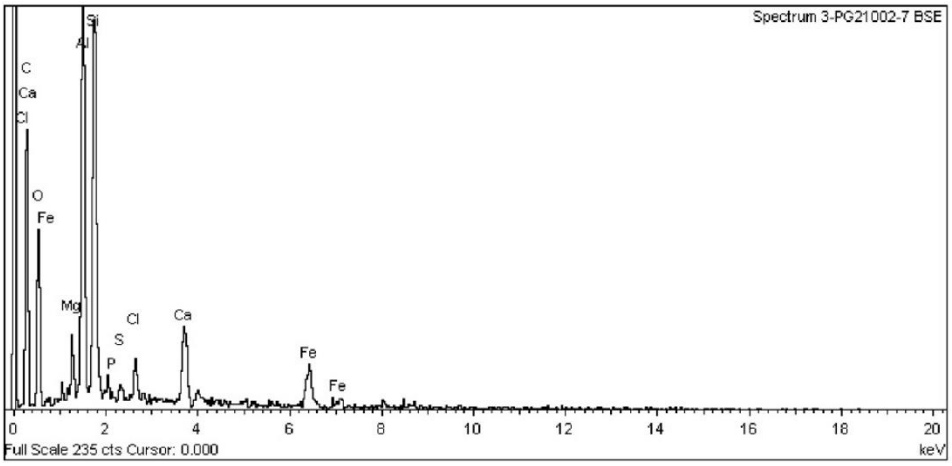

Figure S2. EDX analysis of FeSAC catalyst.

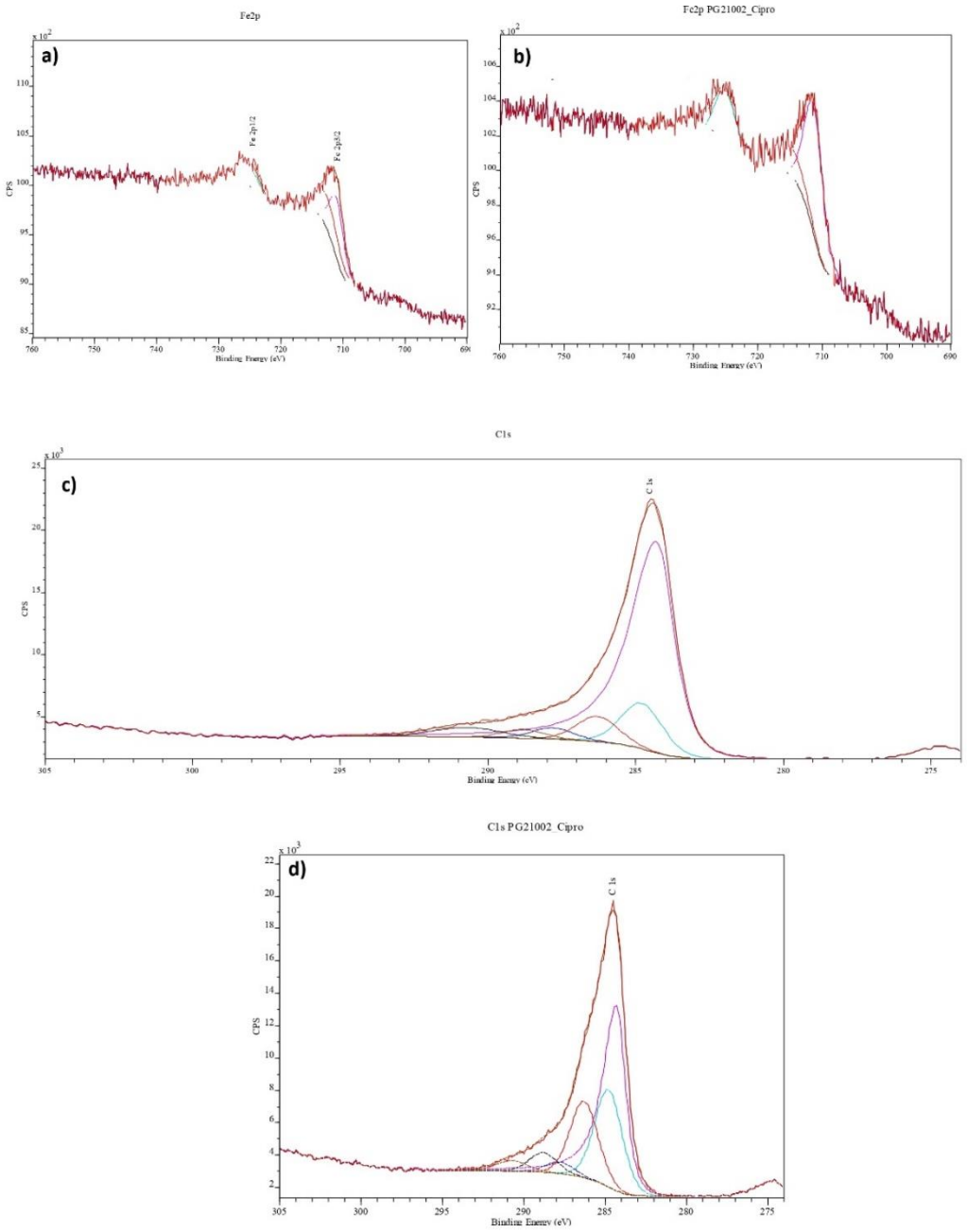

Figure S3. Fe2p, C1s and O1s deconvoluted XPS spectrum of fresh catalyst as prepared (a, c, e) and after used in experiment (b, d, f), respectively.

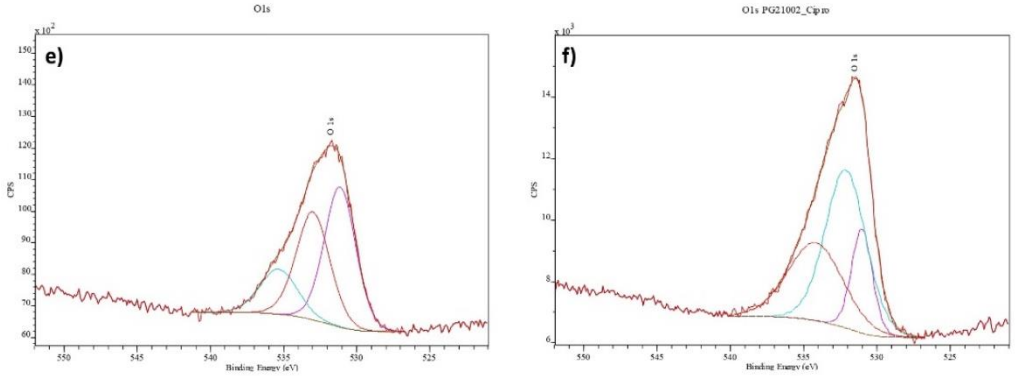

Figure S3. (cont.) Fe2p, C1s and O1s deconvoluted XPS spectrum of fresh catalyst as prepared (a, c, e) and after used in experiment (b, d, f), respectively.

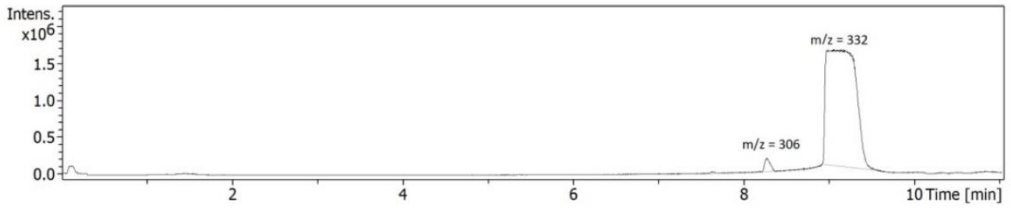

Figure S4. LC-MS chromatogram for the liquid sample at zero time from CWAO reaction.

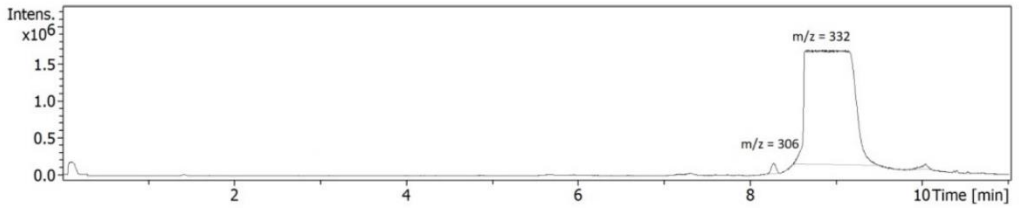

Figure S5. LC-MS chromatogram for the initial ciprofloxacin solution at 50 mg/L.

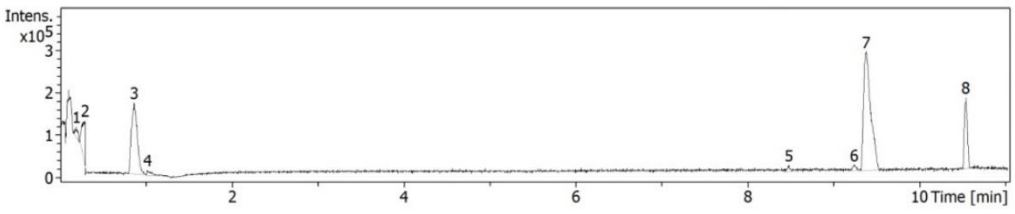

Figure S6. LC-MS chromatogram for the liquid sample after a reaction time of 180 min.

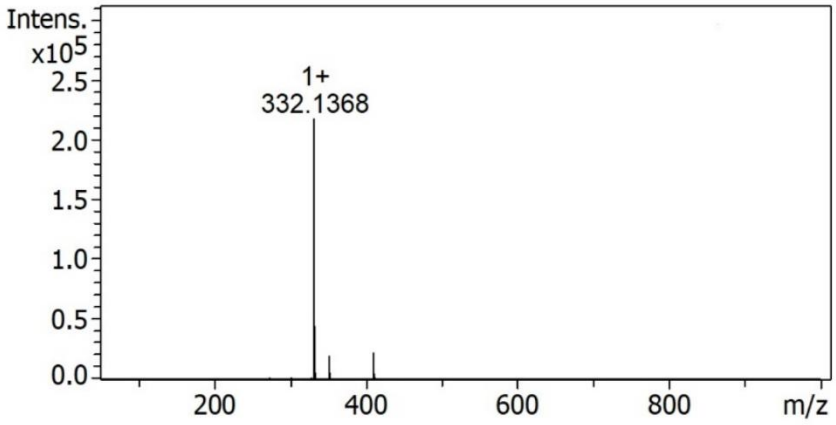

Figure S7. Mass spectrum of ciprofloxacin solution at t_R=9.4 min.

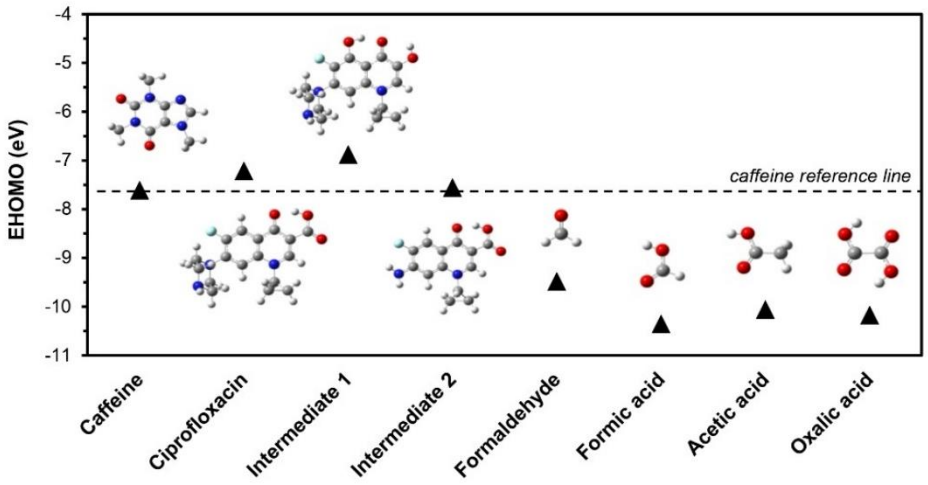

Figure S8. E_{HOMO} (eV) comparative diagram of ciprofloxacin, intermediates, and final products (caffeine as reference).

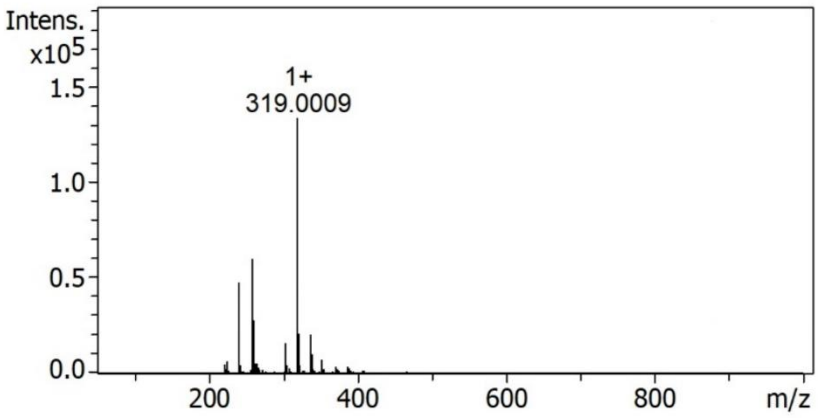

Figure S9. Mass spectrum of ciprofloxacin solution at t_R=0.9 min.

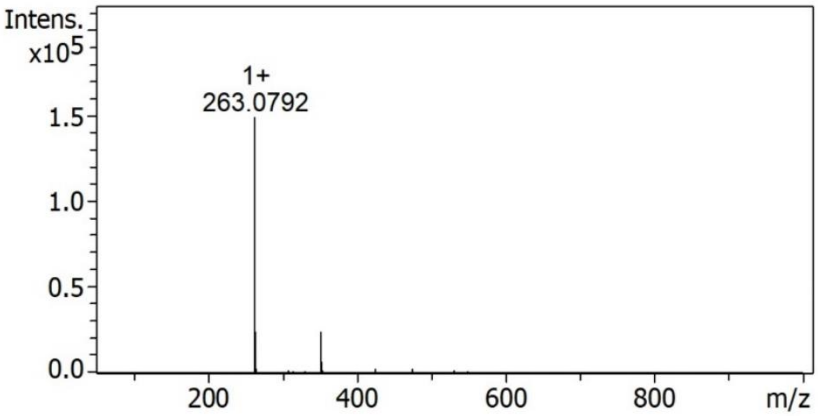

Figure S10. Mass spectrum of ciprofloxacin solution at t_R=10.5 min.

References:

[1] L. Yao, X. He, J. Lv, G. Xu, Z. Bao, J. Cui, D. Yu, Y. Wu, Efficient degradation of ciprofloxacin by Co_3O_4/Si nanoarrays heterojunction activated peroxymonosulfate under simulated sunlight: Performance and mechanism, J. Environ. Chem. Eng. 10 (2022) 107397.

[2] P.B. Patil, P. Thanekar, V.M. Bhandari, Intensified hydrodynamic cavitation using vortex flow based cavitating device for degradation of ciprofloxacin, Chem. Eng. Res. Des. 187 (2022) 623-632.

[3] F. Du, Z. Lai, H. Tang, H. Wang, C. Zhao, Construction and application of BiOCl/Cu-doped Bi_2S_3 composites for highly efficient photocatalytic degradation of ciprofloxacin, Chemosphere 287 (2022) 132391.

[4] J. Li, L. Pan, G. Yu, S. Xie, C. Li, D. Lai, et al., The synthesis of heterogeneous Fenton-like catalyst using sewage sludge biochar and its application for ciprofloxacin degradation, Sci. Total Environ. 654 (2019) 1284–1292.

[5] A. Gupta, A. Garg, Degradation of ciprofloxacin using Fenton's oxidation: Effect of operating parameters, identification of oxidized by-products and toxicity assessment, Chemosphere 193 (2018) 1181–1188.

[6] J. F. Yang, H. H. Chen, Degradation of Ciprofloxacin in Aqueous Solution by the Fenton Process', Adv. Mater. Res. 610–613 (2012) 352–355.